

Drivers of immune resistance in MITF^{low} melanomas



DISSERTATION ZUR ERLANGUNG DES DOKTORGRADES DER
NATURWISSENSCHAFTEN (DR. RER. NAT.) DER FAKULTÄT FÜR BIOLOGIE
UND VORKLINISCHE MEDIZIN DER UNIVERSITÄT REGENSBURG

vorgelegt von
Julian Martin Sax

aus
Bad Kreuznach

im Jahr
2023

Drivers of immune resistance in MITF^{low} melanomas



DISSERTATION ZUR ERLANGUNG DES DOKTORGRADES DER
NATURWISSENSCHAFTEN (DR. RER. NAT.) DER FAKULTÄT FÜR BIOLOGIE
UND VORKLINISCHE MEDIZIN DER UNIVERSITÄT REGENSBURG

vorgelegt von

Julian Martin Sax

aus

Bad Kreuznach

im Jahr

2023

Das Promotionsgesuch wurde eingereicht am:
05.04.2023

Die Arbeit wurde angeleitet von:
Prof. Dr. Philipp Beckhove

Unterschrift:

Julian Martin Sax

Declaration

I herewith declare in lieu of oath that I have composed this thesis without any inadmissible help of a third party and without the use of aids other than those listed. The data and concepts that have been taken directly or indirectly from other sources have been acknowledged and referenced.

Other persons have not helped to produce this work as regards to its content or making. In particular, I have not used the services of any professional agencies in return for payment or those of other persons. Nobody has received payment in kind – neither directly nor indirectly – from me for any work that is connected with the content of this doctoral thesis.

This thesis has not been submitted, wholly or substantially, neither in this country nor abroad for another degree or diploma at any university or institute.

I declare in lieu of oath that I have said nothing but the truth to the best of my knowledge and that I have not withheld any information.

Before the above declaration in lieu of oath had been taken down, I was advised about the significance of a declaration in lieu of oath as well as the legal consequences of an incorrect or incomplete declaration.

Regensburg, 05.04.2023

Julian Martin Sax

Acknowledgments

After a long break following my master's program, I was not quite sure if I should really dare to pursue a PhD. When I decided to do so in AG Beckhove, I had the claim on myself to learn and grow as a scientist as well as a person. Retrospectively, I surely did so but this personal benefit could not have been achieved without the help and company of numerous other people. This chapter is to express my deepest gratitude to everyone who accompanied me through the past four years.

Foremost, I would like to thank my supervisor Prof. Philipp Beckhove. After my first interview with him I was sure that I could learn a lot under his guidance and what should I say – these expectations were met. Thank you, Philipp, for giving me the chance to work on this project and for believing in me to perform bioinformatic analyses when I often did not. Thank you for guiding me through the plenty of experiments in order to focus on the relevant ones that brought me to the completion of this thesis. I very much appreciate your care of building a group that does not work against each other but together and in which everyone likes to support and respects each other.

Also, I would like to thank my PhD mentors Prof. Annette Paschen and Prof. Gernot Längst for their guidance and valuable comments during and beyond the progress reports. As this project is part of the T-Lock consortium, I further thank the Deutsche Krebshilfe for the consortiums funding and Annette for the coordination of the consortium as well as for providing me with the melanoma cell lines.

I would like to express eternal gratitude to my two advisors Vale and Ayşe. I know it wasn't always easy for you, especially in times in which I ignored both of your advice and chose to do the opposite or asking hundreds of questions. No matter when, I could always count on your support. Thank you for teaching me the methods necessary for this project and for the scientific but also personal guidance through the past four years. I strongly appreciated your calming words after exciting meetings or disappointing experimental results. You helped shaping this work to become what it is now.

A big thank you is dedicated to my great students Amelie and Verena. You were an immense support and without your assistance I would still be standing in the lab pipetting kill assays and western blots. I would further like to appreciate the numerous internal and external collaborators that supported this work in any way. Thanks to Dr. Susanne Horn, Prof. Birte Kehr, Prof. Rainer Spang, Christian Kohler, Dr. Nicholas Strieder, Dr. Sebastian Niehus, Dr. Gunter Glehr and Dr. Marian Schön for your advice and expertise on bioinformatic analyses. To Doro and Marianna who I frequently consulted to improve my western blot experiments. And to Prof. Michael Hölzel for the preliminary design to translate my work to *in vivo* experiments. Although not being direct collaborators I would also like to thank all the people that donated healthy or tumor samples for research therefore contributing to the progress in the fields of immunotherapy and others.

A huge thank you goes to all members of the AG Beckhove. Especially when there were super stressful and difficult phases of my PhD, I could always count on your personal and professional support. You were a major reason why I wanted to pursue a PhD in this group and knowing that you were around made me always like to come to work. Today I am happy that I can call some of you not just only colleagues but friends. Teşekkürler to Ayşe for your patience, your energy and endless laughs. I will always remember pipetting the library listening to 'Şıkıdım' and the hardstyle version of 'Für Elise'. Grazie to Vale for introducing me to the world of immune checkpoints, for your kindness and interest in my work. Благодаря to Slava for your professional advice and for my integration into the group by inviting me to social events from the beginning. Ευχαριστώ to my office partner Maria, especially when I had again more questions about FACS and FlowJo and for personal conversations that we shared. நன்றி to Anchana for laughs and making me one unofficial uncle of your daughter. Danke to Franzi who went through all the PhD phases with me as a fellow sufferer. Thanks for sharing your lab skills with me and for many moments off work. شكراً to Abir for being the best office companion. No matter the situation there was always time for a joke or a personal conversation and I will be forever grateful to you and Ralph for taking me and the others with you to Lebanon (سمك بارد). Danke to Alex for taking over the PhD legacy and for being a trustful person and bouldering instructor. Danke to Leo for your energy, for many funny moments and for showing me that I am not the only one with spontaneous crazy behavior. Danke to Jasmin for your great lab support, especially in the past months and for many activities off work. Danke to Nicole for all your contributions to my project in the past months without losing any motivation. Danke an Birgitta for always helping me to find the materials in the lab when I was in need and for great cakes and cookies. Danke to Karin for the laughs we shared and for ordering so much of my lab stuff. Danke to Sabine for your great organizational support with any forms and appointments. Without all of you, the past four years would have been much harder, maybe even impossible, so I deeply thank you for always being around, being supportive and making me welcome and appreciated.

Apart from AG Beckhove, I would also like to appreciate the administrative assistance of Michaela and Sabine at the LIT. Thanks to Heiko for technical support and the drinks we had. To my fellow PhDs for sharing knowledge and concerns and for social activities. Thanks to the LIT for giving me the opportunity to participate in retreats and national and international conferences. And a special appreciation is dedicated to Kinga and Carolin from the RIGeL graduate school for their constant friendly support.

Last but not least, I would like to express my deepest gratitude to the important people who supported me outside of work, my family and friends. Danke Mama, Papa, Daniel, Solveig and Neo. Although we are separated from each other geographically, we are always connected to each other in our hearts.

Without you, I would not be the person that I am today, and I could always count on your trust and encouragement. Thanks to my grandma Mima who always supported me on my personal and professional journeys – I wish I could share this work with you. To Max for having faith in me and for being the one coping with my troubles the most in the past months. To Lena for probably believing in me more than anyone else. To Luca for always making sure that I can be proud of myself. To Simon, Jonas, Mona, Sinje, Teresa, Meike, Nadine and all the other supportive friends from near and far – having a call, a walk, a drink, or a holiday together were the essential things that kept me going on. Finally, special regards go to my godfather Martin who never stopped believing in me that one day, I finally will be Dr. Martin.

Dedicated to

Jutti & Ün

You raised me with endless love and
shaped me to survive in this big world without forgetting
that there is always a place that I can call home.

Summary

Immunotherapy with immune checkpoint inhibitors has largely improved survival of melanoma patients. However, many patients still do not benefit from so far developed strategies due to primary or acquired resistance. In malignant melanoma, increased immune resistance is associated with the downregulation of Microphthalmia-associated transcription factor (MITF). MITF is a key regulator of melanocyte proliferation and survival. In melanoma cells its decrease results in a dedifferentiated phenotype which is concomitant with invasiveness and therapy resistance.

The aim of this work was to identify mechanisms of immune resistance in MITF^{low} human melanoma cells. In order to discover genes that confer immune resistance in MITF^{low} melanomas, I performed a functional high-throughput (HTP) RNAi screen targeting 5202 genes in two melanoma cell lines derived from one immunotherapy refractory melanoma patient. One of these cell lines, Ma-Mel-86a expressed low levels of MITF while the other, Ma-Mel-86c expressed high MITF levels. The use of both cell lines allowed for the discrimination of common and differential effects of the genes in the MITF^{low} and MITF^{high} melanoma cell lines. 91 genes that caused a tumor cell intrinsic resistance against the attack by cytotoxic T cells were identified by this screen and confirmed in secondary validation experiments.

The *in vitro* work was paralleled by extensive bioinformatic analyses using public bulk and single cell RNA-Seq data sets of melanoma samples or patient-derived melanoma cell lines. Immune resistance (IR) genes were shown to be co-expressed in gene expression clusters. IR genes and gene clusters showed heterogeneous expression patterns between patients but homogeneous expression within individual patients and certain genes and clusters could be correlated to a low MITF expression. Furthermore, IR genes were differentially expressed between melanoma cells and healthy cells within the melanoma stroma, and between MITF^{low} and MITF^{high} melanoma cells. Interestingly, MITF^{low} cells still shared features with MITF^{high} cells, but additionally with immunosuppressive cancer-associated fibroblasts.

Several IR genes (*TMCC3*, *SLC39A13*, *MOK* and *ZNF443*) with a particular strong immune resistance potential that were mostly differentially expressed in MITF^{low} melanomas were selected for further functional assessment. These analyses revealed a protective role of these genes against apoptosis induction through stimulation by T cell derived cytotoxic ligands such as TRAIL, TNF α or IFN γ . I performed extensive mode of action analyses for two IR genes, Transmembrane and coiled-coil domain family 3 (*TMCC3*) and Solute carrier family 39 member 13 (*SLC39A13*) to uncover their mechanisms to convey resistance in the MITF^{low} cell line Ma-Mel-86a. *TMCC3* which is located in the membrane of the endoplasmic reticulum (ER) protects MITF^{low} melanoma cells against ER stress and ensures apoptosis resistance by increasing the expression of anti-apoptotic molecules, especially of those involved in death receptor signaling such as CFLAR and BCL-2. Upon treatment with death receptor ligand TRAIL

to which Ma-Mel-86a showed primary resistance, apoptosis is executed in TMCC3 deficient cells. SLC39A13/ZIP13 is a zinc transporter located in the Golgi apparatus that protects MITF^{low} cells against IFN γ -mediated apoptosis. SLC39A13/ZIP13 controls STAT1 and IFN γ R1 expression and induces the expression of anti-apoptotic BCL-2, making the cells resistant against IFN γ -mediated lysis.

In conclusion, I identified a variety of so far unknown immune resistance genes in immunotherapy refractory MITF^{low} melanoma cells that regulate T cell and cytotoxic ligand-mediated rejection which may represent novel targets for future immunotherapeutic interventions in malignant melanoma.

Zusammenfassung

Der Einsatz von Immuncheckpoint-Inhibitoren in Immuntherapien hat das Überleben von Hautkrebspatient:innen stark verbessert. Viele Patient:innen profitieren allerdings nicht von bisher entwickelten Strategien aufgrund von primären oder erworbenen Resistenzmechanismen. Im malignen Melanom steht eine erhöhte Resistenz im Zusammenhang mit der verminderten Expression von Microphthalmia-associated transcription factor (MITF). MITF ist der Haupttranskriptionsfaktor in Melanozyten und wichtig für die Proliferation und das Überleben der Zellen. In Melanomzellen ist eine Abnahme von MITF mit einem de-differenzierten Phänotyp verbunden, einhergehend mit erhöhter Zellinvasion und Therapieresistenz.

Das Ziel dieser Arbeit war die Identifizierung von Immunresistenzmechanismen in humanen Melanomzellen mit geringer MITF-Expression (MITF^{low}). Um Gene zu identifizieren, welche Immunresistenz in MITF^{low}-Melanomen vermitteln, habe ich ein funktionelles Hochdurchsatzscreening auf Basis von RNA-Interferenz durchgeführt, bei dem 5202 Gene in zwei Melanomzelllinien getestet wurden, welche aus einem Immuntherapie-refraktären Patienten generiert wurden. Eine der Zelllinien, Ma-Mel-86a, exprimiert geringe Level von MITF (MITF^{low}), während die andere, Ma-Mel-86c, hohe Level von MITF exprimiert (MITF^{high}). Durch die Verwendung beider Zelllinien konnten gemeinsame und differenzielle Effekte der getesteten Gene zwischen den MITF^{low}- und MITF^{high}-Melanomzelllinien unterschieden werden. 91 Gene, welche intrinsische Resistenz gegenüber der Attacke zytotoxischer T-Zellen verursachten, konnten in diesem Screening identifiziert und in weiteren Validierungsexperimenten bestätigt werden.

Parallel wurden umfassende bioinformatische Analysen mithilfe von öffentlichen Bulk- und Einzelzell-RNA-Seq-Datensätzen von Melanomproben oder Melanomzelllinien, welche aus Patient:innenmaterial gewonnen werden konnten, durchgeführt. Es konnte gezeigt werden, dass Immunresistenz (IR)-Gene in Genexpressionsclustern ko-exprimiert sind. IR-Gene und -Cluster zeigten heterogene Expressionsmuster zwischen Patient:innen, jedoch homogene Expressionen innerhalb individueller Patient:innen. Zusätzlich konnten bestimmte Gene und Cluster mit geringer MITF-Expression korreliert werden. IR-Gene waren außerdem sowohl zwischen Melanomzellen und gesunden Zellen innerhalb des Melanomstromas als auch zwischen MITF^{low}- und MITF^{high}-Melanomzellen differenziell exprimiert. Interessanterweise zeigten MITF^{low}-Zellen einige Merkmale von MITF^{high}-Zellen, jedoch zusätzlich welche von immunsuppressiven Krebs-assoziierten Fibroblasten.

Mehrere Gene (*TMCC3*, *SLC39A13*, *MOK* und *ZNF443*) mit ausgeprägtem IR-Potential, welche zumeist differenziell in MITF^{low}-Zellen exprimiert waren, wurden für weitere funktionelle Analysen ausgewählt. Hier zeigte sich eine protektive Rolle der Gene gegenüber der Induktion von Apoptose durch die Stimulation mit zytotoxischen T-Zell-Liganden wie TRAIL, TNF α oder IFN γ . Umfassendere Analysen zur

Wirkungsweise der beiden Gene Transmembrane and coiled-coil domain family 3 (*TMCC3*) und Solute carrier family 39 member 13 (*SLC39A13*) wurden durchgeführt, um die genauen Mechanismen des Resistenzcharakters der MIF^{low}-Zelllinie Ma-Mel-86a aufzuschlüsseln. *TMCC3* ist in der Membran des Endoplasmatischen Retikulums (ER) lokalisiert und schützt MIF^{low}-Zellen vor ER-Stress. Es stellt die Resistenz gegenüber Apoptose sicher, indem anti-apoptotische Moleküle induziert werden - vor allem jene, welche in Todesrezeptorsignalwegen involviert sind wie CFLAR und BCL-2. Bei Behandlung mit dem Todesrezeptorliganden TRAIL, gegenüber welchem Ma-Mel-86a eine primäre Resistenz zeigt, wird die Apoptose in *TMCC3*-defizienten Zellen ausgelöst. *SLC39A13/ZIP13* ist ein Zinktransporter, welcher im Golgi-Apparat lokalisiert ist, und schützt MIF^{low}-Zellen vor IFN γ -vermittelter Apoptose. *SLC39A13/ZIP13* kontrolliert die Expression von STAT1 und IFN γ R1 und induziert die Expression von anti-apoptotischem BCL-2, wodurch die Zellen resistent gegenüber IFN γ -vermittelter Lyse werden.

Zusammenfassend habe ich eine Auswahl bisher unbekannter Immunresistenzgene in Immuntherapie-refraktären MIF^{low}-Melanomzellen identifiziert, welche den Zelltod durch T-Zellen und zytotoxische Liganden regulieren und welche als neue Angriffspunkte in künftigen immuntherapeutischen Interventionen im malignen Melanom dienen könnten.

Table of contents

Declaration	II
Acknowledgments	III
Summary	VII
Zusammenfassung	IX
Table of contents	XI
List of Figures	XVI
List of Tables	XIX
Abbreviations and symbols	XX
1 Introduction	1
1.1 Cancer immunoediting	1
1.1.1 The Hallmarks of Cancer	1
1.1.2 The three Es of cancer	2
1.1.3 Strategies of tumor elimination	3
1.1.4 Tumor escapes mechanisms	5
1.2 Melanoma	9
1.2.1 Microphthalmia-associated transcription factor (MITF)	9
1.2.2 Melanoma biology	10
1.2.3 Melanoma plasticity and phenotype switching	11
1.2.4 Targeted therapies in malignant melanoma	13
1.3 Immunotherapy	13
1.3.1 Immunotherapies in malignant melanoma	14
1.3.2 Resistance mechanisms in malignant melanoma	15
1.4 High-throughput RNAi screens to identify novel immune resistance genes and pathways in human cancers	17
1.5 Transcriptomics in melanoma	18
2 Objectives of this project	20
3 Materials	21
3.1 Instruments and devices	21
3.2 Consumables	22
3.3 Chemicals, reagents and supplements	23
3.4 Recombinant proteins and peptides	25
3.5 Assay kits	25
3.6 Cell culture media	26
3.7 Buffers	26
3.8 Cells and cell lines	27

3.8.1 Eukaryotic cells and cell lines	27
3.8.2 Bacteria.....	28
3.9 Plasmids and lentiviral particles.....	28
3.10 Oligonucleotides.....	28
3.10.1 Pre-designed primers	28
3.10.2 Individually designed primers	29
3.11 siRNAs.....	29
3.11.1 siRNA libraries	29
3.11.2 siRNAs.....	30
3.12 Antibodies.....	31
3.12.1 FACS antibodies.....	31
3.12.2 Western blot antibodies.....	31
3.13 Software	32
3.14 Additional R packages and software	33
3.15 Data sets.....	33
4 Methods	34
4.1 Cell culture methods	34
4.1.1 Culture of tumor cell lines and T cells	34
4.1.2 Thawing and freezing of tumor cell lines and T cells.....	34
4.1.3 Stable plasmid transfection of Ma-Mel-86.....	34
4.1.4 Lentiviral transduction of Ma-Mel-86	35
4.1.5 Reverse siRNA transfection	36
4.1.6 Expansion of FluT cells.....	36
4.1.7 Polyclonal activation of T cells.....	37
4.2 Molecular biology techniques	37
4.2.1 Transformation of plasmids into competent bacteria	37
4.2.2 RNA isolation and reverse transcription	38
4.2.3 End-point PCR.....	38
4.2.4 Real-time quantitative PCR (qPCR).....	38
4.2.5 Protein isolation	39
4.3 Immunological techniques	39
4.3.1 Western blot.....	39
4.3.2 Enzyme-linked immunosorbent assay (ELISA).....	40
4.3.3 Flow cytometry.....	40
4.4 Cytotoxicity assays.....	41
4.4.1 General setup of cytotoxicity assays	41

4.4.2 Luciferase-based readout.....	41
4.4.3 Real-time live cell imaging.....	42
4.5 High-throughput RNAi screens.....	42
4.5.1 Pipetting of siRNA libraries.....	42
4.5.2 Primary high-throughput RNAi screens.....	42
4.5.3 Secondary validation high-throughput RNAi screens.....	43
4.6 Bioinformatic analyses	43
4.6.1 Analysis of high-throughput RNAi screens	43
4.6.2 ComBat-seq	44
4.6.3 Weighted gene co-expression network analysis (WGCNA).....	44
4.6.4 Generation of heatmaps	45
4.6.5 Seurat	45
4.7 Statistical evaluation	46
5 Results	47
5.1 Characterization of melanoma cell lines	47
5.1.1 Selection of melanoma cell lines.....	47
5.1.2 Level of resistance of MITF ^{low} and MITF ^{high} melanoma cells	48
5.1.3 Expression of apoptosis inducing ligands by CD8+ T cells and their corresponding receptors on the tumor cells	50
5.1.4 Primary resistance of Ma-Mel-86 to death receptor ligands.....	54
5.2 Setup of a high-throughput RNAi screen.....	55
5.2.1 Rapid expansion of flu specific T cells	57
5.2.2 Optimization of siRNA transfection, flu peptide concentration and effector to target ratio for Ma-Mel-86	57
5.2.3 Selection of controls for Ma-Mel-86	60
5.3 High-throughput (HTP) screens reveal novel immune resistance genes	61
5.3.1 Performance of the primary HTP screen.....	61
5.3.2 Design of a siRNA library for a secondary validation screen.....	65
5.3.3 Performance of the secondary validation screen	66
5.4 Bioinformatic analyses reveal clusters of co-expressed immune resistance genes with inter- individual expression patterns.....	70
5.4.1 Melanoma and healthy tissues upregulate different sets of immune resistance genes	71
5.4.2 Immune resistance genes are co-expressed in clusters.....	72
5.4.3 Cluster expression is inter-individually heterogeneous	75
5.4.4 Immune resistance gene expression can be correlated to MITF expression status	77
5.4.5 Patient-derived melanoma samples reveal MITF ^{low} cell subset that shows upregulation of immune resistance genes.....	79

5.5 Functional validation of immune resistance genes.....	82
5.5.1 Primary functional validation of pre-selected immune resistance genes.....	82
5.5.2 Immunoregulatory potential of candidate genes is independent of T cell specificity.....	86
5.5.3 Immune resistance genes show intrinsic protective effects in the tumor cells.....	89
5.5.4 Silencing of immune resistance genes sensitizes tumor cells to death receptor ligands	90
5.6 TMCC3 and SLC39A13 use different mechanisms to prevent tumor cell apoptosis.....	92
5.6.1 The relationship between the expression of MITF and that of TMCC3 or SLC39A13.....	93
5.6.2 Supernatant of activated FluT cells induces TMCC3 expression.....	94
5.6.3 Simultaneous knockdown of TMCC3 and SLC39A13 does not increase tumor cell rejection by FluT cells	95
5.6.4 Co-culture with FluT cells downregulate expression of receptors that are important for antigen expression as well as induction of apoptosis.....	96
5.6.5 Downregulation of TMCC3 and SLC39A13 alter receptor expression <i>per se</i>	100
5.6.6 Downregulation of TMCC3 and SLC39A13 sensitize Ma-Mel-86a to apoptosis by regulating the expression of caspases and BCL-2.....	101
5.6.7 TRAIL treatment increases caspase activity in TMCC3 silenced Ma-Mel-86a.....	103
5.6.8 TMCC3 silencing activates Akt survival pathway.....	103
5.6.9 TMCC3 silencing results in perturbation of ER homeostasis.....	105
5.6.10 IFN γ treatment increases caspase activity in SLC39A13 silenced Ma-Mel-86a	106
5.6.11 SLC39A13 silencing shifts STAT1/STAT3 ratio to induce apoptosis.....	107
5.6.12 Overexpression of TMCC3 decreases FluT cell-mediated tumor cell death	108
6 Discussion	110
6.1 MITF downregulation increases resistance of melanoma cells	110
6.2 A high-throughput RNAi screen in melanoma	111
6.2.1 Rationale and design	112
6.2.2 Optimization of the screening protocol	113
6.2.3 Performance of primary and validation screens	115
6.3 Selection of novel immune resistance genes for functional analyses	117
6.3.1 Performance of bioinformatic analyses	117
6.3.2 Hit selection and refinement.....	120
6.4 TMCC3 and SLC39A13 as immune resistance genes in melanoma.....	123
6.4.1 TMCC3 and SLC39A13 knockdown changes the expression of receptors important for antigen presentation and apoptosis induction	124
6.4.2 Structure and function of TMCC3.....	125
6.4.3 TMCC3 sensitizes melanoma cells to TRAIL-mediated apoptosis	126
6.4.4 Downregulation of TMCC3 induces perturbation of ER homeostasis.....	127
6.4.5 Structure and function of SLC39A13/ZIP13.....	128

6.4.6 SLC39A13/ZIP13 sensitizes melanoma cells to IFN γ -mediated apoptosis by increasing STAT1/STAT3 ratio.....	129
6.5 Translational implications of SLC39A13 and TMCC3 in malignant melanoma.....	130
References.....	132
Appendix.....	146
I. Supplementary Figures.....	146
II. Supplementary Tables.....	151

List of Figures

Figure 1: The Hallmarks of Cancer.....	1
Figure 2: Members of the TNF and TNFR superfamilies as well as IFN γ and IFN γ R.....	5
Figure 3: Immune checkpoint molecules expressed by T cells	7
Figure 4: Regulation of the MITF-M promotor.....	10
Figure 5: The six cell states of melanoma plasticity	12
Figure 6: Phenotype switching and therapy resistance in melanoma	16
Figure 7: Bulk vs. scRNA-Seq	19
Figure 8: Differential expression of MITF between Ma-Mel-86a and Ma-Mel-86c cells	47
Figure 9: Expression of HLA-A2 and GFP on Ma-Mel-86a and Ma-Mel-86c before and after transfection and transduction of cells.....	48
Figure 10: Differential apoptosis sensitivity of Ma-Mel-86a and Ma-Mel-86c and impact of PD-L1 knockdown.	50
Figure 11: Expression of cell death inducing ligands on different T cell sources.....	52
Figure 12: Secretion of TNF α and IFN γ by different T cell sources	53
Figure 13: Expression of death receptors on Ma-Mel-86a and Ma-Mel-86c.....	54
Figure 14: Susceptibility of Ma-Mel-86 to T cell-derived cytotoxic agents.....	55
Figure 15: Experimental set-up of the high-throughput RNAi screens and luciferase-based cytotoxicity assays.....	56
Figure 16: Specificity of FluT cells after rapid expansion	57
Figure 17: Optimization of transfection and co-culture settings for the high-throughput RNAi screens and cytotoxicity assays.....	59
Figure 18: Performance of controls for the high-throughput RNAi screens in Ma-Mel-86a and Ma-Mel-86c.....	61
Figure 19: Performance of the controls in the primary high-throughput (HTP) RNAi screens.....	63
Figure 20: Outcome of the high-throughput (HTP) RNAi screens	64
Figure 21: Selection of library genes for a secondary validation screen.....	65
Figure 22: Performance of the controls in the secondary validation high-throughput (HTP) RNAi screens.....	67
Figure 23: Performance of controls and selected genes in the secondary validation high-throughput (HTP) RNAi screens	69
Figure 24: Expression of Immune resistance (IR) genes in melanoma and different healthy tissues ..	72
Figure 25: Weighted gene co-expression network analysis (WGCNA) in melanoma data sets.....	74
Figure 26: Differential expression patterns of immune resistance (IR) genes in melanoma data sets	76

Figure 27: Significant up- and downregulation of immune resistance (IR) genes with respect to MITF expression in melanoma data sets.....	78
Figure 28: Malignant MITF ^{high} and MITF ^{low} cell subsets in patient-derived melanoma samples.	80
Figure 29: Overexpression of immune resistance (IR) genes in cell clusters of melanoma patients....	81
Figure 30: Performance of validated immune resistance (IR) genes in a de-convolution kill assay.....	84
Figure 31: Knockdown efficiency of selected immune resistance (IR) genes	85
Figure 32: Impact of immune resistance genes on FluT cell-mediated tumor cell rejection.....	86
Figure 33: Impact of immune resistance genes on tumor cell rejection mediated by MART-1 T cells and TIL412.	88
Figure 34: Impact of immune resistance genes on supernatant-mediated tumor cell rejection	89
Figure 35: Impact of immune resistance genes on tumor cell rejection mediated by TRAIL or IFN γ ...	90
Figure 36: Cytotoxicity profiles of the immune resistance (IR) genes.....	92
Figure 37: Relationship of gene expression between MITF and TMCC3 or SLC39A13	93
Figure 38: Expression of TMCC3, SLC39A13 and MITF after various treatments of Ma-Mel-86a	94
Figure 39: Co-knockdown of TMCC3 and SLC39A13 in Ma-Mel-86a	95
Figure 40: Flow cytometry analysis after co-culture of Ma-Mel-86a with FluT cells	97
Figure 41: Regulation of surface receptors after co-culture of Ma-Mel-86a with FluT cells	100
Figure 42: Regulation of surface receptors upon knockdown of TMCC3 and SLC39A13.....	101
Figure 43: Expression of apoptotic genes in TMCC3 or SLC39A13 proficient/deficient Ma-Mel-86a.	102
Figure 44: Expression of apoptotic genes in TMCC3 proficient/deficient Ma-Mel-86a upon TRAIL treatment.	103
Figure 45: Expression of AKT pathway-related genes in TMCC3 proficient/deficient Ma-Mel-86a without and with TRAIL treatment.....	104
Figure 46: Expression of ER stress-related genes in TMCC3 proficient/deficient Ma-Mel-86a without and with TRAIL treatment	106
Figure 47: Expression of apoptotic genes in SLC39A13 proficient/deficient Ma-Mel-86a upon IFN γ treatment.	107
Figure 48: Expression of FAK/Src and IFN γ R pathway-related genes in SLC39A13 proficient/deficient Ma-Mel-86a without and with IFN γ treatment.....	108
Figure 49: Overexpression of TMCC3 and SLC39A13 and their impact on T cell-mediated rejection.	109
Supplementary Figure 1: ComBat-seq to remove dataset specific batch effects	146
Supplementary Figure 2: Knockdown efficiency of selected immune resistance (IR) genes.....	147
Supplementary Figure 3: Impact of immune resistance genes on tumor cell rejection mediated by cytotoxic ligands I	148

Supplementary Figure 4: Impact of immune resistance genes on tumor cell rejection mediated by cytotoxic ligands II 149

Supplementary Figure 5: Expression of control and immune resistance genes in different melanoma cell subsets. 150

List of Tables

Table 1: Instruments and devices.....	21
Table 2: Consumables.....	22
Table 3: Chemicals, reagents and supplements	23
Table 4: Recombinant proteins and peptides	25
Table 5: Assay kits	25
Table 6: Cell culture media.....	26
Table 7: Buffers.....	26
Table 8: Eukaryotic cells and cell lines	27
Table 9: Bacteria.....	28
Table 10: Plasmids and lentiviral particles	28
Table 11: Pre-designed primers	28
Table 12: Individually designed primers.....	29
Table 13: siRNA libraries.....	29
Table 14: siRNAs	30
Table 15: FACS antibodies	31
Table 16: Western blot antibodies	31
Table 17: Software.....	32
Table 18: Additional R packages and software	33
Table 19: Data sets	33
Table 20: Summary of Luciferase-based kill assays and quantitative real-time PCR	83
Supplementary Table 1: siRNA library of the secondary validation screen	151

Abbreviations and symbols

Units

#	Number
%	Percent
°C	Degree Celsius
µg	Microgram
µl	Microliter
µM	Micromolar
µm	Micrometer
cm	Centimeter
g	G force (centrifugation)
g	Gram
h	Hour
kDa	Kilodalton
l	Liter
M	Molar
mg	Milligram
min	Minute
ml	Milliliter
mM	Millimolar
MOI	Multiplicity of infection
ng	Nanogram
nM	Nanomolar
rpm	Rounds per minute
s	Second
TPM	Transcripts per million
U	Enzyme unit
V	Volt
v/v	Volume per volume
w/v	Weight per volume

Chemicals

AMP	Adenosine 5'-monophosphate
ATP	Adenosine 5'-triphosphate
CO ₂	Carbon dioxide
ddH ₂ O	Double-distilled water
DMSO	Dimethylsulfoxid
DTT	Dithiothreitol
EDTA	Ethylenediaminetetraacetic acid
G418	Geneticin
H ₂ O	Water
H ₂ SO ₄	Sulfuric acid
MgSO ₄	Magnesium sulfate
Na ₂ CO ₃	Sodium carbonate
NaCl	Sodium chloride
NaHCO ₃	Sodium hydrogen carbonate
Tris	Tris(hydroxymethyl)aminomethane

Greek letters

α	Alpha
β	Beta
γ	Gamma
δ	Delta
Δ	Delta
κ	Kappa

A

ACT	Adoptive cell therapy
AFBS	Animal-free blocking solution
AG	Adrenal gland
AKT	AKT Serine/Threonine Kinase
AP-1	Activator protein 1
APC	antigen-presenting cell
ASE	Antigen-specific expansion
ATF	Activating Transcription Factor
ATP	Adenosine 5'-triphosphate
AXL	AXL Receptor Tyrosine Kinase

B

β 2M	Beta-2 microglobulin
B2M	Beta-2 microglobulin
BAD	BCL2 Associated Agonist Of Cell Death
BAK	BCL2 Antagonist/Killer
BAX	BCL2 Associated X
BCC	Basal cell carcinoma
Bcl-2	B-cell lymphoma 2
BCL-XL	B-cell lymphoma-extra large
BCSC	Breast cancer stem cell
BH	Bcl-2 homology
bHLH-LZ	Basic domain helix-loop-helix leucine zipper
BID	BH3 interacting domain death agonist
BiP	Binding-Immunoglobulin Protein
BMP	Bone morphogenetic protein
BOK	BCL2 Related Ovarian Killer
BRAF	v-Raf murine sarcoma viral oncogene homolog B
BRN2	Brain-2

C

CAF	Cancer-associated fibroblast
CAMK1D	Calcium/Calmodulin Dependent Protein Kinase ID
cAMP	Cyclic adenosine monophosphate
CAR	Chimeric antigen receptor
CD	Cluster of differentiation
CDH24	Cadherin 24
CDK	Cyclin Dependent Kinase
CEACAM	Carcinoembryonic Antigen-Related Cell Adhesion Molecule
CFLAR	CASP8 And FADD Like Apoptosis Regulator
cFLIP	cellular FLICE-inhibitory protein

CGA	Cancer germline antigen
CHOP	C/EBP homologous protein
CLL	Chronic lymphocytic leukemia
CLM	Complete Lymphocyte Medium
CMV	Cytomegalovirus
CREB	cAMP Responsive Element Binding Protein 1
CRISPR	Clustered regularly interspaced palindromic repeat
Ct	Cycle threshold
CTL	Cytotoxic T lymphocyte
CTLA-4	Cytotoxic T lymphocyte antigen-4
CV ratio	Cytotoxicity/viability ratio
CXCL	C-X-C motif chemokine ligand

D

DC	Dendritic cell
DcR	Decoy receptor
DD	Death domain
DGE	Differential gene expression
DISC	Death-inducing signaling complex
DLL1	Delta Like Canonical Notch Ligand 1
DNA	Deoxyribonucleic acid
DNMT	DNA methyltransferase
DPBS	Dulbecco's Balanced Salt Solution
DR	Death receptor
DSB	Double-strand break
dsRNA	Double-stranded RNA

E

E:T	Effector to target
EC	Endothelial cell
ECM	Extracellular matrix
EGF	Epidermal growth factor
ELISA	Enzyme-linked immunosorbent assay
ELN	Elastin
EMT	Epithelial-mesenchymal transition
ER	Endoplasmic reticulum
ERBB3	Erb-B2 Receptor Tyrosine Kinase 3
ERK	Extracellular signal-regulated kinase

F

FACS	Fluorescence-activated cell sorting
FADD	Fas-associated death domain protein
FAK	Focal adhesion kinase
FAS	Fas Cell Surface Death Receptor
FasL	Fas Ligand
FBS	Fetal Bovine Serum
FluT	Flu peptide specific T cell
FMT	Fecal microbiota transplantation

G

Gal-3	Galectin 3
GAPDH	Glyceraldehyde-3-Phosphate Dehydrogenase
GCK	Glucokinase
GJC2	Gap Junction Protein Gamma 2
gp100	Glycoprotein 100
GRM6	Glutamate Metabotropic Receptor 6
GTEx	Genotype-Tissue Expression
GTPase	Guanosine triphosphate hydrolase enzyme

H

HAT	Histone acetyltransferase
HDAC	Histone deacetylase
HDGF	Heparin Binding Growth Factor
HIF1 α	Hypoxia-inducible factor 1-alpha
HLA	Human leukocyte antigen
HRP	Horseradish peroxidase
HTP	High-throughput
HVEM	Herpesvirus entry mediator

I

IAP	Inhibitor of apoptosis
ICBT	Immune checkpoint blockade therapy
ICI	Immune checkpoint inhibitor
ICM	Immune checkpoint molecule
IFNGR	Interferon-gamma receptor
IFN γ	Interferon-gamma
IgG	Immunoglobulin G
IL	Interleukin
IPRES	Innate anti-PD-1 resistance gene signature
IR	Immune resistance
IRE1	Inositol-Requiring Protein 1
IRF-1	Interferon regulatory factor-1
ISG	Interferon signature genes/Interferon-stimulated gene
ITAM	Immunoreceptor tyrosine-based activation motif
ITGAX	Integrin Subunit Alpha X

J

JAK	Janus kinase
JNK	JUN N-Terminal Kinase
JUN	Jun Proto-Oncogene, AP-1 Transcription Factor Subunit

L

LAG-3	Lymphocyte activation gene-3
LAT	Linker For Activation Of T Cells
Lck	LCK Proto-Oncogene, Src Family Tyrosine Kinase
LGALS3	Galectin 3
LIGHT	TNF Superfamily Member 14 (TNFSF14)
LOESS	Locally estimated scatterplot smoothing
LRRN1	Leucine Rich Repeat Neuronal 1

LT Lymphotoxin
LT β R Lymphotoxin beta receptor
Luc Luciferase

M

MAP Mitogen-activated pathway
MAPK Mitogen-activated pathway kinase
MART-1 Melanoma Antigen Recognized By T Cells 1
MC1R Melanocortin 1 receptor
MCL-1 Myeloid Cell Leukemia Sequence 1
MDA Melanoma differentiation antigen
MDM2 Murine double minute 2
MDSC Myeloid-derived suppressor cell
MEK MAPK/ERK kinase
MFI Mean fluorescence intensity
MHC Major histocompatibility complex
miR microRNA
MiT/TFE Microphthalmia/transcription factor E
MITF Microphthalmia-associated transcription factor
MLANA Melan-A
MMP Matrix metalloproteinase
MOK MOK Protein Kinase
MOMP Mitochondrial outer membrane permeabilization
mRNA Messenger RNA
MSH Melanocyte-stimulating hormone
MW Molecular weight
M Φ Macrophage

N

NBR1 Neighbor of BRCA1 gene 1
NCBI National Center for Biotechnology Information
NCSC Neural crest stem cell
NF-1 Neurofibromin 1
NF- κ B Nuclear factor kappa-light-chain-enhancer of activated B-cells
NGFR Nerve growth factor receptor
NGS Next-generation sequencing
NGS Next generation sequencing
NK cells Natural killer cell
NKG2D Killer Cell Lectin Like Receptor K1 (KLRK1)
NMSC Non-melanoma skin cancer
NRAS Neuroblastoma RAS viral oncogene homolog
NSCLC Non-small-cell lung cancer
NY-ESO-1 New York esophageal squamous cell carcinoma-1

O

OPG Osteoprotegerin
OPN Osteopontin
OR10H1 Olfactory Receptor Family 10 Subfamily H Member 1
ORF Open reading frame
OXPHOS Oxidative phosphorylation

P

p	P-value
p53	Tumor Protein P53
PBMC	Peripheral blood mononuclear cell
PBS	Phosphate buffered saline
PCA	Principle component analysis
PCR	Polymerase chain reaction
PD-1	Programmed cell death 1
PDAC	Pancreatic ductal adenocarcinoma
PD-L	Programmed cell death 1 ligand
PGC1 α	PPARG Coactivator 1 Alpha
PI3K	Phosphoinositol-3-kinase
PKB	Protein kinase B
PLXNA3	Plexin A3
PMEL	Premelanosome protein
POU3F2	POU Class 3 Homeobox 2
PP2A	Protein Phosphatase 2 Phosphatase Activator
PRDX4	Peroxiredoxin-4
PSMC	Proteasome 26S Subunit, ATPase
PSMD	Proteasome 26S Subunit, Non-ATPase
PTEN	Phosphatase and tensin homolog
PUMA	P53-Upregulated Modulator Of Apoptosis

R

RAF	rapidly accelerated fibrosarcoma
RAS	Rat sarcoma
RELA	RELA Proto-Oncogene, NF-KB Subunit p65
REP	Rapid expansion protocol
RIP	Receptor-interacting protein
RISC	RNA-induced silencing complex
RLU	Raw luciferase unit
RNA	Ribonucleic acid
RNAi	RNA interference
RNA-Seq	RNA sequencing
ROR2	Receptor tyrosine kinase like orphan receptor 2
ROS	Reactive oxygen species
RPMI	Roswell Park Memorial Institute
RT	Reverse transcription
RT	Reverse transcription
RTK	Receptor tyrosine kinases

S

S1PR1	Sphingosine-1-Phosphate Receptor 1
SAPK	Stress-Activated Protein Kinase
SCC	Squamous cell carcinoma
scRNA-Seq	Single cell RNA sequencing
SHP	Protein Tyrosine Phosphatase Non-Receptor Type (PTPN)
SIK3	Salt-Inducible Kinase 3
siRNA	Small interfering RNA
SKCM	Skin cutaneous melanoma
SLC13A2	Solute Carrier Family 13 Member 2

SLC39A13	Solute Carrier Family 39 Member 13
SMC	Starved melanoma cell
SOX	SRY-related high-mobility group box
SPNS3	Spinster Homolog 3
SRA	Sequence Read Archive
Src	Sarcoma
STAT	Signal transducer and activator of transcription

T

TAA	Tumor-associated antigen
TAE	Tris-acetate-EDTA
TALEN	Transcription activator-like effector nuclease
TAM	Tumor associated macrophages
TBS	Tris-buffered saline
TCGA	The Cancer Genome Atlas
TCR	T cell receptor
TEAD	Transcriptional enhanced associate domain
TERT	Telomerase reverse transcriptase
TEX28	Testis-expressed 28
TGF	Transforming growth factor
TIGIT	T cell immunoglobulin and ITIM domain
TIL	Tumor-infiltrating lymphocyte
TIM-3	T cell immunoglobulin and mucin domain 3
TLR	Toll-like receptor
TM	Transmembrane
TMCC3	Transmembrane and Coiled-Coil Domain Family 3
TMEM132E	Transmembrane Protein 132E
TNF	Tumor necrosis factor
TNFR	TNF Receptor
TNFRSF	Tumor necrosis factor receptor superfamily
TNFRSF14	TNF Receptor Superfamily Member 14 (HVEM)
TNFSF	Tumor necrosis factor (ligand) superfamily
TOM	Topological overlap matrix
TP53	Tumor Protein P53
TRADD	TNFR1-associated death domain protein
TRAF	TNF Receptor Associated Factor
TRAIL	TNF-related apoptosis-inducing ligand
T _{reg}	Regulatory T cell
T-VEC	Talimogene laherparepvec
TYR	Tyrosinase

U

UBC	Ubiquitin C
UCSC	University of California Santa Cruz
UMAP	Uniform Manifold Approximation and Projection for Dimension Reduction
UPR	Unfolded protein response
UV	Ultraviolet

V

VEGF	Vascular endothelial growth factor
VISTA	V-domain Ig suppressor of T cell activation

W

WGCNA Weighted gene co-expression network analysis
WISP1 Wnt-inducible signaling protein 1
Wnt Wingless/Integrated

X

XIAP X-Linked Inhibitor Of Apoptosis

Z

ZAP-70 Zeta Chain Of T Cell Receptor Associated Protein Kinase 70
ZFN Zinc-finger nuclease
ZIP13 Zinc Transporter 13
ZNF443 Zinc Finger Protein 443

1 Introduction

1.1 Cancer immunoediting

1.1.1 The Hallmarks of Cancer

In 2000, Douglas Hanahan and Robert A. Weinberg published their landmark review ‘The Hallmarks of Cancer’. They looked back at a quarter of a century of cancer research and delineated that healthy cells acquire different genetic capabilities in a multistep process to convert into malignant cells [1]. Six alterations or hallmarks were declared that cells can exploit to circumvent defense mechanisms: self-sufficiency in growth signals, insensitivity to anti-growth signals, tissue invasion & metastasis, limitless replicative potential, sustained angiogenesis and evasion of apoptosis. As almost another quarter of a century has passed since and research has progressed remarkably, new common features of cancer were discovered. In 2011, two emerging hallmarks as well as two enabling characteristics of malignant cells were added to the previous six hallmarks [2]. Among them, ‘evading immune destruction’ described the ability of cancer cells to disable immune cell function. In 2022, that list was complemented by another four proposed features that are commonly existent in cancer, resulting in the current 14 hallmarks [3].

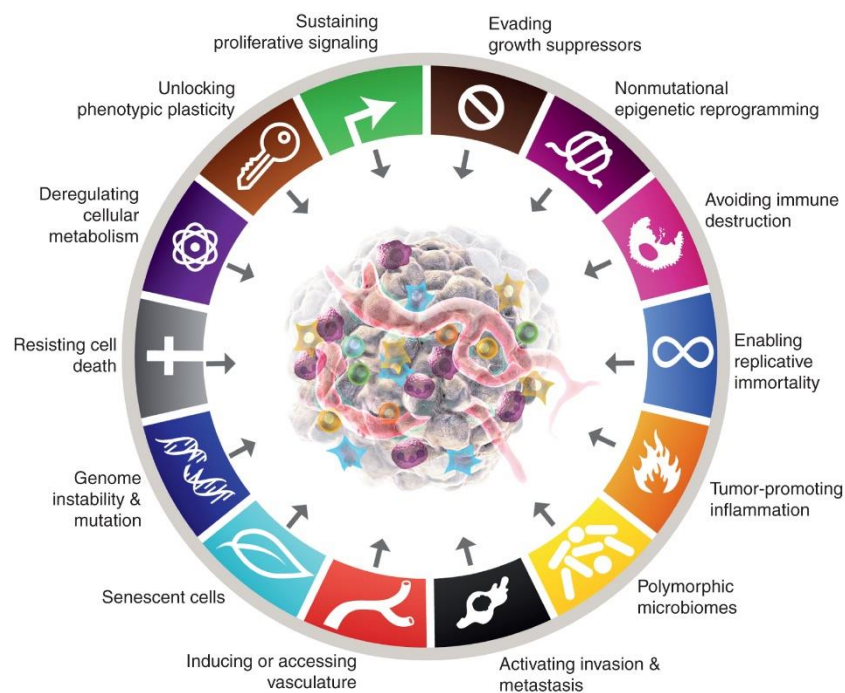


Figure 1: The Hallmarks of Cancer.
Adapted from Hanahan, Cancer Discov. 2022 [3].

Figure 1 illustrates an overview of all hallmarks and characteristics that are so far described to be established by cancer cells for successful tumor development. Since the original six hallmarks in 2000, it is now clearer that not only genetic alterations contribute to the formation of cancer but also

epigenetic and immunoreactive mechanisms as well as non-malignant cells [2, 3]. The tumor microenvironment plays an essential part in which inflammatory immune cells, cancer-associated fibroblasts, endothelial cells and other cell types along with microbes induce heterotypic signaling within the tumor and to malignant cells. Hence, tumor cells can establish phenotypic plasticity and effector immune cell function is impaired, adding complexity to cancer pathogenesis.

1.1.2 The three Es of cancer

A few years after declaration of the first six hallmarks of cancer, another landmark review proposed: 'The Three Es of Cancer Immunoediting' [4]. These were termed elimination, equilibrium and escape, describing the conflicting effects that emerge from the interaction between tumor and immune cells. Paul Ehrlich described in 1909 that immune cells keep the development of tumors in check, assuming the immune system's role in cancer was solely the elimination of malignant cells [5]. In 1957, Sir Macfarlane Burnet introduced the concept of cancer immunosurveillance for the first time by which cancer cells are eliminated by immune cell recognition of neoantigens [6, 7]. Over the 20th century, not only did *in vivo* cancer models improve, but also research conducted on cellular and molecular levels has advanced the field of cancer immunology further [4]. Thus, it was finally demonstrated that the immune system doesn't only eliminate tumor cells but could even promote their growth. Indeed, the term 'immunoediting' was introduced comprising two additional phases: equilibrium and escape.

When cells acquire hallmarks of cancer and tumors evolve, the surrounding tissue is remodeled, and the innate immune system is activated [4]. As a result, a primary antitumor response is initiated and amplified while the cells of the adaptive immune system recognizing tumor antigens are stimulated [4, 8]. The occurring tumor-specific immune response is mainly responsible for the successful rejection of the cancer. When eradication mechanisms fail to reject malignant cells, the elimination phase transitions into the equilibrium phase [4, 9]. Here, the immune system continues to target tumor cells, but mutated and resistant cell variants emerge with reduced immunogenicity. The authors of the initial review consider the equilibrium phase to be probably the longest of the three phases [4]. Finally, tumor cell variants acquire enough immunoevasive capacities enabling their expansion in an immunologically intact environment and the tumor becomes clinically relevant [4, 9]. In the escape phase, malignant cells are either undetectable for immune cells or they establish an immunosuppressive microenvironment that involves different mediators or other cell types. The following chapters will give a deeper insight into how immune cells can fight cancer cells and which resistance mechanisms are established to prevent tumor cell death.

1.1.3 Strategies of tumor elimination

Successful elimination of cancer cells by the immune system is termed antitumor immunity. Innate and adaptive immune responses work mutually and efficiently together in order to eradicate malignant cells [10]. When a tumor emerges, immune cells are able to sense modifications in tissue anatomy and tissue and cell metabolism [11]. Cells of the innate immune system such as natural killer (NK) or $\gamma\delta$ T cells use receptors like NKG2D to recognize ligands that are induced and presented by cancerous cells [4]. In the onset of antitumor immunity, mediators for example Interferon- γ (IFN γ) are produced that have a first antiproliferative, proapoptotic and angiostatic effect on the tumor cells [4, 12]. Furthermore, the production of chemokines amplifies immune cell recruitment. Activated NK cells can kill tumor cells via TNF-related apoptosis-inducing ligand (TRAIL) or perforin-dependent mechanisms leading to the release of cancer cell antigens. The released tumor-associated antigens are collected and processed by dendritic cells (DCs) and finally presented on major histocompatibility complex (MHC) classes I and II to T lymphocytes [8]. In lymph nodes, T cells are primed, activated and they finally infiltrate into the tumor. Here, T cells tap their full potential to recognize and kill tumor cells by a variety of mechanisms [8].

Cytotoxic CD8⁺ T lymphocytes (CTLs) are powerful effector cells that induce apoptosis in their target cells by direct cell-cell interactions [13]. Their T cell receptor (TCR) recognizes the antigenic peptide presented on MHC class I proteins on the tumor cells. Subsequently, an immunological synapse between the tumor cell and T cell is formed and stabilized by intercellular adhesion molecules [14]. Apart from the TCR complex, co-receptor CD8 binds to the MHC- α subunit and the T cell and its killing machinery are activated. As a result, prosurvival pathways and proteins within the CTL enhance persistence of the immune cell. Furthermore, death-inducing ligands are expressed, and cytotoxic granules are released via exocytosis into the synapse in order to kill the cancer cells [13, 14].

Vesicles that are released contain among other proteins perforin and granzymes [13]. Perforins are responsible to create pores in the cell membrane of the target cells to facilitate the entry of granzymes [15, 16]. Alternatively, a cocktail of cytotoxic molecules is endocytosed into the tumor cell and perforin and granulysin perforate the endosomal membrane [16, 17]. Granzymes are serine proteases that, upon entry or release into the cytoplasm of the tumor cells target proteins such as lamin B, α -tubulin and caspases [15]. Granzyme B is the best studied member and doesn't only activate executioner caspases like caspase-3 and -7 but as well their direct substrates in order to induce apoptosis [18]. Of note, the T cell protects itself from damage by production of granzyme inhibitors called serpins or by surface expression of cathepsin B that disables perforin by proteolysis [15]. On the other hand, granzyme B targets extracellular proteins such as fibronectin and laminin in order to restrict cancer cell invasion and enhance lymphocyte infiltration [19].

As mentioned previously, IFN γ is a cytokine that is secreted by NK cells. CTLs are also capable to produce large amounts of IFN γ after activation [12, 20]. It binds as dimer to the interferon-gamma receptor (IFNGR) on the target cell that consists of two monomers IFNGR1 and IFNGR2 [21, 22]. Binding induces janus kinase-signal transducer and activator of transcription (JAK-STAT) signaling, in which mainly STAT1 activation induces Interferon Signature Genes (ISG) such as interferon regulatory factor-1 (IRF-1). IRF-1 activation can further induce apoptosis and tumor suppression and furthermore, upregulation of MHC class I [21, 23]. Hence, tumor cells increase their presentation of tumor-associated antigens and can therefore be targeted more efficiently by CTLs.

Another group of ligands that are expressed by cytotoxic T cells belongs to the tumor necrosis factor (TNF) ligand superfamily that bind to respective members of the TNF receptor (TNFR) superfamily. Overall, both superfamilies include 19 ligands and 29 receptors that regulate diverse events in target cells such as survival and apoptosis as well as differentiation [24]. Not all ligands are expressed by CTLs and not all receptors are expressed by tumor cells, that being the case, I here focus on the most relevant ones for this project.

The ligands TNF α (TNFSF2), FasL (TNFSF6), TRAIL (TNFSF10) and LIGHT (TNFSF14) are expressed on the surface of the T cells and can be proteolytically cleaved and released into the extracellular space, all as homotrimers [25, 26]. While Lymphotoxin- α (LT α /TNFSF1) doesn't possess transmembrane domains and is directly secreted and builds trimers, LT β (TNFSF3) remains bound to the cell membrane via its transmembrane domain and forms homotrimers or heterotrimers with LT α [25, 27]. Several ligands can bind to multiple trimeric receptors, namely TNFR1 (TNFRSF1A), TNFR2 (TNFRSF1B), FAS (TNFRSF6), Death receptor 4 (DR4/TNFRSF10A), DR5 (TNFRSF10B), Herpesvirus entry mediator (HVEM/TNFRSF14) and Lymphotoxin beta receptor (LT β R/TNFRSF3) [25]. Figure 2 illustrates the different ligand-receptor interaction possibilities. Of note, membrane-bound and soluble forms of TNFR ligands can induce downstream signaling with varying degree, always depending on the ligand-receptor pair. After receptor ligation, different pathways are activated in the target cell that can lead to apoptosis and necroptosis or alternatively, to proliferation [28]. FAS, TNFR1, DR4 and DR5 possess intracellular so-called death domains (DD) that are crucial for apoptosis and necroptosis induction. In case of insufficient pro-survival and anti-apoptotic signaling, ligand-receptor complexes recruit Fas-associated death domain protein (FADD) as well as procaspase-8 [25, 29]. The resulting death-inducing signaling complex (DISC) finally induces tumor cell apoptosis. Alternatively, low caspase-8 activity results in induction of necroptosis by receptor-interacting protein 3 (RIP3) binding to RIP1 [28]. TNFR2, HVEM and LT β R don't possess death domains but rather induce nuclear factor kappa-light-chain-enhancer of activated B-cells (NF- κ B) and Activator protein 1 (AP-1) signaling by recruitment of TNF Receptor Associated Factor (TRAF) proteins [25]. While this is more associated with pro-survival functions, LT β R

is able to induce tumor cell death in a reactive oxygen species (ROS) dependent way. This mechanism was shown to activate caspase signaling or to induce apoptosis in a caspase-independent way [30, 31].

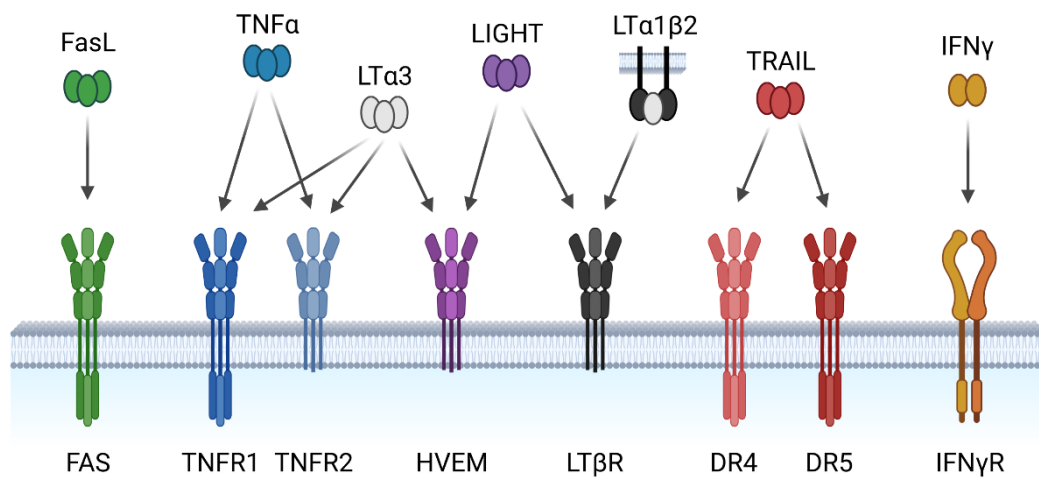


Figure 2: Members of the TNF and TNFR superfamilies as well as IFN γ and IFN γ R.

Ligands on top are expressed and mostly released by immune cells and bind to their respective receptors on the target cells to regulate diverse cell functions or, as in tumor cells, to induce apoptosis. Adapted from Suo *et al.*, *Pharmaceutics*. 2022 [25]. Created with BioRender.com [32].

1.1.4 Tumor escapes mechanisms

When cancer cells develop features in order to grow in an intact immune environment, the third phase of immunoediting begins termed the 'escape phase' [4]. Here, strategies of tumor elimination by the immune system fail as the cancer cells developed various resistance mechanisms to avoid immune cell-mediated cytotoxicity or to suppress immune cell functions. Some tumors are infiltrated with immune cells such as NK and T cells and referred to as 'hot' tumors, but tumor can also be 'cold', characterized by immune non-infiltration [33].

Cold tumors show reduced levels of attractants such as C-X-C motif chemokine ligand 9 (CXCL9) or CXCL10 which results in decreased T cell infiltration [34]. This is enhanced by expression of Vascular Endothelial Growth Factor (VEGF) resulting in the downregulation of adhesion molecules for T cells on endothelial cells of the blood vessels [35]. At the same time, production of Interleukin 10 (IL-10) and prostaglandin E₂ by the malignant cells induces expression of FasL on the endothelial cells that stimulates apoptosis of emerging effector T cells. Within the tumor, an immunosuppressive microenvironment is promoted by the presence of immunosuppressive cells such as regulatory T cells (T_{reg}) or cancer-associated fibroblasts (CAF) that produce extracellular matrix (ECM) proteins like collagen and laminin [36]. Also, factors such as IL-10 and Transforming growth factor β (TGF β) inhibit the function and maturation of dendritic cells [37]. Hence, DCs downregulate co-stimulatory molecules like CD80/CD86 and MHC preventing T cell activation and proliferation. If the TCR complex is formed but co-stimulation is missing, the T cells become unresponsive, commonly termed T cell anergy [38].

In hot tumors, partially similar mechanisms are exploited by tumor cells. Downregulation of MHC class I molecules on the surface and decreased antigen presentation on tumor cells leads to reduced recognition by CTLs [33]. This is achieved through various mechanisms such as antigen depletion or genetic or transcriptional alterations for MHC I [39]. Besides, immunosuppressive cells and molecules in the tumor microenvironment are part of the tumor escape mechanisms. M2 tumor-associated Macrophages (TAM) express IL-10, VEGF and matrix metalloproteinases (MMP) promoting tissue remodeling, angiogenesis and tumor progression [40]. Myeloid-derived suppressor cells (MDSCs) increase the suppression of immune cells by production of arginase 1, prostaglandin E₂, IL-10 and TGFβ [41]. TGFβ has a broad range of functions from tissue regeneration to proliferation and apoptosis. In the context of immunosuppression in the tumor, TGFβ inhibits effector T and NK cells and at the same time promotes the generation of T_{reg} cells [42]. T_{reg} cells themselves show immunosuppressive features as they are able to produce IL-10 and TGFβ thereby impairing DC and T cell function [43]. Additionally, T_{reg} cells express cytotoxic T lymphocyte antigen-4 (CTLA-4) which binds like CD28 to CD80/CD86 on antigen-presenting cells (APC) therefore reducing co-stimulatory signals to effector T cells.

CTLA-4 belongs to a group of proteins called immune checkpoint molecules (ICM). When immune cells are activated due to infections or by transformed cells, ICM are important to limit effector functions in order to protect healthy tissue from damage [44]. As previously described, CD8⁺ T cells are fully activated when T cells receive multiple signals through the TCR, CD8 and co-stimulatory receptor CD28 [14]. Upon binding of CD8 to MHC I on APCs, tyrosine kinase Lck phosphorylates immunoreceptor tyrosine-based activation motifs (ITAMs) of the intracellular CD3 domains of the TCR. Recruitment, phosphorylation, and activation of downstream signaling proteins such as ZAP-70 and LAT are important for TCR signaling [14, 45]. Activation of CD28 follows TCR/CD8 activation by binding to its ligands CD80 or CD86 expressed by the APC leading to intracellular phosphorylation events that promote survival signaling through PI3K/AKT and NF-κB [14]. Without CD28 activation, the killing machinery cannot be activated, and T cells get anergic. Activation of T cells involves the upregulation of co-inhibitory ICM as a feedback mechanism [46]. Most prominent members are CTLA-4, programmed cell death 1 (PD-1), Lymphocyte activation gene-3 (LAG-3), T cell immunoglobulin and mucin domain 3 (TIM-3) and T cell immunoglobulin and ITIM domain (TIGIT). For example, CTLA-4 binds to CD80/86 with higher affinity and avidity than CD28 [47, 48]. The intracellular domain of CTLA-4 is subsequently phosphorylated, resulting in activation of phosphatases SHP2 and PP2A that abrogate PI3K/AKT and TCR signaling [49]. Similarly, PD-1 has inhibitory intracellular domains that are phosphorylated after binding of PD-1 to its ligands Programmed Cell Death 1 Ligand 1 (PD-L1) and PD-L2. Phosphatases SHP1/SHP2 are recruited resulting in inhibition of PI3K/AKT and ZAP-70 signaling [49].

Classically, ligands of inhibitory signaling are expressed by APCs, but tumor cells exploit this mechanism to impair immune cell activity [50]. Ligands such as PD-L1, PD-L2 and Galectin-9 are upregulated on the surface of malignant cells in order to suppress CTL activity resulting in increased tumor cell survival [51]. PD-L1 expression for example is hereby induced by IFN γ that is secreted by infiltrating T cells as an adaptive resistance mechanism [52]. Figure 3 illustrates ICM and their ligands and how their interactions impair TCR signaling and T cell function.

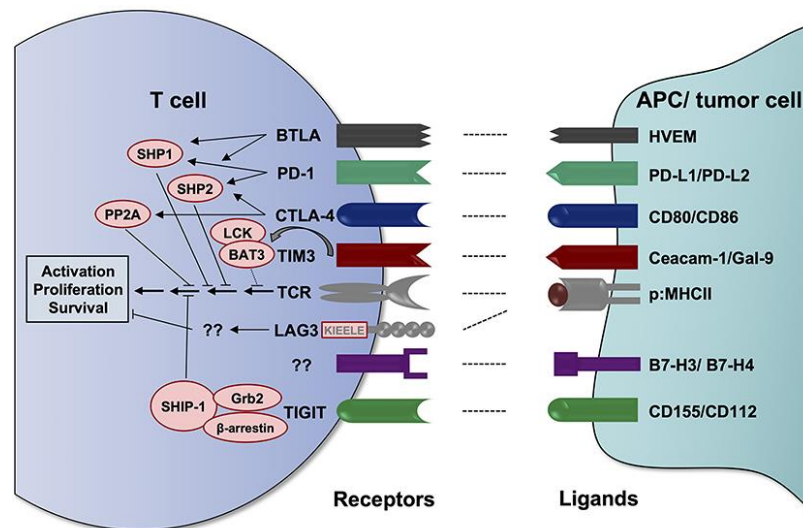


Figure 3: Immune checkpoint molecules expressed by T cells.

Their ligands are expressed on antigen presenting cells (APC) or can be exploited by tumor cells to abrogate TCR signaling and immune cell function. Original figure was modified from Köhler *et al.*, Front Immunol. 2021 [50].

Another way of tumor escape is increased resistance to cell death of the malignant cell. This can be achieved by different ways such as the regulation of apoptosis, autophagy and necroptosis and of signaling of heat shock and proteasomal proteins as well as by epigenetic mechanisms [53]. Next, I will focus on mechanisms of three important groups of proteins: receptors that regulate apoptosis upon binding of cognate ligands, the enzyme family of caspases and apoptosis regulating proteins like the Bcl-2 family.

As mentioned before, death receptors such as TNFR1, DR4 and DR5 don't only activate apoptosis by recruitment of FADD upon binding of TNF ligands. Additionally, TNFR1-associated death domain protein (TRADD) and inhibitor of apoptosis (IAP) proteins are recruited which activate NF- κ B and AP-1 signaling that are important for survival of the tumor cell, thus counteracting apoptosis induction [25, 54]. Also, the expression of death receptors itself can be regulated. The main mechanism of downregulation of FAS, DR4 and DR5 is by methylation of the gene and/or promotor [28]. Another mechanism that can reduce or prevent TNFR family induced apoptosis is the simultaneous expression of decoy receptors (DcR). While TRAIL is bound by DcR1, DcR2 and osteoprotegerin (OPG), FasL and LIGHT bind to DcR3. These receptors are either expressed on the cell surface but lack intracellular

domains important for the induction of apoptosis or are secreted into the extracellular milieu. Decoy receptors expressed by tumor cells bind to the ligands in order for the tumor cells to escape immunosurveillance and promote tumor growth [55, 56]. Finally, tumor cells can secrete proteins like matrix metalloproteinases (MMP) into the tumor environment that cleave FasL and TRAIL off the surface of effector cells, thereby reducing their cytotoxic potential [28].

Furthermore, apoptosis of tumor cells is prevented by dysregulation of caspases [57]. Most of the members of this enzyme family of endoproteases is involved in apoptosis induction. Caspases-8 and -9 are so-called initiator caspases which are activated by dimerization and subsequently cleaved autocatalytically [57, 58]. Dimers of the executioner caspases-3, -6 and -7 are activated by cleavage by the initiator caspases. Cleaved subunits build mature proteases that finally induce apoptosis by destroying important structural proteins and enzymes [57]. Caspase-9 is activated during the intrinsic pathway of apoptosis, in which different cellular stresses lead to the release of mediators such as cytochrome c from the mitochondria. Caspase-8 is activated during the extrinsic pathway mediated by extracellular ligands that bind to death receptors such as TNFR1 or DR5 resulting in recruitment to the receptor complex and dimerization of caspase-8. Active caspase-8 is also able to induce the intrinsic pathway of apoptosis by cleaving BH3 Interacting Domain Death Agonist (BID) [59]. In tumor cells, these pathways can be dysregulated to prevent apoptosis [57]. The gene of caspase-8 can be silenced by CpG methylation or deleted [28]. Furthermore, both Caspase-8 and FADD can be M1 ubiquitinated to inhibit their function [60].

However, most of the regulation of the extrinsic and intrinsic apoptosis pathway is caused by other pro- and anti-apoptotic proteins. Due to high homology, cellular FLICE-inhibitory protein (cFLIP/CFLAR) competes with caspase-8 in building the DISC [28]. cFLIP has three different splice variants and all inhibit initiation of the apoptosis signaling cascade by different mechanisms. Large cFLIP_L is cleaved by caspase-8 and can subsequently induce additional pro-survival NF- κ B signaling. The previously mentioned inhibitor of apoptosis proteins (IAPs) is another group that regulate programmed cell death [61]. While XIAP prevents apoptosis signaling by binding to caspase-3, -7 and -9, cIAP1 and cIAP2 mediate resistance differently. Both proteins are recruited by death receptors like TNFR1 upon binding of its ligand in order to ubiquitinate proteins, thus preventing formation of the DISC and promoting NF- κ B signaling. Finally, the B-cell lymphoma 2 (Bcl-2) family of pro- and anti-apoptotic proteins regulate the intrinsic apoptosis pathway [62]. The amount of different Bcl-2 Homology (BH) motifs divides the members into three subfamilies that characterize their function. Pro-apoptotic members BAX, BAK and BOK promote mitochondrial outer membrane permeabilization (MOMP), thereby initiating apoptosis [63]. To counteract induction of cell death, pro-survival genes such as BCL-2, BCL-XL and MCL-1 are expressed. BCL-2 for instance, prevents apoptosis by either binding to BAX or by

inhibiting caspase activity [64]. BH3-only subfamily members like BID, BAD or PUMA can either antagonize pro-survival genes or activate BAX and BAK. Tumor cells enhance escape mechanisms by dysregulating the expression of pro- and anti-apoptotic proteins. Here, expression of pro-survival members like BCL-2 and BCL-XL are frequently increased. Alternatively, tumor cells can downregulate the expression of pro-apoptotic proteins, for example, the lack of expression of BAK and BH3-only members is observed regularly in human cancers [62, 64].

1.2 Melanoma

Skin cancer is a worldwide public health concern, and the prevalence is on the rise [65]. In Germany, more than 300.000 people are diagnosed with skin cancer every year, hence being the most frequent cancer type [66]. Skin cancer is divided into two subgroups: non-melanoma skin cancer (NMSC) and melanoma. NMSC represent about 95 % of skin cancers with cutaneous squamous cell carcinoma (SCC) and basal cell carcinoma (BCC) being the most frequent types [65]. Although melanoma represents only the remaining 5 % of skin cancers, it is responsible for almost two thirds of all skin cancer-related fatalities [67]. The four main subtypes of melanoma are acral lentiginous melanoma, lentigo melanoma, nodular melanoma and superficial spreading melanoma, the latter being responsible for about 70 % of all melanomas [68].

Malignant melanoma is derived from melanocytes. These cells originate from the neural crest and are finally distributed in the basal layer of the epidermis and produce melanin, the pigment that is responsible for the coloring of the skin [65, 67]. As the most abundant cell type of the epidermis are keratinocytes, melanin produced by the melanocytes are transferred to the keratinocytes via organelles called melanosomes [68]. Multiple factors are involved in melanocyte and melanoma development that play important roles in skin homeostasis as well as the pathophysiology of melanoma, one of them being MITF [69].

1.2.1 Microphthalmia-associated transcription factor (MITF)

Microphthalmia-associated transcription factor (MITF) is the key transcriptional regulator in melanocytes regulating cell metabolism, proliferation and differentiation but also DNA damage repair, cell survival and invasion [70, 71]. It belongs to the MiT subfamily together with TFEB, TFE3 and TFEC as well as to the basic domain helix–loop–helix leucine zipper (bHLH-LZ) class of transcription factors that are able to bind DNA as dimers at so-called E-box sequences [71]. The *MITF* gene contains many exons with several transcriptional start sites, resulting in different isoforms, of which MITF-M is the one specific for melanocytes. Directly upstream of this isoforms promotor, different transcription

factors can regulate the expression of MITF such as SRY-related high-mobility group box 10 (SOX10), cAMP Responsive Element Binding Protein 1 (CREB) and Activating Transcription Factor 4 (ATF4) [72, 73]. These can promote or repress transcription of *MITF* and are regulated by different signaling pathways which is represented in more detail in Figure 4 [71]. The synthesized MITF protein undergoes posttranslational modifications such as phosphorylation, ubiquitylation and SUMOylation that regulate its cellular localization, activity as well as its stability and degradation. MITF is able to bind to tens of thousands of sites in the genome. However, in a study from Strub *et al.* it was reported that MITF positively or negatively regulates 465 target genes effectively [74]. As mentioned before, it regulates a diverse set of cell functions [71]. One typical function of differentiated melanocytes induced by MITF is pigment biogenesis by upregulation of Tyrosinase (TYR) and Melan-A (MLANA), but it also regulates the cell cycle by enhancing Cyclin Dependent Kinase 2 (CDK2) [75]. Additionally, MITF can induce expression of BCL-2, therefore contributing to cell survival by inhibition of apoptosis. As an example of MITF in a biological context, it mediates a skin protection mechanism as a response to UV radiation [76]. UV radiation stimulates keratinocytes to secrete melanocyte-stimulating hormone (α MSH), a ligand of the melanocortin 1 receptor (MC1R) on melanocytes. Downstream, cAMP levels are increased and CREB induces MITF expression that itself drives cell survival and pigmentation processes to protect cells of the skin from damage caused by the UV radiation [76].

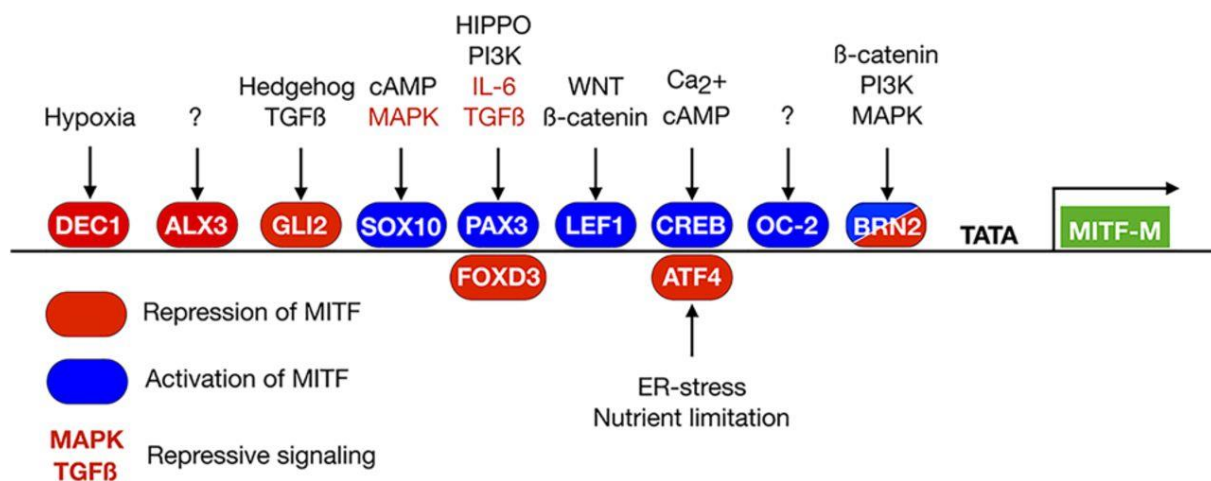


Figure 4: Regulation of the MITF-M promoter.

Pathways and downstream transcription factors positively and negatively regulate the transcription of the *MITF-M* isoform of Microphthalmia-associated transcription factor. Adapted from Goding *et al.*, *Genes Dev.* 2019 [71].

1.2.2 Melanoma biology

Different genetic, biological and environmental factors are contributing to melanomagenesis, in which melanocytes are characterized by abnormal proliferation [65]. UV radiation is the main trigger for melanoma development as it can cause genetic damage and induce or repress several signaling programs in the cell. Upon transformation, oncogenes are activated, tumor suppressor genes are

repressed, and genetic and epigenetic processes finally trigger cell proliferation, prevention of apoptosis, angiogenesis, tissue invasion and metastasis, making melanoma the most aggressive type of skin cancer [65].

Some mutations are very common between most melanomas. The kinase BRAF is in about half of all melanomas hyperactivated usually due to a point mutation at codon 600 (mainly BRAF^{V600E}) [68]. BRAF is a member of the rapidly accelerated fibrosarcoma (RAF) family of serine/threonine kinases [77]. It is part of the Mitogen-activated pathway (MAP) kinase/ERK signaling pathway that is induced upon activation of receptor tyrosine kinases (RTKs) due to binding of respective ligands like epidermal growth factor (EGF). Phosphorylation of RTK activates GTPases of the RAS-family resulting in dimerization of RAF family proteins and further activation of the kinases MEK1/2 and ERK1/2 [78]. Finally, cell survival and proliferation are induced due to transcriptional regulation by the kinases. Hence, BRAF mutations in melanoma cells drive cell growth, but they are also associated to tumor cell escape and metastasis [68, 78]. The GTPase NRAS is mutated in approximately 20 % of all melanomas, usually at codon 61 (NRAS^{Q61K/R/L}) [68]. Here, GTPase activity is compromised leading to accumulation of RAS-GTP that promotes the MAPK/ERK signaling pathway as well as pro-survival phosphoinositol-3-kinase (PI3K) pathways. Neurofibromin 1 (NF-1) is a protein that controls RAS activity by RAS-GTP inhibition [67]. However, NF-1 is frequently mutated in malignant melanoma which again promotes MAPK and PI3K pathways. The PI3K/AKT pathway can further be constitutively enhanced by inactivation of the tumor suppressor Phosphatase and Tensin Homolog (PTEN) due to genetic mutations or epigenetic changes [68]. In 70 % of all melanomas, mutations in the promotor gene of Telomerase Reverse Transcriptase (TERT) can be found. Activation of the TERT accordingly increases telomerase production causing melanoma cell immortality [68].

Melanoma has a high metastatic potential and distant metastases are the main cause of melanoma patient deaths. Genetic alterations and induction of osteopontin (OPN) results in upregulation of NF- κ B-mediated activation of matrix metalloproteinases (MMPs) [67, 79, 80]. MMPs like MMP-9 remodel the extracellular matrix facilitating the invasion of melanoma cells and finally leading to infiltration into the blood stream. The expression of Wnt-inducible signaling protein 1 (WISP1) contributes to remodeling of the microenvironment [68]. WISP1 enables melanoma invasion by inhibiting E-cadherin and MITF promoting epithelial-mesenchymal transition (EMT) [81]. The following chapter will give a deeper insight into EMT and phenotype switching in dependence of MITF.

1.2.3 Melanoma plasticity and phenotype switching

The expression of MITF can be used to measure the degree of differentiation in melanoma cells. MITF is important for the differentiation from neural crest precursors to melanocytes, thus showing high

expression in differentiated melanocytes as well as melanoma cells [70]. Dedifferentiated melanoma occurs when melanoma cells lose their typical morphological phenotype in which MITF and immunohistochemical markers are downregulated [82]. Accordingly, different transcriptional programs are driving the differentiated and dedifferentiated along with intermediate melanoma subtypes [70, 83]. Different cell states co-exist within the same tumor and the phenotype of one cell is not static [70]. These dynamics of the high plasticity in melanoma is often termed as phenotype switching.

In recent years, states of melanoma cells were defined and characterized by their transcriptional landscapes and expression of cell markers and by their features concerning proliferation, invasion, and therapy resistance. This was mainly achieved by experimental data and bioinformatic analyses of patient-derived melanoma cell lines or melanoma patient material [83-86]. So far, six states were described: hyperdifferentiated (pigmented), melanocytic (differentiated), intermediate (transitory), starved (SMC), dedifferentiated (undifferentiated) and neural crest stem cell (NCSC)-like [87, 88]. Figure 5 illustrates the characteristics of the different states of melanoma plasticity. As aforementioned, features of dedifferentiation are especially present in melanoma cells that are becoming invasive and metastatic, and these are characterized by reduced proliferation [70]. While *MITF* is downregulated, other marker genes such as Nerve Growth Factor Receptor (*NGFR*) or *AXL* Receptor Tyrosine Kinase are upregulated.

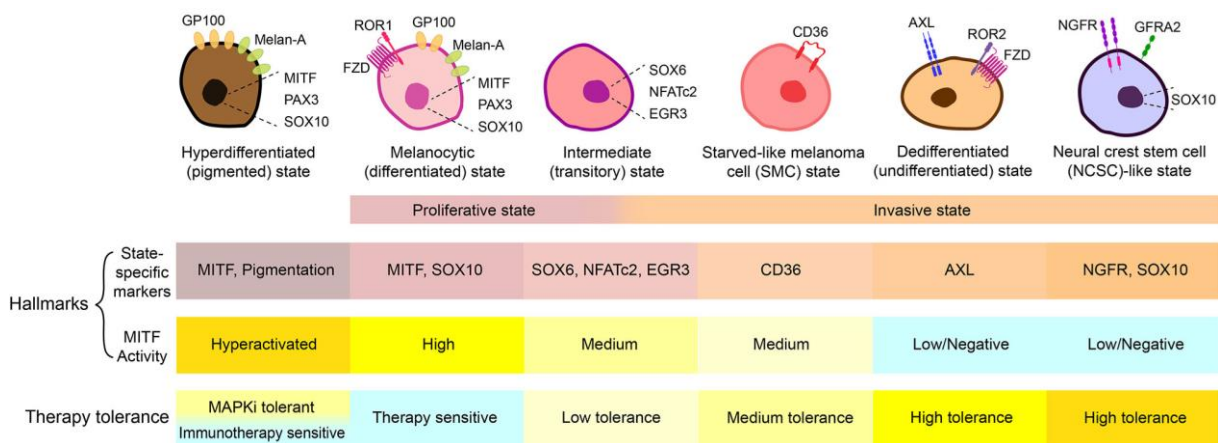


Figure 5: The six cell states of melanoma plasticity.

Each melanoma cell state is characterized by the expression of distinctive markers as well as by MITF activity and features concerning proliferation, invasion, and therapy tolerance. Original figure was modified from Huang *et al.*, Front Oncol. 2021 [88].

Epithelial to mesenchymal transition (EMT) is an important process in embryonic development that is hijacked by cancer cells to dissociate and metastasize [89]. Microenvironmental conditions such as inflammation or metabolic stress activate pathways in melanoma cells and induce reprogramming to a dedifferentiated and mesenchymal-like cell state independent of genetic alterations [88]. General transcriptional drivers of EMT in melanoma are POU Class 3 Homeobox 2 (POU3F2/BRN2), Activator

protein 1 (AP-1) and the family of Transcriptional enhanced associate domain (TEAD) transcription factors. BRN2 can be induced by high MAPK and PI3K signaling and binds to the *MITF* promoter repressing its expression [88, 90]. These signaling pathways and regulators can be activated by cytokines such as TNF α , IL-1 or TGF β [88]. TGF β is generally expressed by melanocytes to downregulate proliferation and is often involved in phenotype switching. In EMT, it is associated to BRN2 and AP-1 but is also able to induce ATF4 and HIF1 α , two regulators that are usually induced by metabolic stress and finally suppress *MITF* while promoting dedifferentiation and the expression of marker genes like *AXL* and Receptor Tyrosine Kinase Like Orphan Receptor 2 (*ROR2*) [73, 88, 91]. The upcoming chapters offer closer reviews on how the high plasticity and EMT in melanoma contribute to therapy resistance.

1.2.4 Targeted therapies in malignant melanoma

Due to frequent genetic alterations such as *BRAF* and *NRAS* mutations, targeted therapies for melanoma have been developed aiming to downregulate hyperactivated MAPK signaling [68, 70]. BRAF and MEK inhibitors like vemurafenib and trametinib, respectively, are widely used in combination in BRAF^{V600}-mutated melanoma patients [70]. Despite clinical benefit of targeted therapy, most tumors acquire resistance within a few months to years. Initially, loss of MAPK signaling consequently downregulates ERK activity and reprograms tumor cell signaling [92]. Alternative transcription factors enhance and stabilize RTKs like Erb-B2 Receptor Tyrosine Kinase 3 (ERBB3), inducing pro-survival pathways such as PI3K/AKT. Melanoma cells that upregulate ERBB3 as well as *AXL* and other RTKs are able to generate dedifferentiated and invasive signatures with low *MITF* expression and a resistant phenotype [70]. On the other hand, MAPK pathway inhibition can also increase *MITF* expression, resulting in transcription of PPARG Coactivator 1 Alpha (*PGC1 α*) that drives oxidative phosphorylation (OXPHOS) [93]. Cancer cells which upregulate OXPHOS increase ATP synthesis in order to maintain cell proliferation [94, 95]. Apart from intrinsic signaling, alterations in the microenvironment of the tumor contributes to melanoma plasticity and resistance to BRAF and MEK inhibition. Finally, resistance can be further achieved by reactivation of MAPK signaling due to additional mutations like gene amplification of *BRAF* [70]. Figure 6 in chapter 1.3.2 illustrates phenotype switching and acquired resistance during MAPK-targeted therapy.

1.3 Immunotherapy

Immunotherapy is regarded as the fifth pillar of cancer therapy alongside surgery, chemotherapy, radiation and targeted therapy [96]. It utilizes and enhances the immune system's ability to fight tumor cells in order to eradicate cancer and has prolonged survival of cancer patients [7]. Immunotherapy

dates back to the 19th century when Wilhelm Busch and Friedrich Fehleisen observed regression of tumors after accidental infections with *Streptococcus pyogenes*. Discoveries in immunological research such as the TCR, CTLA-4 or monoclonal antibodies led to clinical applications of engineered T cells or inhibitory checkpoint inhibitors in 2010 and 2011, respectively [96].

Cancer immunotherapy is diverse as it comprises the application of oncolytic viruses that selectively lyse tumor cells or cytokines and vaccines promoting immune cell function [96-98]. In adoptive cell transfer, autologous or allogenic T cell, NK cell or dendritic cell numbers and/or functions are improved and administered to cancer patients to eradicate tumor cells [97]. Here, T cells as strong effector cells play a major role in cancer immunotherapy. In adoptive T cell therapies, tumor-infiltrating lymphocytes (TILs) recognizing tumor-associated antigens (TAAs) are expanded from biopsies by using Interleukin-2 (IL-2) to effectively kill cancer cells after re-infusion into the patient [7]. Alternatively, the TCR can be genetically modified to increase specificity to tumor neoantigens. Finally, chimeric antigen receptors (CARs) are engineered to express a specific set of extracellular and intracellular domains. These are designed to maintain T cell viability and antitumor efficacy and are not restricted to antigen recognition on MHC molecules. CAR T cell therapy shows severe toxicities as well as limited persistence of CAR T cells and it is restricted to B cell leukemia or lymphoma due to reduced antigen variety and limited tumor infiltration [7, 99, 100]. Immune checkpoint blockade therapy (ICBT) represents another approach in cancer immunotherapy that enhances T cell function to fight tumor cells. As described in 1.1.4 immune checkpoint signaling is an important mechanism of the immune system to limit immune responses and prevent autoimmunity [101]. Tumor cells upregulate molecules such as PD-L1 in order to abrogate TCR signaling and T cell activation by ligation of their cognate receptor PD-1. Immune checkpoint inhibitors (ICI) represent a group of antibodies or small molecules that prevent inhibitory interactions of T cells [97, 101]. ICIs boost immune cell function and have demonstrated strong antitumor effects in solid tumors like NSCLC and melanoma [97, 102, 103]. However, ICBT show immune-related adverse effects as well as limited response rates, especially treatment with single ICIs [101].

1.3.1 Immunotherapies in malignant melanoma

Due to high mutational burden in melanoma, the disease is well eligible for immunotherapy [104]. The treatment of advanced melanoma with immunotherapies has improved median survival of patients from six months to six years in stage IV disease in the past decade [105, 106]. IL-2 was the first immunotherapy agent in clinical use from 1998 but showed strong toxicity in patients [105]. Since then, adoptive cell therapy (ACT), melanoma vaccines and oncolytic virus therapy like talimogene

laherparepvec (T-VEC) were developed until in 2011, the first ICI was approved for metastatic melanoma.

Ipilimumab is a human IgG1 monoclonal antibody inhibiting CTLA-4 which improved overall patient survival [103, 107]. Another immune checkpoint mechanism that is targeted by ICIs is the PD-1/PD-L1 axis. Melanoma cells overexpress PD-L1 to circumvent immune responses by abrogating TCR signaling in order to prevent effector T cell function [105]. Pembrolizumab and Nivolumab are IgG4 monoclonal antibodies both targeting PD-1 expressed on T cells. Treatment with these antibodies improved patient survival and showed less adverse events compared to chemotherapy as well as ipilimumab [108-112]. Combination of anti-CTLA-4 and anti-PD-1 with ipilimumab and nivolumab showed synergistic effects in the treatment of advanced melanoma and finally pushed response rates and median overall survival to more than six years, in spite of increasing high-grade adverse events [106, 113]. Since then, other combination therapies have been investigated and further proposed. Nivolumab was administered in melanoma patients together with relatimab, an IgG4 LAG-3 blocking antibody [105]. LAG-3 is related to CD4 and is expressed by activated T cells binding with high affinity to MHC II [114]. Melanoma cells that express MHC II therefore downregulate T cell function and promote tumor cell survival [115]. Toll-like receptor 9 (TLR-9) agonists have been administered intra-lesionally or subcutaneously to drive the expression of cytokines in order to increase recruitment and activation of effector T cells, turning cold tumors into hot tumors [105]. So far, anti-CTLA-4 and anti-PD-1 antibodies are part of combination therapies with TLR-9 agonists, T-VEC or ACT, but also fecal microbiota transplantation (FMT) from anti-PD-1 responder patients is tested to have an effect on response rates as the microbiome can influence adaptive immune responses [105, 116-120].

Besides partially severe adverse events, the success of ICBT is limited by the expression of inhibitory ligands on the tumor cells. Low expression of PD-L1 or LAG-3 consequently reduced progression-free survival in melanoma patients [121]. In general, still many patients do not benefit from immunotherapy due to primary or acquired resistance mechanisms of melanoma in most cases [105].

1.3.2 Resistance mechanisms in malignant melanoma

Despite a plethora of strategies of tumor elimination by effector cells and various targeted therapies and immunotherapies improving median overall survival, primary and acquired resistance mechanisms in melanoma allow malignant cells to escape immune responses finally preventing tumor eradication [105, 106]. Broadly, resistance in melanoma as in other tumor types can be divided into two categories: either, resistant clones exist prior to immunotherapy and outgrow, or adaptive changes are initiated during the immunotherapy [122].

Cell plasticity plays a critical role in the resistance of melanoma cells [88]. A transcriptional innate anti-PD-1 resistance gene signature (IPRES) was proposed by Hugo *et al.* in which markers of dedifferentiated melanoma such as *AXL* and *ROR2* together with immunosuppressive genes like *IL-10* and *VEGF* were higher expressed in non-responder patients [123]. Phenotype switching also occurs during immunotherapy leading to acquired resistance of melanoma [70, 88]. ACT or ICIs that promote immune function drive inflammation in the tumor which induces dedifferentiation of melanoma cells [85, 124]. Melanocytic antigens like Melan-A are downregulated, resulting in decreased recognition and elimination by T cells. Phenotype switching facilitates the infiltration of MDSCs that enhance inflammation-induced dedifferentiation through the expression of WNT5A and TGFβ and the development of an immunosuppressive microenvironment [125]. Dedifferentiated and invasive MITF^{low}/*AXL*^{high} cells further express CD73 through c-Jun/AP-1 signaling. CD73 increases the immunosuppressive characteristics of the tumor microenvironment by generation of adenosine [88, 126]. Dedifferentiated neural crest stem cell (NCSC)-like MITF^{low}/*NGFR*^{high} cells show increased expression of PD-L1 that drives T cell exhaustion through ICM signaling [127]. Figure 6 illustrates phenotype switching and acquired resistance during immunotherapy in malignant melanoma.

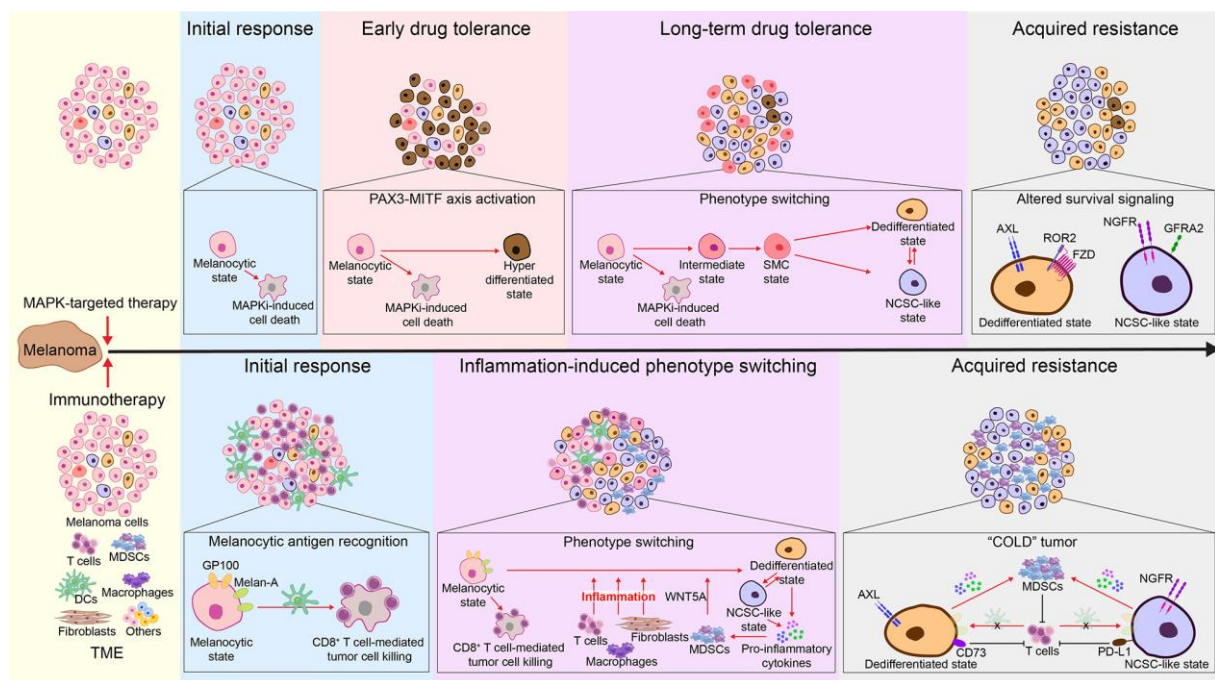


Figure 6: Phenotype switching and therapy resistance in melanoma.

Melanoma cells convert from a melanocytic MITF^{high} to a dedifferentiated MITF^{low} phenotype. Despite initial response to MAPK-targeted therapy (top) and immunotherapy (bottom), some melanoma cells acquire resistance mechanisms that helps the tumor cells to survive and the cancer to progress. Adapted from Huang *et al.*, Front Oncol. 2021 [88].

Like PD-L1, expression of NGFR can be induced by IFNγ that is primarily released by cytotoxic T cells to stimulate tumor cell death through JAK/STAT signaling [127, 128]. IFNγ also drives expression of MHC I in order to increase antigen presentation to effector T cells. During immunotherapy, subclones with

mutations in JAK1/JAK2 develop in melanoma that are resistant to IFN γ [128, 129]. These clones develop resistance to IFN γ -induced apoptosis but are further unable to upregulate MHC I. However, loss of *HLA* or *B2M* is another reason why tumor cells acquire resistance to T cell-mediated rejection and hence T cell-based immunotherapy [130-133].

Resistance to ICBT can additionally be achieved in tumors by T cell upregulation of alternative immune checkpoints not targeted by the therapy such as TIM-3, LAG-3, TIGIT and V-domain Ig suppressor of T cell activation (VISTA) [105, 122]. In a lung adenocarcinoma mouse model, Koyama *et al.* interestingly showed that in anti-PD-1 resistant tumors, binding of the antibodies to PD-1 induced upregulation of *LAG-3*, *CTLA-4* and especially *TIM-3* causing T cell exhaustion and acquired resistance [134]. Even in matched samples from human melanoma patients anti-PD-1 treatment induced the expression of alternative immune checkpoints such as *LAG-3* and *VISTA* on T cells [135, 136].

Despite improved patient survival since the advent of immunotherapy, many patients do not benefit from therapy on a long-term basis as innate and acquired resistance mechanisms help melanoma cells to efficiently evade immune responses. It is therefore inevitable that current therapies are improved, and novel targets are identified to further improve therapy success.

1.4 High-throughput RNAi screens to identify novel immune resistance genes and pathways in human cancers

High-throughput (HTP) genetic screening approaches are effective tools to discover novel genes and mechanisms by disrupting the expression of target genes and studying their phenotypic consequences [137, 138]. Fire *et al.* showed in 1998 in *Caenorhabditis elegans* that double-stranded RNA (dsRNA) caused interference stronger than single strands [139]. Shortly afterwards, RNA interference was introduced to human cell lines using 21-nucleotide small interfering RNA (siRNA) duplexes homologous to the sequence of a target gene to downregulate gene expression [140]. As genetic mutations often lead to complete loss-of-function, other tools were developed such as zinc-finger nucleases (ZFNs) and later, transcription activator-like effector nucleases (TALENs) inserting mutations through double-strand breaks (DSBs) [137]. More recently, the advent of the clustered regularly interspaced palindromic repeat (CRISPR)-Cas9 system transformed the landscape of genomic manipulations [141]. Originally discovered as an adaptive immune mechanism against viruses, a guide RNA directs the endonuclease Cas9 to specific regions of the human DNA introducing DSBs. HTP genome-wide screens enable simultaneous investigation of many phenotypes upon loss-of function of genes. Accordingly, this was first introduced with RNAi screens, although CRISPR screens became quite popular in recent years [138, 142].

Within this context, our group has developed a luciferase-based RNAi screening approach to discover novel immune resistance genes that cancer cells employ to prevent elimination by T cells [143-145]. Upon transfection of cells, 21-23 nucleotide siRNA duplexes are incorporated into the RNA-induced silencing complex (RISC) [142, 146]. The siRNA is unwound within the RISC and guides it to the target mRNA. siRNA-mRNA base pairing activates the ribonuclease of the RISC effector complex to degrade the mRNA, resulting in silencing of gene expression [146]. In our HTP assay system, luciferase-expressing cancer cell lines were transfected with siRNA libraries targeting hundreds to thousands of genes in a multi-well format [143-145]. Tumor cells were subsequently co-cultured with cytotoxic T cells in order to investigate if the knockdown of single genes increase T cell-mediated lysis of tumor cells which is measured by the remaining luciferase activity during the readout. In order to increase the confidence in HTP RNAi screening approaches, positive and negative controls have to be included and effects in large-scale primary screens need to be validated in secondary screens [142]. Overall, RNAi provides a straightforward and fast method for HTP screens and so far several immune resistance genes in different tumor entities were identified by our group and successfully characterized [143-145].

1.5 Transcriptomics in melanoma

Multiomics analyzes multiple 'omes' such as the genome, epigenome, proteome, or transcriptome [147]. Hereby, the insight into a biological system and associations is facilitated to finally be able to better understand mechanisms of different phenotypes and diseases. While bulk multiomics mainly measured the average signal of many cells in one sample, single cell multiomics increased the resolution and gave insight into the cellular heterogeneity of a bulk sample. Due to the relevance in this project, I will focus here on transcriptomic data.

With Sanger sequencing as the first-generation sequencing technology in 1977, RNA sequencing has enormously progressed over the past decades and has become the method primarily used in transcriptome profiling [148]. Next generation sequencing (NGS) sped up RNA-Seq at low cost and high accuracy and is nowadays widely used in cancer research. Especially the advent of single cell RNA-sequencing delineated intratumoral heterogeneity, therefore contributing to the understanding of cancer evolution, the interplay of cells in the tumor microenvironment and drug resistance [104, 148].

As with other tumors, patient-derived melanomas as well as melanoma cell lines were subjected to RNA-sequencing. In 2015, The Cancer Genome Atlas (TCGA) Network presented work on primary and metastatic melanomas with bulk RNA-Seq data of 329 samples [149]. Hierarchical clustering revealed the three clusters 'immune', 'keratin' and 'MITF-low'. Genes higher expressed in the MITF-low cluster

were more associated with the nervous system and embryonic development. Others performed bulk RNA-Seq on melanoma samples of patients undergoing targeted or immunotherapies in order to identify gene expression patterns that can predict therapy outcome [123, 150, 151]. Here, matched patient samples before and after immunotherapy were useful to elucidate tumor evolution or the development of resistance during therapy [135]. RNA-Seq data on patient-derived melanoma cell lines enabled interpretation of melanoma plasticity and categorization into different phenotypes *e.g.*, melanocytic, mesenchymal, and NCSC-like [83, 85]. Plasticity marker genes such as *MITF*, *AXL* and *NGFR* and gene regulatory networks were identified increasing the complexity as well as understanding of melanoma biology. Single-cell RNA-Seq data finally pushed the molecular resolution to the next level, giving insight into the cellular heterogeneity of one melanoma tumor. While on the bulk level, tumors were classified as $MITF^{\text{high}}$ or AXL^{high} , it was now shown that both phenotypes coexist in the same tumor [70, 86]. Transcriptional heterogeneity separated malignant cells from the tumor microenvironment, revealing T cell exhaustion and drug resistance programs [86, 152, 153]. Jerby-Arnon *et al.* showed that a resistance program is expressed before the application of immunotherapy as it is present in cold niches of the tumor [152]. In this context, CDK4/6 inhibition seemed to have beneficial effects on melanoma progression and therapy outcome.

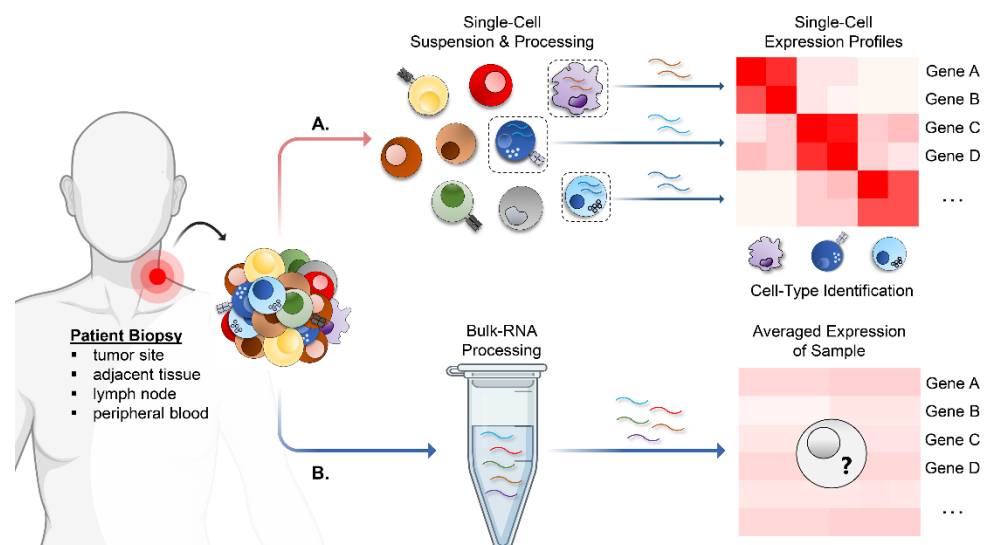


Figure 7: Bulk vs. scRNA-Seq.

While for bulk RNA-Seq (B) approaches one sample provides averaged gene expression levels, scRNA-Seq (A) delineates cellular heterogeneity with cell type specific expression patterns. Adapted from Guruprasad *et al.*, *J Exp Med.* 2021 [104].

Single-cell transcriptomics have highly improved the resolution of tumors uncovering transcriptional programs of cancer cells and the microenvironment [104]. Despite better understanding of T cell exhaustion and cancer cell heterogeneity and resistance, much remains to be unknown. Increased number of therapy-matched samples as well as new technologies in multiomics will further facilitate the interpretation of the complexity of cancer and treatment response.

2 Objectives of this project

Despite the successful application of immune checkpoint inhibitors such as monoclonal antibodies against CTLA-4 or PD-1 in malignant melanoma, many patients still do not benefit from this therapy on the long term due to primary and acquired cancer resistance mechanisms [105]. In melanoma, resistance to immunotherapies is associated with the downregulation of the master regulator of melanocytes MITF which is concomitant with a dedifferentiated and invasive phenotype of melanoma cells [88].

I hypothesized that melanoma cells, especially those with a low MITF expression use so far unknown immune resistance mechanisms to circumvent immune responses. Furthermore, genes that convey immune resistance are co-expressed in clusters working in tandem and can be correlated to low MITF expression. In this project, I therefore aimed to identify complementary immune resistance genes and pathways that are responsible for the unresponsiveness to immunotherapies, especially in MITF^{low} melanoma. I combined *in vitro* and *in silico* approaches to finally achieve the following objectives:

1. Implementation of a high-throughput RNAi screen for the identification of novel immune resistance genes in melanoma using MITF^{high} and MITF^{low} cell lines derived from the same immunotherapy non-responder patient.
2. *In silico* analyses for the identification of expression and co-expression patterns of immune resistance genes that are associated to a MITF^{low} phenotype in melanoma.
3. *In vitro* mode of action analyses of selected immune resistance genes for the discovery of the mechanisms that MITF^{low} melanoma cells use to evade immune responses.
4. Evaluation on the applicability of selected immune resistance genes as novel therapeutic interventions for malignant melanoma.

3 Materials

3.1 Instruments and devices

Table 1: Instruments and devices

Instrument	Company
3D shaker SU1030	Sunlab Instruments
ASSIST PLUS Pipetting robot	Integra Biosciences
Axio Vert.A1 Microscope	ZEISS
Bolt® Mini Gel Tank	Life Technologies
ChemiDoc Imaging System	Bio-Rad
Cold Plate Air Cooled Heater/Cooler (CPAC)	Inheco
CoolCell LX Freezing container	BioCision
CryoCube® F740hi	Eppendorf
DNA/RNA UV-cleaver box UVC/T-M-AR	Biosan
E1-ClipTip™ Electronic Adjustable Tip Spacing Multichannel Equalizer Pipettes	Thermo Scientific
F1-ClipTip™ Multichannel Pipettes	Thermo Scientific
F1-ClipTip™ Variable Volume Single Channel Pipettes	Thermo Scientific
FACSAria™ II Cell sorter	BD Biosciences
FACSLyric™	BD Biosciences
HEco™ 818P-190 freezer	MVE
Heracell™ 240i CO ₂ Incubator	Thermo Scientific
HeraSafe™ 2030i Biosafety Cabinet	Thermo Scientific
Heraeus Fresco™ 17 Centrifuge	Thermo Scientific
Heraeus Multifuge™ X3FR	Thermo Scientific
IBL 437C Blood Irradiator	CIS Bio International
Incucyte® SX5 Live-Cell Analysis Instrument	Sartorius
KS 4000 i control shaker	IKA
LGex 3410 MediLine freezer	LIEBHERR
LKv 3910 MediLine fridge	LIEBHERR
MIX 6 Magnetic stirrer	2mag
Multidrop™ Combi Reagent Dispenser	Thermo Scientific
NanoDrop™ 2000c Spectrophotometer	Thermo Scientific
Neubauer improved Hemacytometer	Assistent
Owl™ EasyCast™ B2 Mini Gel Electrophoresis Systems	Thermo Scientific
PIPETBOY acu 2 Pipette controller	Integra Biosciences
PowerEase™ 300W Power Supply	Thermo Scientific
QuantStudio™ 3 Real-Time PCR System	Applied Biosystems
Rotating mixer RM5	Hecht Assistent
SCALA XPRESS fume hood	Waldner

Single TEC Control (STC) with Blue Slot Module	Inheco
SimpliAmp™ Thermocycler	Applied Biosystems
Tecan Spark 10M Microplate Reader	TECAN
ThermoMixer C	Eppendorf
Trans-Blot Turbo Transfer System	Bio-Rad
VOYAGER Electronic Pipette 8 Channels	Integra Biosciences
Vortex-Genie 2 Mixer	Scientific Industries
TW12 Water Bath	Julabo

3.2 Consumables

Table 2: Consumables

Material	Company	Catalog#
Cap for PCR microcentrifuge tubes	nerbe plus	04-042-0500
Cell Culture Flask, 25 cm ²	Greiner Bio-One	690175
Cell Culture Flask, 75 cm ²	Greiner Bio-One	658175
Cell Culture Flask, 175 cm ²	Greiner Bio-One	660175
CELLSTAR® serological pipette 5 ml	Greiner Bio-One	606180
CELLSTAR® serological pipette 10 ml	Greiner Bio-One	607180
CELLSTAR® serological pipette 25 ml	Greiner Bio-One	760180
ClipTip™ Pipette tips, 20 µl	Thermo Scientific	94410213
ClipTip™ Pipette tips, 200 µl	Thermo Scientific	94410313
ClipTip™ Pipette tips, 1250 µl	Thermo Scientific	94410813
ClipTip™ Pipette tips with filter, 20 µl	Thermo Scientific	94420213
ClipTip™ Pipette tips with filter, 125 µl	Thermo Scientific	94420153
ClipTip™ Pipette tips with filter, 200 µl	Thermo Scientific	94420313
ClipTip™ Pipette tips with filter, 1250 µl	Thermo Scientific	94420813
CRYO.S, 2 ML	Greiner Bio-One	122278
CulturPlate, white 96-well	Perkin Elmer	6005680
CulturPlate, white 384-well	Perkin Elmer	6007680
FACS tubes - Falcon® 5 mL Round Bottom	Corning	352008
FACS tubes - Falcon® 5 mL with Cell Strainer	Corning	352235
Falcon® 6-well clear flat Microplates	Corning	351146
Falcon® 24-well clear flat Microplates	Corning	353047
Falcon® 96-well clear round Microplates	Corning	351177
GRIPTIP 12,5 µl Filter Tips, Low Retention	Integra Biosciences	6505
GRIPTIP 300 µl Filter Tips, Low Retention	Integra Biosciences	6535
MaxiSorp™ Clear Flat-Bottom Plate, 96-well	Thermo Scientific	439454
MicroAmp™ Clear Adhesive Film	Applied Biosystems	4306311
MicroAmp® Optical 96-Well Reaction Plate	Applied Biosystems	N8010560

Microcentrifuge tube PP, 5ml	nerbe plus	04-252-1000
Microplate, 96-well, V-bottom clear	Greiner Bio-One	651101
Multichannel Reagent Reservoirs, 10 ml	Integra Biosciences	4332
Multichannel Reagent Reservoirs, 25 ml	Integra Biosciences	4312
Parafilm® M	VWR	291-1212
PCR microcentrifuge tube PP, 0.2ml	nerbe plus	04-032-0500
Safelock-Cap microcentrifuge tube PP, 1.5ml	nerbe plus	04-212-1206
SafeSeal reaction tube, 0.5 ml, PP	Eppendorf	72.704
SafeSeal reaction tube, 1.5 ml, PP	Eppendorf	72.706
SafeSeal reaction tube, 2 ml, PP	Eppendorf	72.695.500
Screw cap tube, 15 ml	Sarstedt	62.554.001
Screw cap tube, 15 ml	Greiner Bio-One	188271
Screw cap tube, 50 ml	Sarstedt	62.547.254
Screw cap tube, 50 ml	Greiner Bio-One	227261
Tissue Culture Test Plates, 6-well	TPP	92006
Tissue Culture Test Plates, 96-well	TPP	92096

3.3 Chemicals, reagents and supplements

Table 3: Chemicals, reagents and supplements

Material	Company	Catalog#
2-Mercaptoethanol ≥99.0%	Sigma-Aldrich	M6250
Adenosine 5'-monophosphate disodium salt (AMP)	Sigma-Aldrich	01930
Adenosine 5'-triphosphate disodium salt hydrate (ATP)	Sigma-Aldrich	A2383
Agarose NEEO ultra-quality	Roth	2267.4
AIM V™ Medium	Gibco	12055091
Ampicillin	ratiopharm	6613441.00.00
Animal-Free Blocking Solution (5X)	Cell Signaling	15019
BD® Assay Diluent	BD Biosciences	555213
BD® Clean Solution	BD Biosciences	340345
BD® CS&T	BD Biosciences	656505
BD FACSTFlow™ Sheath Fluid	BD Biosciences	342003
Bio-Safe™ Coomassie Stain	Bio-Rad	1610786
CD3 Monoclonal Antibody (OKT3), eBioscience™	Invitrogen	16-0037-81
D-Luciferin Firefly	Biosynth	L-8200
Dimethylsulfoxid (DMSO)	Sigma-Aldrich	D2650
DNA Gel Loading Dye (6X)	Thermo Scientific	R0611
Dulbecco's Balanced Salt Solution (DPBS)	Gibco	14190250
Dulbecco's Phosphate Buffered Saline (10x)	Sigma-Aldrich	D1408
DTT BioChemica	AppliChem	A1101

Ethanol ROTIPURAN® ≥99,8 %, p.a.	Roth	9065.3
Fetal Bovine Serum (FBS)	Sigma-Aldrich	F7524
GelRed® Nucleic Acid Gel Stain	Biotium	41003
Geneticin™ Selective Antibiotic (G418 Sulfate)	Gibco	11811031
GeneRuler 50 bp DNA Ladder	Thermo Scientific	SM0371
HEPES solution	Sigma-Aldrich	H0887
Human AB Serum Heat-Inactivated	Valley Biomedical	HP1022 HI
Hygromycin B	Gibco	10687010
IL-2 Proleukin® S	Novartis	1003780
Incucyte® Cytotox Red Dye	Sartorius	4632
KIOVIG Human normal immunoglobulin (IVIg)	Baxter	EU/1/05/329
LB Broth (Luria/Miller)	Roth	X968
LB Agar (Luria/Miller)	Roth	X969
Lipofectamine™ 3000 Transfection Reagent	Invitrogen	L3000008
Lipofectamine™ RNAiMAX Transfection Reagent	Invitrogen	13778150
Magnesium sulfate (MgSO ₄)	Sigma-Aldrich	M2643
MILLIPLEX MAP Lysis buffer for Multiplexing	Merck Millipore	43-040
Nonfat dried milk powder	AppliChem	A0830
Nuclease-Free Water (not DEPC-Treated)	Ambion	AM9937
NuPAGE™ 4 bis 12 %, Bis-Tris	Invitrogen	NP0335BOX
NuPAGE™ LDS Sample Buffer (4X)	Invitrogen	NP0007
NuPAGE™ MOPS SDS Running Buffer (20X)	Invitrogen	NP0001
Opti-MEM™ Reduced Serum Medium	Gibco	31985062
Oxalic acid, ReagentPlus	Sigma-Aldrich	241172
PageRuler™ Prestained Protein Ladder	Thermo Scientific	26616
Penicillin-Streptomycin	Sigma-Aldrich	P4333
Phenylacetic acid	Sigma-Aldrich	P16621
Phosphatase Inhibitor Cocktail 3	Sigma-Aldrich	P0044
Ponceau S solution	Sigma-Aldrich	P7170
Protease Inhibitor Cocktail Set III, EDTA-Free	Calbiochem	539134
Puromycin Dihydrochloride	Gibco	A1113803
Recombinant BenzNuclease / Benzonase Protein	SPEED Biosystems	YCP1200
RPMI 1640 Medium	Gibco	21875091
RPMI-1640 Medium	Sigma-Aldrich	R8758
S.O.C. Medium	Invitrogen	15544034
Sodium carbonate (Na ₂ CO ₃)	Roth	8563
Sodium chloride (NaCl)	VWR	27810
Sodium hydrogen carbonate (NaHCO ₃)	Merck Millipore	106329
Sulfuric acid (H ₂ SO ₄)	Sigma Aldrich	30743
TAE Buffer (Tris-acetate-EDTA) (50x)	Thermo Scientific	B49

Tris(hydroxymethyl)aminomethane (Tris)	Merck Millipore	108382
Triton™ X-100 solution 10 %	Sigma-Aldrich	93443
Trypan Blue solution	Sigma-Aldrich	T8154
Trypsin-EDTA solution 10x	Sigma-Aldrich	T4174
Tween® 20 for molecular biology	AppliChem	A4974
UltraPure™ 0,5 M EDTA, pH 8,0	Invitrogen	15575020
Zombie Aqua™ Fixable Viability Kit	BioLegend	423102
Zombie NIR™ Fixable Viability Kit	BioLegend	423106

3.4 Recombinant proteins and peptides

Table 4: Recombinant proteins and peptides

Protein/Peptide	Company	Catalog#
Matched peptide A*02:01-GILGFVFTL (Flu)	ProlImmune	P007-0A-E
Matched peptide A*02:01- ELAGIGILTV (MART-1)	ProlImmune	P082-0A-E
Recombinant Human FASL (TNFSF6)	BioLegend	589404
Recombinant Human IFN-γ	PeproTech	300-02
Recombinant Human Light (TNFSF14)	BioLegend	762304
Recombinant Human LT-α (TNF-β)	BioLegend	562604
Recombinant Human TRAIL (TNFSF10)	BioLegend	752904
Recombinant Human TNF-α	Kindly provided by Daniela Männel, University of Regensburg	-

3.5 Assay kits

Table 5: Assay kits

Material	Company	Catalog#
BD OptEIA™ Human IFN-γ ELISA Set	BD Biosciences	555142
BD OptEIA™ Human TNF ELISA Set	BD Biosciences	555212
BD OptEIA™ TMB Substrate Reagent Set	BD Biosciences	555214
MyTaq™ HS Red Mix	Bioline	BIO-25047
Pierce™ BCA Protein Assay Kit	Thermo Scientific	23225
Pierce™ ECL Western Blotting Substrate	Thermo Scientific	32209
PureLink™ HiPure Plasmid Midiprep Kit	Invitrogen	K210005
QuantiFast SYBR Green PCR Kit	Qiagen	204056
QuantiNova SYBR Green PCR Kit	Qiagen	208056
QuantiTect Rev. Transcription Kit	Qiagen	205313
RNeasy Mini Kit	Qiagen	74106
Trans-Blot Turbo RTA Mini 0.2 μm Nitrocellulose Transfer Kit	Bio-Rad	1704270

Trident femto Western HRP Substrate	GeneTex	GTX14698
-------------------------------------	---------	----------

3.6 Cell culture media

Fetal Bovine Serum (FBS) was heat-inactivated by an incubation of 30 min at 56 °C before application in the cell culture media.

Table 6: Cell culture media

Medium	Ingredient	Amount
Complete Lymphocyte Medium (CLM)	RPMI (Gibco)	500 ml
	Human AB Serum	50 ml
	Penicillin-Streptomycin	5 ml
	HEPES	5 ml
	2-Mercaptoethanol	50 µl
Complete RPMI	RPMI (Sigma-Aldrich)	500 ml
	FBS	50 ml
	Penicillin-Streptomycin	5 ml
FluT cell expansion medium	CLM	50 %
	AIM-V	50 %
Freezing medium A for FluT cells	Fetal Bovine Serum (FBS)	60 %
	RPMI	40 %
Freezing medium B for FluT cells	Fetal Bovine Serum (FBS)	80 %
	DMSO	20 %
Freezing medium A for TIL412/MART-1 T cells	Human AB Serum	60 %
	RPMI	40 %
Freezing medium B for TIL412/MART-1 T cells	Human AB Serum	80 %
	DMSO	20 %
Freezing medium for tumor cells	Fetal Bovine Serum (FBS)	90 %
	DMSO	10 %

3.7 Buffers

Table 7: Buffers

Buffer	Ingredient	Amount/ Concentration
1 % milk in TBS-T (Staining/washing solution for western blot)	TBS-T	
	Nonfat dried milk powder	1 % (w/v)
10 % milk in TBS-T (Blocking solution for western blot)	TBS-T	
	Nonfat dried milk powder	10 % (w/v)
Animal-Free Blocking Solution (Blocking/staining solution for western blot)	ddH ₂ O	
	Animal-Free Blocking Solution (5X)	20 % (v/v)
B2 Buffer	ddH ₂ O	
	AMP	1 mM
	ATP	35 mM
	DTT	415 mM
BL Buffer (pH 7,6)	ddH ₂ O	
	EDTA	0,5 mM
	HEPES	50 mM

	Oxalic acid Phenylacetic acid	0,07 mM 0,033 mM
Coating buffer (pH 9,5) (ELISA)	ddH ₂ O NaHCO ₃ Na ₂ CO ₃	100,0 mM 33,6 mM
FACS buffer	PBS FBS	2 % (v/v)
Luciferin solution	ddH ₂ O D-Luciferin Firefly	45 mM
Luciferase buffer (Luciferase-based cytotoxicity assay)	BL Buffer B2 Buffer Luciferin solution 1 M MgSO ₄	2,2 % (v/v) 0,4 % (v/v) 2,8 % (v/v)
Lysis buffer (Luciferase-based cytotoxicity assay)	BL Buffer Triton™ X-100 solution 10 %	3 % (v/v)
MOPS SDS running buffer 1x (Western blot)	ddH ₂ O MOPS SDS Running Buffer (20X)	5 % (v/v)
PBS-T (ELISA washing buffer)	ddH ₂ O PBS (10x) Tween 20	10,00 % (v/v) 0,05 % (v/v)
TAE Buffer 0,5x (Agarose gel electrophoresis)	ddH ₂ O TAE Buffer (50x)	1 % (v/v)
TBS-T (Western blot washing solution)	TBS Tween 20	0,05 % (v/v)
Tris-buffered saline (TBS) 1x	ddH ₂ O TBS (10x)	10 % (v/v)
Tris-buffered saline (TBS) 10x	ddH ₂ O Tris NaCl	150 mM 100 mM
Trans-Blot Turbo Transfer buffer 1x (Western blot)	ddH ₂ O Ethanol ≥99,8 % Trans-Blot Turbo Transfer buffer (5X)	20 % (v/v) 20 % (v/v)

3.8 Cells and cell lines

3.8.1 Eukaryotic cells and cell lines

Table 8: Eukaryotic cells and cell lines

Cells/Cell line	Origin	Culture medium
FluT cells	Healthy donor PBMCs	CLM
Ma-Mal-86	Human metastatic melanoma (University Hospital Essen, Department of Dermatology)	Complete RPMI
Ma-Mal-86 HLA-A2+	Human metastatic melanoma (University Hospital Essen, Department of Dermatology)	Complete RPMI + 0,9 mg/ml G418
Ma-Mal-86 HLA-A2+ Luc+	Human metastatic melanoma (University Hospital Essen, Department of Dermatology)	Complete RPMI + 0,9 mg/ml G418 + 0,6 µg/ml Puromycin

Ma-Mal-86a HLA-A2+ Luc+ transfected with an overexpression plasmid	Human metastatic melanoma (University Hospital Essen, Department of Dermatology)	Complete RPMI + 0,9 mg/ml G418 + 0,6 µg/ml Puromycin + 0,2 mg/ml Hygromycin
MART-1 T cells	Human primary tumor tissue	CLM
TIL412	Human primary tumor tissue	CLM

3.8.2 Bacteria

Table 9: Bacteria

Bacteria	Origin
DH5α competent <i>Escherichia coli</i>	Kindly provided by the Division of Genetic Immunotherapy, Leibniz Institute for Immunotherapy (LIT), Regensburg

3.9 Plasmids and lentiviral particles

Table 10: Plasmids and lentiviral particles

Product	Company	Catalog# / Clone ID
HLAA2_pcDNA3.1/G418(+) plasmid	GenScript	Customized
Luciferase (firefly)-2A-GFP (CMV, Puro) Lentivirus	GenTarget Inc	LVP020
SLC39A13_pcDNA3.1/Hygro(+) plasmid	GenScript	OHu74313C
TMCC3_pcDNA3.1/Hygro(+) plasmid	GenScript	OHu107341C

3.10 Oligonucleotides

3.10.1 Pre-designed primers

Table 11: Pre-designed primers

Primers	Company	Catalog#
RT ² qPCR Primer Assay for Human AXL	Qiagen	PPH00248E
RT ² qPCR Primer Assay for Human CD274	Qiagen	PPH21094A
RT ² qPCR Primer Assay for Human CDH24	Qiagen	PPH12992A
RT ² qPCR Primer Assay for Human CFLAR	Qiagen	PPH00333B
RT ² qPCR Primer Assay for Human DLL1	Qiagen	PPH06024E
RT ² qPCR Primer Assay for Human ELN	Qiagen	PPH06895F
RT ² qPCR Primer Assay for Human GCK	Qiagen	PPH02294B
RT ² qPCR Primer Assay for Human GJC2	Qiagen	PPH10823B
RT ² qPCR Primer Assay for Human GRM6	Qiagen	PPH02353B
RT ² qPCR Primer Assay for Human ITGAX	Qiagen	PPH00661F
RT ² qPCR Primer Assay for Human LRRN1	Qiagen	PPH11746A
RT ² qPCR Primer Assay for Human MOK	Qiagen	PPH10931A
RT ² qPCR Primer Assay for Human NGFR	Qiagen	PPH00821A
RT ² qPCR Primer Assay for Human PLXNA3	Qiagen	PPH08323A

RT ² qPCR Primer Assay for Human S1PR1	Qiagen	PPH01350F
RT ² qPCR Primer Assay for Human SIK3	Qiagen	PPH21242A
RT ² qPCR Primer Assay for Human SLC13A2	Qiagen	PPH10865A
RT ² qPCR Primer Assay for Human SLC39A13	Qiagen	PPH06304A
RT ² qPCR Primer Assay for Human SPNS3	Qiagen	PPH22972A
RT ² qPCR Primer Assay for Human TMCC3	Qiagen	PPH13586A
RT ² qPCR Primer Assay for Human TMEM132E	Qiagen	PPH13922A
RT ² qPCR Primer Assay for Human ZNF443	Qiagen	PPH12425A

3.10.2 Individually designed primers

All primer sequences were synthesized by Sigma-Aldrich/Merck and reconstituted in nuclease-free water.

Table 12: Individually designed primers

Primers	Sequence
Human β -Actin	Forward: TGGAGCGAGCATCCCCAAA Reverse: TGGAGCGAGCATCCCCAAA
Human HDGF	Forward: CCAAAGACCTCTTCCCTTACGAG Reverse: TGGTTCAGGCTCTCCACACAG
Human MITF	Forward: GAAATCTTGGGCTTGATGGA Reverse: AGGAGTTGCTGATGGTGAGG
Human MOK	Forward: TGTCCCCACAATGCCTCTCC Reverse: GCCCGCTTCTCTGTTTTCTC
Human SLC39A13	Forward: TTCCCGTTGCTTGTCATTCCC Reverse: AAACACATTGCCAAGAGTCCC
Human TMCC3	Forward: CATCAGACTCAGCGTGGGCT Reverse: AATGGTGTGGGCTGGTGTGA
Human TMCC3 - ORF	Forward: GCTGCAAGAGCCGGGTAGAA Reverse: GGCTGTCTGCAGTGAGTTTGAC
Human ZNF443	Forward: CTGGCTGGAACACGCATTGG Reverse: AAGCCCACTTCTCGGGTG
Human ZNF443 - ORF	Forward: TGCAAACCTTGGGAAAGCCTG Reverse: GTCGTAGAAAGCAAGTGAGCCA

3.11 siRNAs

3.11.1 siRNA libraries

Table 13: siRNA libraries

Library	Company
Custom Cherry-Pick siRNA Library, siGENOME SMARTpools, 5202 target genes, 384 well format, vertical	Horizon Discovery
RNAi Cherry-pick Library 0.1 nmol, 174 wells, 3 plates, plate type 96, Vertical (siGENOME SMARTpools)	Horizon Discovery
RNAi Cherry-pick Library 0.1 nmol, 696 wells, 9 plates, plate type 96, Vertical (siGENOME individual siRNAs)	Horizon Discovery

3.11.2 siRNAs

Table 14: siRNAs

siRNA	Company	Catalog#
AllStars Hs Cell Death siRNA	Qiagen	1027299
ON-TARGETplus Human MITF siRNA, Set of 4	Horizon Discovery	LQ-008674-00
ON-TARGETplus Human OR10H1 siRNA, s5	Horizon Discovery	J-020479-05
ON-TARGETplus Human SIK3 siRNA, s11	Horizon Discovery	J-004779-11
ON-TARGETplus Non-targeting siRNA #2	Horizon Discovery	D-001810-02
ON-TARGETplus Non-targeting siRNA #3	Horizon Discovery	D-001810-03
ON-TARGETplus Non-targeting siRNA #4	Horizon Discovery	D-001810-04
siGENOME Human AXL siRNA, set of 4	Horizon Discovery	MQ-003104-03
siGENOME Human CAMK1D siRNA, set of 4	Horizon Discovery	MQ-004946-01
siGENOME Human CD274 siRNA, set of 4	Horizon Discovery	MQ-015836-01
siGENOME Human CDH24 siRNA, set of 4	Horizon Discovery	MQ-018985-00
siGENOME Human CFLAR siRNA, set of 4	Horizon Discovery	MQ-003772-06
siGENOME Human DLL1 siRNA, set of 4	Horizon Discovery	MQ-013302-02
siGENOME Human ELN siRNA, set of 4	Horizon Discovery	MQ-009306-01
siGENOME Human GCK siRNA, set of 4	Horizon Discovery	MQ-010819-01
siGENOME Human GJC2 siRNA, set of 4	Horizon Discovery	MQ-020380-02
siGENOME Human GRM6 siRNA, set of 4	Horizon Discovery	MQ-005621-02
siGENOME Human HDGF siRNA, set of 4	Horizon Discovery	MQ-019782-00
siGENOME Human ITGAX siRNA, set of 4	Horizon Discovery	MQ-008009-02
siGENOME Human LGALS3 siRNA, SMARTPool	Horizon Discovery	M-010606-02
siGENOME Human LRRN1 siRNA, set of 4	Horizon Discovery	MQ-019481-02
siGENOME Human MOK siRNA, set of 4	Horizon Discovery	MQ-004838-01
siGENOME Human NGFR siRNA, set of 4	Horizon Discovery	MQ-009340-02
siGENOME Human OR10H1 siRNA, s1	Horizon Discovery	D-020479-01
siGENOME Human PLXNA3 siRNA, set of 4	Horizon Discovery	MQ-020933-01
siGENOME Human S1PR1 siRNA, set of 4	Horizon Discovery	MQ-003655-02
siGENOME Human SIK3 siRNA, s1	Horizon Discovery	D-004779-01
siGENOME Human SLC13A2 siRNA, set of 4	Horizon Discovery	MQ-007392-01
siGENOME Human SLC39A13 siRNA, set of 4	Horizon Discovery	MQ-007568-00
siGENOME Human SPNS3 siRNA, set of 4	Horizon Discovery	MQ-018953-00
siGENOME Human TMCC3 siRNA, set of 4	Horizon Discovery	MQ-013877-01
siGENOME Human TMEM132E siRNA, set of 4	Horizon Discovery	MQ-023299-00
siGENOME Human TNFRSF14 siRNA, set of 4	Horizon Discovery	MQ-008096-00
siGENOME Human UBC siRNA, SMARTPool	Horizon Discovery	M-019408-01
siGENOME Human ZNF443 siRNA, set of 4	Horizon Discovery	MQ-018335-01

3.12 Antibodies

3.12.1 FACS antibodies

Table 15: FACS antibodies

Antibody	Company	Catalog#	Dilution
Alexa Fluor® 700 anti-human CD3 Antibody	BioLegend	300424	1:50
APC anti-human CD120a Antibody	BioLegend	369906	1:20
APC anti-human CD253 (TRAIL) Antibody	BioLegend	308210	1:20
APC anti-human CD258 (LIGHT) Antibody	BioLegend	318709	1:20
APC anti-human CD261 (DR4, TRAIL-R1) Antibody	BioLegend	307208	1:20
APC anti-human CD270 (HVEM, TR2) Antibody	BioLegend	318808	1:20
APC anti-human CD274 (B7-H1, PD-L1) Antibody	BioLegend	329708	1:20
APC Flu Pentamer (A*02:01 - GILGFVFTL)	ProlImmune	F007-4A-E	1:10
APC Mouse Anti-Human HLA-A2	BD Biosciences	561341	1:20
Brilliant Violet 421™ anti-human CD95 (Fas) Antibody	BioLegend	305624	1:20
PE anti-human CD119 (IFN-γ R α chain) Antibody	BioLegend	308606	1:20
PE anti-human CD120b Antibody	BioLegend	358404	1:20
PE anti-human CD178 (Fas-L) Antibody	BioLegend	306407	1:20
PE anti-human CD262 (DR5, TRAIL-R2) Antibody	BioLegend	307406	1:20
PE anti-human LT-α (TNF-β) Antibody	BioLegend	503105	1:80
PE anti-human Lymphotoxin beta receptor (LT-βR) Antibody	BioLegend	322008	1:20
V450 Mouse Anti-Human CD8	BD Biosciences	560347	1:200

Isotype antibody	Company	Catalog#
APC Mouse IgG1, κ Isotype Ctrl (FC) Antibody	BioLegend	400122*
APC Mouse IgG2a, κ Isotype Ctrl (FC) Antibody	BioLegend	400222*
APC Mouse IgG2b κ Isotype Control	BD Biosciences	555745*
APC Mouse IgG2b, κ Isotype Ctrl Antibody	BioLegend	400322*
Brilliant Violet 421™ Mouse IgG1, κ Isotype Ctrl Antibody	BioLegend	400158*
PE Mouse IgG1, κ Isotype Ctrl Antibody	BioLegend	400112*
PE Mouse IgG2b, κ Isotype Ctrl Antibody	BioLegend	400314*
PE Rat IgG2a, κ Isotype Ctrl Antibody	BioLegend	400508*

*Concentration of the isotype antibody was adjusted to the respective antigen-specific antibody.

3.12.2 Western blot antibodies

Table 16: Western blot antibodies

Antibody	Company	Catalog#	Dilution
Akt (pan) (40D4) Mouse mAb	Cell Signaling	2920	1:2000
Anti-TMCC3 antibody produced in rabbit	Sigma-Aldrich	HPA014272	1:500

Anti-mouse IgG, HRP-linked Antibody	Cell Signaling	7076	1:2000
Anti-rabbit IgG, HRP-linked Antibody	Cell Signaling	7074	1:2000
Bcl-2 (124) Mouse mAb	Cell Signaling	15071	1:1000
BiP (C50B12) Rabbit mAb	Cell Signaling	3177	1:1000
Caspase-3 (D3R6Y) Rabbit mAb	Cell Signaling	14220	1:1000
Caspase-8 (1C12) Mouse mAb	Cell Signaling	9746	1:1000
Caspase-9 Antibody (Human Specific)	Cell Signaling	9502	1:1000
CHOP (L63F7) Mouse mAb	Cell Signaling	2895	1:1000
FLIP (D5J1E) Rabbit mAb	Cell Signaling	56343	1:1000
GAPDH Antibody (0411)	Santa Cruz	sc-47724	1:2000
IRE1 α (14C10) Rabbit mAb	Cell Signaling	3294	1:1000
Monoclonal Anti-Microphthalmia (MITF) antibody produced in mouse	Sigma-Aldrich	M6065	1:1667
MOK Antibody	Aviva	OAAN03251	1:500
p53 (7F5) Rabbit mAb	Cell Signaling	2527	1:1000
Phospho-Akt (Ser473) Antibody	Cell Signaling	9271	1:1000
Phospho-Bad (Ser136) (D25H8) Rabbit mAb	Cell Signaling	4366	1:1000
Phospho-NF- κ B p65 (Ser536) (93H1) Rabbit mAb	Cell Signaling	3033	1:1000
Phospho-SAPK/JNK (Thr183/Tyr185) (81E11) Rabbit mAb	Cell Signaling	4668	1:1000
Phospho-Stat1 (Tyr701) (D4A7) Rabbit mAb	Cell Signaling	7649	1:1000
Phospho-Stat3 (Ser727) Antibody	Cell Signaling	9134	1:1000
SLC39A13 Antibody - middle region	Aviva	ARP78987	1:500
Stat1 (D1K9Y) Rabbit mAb	Cell Signaling	14994	1:1000
Stat3 (124H6) Mouse mAb	Cell Signaling	9139	1:1000
XIAP (3B6) Rabbit mAb	Cell Signaling	2045	1:1000
ZNF443 antibody [N1N2], N-term	GeneTex	GTX115372	1:500

3.13 Software

Table 17: Software

Software	Developer
EndNote X7.8	Clarivate Analytics
FlowJo 10.8.1	Becton Dickinson & Company (BD)
GraphPad Prism 9.4.1	GraphPad Software, Inc.
ImageJ 1.53t	Wayne Rasband (NIH)
Incucyte 2021C	Essen BioScience Inc.
Microsoft 365 Apps for Business	Microsoft
R 4.1.1	R Core Team
Vialab	Integra Biosciences
Vialink	Integra Biosciences

3.14 Additional R packages and software

Apart from the base packages, additional packages were installed and used to conduct bioinformatic analyses with the programming language R for statistical computing.

Table 18: Additional R packages and software

R package/software	Publication
Bioconductor	Gentleman <i>et al.</i> , Genome Biol. 2004 [154]
cellHTS2	Boutros <i>et al.</i> , Genome Biol. 2006 [155]
ComBat-seq	Zhang <i>et al.</i> , NAR Genom Bioinform. 2020 [156]
ggfortify	Tang <i>et al.</i> , R J. 2016 [157]
harmony	Korsunsky <i>et al.</i> , Nat Methods. 2019 [158]
network	Butts, J. Stat. Softw. 2008 [159]
Seurat	Stuart <i>et al.</i> , Cell. 2019 [160]
tidyverse	Wickham <i>et al.</i> , J. Open Source Softw. 2019 [161]
WGCNA	Langfelder <i>et al.</i> , BMC Bioinformatics. 2008 [162]

R package	Author
aroma.light	Bengtsson [163]
data.table	Dowle <i>et al.</i> [164]
dynamicTreeCut	Langfelder <i>et al.</i> [165]
dplyr	Wickham <i>et al.</i> [166]
ggplot2	Wickham <i>et al.</i> [167]
gplots	Warnes <i>et al.</i> [168]
gprofiler2	Kolberg <i>et al.</i> [169]
hwriter	Pau [170]
pheatmap	Kolde [171]
splots	Huber <i>et al.</i> [172]
sva	Leek <i>et al.</i> [173]
xlsx	Dragulescu <i>et al.</i> [174]

3.15 Data sets

Table 19: Data sets

Data set	Publication
GSE115978	Jerby-Arnon <i>et al.</i> , Cell 2018 [152]
GSE134432	Wouters <i>et al.</i> , Nat Cell Biol. 2020 [83]
SRP068803	Zhao <i>et al.</i> , Cancer Res. 2016 [130]
TCGA TARGET GTEx	Vivian <i>et al.</i> , Nat Biotechnol. 2017 [175-177] https://gtexportal.org/home/

4 Methods

4.1 Cell culture methods

4.1.1 Culture of tumor cell lines and T cells

Wildtype and genetically modified Ma-Mel-86 were cultured in complete RPMI supplemented with the required antibiotics as described in 3.8.1. When cells reached more than 80-90% confluency, cells were washed once with DPBS and treated with 1x trypsin/EDTA for several minutes at 37 °C to detach from the culture flask. Detachment was stopped by adding complete medium and cells were centrifuged for 10 min at 500 g and room temperature (RT). Cells were subcultured twice a week.

FluT cells were thawed 6 h prior to each experiment and cultured in plain CLM at a concentration of 1×10^6 cells per ml. MART-1 T cells and TIL412 were thawed 3 days prior to each experiment and cultured in CLM supplemented with 6000 U/ml of IL-2 at a concentration of $0,6 \times 10^6$ cells per ml. 24 h before the experiment, they were IL-2 depleted and cultured in plain CLM at a concentration of $0,6 \times 10^6$ cells per ml.

All cells were cultured at 37 °C and 5 % CO₂.

4.1.2 Thawing and freezing of tumor cell lines and T cells

Tumor cell lines and T cells were thawed using their respective medium as described in 3.8.1. Culture medium was supplemented with 75 U/ml Benzonase. Cryovials with frozen cells were thawed at 37 °C. When defrosting was almost completed, prewarmed thawing medium was added dropwise to the cells and cells were transferred to 10 ml of thawing medium in a Falcon® tube. Cells were centrifuged for 10 min at 500 g and RT and were subsequently taken into culture as described in 4.1.1.

Before freezing, cells were collected and counted using a hemocytometer. Cells were pelleted for 10 min at 500 g and RT, tumor cell pellets were then directly resuspended in freezing medium. Lymphocyte pellets were resuspended in freezing medium A and freezing medium B was added dropwise in a ratio of 1:1. Cells were pipetted into cryovials which were immediately transferred to a CoolCell LX Freezing container and stored at -80 °C for at least 2 h. Afterwards, vials were moved to the liquid nitrogen tank.

4.1.3 Stable plasmid transfection of Ma-Mel-86

To stably express HLA-A2 in Ma-Mel-86 wildtype cells, a customized pcDNA3.1 plasmid was used containing the ORF encoding for HLA-A2 as well as for a geneticin (G418) resistance. Plasmid

transfection was conducted using Lipofectamine P3000 according to the manufacturer's instructions. Briefly, $2,5 \times 10^5$ cells per well were seeded into a treated 6-well plate one day before the transfection. Per well, 5 µg of plasmid DNA, 10 µl of P3000 reagent and 7,5 µl of Lipofectamine 3000 were combined in a total of 250 µl Opti-MEM™. Upon transfection, cells were incubated in RPMI supplemented with 10 % FBS in the absence of antibiotics for 20 h at 37 °C and 5 % CO₂. Then, medium was changed to complete RPMI for 24 h and finally to complete RPMI supplemented with G418 in order to restrict cell growth only to transfected cells. The correct concentration of the selection antibiotic was determined previously in a titration experiment. Transfected Ma-Mel-86a and Ma-Mel-86c were cultured in 0,4 mg/ml and 0,8 mg/ml G418, respectively, as these concentrations showed high toxicity in wildtype cells. Approximately two weeks after transfection, HLA-A2 expression was measured by flow cytometry and Ma-Mel-86 HLA-A2+ were continuously cultured in 0,9 mg/ml G418 containing culture medium to keep HLA-A2 expression stable.

The protocol for stable overexpression of immune resistance genes in Ma-Mel-86a HLA-A2+ Luc+ was similar. Here, customized pcDNA3.1 plasmids contained a gene for a hygromycin resistance and either an ORF encoding for the respective immune resistance gene or no additional gene (empty vector). 2,5 µg of plasmid DNA, 5 µl of P3000 reagent and 3,75 µl of Lipofectamine 3000 per well were used and the final culture medium contained 0,9 mg/ml G418, 0,6 µg/ml puromycin and 0,2 mg/ml hygromycin. Gene expression was measured by quantitative PCR, cells transfected with an empty vector served as a negative control.

4.1.4 Lentiviral transduction of Ma-Mel-86

For stable expression of luciferase, pre-made lentiviral transducing particles were used that expressed firefly luciferase 3 as well as green fluorescent protein (GFP) under the same CMV promotor. Additionally, the vector encodes for a puromycin resistance gene under an RSV promotor. One day before transduction $2,5 \times 10^5$ Ma-Mel-86 HLA-A2+ per well were seeded into a treated 6-well plate. On the day of transduction, medium was replaced with plain RPMI supplemented with 10 % FBS without antibiotics and tumor cells were transduced with lentivirus at a multiplicity of infection (MOI) of 1. Cells were incubated for 20 h at 37 °C and 5 % CO₂. Afterwards, medium was changed to complete RPMI supplemented with 0,9 mg/ml G418 for 24 h. Finally, medium was replaced again, and cells were continuously cultured in complete RPMI containing 0,9 mg/ml G418 and puromycin. As previously, the appropriate concentration of the selection antibiotic was determined in a titration experiment. Ma-Mel-86a and Ma-Mel-86c required a concentration of 0,6 µg/ml and 0,4 µg/ml of puromycin, respectively. Approximately two weeks after transduction, transduction efficiency and GFP expression

was measured by flow cytometry. Ma-Mel-86 HLA-A2+ Luc+ were then cultured in complete RPMI supplemented with 0,9 mg/ml G418 and 0,6 µg/ml puromycin.

4.1.5 Reverse siRNA transfection

In order to silence the gene expression of different target genes, cells were transfected with the respective siRNA. siRNA stocks were diluted with nuclease-free water to 250 nM. 200 µl of siRNA solution were pipetted into a 6-well plate. For successful transfer of siRNA into the target cells, the RNAiMAX transfection reagent was used. Per well, 4 µl RNAiMAX were added to 196 µl RPMI and the mix was incubated for 10 min at RT. Subsequently, 400 µl RPMI were added to the mix and the total volume was added to the siRNA in the 6-well plate. RNAiMAX-siRNA mix was incubated for 25 min at RT allowing for formation of siRNA-lipid complexes. Meanwhile, wildtype or genetically modified Ma-Mel-86 were collected from culture flasks. Per well, $2,5 \times 10^5$ tumor cells were diluted in 1,2 ml of complete RPMI to be added to the RNAiMAX-siRNA mix, resulting in a final siRNA concentration of 25 nM. Cells were transfected for 48 h at 37 °C and 5 % CO₂. For transfection experiments in 96-well and 384-well plates, the described protocol was adapted proportionally, maintaining a final siRNA concentration of 25 nM. In 96-well plates, 5000 Ma-Mel-86a and 10000 Ma-Mel-86c cells were seeded per well and in 384-well plates, 2000 Ma-Mel-86a and 4000 Ma-Mel-86c cells were seeded.

4.1.6 Expansion of FluT cells

Flu peptide specific T (FluT) cells were previously generated by Dr. Ayşe Nur Menevşe and frozen in aliquots for later expansion experiments [178]. Briefly, CD8+ T cells were isolated from peripheral blood mononuclear cells (PBMCs) from healthy donors. Flu peptide specific CD8+ T cells were expanded by antigen-specific expansion (ASE) in the presence of HLA-A2 matched flu peptide (GILGFVFTL), IL-2 and IL-15 as well as irradiated feeder cells [144, 178].

For efficient expansion, the rapid expansion protocol introduced by Rosenberg *et al.* was used [179]. T cells that were generated by the ASE were thawed in CLM and stained with Flu Pentamer (A*02:01 - GILGFVFTL) as described in 4.3.3 in order to identify flu peptide specific T (FluT) cells which were sorted by FACS. During the sorting, previously isolated PBMCs from three different donors were irradiated with 60 Gray and used as feeder cells for the expansion. Expansion medium (described in 3.6) was prepared and supplemented with 3000 U/ml IL-2 and 30 ng/ml anti-CD3 antibody (clone: OKT3). 1×10^6 sorted FluT cells were co-cultured with 200×10^6 irradiated PBMCs (ratio 1:200) in 150 ml of supplemented expansion medium in an upright T175 cell culture flask. Cells were incubated at 37 °C and 5 % CO₂ for 4 days. On day 5 after start of the REP, 100 ml of the medium was discarded and

replenished with fresh expansion medium supplemented with 3000 U/ml IL-2. On days 7 and 11 after start of the REP, 2/3 of the culture medium was discarded, cells were counted using a hemocytometer, and remaining medium was replenished with fresh expansion medium supplemented with 3000 U/ml to adjust the cell number to $0,6 \times 10^6$ cells per ml. REP was completed after 14 days. $0,3 \times 10^6$ FluT cells were used for a staining with Flu Pentamer to conduct flow cytometry in order to measure the proportion of flu peptide specific CD8+ T cells. Subsequently, expanded FluT cells were frozen as described in 4.1.2.

4.1.7 Polyclonal activation of T cells

Activation was performed in an untreated 6-well plate. Wells were coated with 4 µg/ml anti-CD3 antibody in 2 ml of DPBS overnight at 4°C. The plate was then washed twice with DPBS. T cells were seeded in CLM supplemented with 1 µg/ml anti-CD28 antibody at a concentration of 1×10^6 cells per ml. 1,5-4 ml of cell suspension were used per well. Cells were stimulated for 20-24 h at 37 °C and 5 % CO₂. Afterwards, T cell suspension was transferred to a Falcon® tube and centrifuged for 10 min at 500 g and RT. The supernatant was collected in a fresh tube and used directly in experiments or alternatively stored at -20 °C for future use.

4.2 Molecular biology techniques

4.2.1 Transformation of plasmids into competent bacteria

Chemically competent DH5α *E. coli* were used for transformation and amplification of overexpression plasmids encoding *TMCC3* or *SLC39A13* as well as an empty vector. 1 µg of plasmid was added to one vial of 50 µl competent bacteria suspension and the mix was incubated for 10 min on ice. After a heat-shock of 45 s at 42 °C, cells were incubated for another 2 min on ice. 200 µl of S.O.C. medium was added, and suspension was incubated for 1 h at 37 °C, shaking at 300-500 rpm. 50 µl of the bacteria suspension was transferred to an agar plate containing 100 µg/ml ampicillin and distributed by the quadrant streaking method. The plate was incubated overnight at 37 °C. The next day, a single colony was picked and inoculated in 10 ml of LB medium supplemented with 100 µg/ml ampicillin. The culture was incubated for 8 h shaking at 37 °C and 300 rpm. 100 µl of the culture was subsequently transferred to 200 ml LB medium supplemented with 100 µg/ml ampicillin and incubated overnight shaking at 37 °C and 300 rpm. Finally, bacteria from the overnight culture were harvested by centrifugation for 15 min at 4000 g. Plasmid DNA was purified using the PureLink™ HiPure Plasmid Midiprep Kit following the manufacturer's instructions. DNA was eluted in 100 µl of nuclease-free water. Concentration was determined using the NanoDrop™ 2000c Spectrophotometer. DNA was stored at -20 °C.

4.2.2 RNA isolation and reverse transcription

RNA was isolated from cell pellets of tumor cells. For pellet collection, cells were washed once with DPBS and detached with trypsin/EDTA. Complete RPMI was added, and cell suspension was centrifuged for 5 min at 500 g and 4 °C. Pellets were washed once with cold DPBS. Supernatant was discarded and pellets were stored at -20 °C or used immediately for RNA isolation.

RNA isolation was conducted using the RNeasy Mini Kit from Qiagen according to the manufacturer's instructions. RNA purity and concentration was measured using the NanoDrop™ 2000c Spectrophotometer. RNA was stored at -80 °C. Measurement of the concentration was repeated after each freeze-thaw cycle. Reverse transcription was conducted using the QuantiTect Rev. Transcription Kit from Qiagen following the manufacturer's instructions. 1 µg of previously isolated RNA was used per reaction.

4.2.3 End-point PCR

In order to determine gene expression at mRNA level, PCR was performed using the 2x MyTaq™ HS Red Mix in a reaction volume of 25µl. Per reaction, 1 µl of pre-designed primers or 500 nM self-designed primers were used. 100 ng of cDNA was used as template and water was used to reach final reaction volume. Water additionally served as contamination control in a sample without cDNA. Default PCR program was initiated for 3 min at 95 °C, followed by 35 cycles of the following three steps: denaturation for 30 s at 95 °C, primer annealing for 30 s at 60 °C and elongation for 30 s at 72 °C. PCR was completed by a final step at 72 °C for 5 min.

A 2 % agarose gel was prepared with agarose in 0,5x TAE buffer and GelRed® Nucleic Acid Gel Stain (1:12.000). 23 µl of PCR samples were loaded on the agarose gel and run at a constant voltage of 120 V. Finally, DNA bands were visualized using the ChemiDoc Imaging System.

4.2.4 Real-time quantitative PCR (qPCR)

In order to quantify mRNA expression, real-time quantitative PCR (qPCR) was performed. The QuantiFast and QuantiNova SYBR Green PCR Kits were used in a total reaction volume of 20 µl. Per reaction, 10 µl of 2x SYBR Green mix and 10 ng of cDNA were applied as a template. When pre-designed primers were used in the PCR, 1 µl was used per reaction. Self-designed primers were applied at 300 nM end concentration for each primer. Water was used to reach final reaction volume and as contamination control in a sample without cDNA. Each sample was run in triplicates and qPCR was performed using the QuantStudio™ 3 Real-Time PCR System. In subsequent analysis, expression (Ct value) of target gene was subtracted by the expression (Ct value) of the housekeeper gene *β-Actin* as

a normalization step. In order to calculate relative fold gene expression between different conditions, analysis was performed using the $2^{-\Delta\Delta Ct}$ method [180].

4.2.5 Protein isolation

Whole protein lysates were extracted from cell pellets of tumor cells. Pellet collection was performed in the same manner as described in 4.2.2. Pellets were resuspended in MILLIPLEX MAP Lysis buffer supplemented with protease and phosphatase inhibitors (each 1:100). The resulting cell lysis was performed at 4°C for 15 min under constant rotation. Afterwards, samples were centrifuged for 15 min at 17.000 g and 4 °C. Supernatant containing the proteins was collected in fresh reaction tubes. For measurement of protein concentration, the Pierce™ BCA Protein Assay Kit was used according to the manufacturer's instructions. Absorbance at a wavelength of 562 nm was measured using the Tecan Spark 10M Microplate Reader. Protein concentration was determined using a regression model of the standards provided by the kit.

4.3 Immunological techniques

4.3.1 Western blot

To determine the expression of target genes at protein level, western blot was performed. 30 µg of protein extracted in 4.2.5 were diluted in water to a total volume of 18,75 µl. 6,25 µl of NuPAGE™ LDS Sample Buffer (4X) supplemented with 10 % 2-Mercaptoethanol were added, and samples were incubated for 10 min at 70 °C. NuPAGE™ 4 - 12 %, Bis-Tris gel and 1X MOPS SDS Running Buffer were prepared in the electrophoresis chamber and 23 µl of each sample were loaded onto the gel. Electrophoresis was performed for 15 min at 80 V, then for 90 min at 120 V.

For transfer of proteins onto a nitrocellulose membrane, the Trans-Blot Turbo RTA Mini 0.2 µm Nitrocellulose Transfer Kit was used. Transfer buffer was prepared according to the manufacturer's instructions and membrane and two transfer stacks were equilibrated for 10 min in transfer buffer. After gel electrophoresis was completed, the gel was removed from the chamber and transferred to transfer buffer. One transfer stack was placed on the anode of the Trans-Blot Turbo Transfer System, followed by the membrane, the gel and the second transfer stack. A blot roller was used after each step to remove air bubbles between the components, excessive transfer buffer was removed, and the cathode was used to seal the system. Protein transfer was performed with the preprogrammed protocol "High MW" with a prolonged duration of 30 min.

After completion of the protocol, successful transfer of protein from gel onto membrane was verified by staining the nitrocellulose membrane with Ponceau S solution according to the manufacturer's instructions. Solution was removed by washing the membrane several times in TBS-T. The remaining protein in the gel was stained using Bio-Safe™ Coomassie Stain according to the manufacturer's instructions.

For the development of the membrane, it was blocked for 1,5 h at RT in 10 % milk in TBS-T or Animal-Free Blocking Solution (AFBS) for detection of total or phospho-proteins, respectively. After a washing step for 5 min in TBS-T, membrane was stained with the primary antibody (see 3.12.2) in 1 % milk in TBS-T or AFBS overnight at 4 °C. On the next day, the membrane was washed thrice for 10 min at RT in 1 % milk in TBS-T or in case phospho-protein specific antibodies were used previously, in plain TBS-T. Subsequently, the membrane was incubated for 1 h at RT with the appropriate secondary HRP-conjugated antibody diluted in 1 % milk in TBS-T or AFBS. Antibodies were diluted as described in 3.12.2. Afterwards, membrane was washed once with 1 % milk in TBS-T or plain TBS-T (phospho-proteins) for 10 min at RT. This was followed by a washing step in TBS-T and finally in TBS, each for 10 min at RT. Lastly, membrane was dried and Trident femto Western HRP Substrate was added onto the membrane and incubated for 5 min in the dark for detection of proteins. For detection of the housekeeper gene *GAPDH*, Pierce™ ECL Western Blotting Substrate was applied for 1 min due to high protein expression of the gene. Membrane was dried and protein bands were visualized using the ChemiDoc Imaging System.

4.3.2 Enzyme-linked immunosorbent assay (ELISA)

In order to measure secreted cytokines TNF α or IFN γ , cell supernatant was collected and centrifuged for 5 min at 500 g to deposit cell debris. Supernatant was transferred to an untreated microplate or reaction tubes and stored at -20 °C until the ELISA was performed. For conducting a sandwich ELISA, BD OptEIA™ ELISA kits were used according to the manufacturer's instructions. Using the Tecan Spark 10M, absorbance at a wavelength of 450 nm was measured with a reference wavelength of 570 nm. Cytokine concentration was determined by subtraction of the reference absorbance and a regression model of the standards.

4.3.3 Flow cytometry

Surface protein expression was measured by flow cytometry. Adherent tumor cells were detached with 0,02 % EDTA in DPBS. During the staining, cold buffers were used, and all steps were followed by washing steps, centrifugation for 5 min at 600 g and 4 °C and disposal of the supernatant. Up to 3×10^5

tumor or T cells were transferred to one well of a V bottom microplate and washed with FACS buffer. After centrifugation, Kiovig solution (1:20 in FACS buffer) was added and cells were incubated for 20 min on ice. Cells were washed with DPBS and stained with Zombie Aqua™/NIR™ (1:1000 in PBS) for 15 min at RT in the dark. Staining was followed by a washing step with FACS buffer. Flu Pentamer was centrifuged for 5 min at 14000 g and 4 °C to dispose protein aggregates prior to use for staining. FluT cells were stained with Flu Pentamer (1:10 in FACS buffer) for 10 min at RT in the dark and washed afterwards with FACS buffer. For the following surface protein staining, monoclonal fluorophore-conjugated antibodies were diluted in FACS buffer at a suitable concentration (see 3.12.1) and applied to the cells for 30 min on ice in the dark. Appropriate isotype antibodies with the same Ig subclass and fluorophore as the target antibody were applied in the same concentration as staining controls. After the surface staining, cells were washed twice and afterwards resuspended in FACS buffer and transferred to a FACS tube through a cell strainer. Samples were acquired with the FACSLyric™ and FluT cells were sorted using the FACS Aria™ II. Appropriate laser voltages and fluorophore signal compensation was applied by using unstained and single stain controls. Flow cytometry was subsequently analyzed using the software FlowJo. Compensation was re-applied and, if required, geometric mean was used for measurement of mean fluorescence intensity (MFI) values.

4.4 Cytotoxicity assays

4.4.1 General setup of cytotoxicity assays

Genetically modified Ma-Mel-86 were seeded to 6-well, 96-well or 384-well plates without treatment or transfected with siRNAs as described in 4.1.5. In luciferase-based cytotoxicity assays, cells were seeded into white microplates, otherwise transparent plates were used. If not stated otherwise, cells were cultured for 48h until further treatment. In cytotoxicity assays with FluT or MART-1 T cells, Ma-Mel-86 were pulsed for 1 h at 37 °C and 5 % CO₂ with 0,01 µg/ml flu peptide GILGFVFTL and 10 µg/ml MART-1 peptide ELAGIGILTV, respectively. Medium of untreated or pulsed cells was removed and melanoma cells were co-cultured with FluT, MART-1 T cells or TIL412. Alternatively, cells were treated with supernatant of polyclonally activated FluT cells or with 100 ng/ml of recombinant human TNF α , TRAIL, FasL, LT α , LIGHT or IFN γ . Cells were subsequently cultured at 37 °C and 5 % CO₂.

4.4.2 Luciferase-based readout

In luciferase-based cytotoxicity assays, Ma-Mel-86 HLA-A2+ Luc+ were treated for 20 h. Subsequently, cell supernatant was discarded, and cells were lysed with 40 µl or 20 µl of lysis buffer per well in 96-well and 384-well plates, respectively. After an incubation of 10 min at RT, equal amount of luciferase

buffer was added per well and readout was performed immediately by measuring raw luciferase units by luminescence with the Tecan Spark 10M.

4.4.3 Real-time live cell imaging

In real-time cytotoxicity assays, Incucyte® Cytotox Red Dye was added to Ma-Mel-86 HLA-A2+ Luc+ at start of treatment at a final dilution of 1:4000. Microplates were transferred into the Incucyte SX5® device for at least 20 h at 37 °C and 5 % CO₂. Every two hours, the device acquired the red signal of dying cells indicated by Cytotox Red binding to DNA due to disrupted cell membrane integrity. Additionally, GFP expression of cells was acquired. In the subsequent analysis with the Incucyte 2021C software, the area per well of the red signal was normalized to the green signal for determination of cytotoxicity.

4.5 High-throughput RNAi screens

4.5.1 Pipetting of siRNA libraries

For conduction of the high-throughput (HTP) RNAi screens, customized siRNA libraries were delivered in 384-well or 96-well microplates as stocks from Horizon Discovery. The library was designed with the first four or two columns to be empty for later addition of control siRNAs. To conduct the screens in technical duplicates with viability and cytotoxicity setting, siRNAs were diluted and distributed to white microplates using the ASSIST PLUS pipetting robot and electronic pipettes. Pipettes were programmed using the Vialab software. Nuclease-free water was used to dilute the siRNAs to a concentration of 250 nM. Microplates were kept continuously on ice or during pipetting at 4 °C using a cooling unit on the robot to prevent siRNA degradation. Until implementation of the screen, plates were stored at -20 °C.

4.5.2 Primary high-throughput RNAi screens

In the primary HTP screens, a siRNA library was used comprising 5202 genes encoding for the whole surfaceome as well as kinases and cell metabolism-related genes. Each gene was targeted by a SMARTpool of four non-overlapping siRNAs targeting the mRNA of the respective gene. The setup of the screen was adapted from Khandelwal *et al.* [143] and was conducted in 384-well microplates. The library stocks were diluted and distributed as described in 4.5.1 with the first four columns left empty. Control siRNAs were diluted with nuclease-free water to 250 nM on the day of the screen and pipetted to the first four columns of the microplate. The read-out was conducted similar to the reverse siRNA transfection and luciferase-based cytotoxicity assay as described in 4.1.5 and 4.4, respectively. Per well, 0,05 µl of RNAiMAX transfection reagent was used and 2000 Ma-Mel-86a HLA-A2+ Luc+ and 4000

Ma-Mel-86c HLA-A2+ Luc+ were seeded, respectively. Final siRNA concentration was 25 nM in a final volume of 50 μ l. After 48 h of transfection, melanoma cells were pulsed with 0,01 μ g/ml flu peptide for 1 h at 37 °C and 5 % CO₂. Subsequently, peptide containing medium was removed and Ma-Mel-86 were cultured in plain medium in the viability setting or co-cultured with FluT cells in the cytotoxicity setting. Ma-Mel-86a were co-cultured at an E:T ratio of 1:1 while Ma-Mel-86c were co-cultured at an E:T ratio of 0,5:1. After 20 h, tumor cells were lysed, and remaining luciferase activity was measured as described in 4.4.2.

4.5.3 Secondary validation high-throughput RNAi screens

The secondary validation screens were conducted similarly to the primary HTP screens described in 4.5.2. The library of the validation screen comprised 174 genes encoding for strong immunoregulatory genes identified in the primary HTP screens as well as MITF and PD-L1. As in the primary screens, each gene was targeted by a pool of four siRNAs. Additionally, each of the four siRNAs was used individually to investigate off-target effects and different effect sizes of the single siRNAs. The secondary screen was conducted in 96-well plates with the first two columns used for control siRNAs. Per well, 5000 Ma-Mel-86a HLA-A2+ Luc+ and 10000 Ma-Mel-86c HLA-A2+ Luc+ were seeded, respectively.

4.6 Bioinformatic analyses

Bioinformatic analyses were conducted using the programming language R for statistical computing. Default R packages were complemented by specific packages important for the respective analysis. If not stated otherwise, default arguments of functions were applied.

4.6.1 Analysis of high-throughput RNAi screens

The HTP RNAi screens were analyzed using the package 'CellHTS2'. Analysis was performed on viability and cytotoxicity settings of the screens in Ma-Mel-86a and Ma-Mel-86c. The function `normalizePlates(scale="multiplicative", log=TRUE)` was used in order to eliminate inter-plate variability of raw luciferase units (RLU). This was followed by assigning a z-score to each gene, estimating its effect on the viability of cells compared to all other genes. Here, the function `scoreReplicates()` was used with `sign="-"` as increased melanoma cell death mediated by FluT cells should result in positive scores, followed by `summarizeReplicates(summary="mean")`. The script of the downstream analysis was adapted from my former colleague Tillmann Michels [181]. The z-scores of viability and cytotoxicity setting were first quantile normalized using the `normalizeQuantileRank()` function of the 'aroma.light'

package. In order to identify each gene's immunomodulatory potential on FluT cell-mediated tumor cell rejection, a regression model was applied to predict the cytotoxicity score from the viability score using locally estimated scatterplot smoothing (LOESS). LOESS scores were calculated as difference between the cytotoxicity z-score and the prediction model, and all genes were ranked by their LOESS score with positive scores for genes that increased tumor cell death upon knockdown.

4.6.2 ComBat-seq

To combine different transcriptomic data sets and correct batch effects that were introduced due to varying origins of the data sets, ComBat-seq from the package 'sva' was used to adjust the data resulting in high statistical power while maintaining integer values of the raw count data. RNA-Seq data from melanoma cell lines Ma-Mel-86a and Ma-Mel-86c were publicly available via NCBI SRA (project ID SRP068803). Raw transcriptome data (FASTQ) was processed to a raw count matrix by our institute's Next-Generation Sequencing (NGS) core facility. Wouters *et al.* published RNA-Seq data on patient-derived melanoma cell lines accessible via the Gene Expression Omnibus (GSE134432). Gene names of the Wouters *et al.* data sets were converted to Ensembl IDs using the R package 'gprofiler2' in order to merge the raw count data with the Ma-Mel-86 cell lines' data set. Principle component analysis (PCA) was conducted on log₂-transformed raw count data using the `prcomp()` function before and after the ComBat-seq batch effect correction to investigate similarities of the different melanoma cell lines according to dataset and melanoma phenotype as well as efficiency of batch effect correction. PCA was visualized with the `autoplot()` function of the 'ggfortify' package.

4.6.3 Weighted gene co-expression network analysis (WGCNA)

To identify co-expression modules from a correlation matrix of RNA-Seq data, the package 'WGCNA' was used together with 'dynamicTreeCut'. As genes with a positive correlation to each other should be assigned to a cluster, signed networks were generated. If required, the analysis was conducted on a specific sample subset like malignant cells in the Jerby-Arnon *et al.* single cell RNA-Seq data set. The total list of genes in the data set was reduced to a list of 265 validated immune resistance genes and controls. Normalized count or TPM expression data was log₂-transformed and genes that didn't show expression in any sample were excluded. In WGCNA, a correlation matrix is transformed into a weighted adjacency matrix by applying soft thresholding. A power value is applied to the correlation matrix to emphasize on strong correlations. The function `pickSoftThreshold(verbose = 5, networkType="signed")` was used to determine the appropriate power value to obtain high similarity and scale-free topology. If a network is scale-free, a few genes interact with a large number of other genes while the majority wouldn't have high connectivity, which is usually the case in biological

networks. Taking the power value into account, the adjacency matrix was generated with the function `adjacency(type = "signed")`. To cluster the genes from the adjacency matrix, a proximity measure was applied, resulting in a topological overlap matrix (TOM) to minimize noise and spurious associations. The dissimilarity TOM was then used for hierarchical clustering with the function `hclust(method="average")` to finally create a dendrogram. With the function `cutreeDynamic(method = "hybrid", deepSplit = 2, pamStage = FALSE, minClusterSize = 3)`, genes were assigned to modules of at least three genes. Resulting clusters with module eigengenes, representing the general expression of the majority of a cluster, were correlated to each other and to marker genes as well as external traits. Clusters with a module eigengene correlation coefficient of 0,75 were merged. The cluster dendrogram was visualized with the function `plotDendroAndColors()` while the correlation heatmaps were generated using the function `plotEigengeneNetworks(plotAdjacency = F)`.

4.6.4 Generation of heatmaps

Apart from the WGCNA and Seurat analysis, heatmaps were generated with the package 'pheatmap'. Data matrices were log₂-transformed with samples as rows and genes as columns. If required, genes were ordered from previous WGCNA by using `setcolorder()` from the package 'data.table'. Samples were either ordered manually or by hierarchical clustering by setting `cluster_rows=T` in the `pheatmap()` function. In analyses comparing the expression of immune resistance genes with statistical tests, sample groups were defined and `wilcox.test()` was applied to implement a Mann–Whitney U test in a gene-wise manner. Mann-Whitney U test was chosen due to the assumption that gene expression did not follow normal distribution as some genes showed expression only in a subset of samples. The p-values were adjusted for multiple testing using `p.adjust(method="fdr")` and genes were ordered by their adjusted p-value.

4.6.5 Seurat

Single cell RNA-Seq analysis was performed with the specialized package 'Seurat' to identify cell types and different subsets of malignant cells in patient melanomas. Raw count data from the Jerby-Arnon *et al.* data set was used to create a Seurat object with `CreateSeuratObject(min.cells = 3, min.features = 100)`. Quality control was performed and cells were filtered with `subset(subset = nFeature_RNA > 200 & nFeature_RNA < 10000 & nCount_RNA < 2e6)`. Data was subsequently normalized and scaled and the top 2000 variable features were integrated to perform PCA. The function `RunHarmony()` from the package 'harmony' was used to remove patient-specific batch effects. Subsequently, cells were clustered with the functions `FindNeighbors(reduction = "harmony", dims = 1:30)` and `FindClusters(resolution = 0.5)` followed by `RunUMAP(reduction = "harmony", dims = 1:30)` to perform

Uniform Manifold Approximation and Projection for Dimension Reduction (UMAP). UMAP plots were visualized using the function `DimPlot(reduction = "umap")`. In order to assign cell type identities to the clusters, the expression of marker genes in the different clusters was visually investigated with the `DotPlot()` function. According to marker gene expression, clusters were relabeled, merged or excluded. To identify immune resistance genes as cluster marker genes the function `FindAllMarkers(only.pos = TRUE, min.pct = 0.25, logfc.threshold = 0.25)` was applied and the resulting list of marker genes was intersected with the list of immune resistance genes. Expression of genes was visualized with the functions `DotPlot()` or with averaged expression levels by `DoHeatmap()`.

4.7 Statistical evaluation

To measure statistical significances between different conditions in the experiments, the software GraphPad Prism 9 was used. The choice of the statistical test was dependent on the data that was compared in the test. In single experiments or representative data an unpaired two-tailed t-test was chosen. For compiled data, a two-tailed paired t-test between conditions that were not normalized to each other, and a two-tailed ratio paired t-test for normalized conditions were used. In case the hypothesis implied a clear reduction in measured values, the tests were changed from two-tailed to one-tailed t-tests. In all cases, p-values below 0,05 were considered significant with * $p < 0,05$, ** $p < 0,01$, *** $p < 0,001$ and **** $p < 0,0001$.

5 Results

5.1 Characterization of melanoma cell lines

5.1.1 Selection of melanoma cell lines

MITF, as the master regulator in melanocytes, plays an important role in cell plasticity and melanomagenesis [70]. In order to identify novel immune resistance genes two melanoma cell lines with different MITF expression levels were selected. In collaboration with the Department of Dermatology from the University Hospital in Essen, the previously characterized melanoma cell lines Ma-Mel-86a (MITF^{low}) and Ma-Mel-86c (MITF^{high}) were chosen [130]. Ma-Mel-86a and -86c are cell lines that were derived from the same melanoma patient originating from different lymph node lesions two months (Ma-Mel-86a) and three years (Ma-Mel-86c) after diagnosis, respectively. The melanoma patient received several immunotherapies including different peptide-based vaccines as well as IFN α and tumor lysate loaded dendritic cell vaccine. Immunotherapies and surgery led to a 3-year disease-free period, yet the patient deceased rapidly after melanoma recurrence [130].

In order to validate differences in MITF expression, cDNA and protein lysates of the Ma-Mel-86 pair were generated and MITF mRNA and protein expression was measured by PCR and western blot (Figure 8). Quantitative PCR confirmed that *MITF* expression on the mRNA level was reduced in Ma-Mel-86a by more than 95 % compared to Ma-Mel-86c (Figure 8B). Western blot results showed that MITF protein expression was only detected in Ma-Mel-86c (Figure 8C).

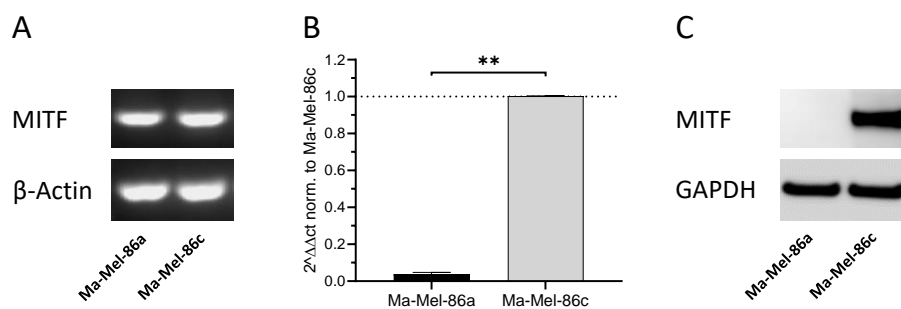


Figure 8: Differential expression of MITF between Ma-Mel-86a and Ma-Mel-86c cells.

PCR and western blot analysis to measure the expression of MITF in Ma-Mel-86a and Ma-Mel-86c. Ma-Mel-86 were lysed for RNA and protein isolation. (A-B) RNA was reversely transcribed into cDNA and gene expression of *MITF* was measured by (A) conventional or (B) quantitative real-time PCR (qPCR). Expression of Actin-beta was measured as reference gene and used for normalization of *MITF* expression in the qPCR. *MITF* expression in Ma-Mel-86a is normalized to the *MITF* expression in Ma-Mel-86c. Bars represent the mean of technical replicates and error bars indicate standard deviation. Significance between both cell lines was calculated by applying an unpaired two-tailed t-test (**p<0,01). (C) Western Blot was performed to analyze MITF protein expression. GAPDH expression was acquired as reference gene. (B-C) Representative data of three independent experiments. Verena Babl contributed to the generation of the data as a Master's student under my co-supervision.

Ma-Mel-86 were characterized to be negative for HLA-A2 (Figure 9, left panel). To make both cell lines eligible for various co-culture and cytotoxicity experiments, cells were stably transfected with HLA-A2 on which selected peptides could be presented to cytotoxic T cells. After transfection, flow cytometry analysis showed HLA-A2 expression in 98 % and 78 % of cells in Ma-Mel-86a and -86c, respectively (Figure 9). For luciferase-based cytotoxicity assays, Ma-Mel-86 HLA-A2+ cells were transduced with a lentivirus expressing firefly luciferase. Under the same CMV promotor *GFP* was co-expressed to determine the transduction efficiency by flow cytometry. After transduction, GFP and therefore luciferase was expressed by 100 % of Ma-Mel-86a HLA-A2+ cells and 91 % of Ma-Mel-86c HLA-A2+ cells (Figure 9). Furthermore, HLA-A2 expression increased in Ma-Mel-86c to 92 %, making both Ma-Mel-86 HLA-A2+ Luc+ cell lines positive for both HLA-A2 and luciferase more than 90 %.

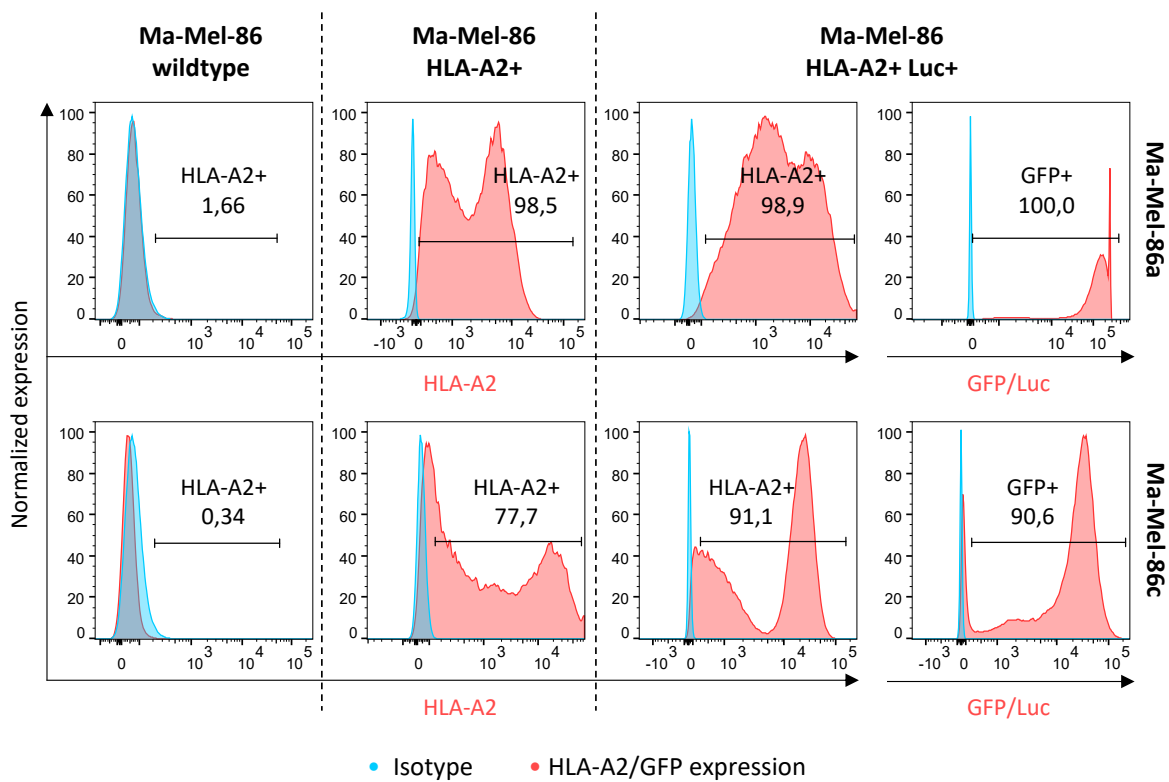


Figure 9: Expression of HLA-A2 and GFP on Ma-Mel-86a and Ma-Mel-86c before and after transfection and transduction of cells.

Flow cytometry analysis to measure the expression of HLA-A2 and GFP in wild-type Ma-Mel-86, HLA-A2 transfected Ma-Mel-86 and luciferase/GFP transduced Ma-Mel-86 HLA-A2+ cells. Melanoma cells were stained with isotype or HLA-A2 specific antibodies. GFP expression was acquired simultaneously. Isotype control for GFP were Ma-Mel-86 HLA-A2+ GFP negative cells. The blue histogram represents the isotype and the red one the expression of HLA-A2 and GFP, respectively. Gates indicate the percentage of cells expressing HLA-A2 and GFP, respectively.

5.1.2 Level of resistance of MITF^{low} and MITF^{high} melanoma cells

A decrease of MITF activity is associated with a more immune resistant phenotype in melanoma patients [88]. Furthermore, MITF^{low} cells show reduced expression of melanoma-associated antigens

such as MART-1 and gp100. To investigate whether Ma-Mel-86 shows a different level of resistance to T cell-mediated melanoma cell killing, the cell line pair was first co-cultured with CD8⁺ melanoma specific tumor infiltrating lymphocytes (Figure 10). TIL412 which show specificity against MART-1 and gp100 as well as MART-1 specific TILs were used for the experiment (Figure 10A&B). The cytotoxicity assays showed that Ma-Mel-86c (MITF^{high}) were strongly killed upon T cell encounter with increasing tumor cell death in higher E:T ratios. Here, almost 70 % of tumor cells could be lysed by MART-1 T cells. Ma-Mel-86a (MITF^{low}) were neither killed by TIL412 nor MART-1 T cells.

Additionally, MART-1 T cells and flu peptide specific CD8⁺ T (FluT) cells in the presence of their respective antigenic peptide as well as supernatant of polyclonally activated FluT cells were used to induce cell death (Figure 10C). Altogether, the results showed a higher tumor cell death of the MITF^{high} cell line Ma-Mel-86c (up to 90 %) compared to Ma-Mel-86a (55%). PD-L1 is a well characterized immune checkpoint molecule (ICM), expressed on cancer cells to abrogate T cell receptor signaling and decrease T cell function [51]. Flow cytometry analyses showed expression of PD-L1 in both cell lines with higher expression in Ma-Mel-86a (Figure 10D, left panel). To determine whether PD-L1 protects Ma-Mel-86 with different MITF status, melanoma cells were co-cultured with FluT cells upon PD-L1 silencing. Downregulation of PD-L1 increased tumor cell rejection by FluT cells in MITF^{high} Ma-Mel-86c, but not in MITF^{low} Ma-Mel-86a cells (Figure 10D, right panel). Taken together, Ma-Mel-86c showed increased susceptibility to T cell-mediated tumor cell lysis and increased cell death upon knockdown of classical ICM PD-L1 in contrast to Ma-Mel-86a.

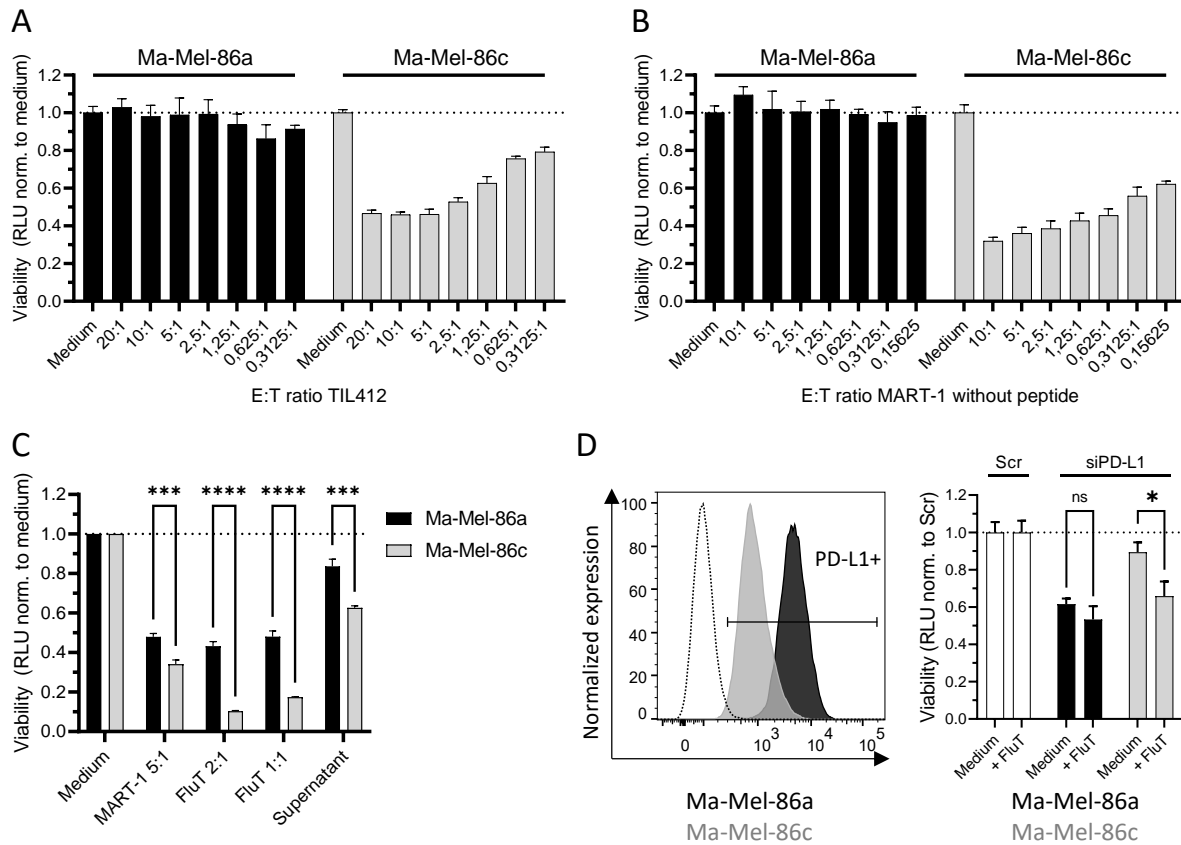


Figure 10: Differential apoptosis sensitivity of Ma-Mel-86a and Ma-Mel-86c and impact of PD-L1 knockdown. (A-C) Luciferase-based cytotoxicity assay to measure the susceptibility of Ma-Mel-86 to CD8⁺ T cells and supernatant of polyclonally activated T cells. Ma-Mel-86 HLA-A2⁺ Luc⁺ were cultured in plain medium, co-cultured with different T cell sources or treated with supernatant. After 20 h of (co-)culture/treatment, cells were lysed, and remaining luciferase activity was measured by luminescence. Raw luciferase units (RLU) were normalized to RLU of cells cultured in plain medium. (A-B) Melanoma cells were co-cultured with melanoma specific T cell sources (A) TIL412 or (B) MART-1 specific T cells in different effector to target (E:T) ratios. (C) Ma-Mel-86 were pulsed with MART-1 or flu peptide for 1 h and subsequently co-cultured with MART-1 specific T cells or flu peptide specific T cells in different E:T ratios or treated with supernatant of FluT cells that were polyclonally activated for 24 h. (D) (Left panel) Flow cytometry analysis to measure the expression of PD-L1 expression on Ma-Mel-86. Cells were stained with isotype or antigen-specific antibodies. Grey histogram represents PD-L1 expression on Ma-Mel-86c and the black one the PD-L1 expression on Ma-Mel-86a while the isotype control is represented by the dashed line. (Right panel) Luciferase-based cytotoxicity. Ma-Mel-86 HLA-A2⁺ Luc⁺ were reversely transfected with a non-targeting Scr or PD-L1 targeting siRNA for 48 h. Cells were pulsed with flu peptide for 1 h and subsequently, melanoma cells were either cultured in plain medium or co-cultured with FluT cells for 20 h. RLU were normalized to the Scr control. (C-D) Representative data of $n \geq 2$. Bars represent the mean of technical replicates + standard deviation. Significances between both cell lines were calculated by applying an unpaired two-tailed t-test (* $p < 0,05$, ** $p < 0,01$, *** $p < 0,001$, **** $p < 0,0001$, ns = not significant).

5.1.3 Expression of apoptosis inducing ligands by CD8⁺ T cells and their corresponding receptors on the tumor cells

Upon target cell encounter, CD8⁺ T cells secrete multiple mediators such as TNF α , TRAIL and IFN γ to induce apoptosis in the tumor cells [20, 25]. As Ma-Mel-86 were killed upon co-culture with cytotoxic T cells or treatment with supernatant of polyclonally activated T cells, expression of apoptosis inducing

ligands by T cells as well as the expression of their corresponding receptors on the tumor cells were investigated by flow cytometry (Figure 11-13). Figure 2 in chapter 1.1.3 illustrates ligands and their cognate receptors. As those death ligands are mainly induced after activation of T cells [20, 25], ligand expression was compared between non-activated and polyclonally activated T cells. Flow cytometry analysis showed that non-activated T cells did not show expression of cytotoxic ligands (data not shown). However, polyclonally activated FluT cells, MART-1 T cells and TIL412 expressed all tested death inducing ligands TRAIL, FasL, Lymphotoxin- α (LT α) and LIGHT (Figure 11). FluT cells showed the highest surface expression of all four ligands ($\geq 50\%$). Additionally, ELISA was performed to determine secreted levels of TNF α and IFN γ in the T cell supernatant. Both TNF α and IFN γ were secreted only upon activation by all tested polyclonally activated T cell sources (Figure 12).

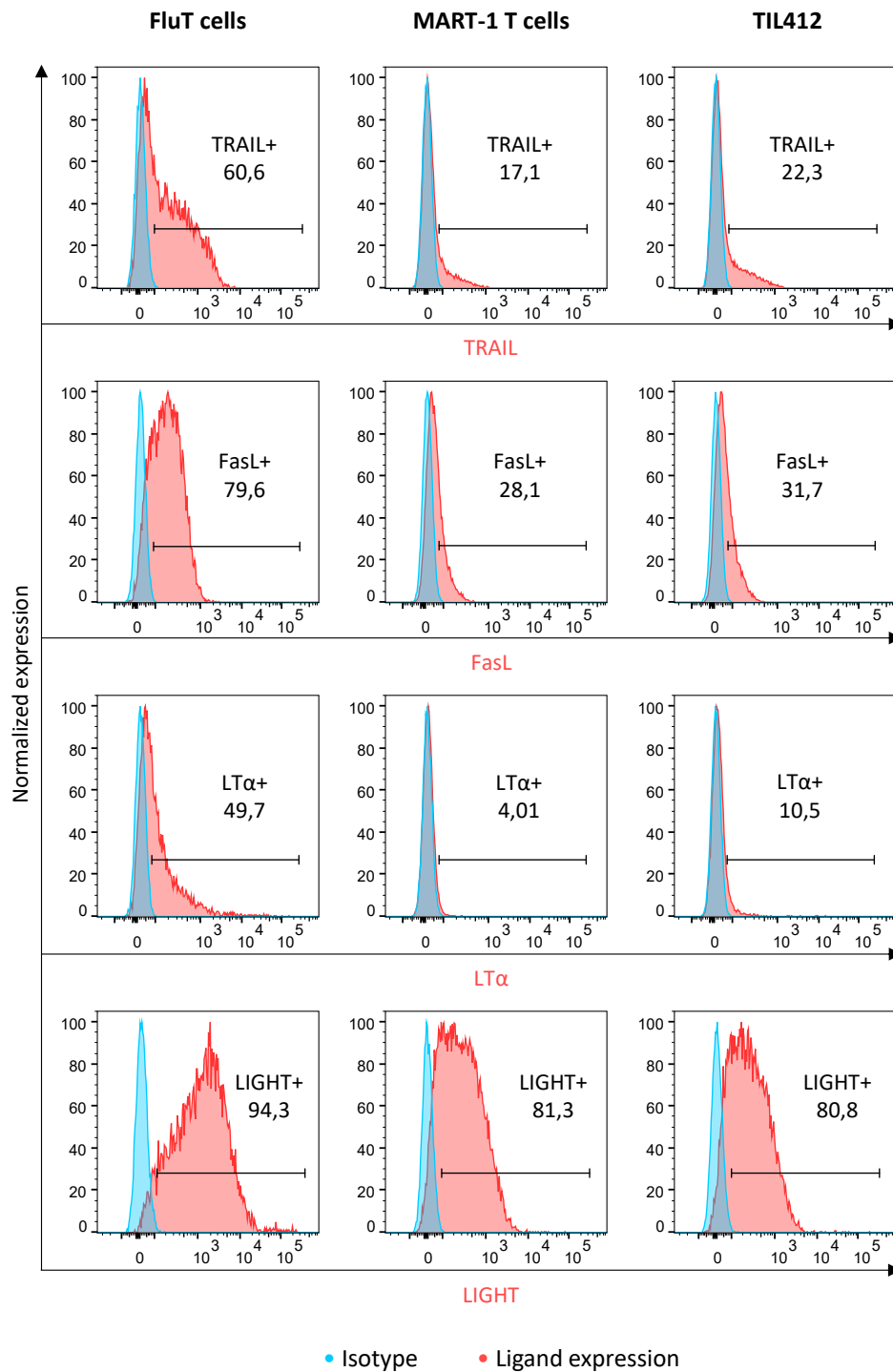


Figure 11: Expression of cell death inducing ligands on different T cell sources.

Flow cytometry analysis to measure the expression of TRAIL, FasL, LTα and LIGHT on polyclonally activated FluT cells (left panel), MART-1 T cells (middle panel) and TIL412 (right panel). T cells were stained with isotype or antigen-specific antibodies. The blue histogram represents the isotype and the red one the surface expression of the ligand. Indicated gates describe the percentage of cells expressing the respective ligand.

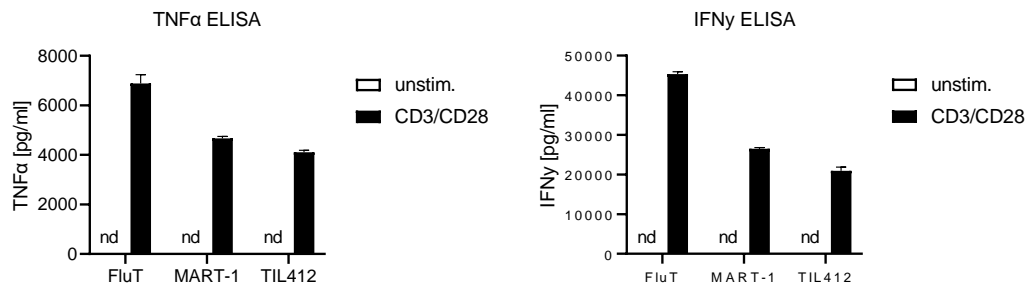


Figure 12: Secretion of TNF α and IFN γ by different T cell sources.

Sandwich ELISA to detect secreted TNF α and IFN γ in the supernatant of FluT cells, MART-1 T cells and TIL412 that were either unstimulated or polyclonally activated for 24 h. Concentration of cytokines was measured by absorbance. Bars represent the mean of technical replicates + standard deviation.

Flow cytometry analysis of the tumor cells to investigate death receptor expression showed expression of DR5/TRAILR2, TNFR1, FAS, IFN γ R1, LT- β R and HVEM in both melanoma cell lines, Ma-Mel-86a and -86c (Figure 13). Both cell lines were negative for DR4/TRAILR1 as well as TNFR2. IFN γ R1 was expressed at similar levels while HVEM was higher expressed in the MITF^{high} cell line Ma-Mel-86c. The remaining receptors showed higher expression on the MITF^{low} cell line Ma-Mel-86a.

In summary, all tested activated T cells were able to express or secrete cytotoxic ligands while both melanoma cell lines expressed most apoptosis-related receptors to a high degree which did not correlate to the susceptibility to T cell-mediated tumor cell rejection.

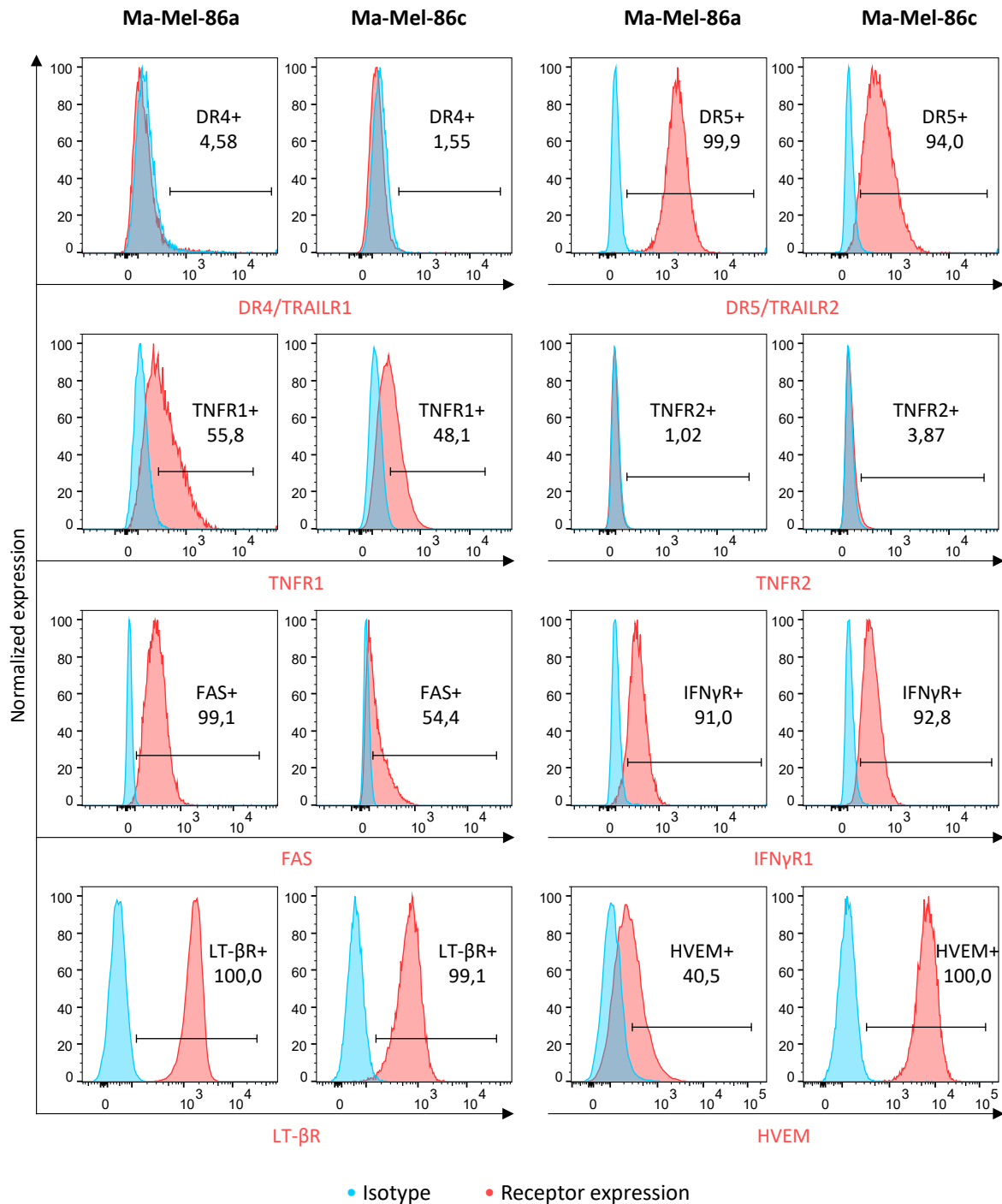


Figure 13: Expression of death receptors on Ma-Mel-86a and Ma-Mel-86c.

Flow cytometry analysis to measure the expression of DR4/TRAILR1, DR5/TRAILR2, TNFR1, TNFR2, FAS, IFN γ R1, LT- β R and HVEM on Ma-Mel-86 cells. Cells were stained with isotype or antigen-specific antibodies. The blue histogram represents the isotype and the red one the expression of the receptor. Gates indicate the percentage of cells expressing the respective receptor.

5.1.4 Primary resistance of Ma-Mel-86 to death receptor ligands

To investigate to which extent single agents of the supernatant can induce apoptosis in the tumor cells and to determine if there are differences in the capacities between the ligands to induce tumor cell death, Ma-Mel-86a and -86c were treated with TRAIL, TNF α , FasL, LT α , LIGHT as well as IFN γ

individually (Figure 14). The results showed that neither TRAIL, TNF α , FasL, LT α nor LIGHT could induce apoptosis in the tumor cells. Only when the cells were treated with IFN γ , tumor cell death was observed in both cell lines. MITF^{high} melanoma cell line Ma-Mel-86c showed 38 % viability reduction while 25 % of Ma-Mel-86a died, similar to previous results in which co-culture with T cells and treatment with supernatant showed higher impact in Ma-Mel-86c (Figure 14). In summary, Ma-Mel-86 showed primary resistance to death receptor ligands but not to IFN γ .

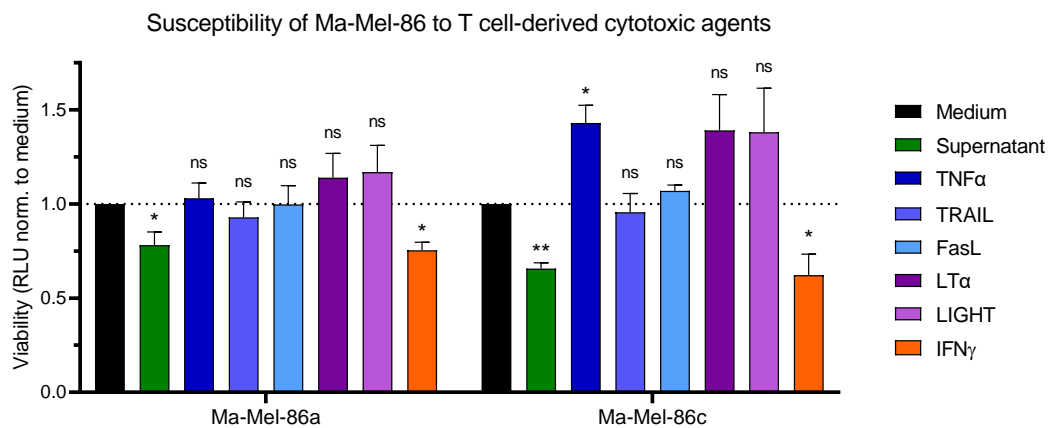


Figure 14: Susceptibility of Ma-Mel-86 to T cell-derived cytotoxic agents.

Luciferase-based cytotoxicity assay to measure the susceptibility of Ma-Mel-86 HLA-A2+ Luc+ to supernatant of FluT cells that were polyclonally activated for 24 h or single ligands expressed by T cells. After 20 h of treatment, cells were lysed, and remaining luciferase activity was measured by luminescence. Raw luciferase units (RLU) were normalized to RLU of untreated cells cultured in plain medium. Bars represent the mean + standard deviation of three independent experiments. Significances between individual treatment to medium were calculated by applying a two-tailed ratio paired t-test (*p<0,05, **p<0,01, ns = not significant).

5.2 Setup of a high-throughput RNAi screen

In order to identify novel immune resistance genes in Ma-Mel-86, small interfering RNA (siRNA)-based high-throughput (HTP) RNA interference (RNAi) screens were performed. The original method of the screen was established in our group by Dr. Nisit Khandelwal [143]. Dr. Ayşe Nur Menevşe established a protocol in our group to generate and expand efficiently flu antigen specific T cells (FluT cells) as effector T cells from peripheral blood mononuclear cells (PBMCs) of HLA-A2+ healthy donors [144]. To successfully conduct the HTP RNAi screen, tumor cells stably expressed HLA-A2 for HLA-A2-matched flu peptide antigen presentation to FluT cells as well as luciferase to perform a reporter gene-based readout after co-culture of tumor and T cells.

Figure 15 shows a sketch of the HTP screen set-up. Briefly, Ma-Mel-86 HLA-A2+ Luc+ were reversely transfected with siRNAs. After 48 h of transfection, cells were pulsed for 1 h with the flu peptide GILGFVFTL that originates from the Influenza M1 protein. Subsequently, Ma-Mel-86a were co-cultured with flu specific T cells (FluT). Apart from this co-culture setting called the cytotoxicity setting, there is also a viability setting of tumor cell culture in plain medium without FluT cells to determine the effect

on the tumor cell viability by the siRNA transfection and/or downregulation of the target gene *per se*. The immunomodulatory effect of a gene is therefore apparent if there is a higher tumor cell death in the cytotoxicity setting compared to the viability setting, each compared to a non-targeting siRNA control. After 20 h of co-culture, the remaining tumor cells were lysed, and luciferase activity was measured which is proportional to the remaining number of Ma-Mel-86. Immunomodulatory genes would ideally not show an impact on the viability of the cells but increase tumor cells lysis upon co-culture with FluT cells represented by lower luciferase activity.

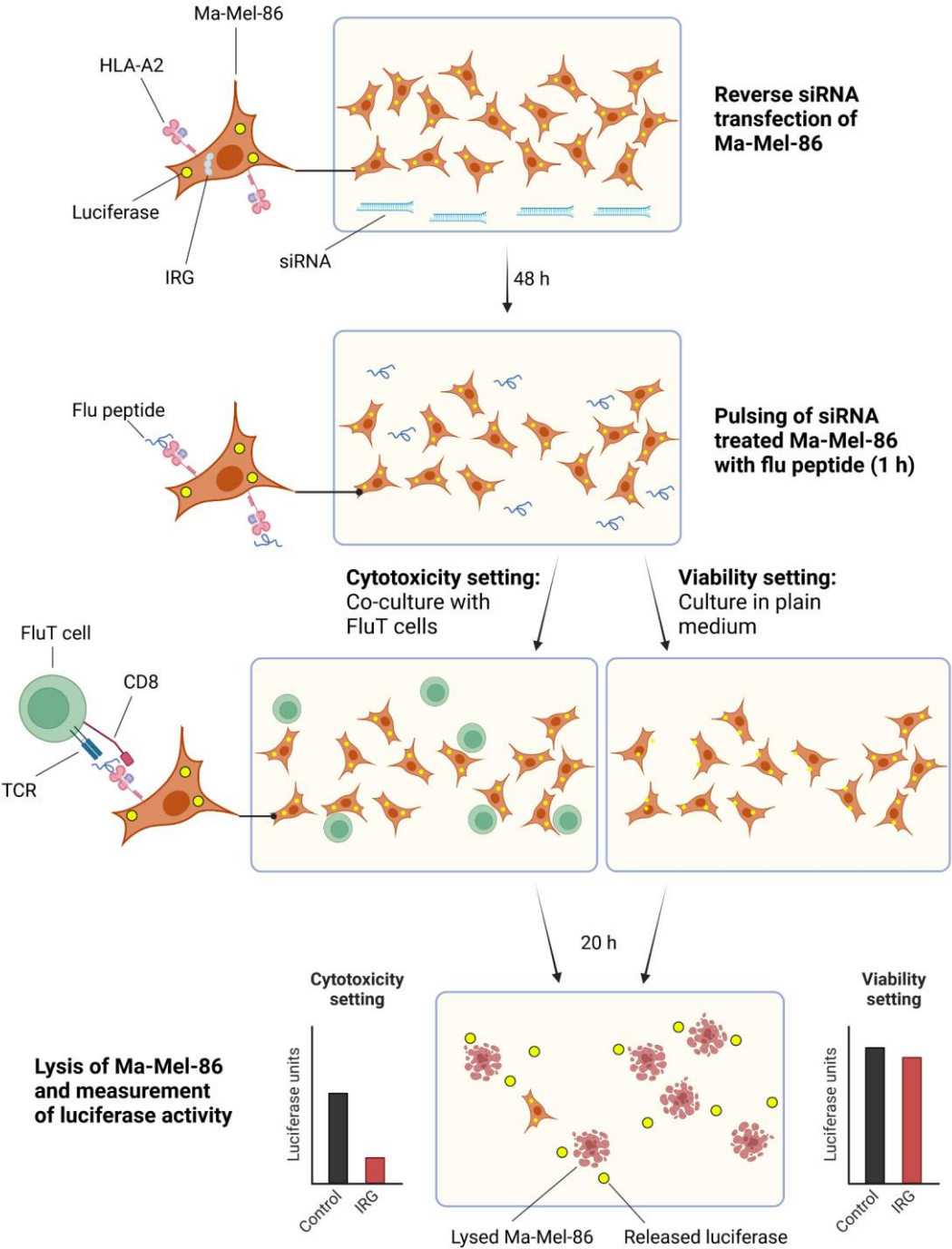


Figure 15: Experimental set-up of the high-throughput RNAi screens and luciferase-based cytotoxicity assays.

Ma-Mel-86 HLA-A2+ Luc+ cells were reversely transfected with siRNAs for 48 h. Tumor cells were pulsed with HLA-A2-matched flu peptide for 1 h and subsequently either cultured in plain medium (viability setting) or co-cultured with flu specific T (FluT) cells (cytotoxicity setting) for 20 h. Finally, remaining Ma-Mel-86 HLA-A2+ Luc+ were lysed and remaining luciferase activity was measured by luminescence. Created with BioRender.com [32].

5.2.1 Rapid expansion of flu specific T cells

As mentioned before, Dr. Ayşe Nur Menevşe established an antigen-specific expansion protocol in our group to generate flu specific T cells and subsequently expand them using the rapid expansion protocol (REP) previously introduced by Rosenberg *et al.* [179]. Briefly, CD8+ T cells were isolated from peripheral blood mononuclear cells (PBMCs) of HLA-A2+ healthy donors and antigen-specifically expanded in the presence of flu peptide for two weeks (Data not shown). In order to increase the specific population and the number of CD8+ flu antigen specific T cells, antigen specifically expanded FluT were FACS-sorted by pentamer staining. Sorted cells (1×10^6) were expanded using the REP in which cells were cultured in the presence of high IL-2, anti-CD3 antibody and irradiated feeder cells from three different healthy donors. After 14 days, cells were expanded 120-fold and flow cytometry analysis showed a proportion of 82 % of FluT cells (Figure 16).

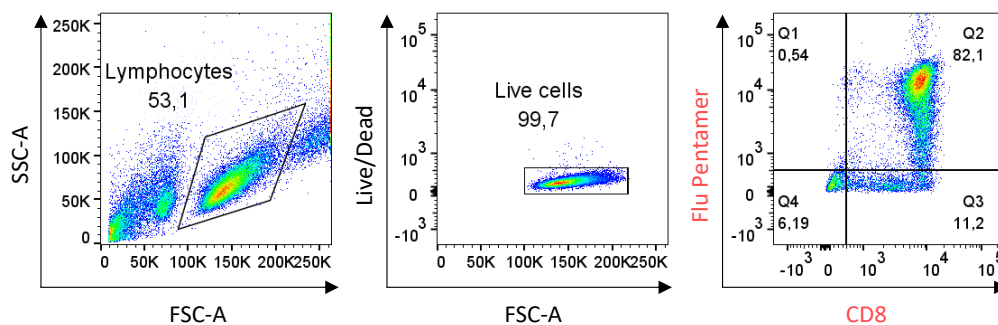


Figure 16: Specificity of FluT cells after rapid expansion.

Flow cytometry analysis to measure the proportion of flu specific CD8+ T cells after 14 days of expansion with the rapid expansion protocol. Cells were stained with anti-CD8 antibody and Flu pentamer. All acquired events were gated on lymphocytes and live cells to determine the proportion of CD8+ flu specific T cells.

5.2.2 Optimization of siRNA transfection, flu peptide concentration and effector to target ratio for Ma-Mel-86

To investigate the optimal duration of siRNA-mediated knockdown of target genes in Ma-Mel-86, melanoma cells were transfected with siRNAs targeting Programmed Cell Death 1 Ligand 1 (*PD-L1/CD274*) and Salt-Inducible Kinase (*SIK3*) for 48 h and 72 h. Non-targeting siRNA controls (Scr 2-4) were used additionally in which no alteration of gene expression was expected. Gene expression of *PD-L1* and *SIK3* was evaluated by quantitative PCR after the described time points. Normalization to non-transfected cells (Mock) showed a stronger downregulation of *PD-L1* and *SIK3* after 48 h (85-94

%) compared to 72 h (24-76 %) (Figure 17A). Also the Scr controls had less impact on the expression of *PD-L1* and *SIK3* after a transfection period of 48 h.

Co-culture of Ma-Mel-86 HLA-A2+ Luc+ with FluT require pulsing of melanoma cells with flu peptide for recognition of tumor cells by FluT. In order to investigate the optimal co-culture settings, a cytotoxicity assay was performed in which tumor cells were pulsed with different flu peptide concentrations (Figure 17B). The peptide concentrations 0.01, 0.001 and 0.0001 µg/ml were tested for both melanoma cell lines Ma-Mel-86a HLA-A2+ Luc+ and -86c HLA-A2+ Luc+ at an E:T ratio of 2:1. The results of the luciferase-based readout confirmed that tumor cells were only effectively killed when peptide was present (Figure 17B). The peptide concentration 0.0001 µg/ml didn't induce a strong tumor cell rejection by FluT cells while 0.01 and 0.001 µg/ml both led to tumor cell lysis. I decided to use the higher concentration of 0.01 µg/ml for future experiments and rather adapt the E:T ratios for determination of the degree of the tumor cell death.

Consequently, I aimed to find an appropriate effector to target (E:T) ratio for both melanoma cell lines. The E:T ratios 2:1, 1:1 and 0.5:1 for Ma-Mel-86a HLA-A2+ Luc+ and 1:1, 0.5:1 and 0.25:1 for Ma-Mel-86c HLA-A2+ Luc+ were used in a cytotoxicity assay. The results indicated that increasing E:T ratios have higher impact in the MITF^{high} melanoma cell line Ma-Mel-86c (Figure 17C). While all E:T ratios resulted in a tumor cell death of approximately 50 % in Ma-Mel-86a, tumor cell lysis was increased from 65 to 90 % in Ma-Mel-86c with growing E:T ratios. The ratios 0.5:1 and 1:1 were chosen for Ma-Mel-86c and Ma-Mel-86a, respectively.

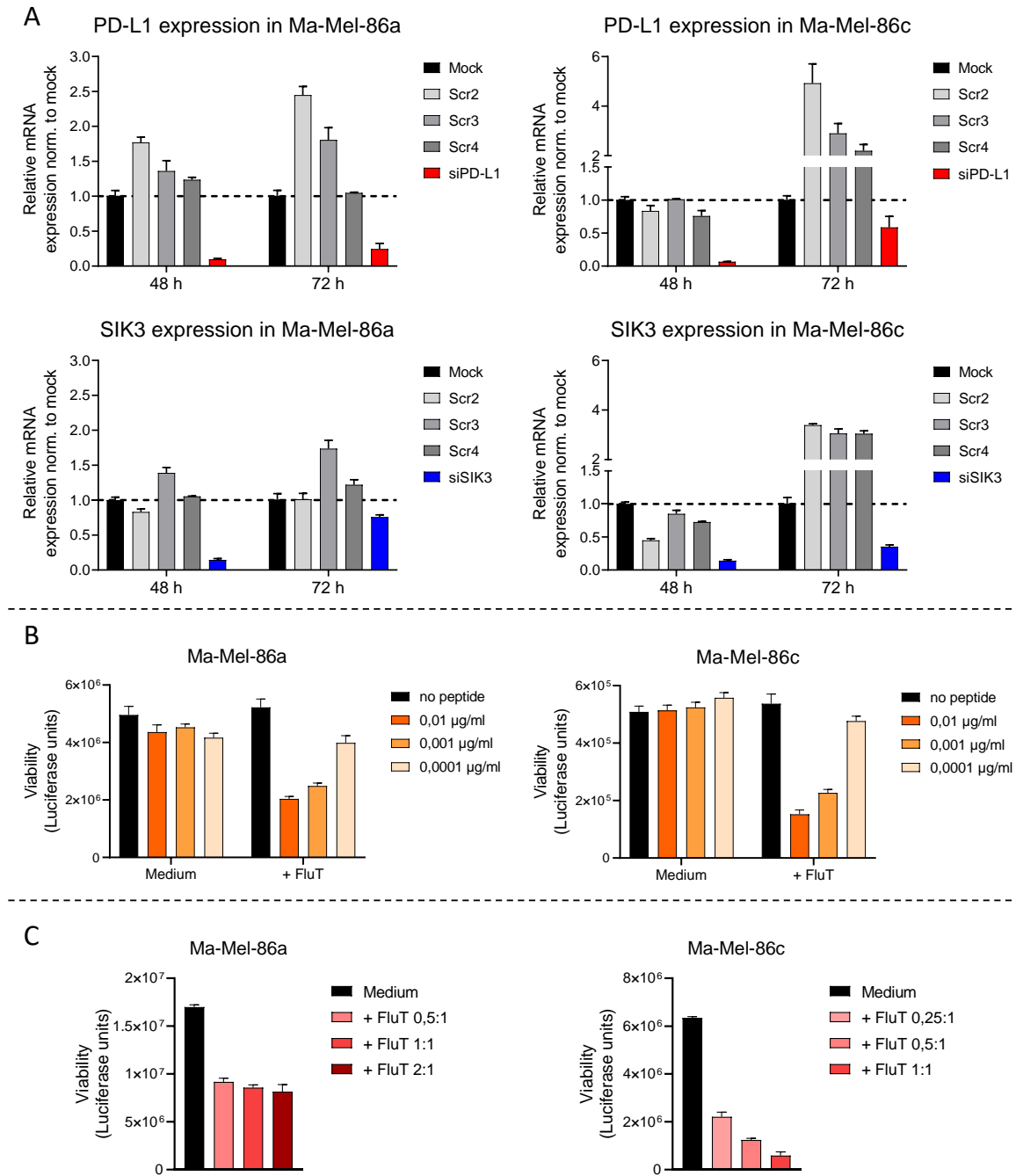


Figure 17: Optimization of transfection and co-culture settings for the high-throughput RNAi screens and cytotoxicity assays.

(A) Ma-Mel-86 were transfected with Scr2/3/4 or a pool of four *PD-L1* or single s1 *SIK3* siRNAs for 48 or 72 h. Additionally, melanoma cells were cultured without transfection (mock control). Cells were lysed for RNA isolation and RNA was reversely transcribed to cDNA. Quantitative real-time PCR was performed to measure gene expression of *PD-L1* and *SIK3*. Expression of Actin-beta was measured as reference gene and used for normalization of *PD-L1* and *SIK3*. Gene expression was normalized to expression levels of the mock control. Bars represent the mean of technical replicates + standard deviation. **(B)** Ma-Mel-86 HLA-A2+ Luc+ were pulsed with different concentrations of flu peptide for 1 h or cultured in the absence of flu peptide. Subsequently, melanoma cells were either cultured in plain medium or co-cultured with FluT cells in a 2:1 effector to target (E:T) ratio for 20 h. Cells were lysed, and remaining luciferase activity was measured by luminescence. Bars represent the mean of technical replicates + standard deviation. **(C)** Ma-Mel-86 HLA-A2+ Luc+ were pulsed with flu peptide for 1 h and subsequently, melanoma cells were either cultured in plain medium or co-cultured with FluT cells in different E:T ratios for 20 h. Cells were lysed, and remaining luciferase activity was measured by luminescence. Bars represent the mean of technical replicates + standard deviation.

5.2.3 Selection of controls for Ma-Mel-86

The surface molecule PD-L1 is expressed by tumor cells to shift T cells expressing Programmed Cell Death 1 (PD-1) into an exhausted cell state. Both molecules are used as targets in antibody-based immunotherapies [105]. In the HTP screens, I aimed to identify novel immune resistance genes that exert stronger immune resistance compared to already established immune checkpoint genes like PD-L1. Immunoregulatory genes identified by our group or described in literature that increase T cell-mediated rejection upon downregulation are used as positive controls and help to interpret the outcome of the screen and the impact of novel genes (Figure 18).

Scrambled siRNA controls (Scr2-4) do not target any gene and were used as negative controls in the kill assays and the HTP screens showing a similar phenotype as non-transfected wild-type cells (Mock). The Scr controls represent the condition to which the impacts of the gene knockdowns will be normalized to. Finally, siRNAs targeting survival genes such as Ubiquitin C (*UBC*), or the commercially available 'Cell Death' siRNA cocktail were used. These indicated on the one hand the transfection efficiency but also helped to better assess the viability impact of the siRNA transfection or gene knockdown.

The results of the viability setting in the assay without FluT cell co-culture showed that the MITF^{low} melanoma cell line Ma-Mel-86a was more susceptible to cell death after siRNA transfection compared to Ma-Mel-86c (Figure 18). Reduced cell viability was measured when *SIK3* s1 siRNA or a pool of four individual *PD-L1* or Calcium/Calmodulin Dependent Protein Kinase ID (*CAMK1D*) siRNAs was used. In agreement to that, using siRNA for *UBC* or Cell Death resulted almost in a complete eradication of Ma-Mel-86a but only a fraction of around 35-50 % of Ma-Mel-86c.

With regard to the immunomodulatory effects the results showed that there were differences for the MITF^{low} and MITF^{high} melanoma cell lines of Ma-Mel-86 in the selection of positive controls. For Ma-Mel-86a downregulation of *SIK3* and also *CAMK1D* improved T cell-mediated killing, whereas for Ma-Mel-86c downregulation of Olfactory Receptor Family 10 Subfamily H Member 1 (*OR10H1*), Galectin 3 (*LGALS3/Gal-3*) as well as *SIK3* sensitized tumor cells to T cell attack (Figure 18). As observed previously, knockdown of the well-established molecule *PD-L1* did not result in an increased tumor cell rejection in Ma-Mel-86a and demonstrated a weak effect in Ma-Mel-86c. The Scr controls showed similar phenotypes as the mock condition in both, the viability and cytotoxicity settings. All mentioned positive and negative controls were included in the primary HTP screens.

Taken together, for both cell lines suitable control siRNAs were identified with differences between MITF^{low} and MITF^{high} cell lines Ma-Mel-86a and Ma-Mel-86c, respectively.

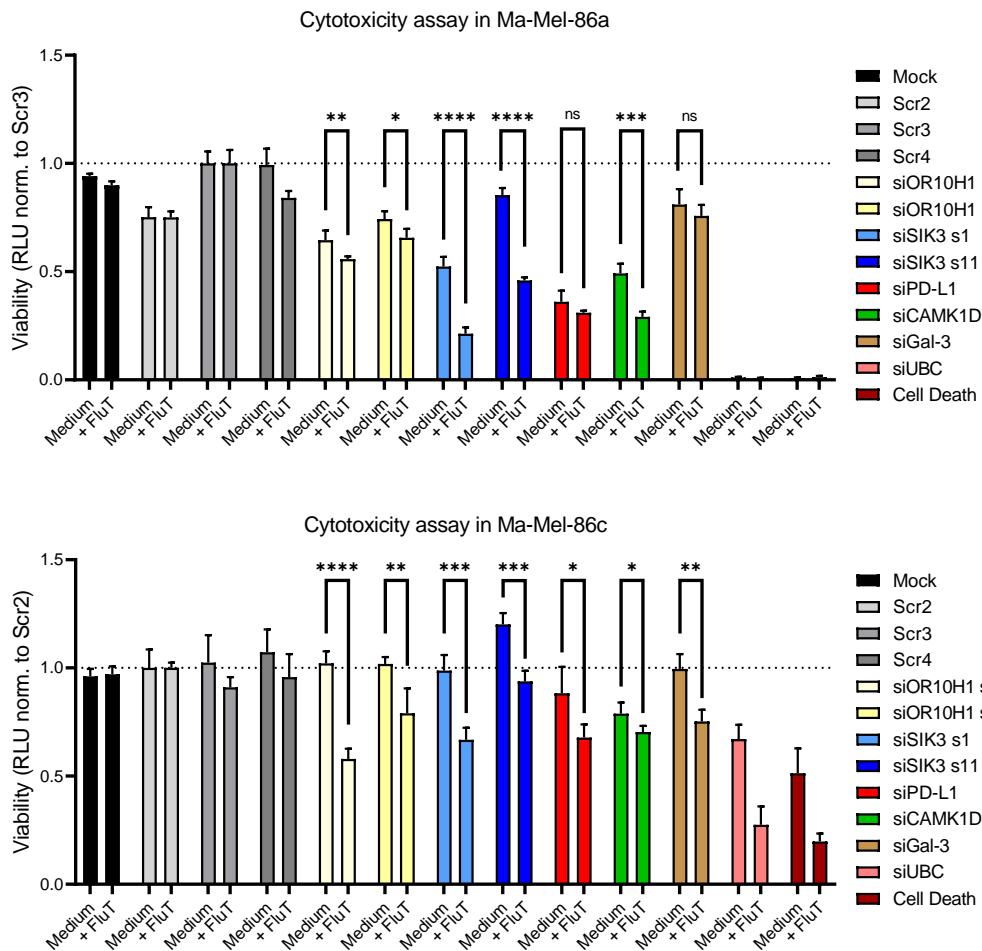


Figure 18: Performance of controls for the high-throughput RNAi screens in Ma-Mel-86a and Ma-Mel-86c.

Luciferase-based cytotoxicity assay to measure the impact of different controls on the viability of the melanoma cells and the T cell-mediated rejection. Ma-Mel-86 HLA-A2+ Luc+ were transfected with the indicated siRNAs for 48 h or not transfected (mock control). If not stated with single numbers, a pool of four individual siRNAs for the respective gene was used. Melanoma cells were pulsed for 1 h with flu peptide and subsequently cultured in plain medium (viability setting) or co-cultured with FluT cells with an E:T ratio of 1:1 for Ma-Mel-86a and 0,5:1 for Ma-Mel-86c (cytotoxicity setting) for 20 h. Cells were lysed, and remaining luciferase activity was measured by luminescence. Raw luciferase units (RLU) were normalized to RLU of Scr3 and Scr2, respectively. Bars represent the mean of technical replicates + standard deviation. Significances between viability and cytotoxicity setting were calculated by applying an unpaired two-tailed t-test (* $p < 0,05$, ** $p < 0,01$, *** $p < 0,001$, **** $p < 0,0001$, ns = not significant). Representative data of three independent experiments.

5.3 High-throughput (HTP) screens reveal novel immune resistance genes

5.3.1 Performance of the primary HTP screen

In the primary HTP screens a siRNA library comprising 5202 genes was used encoding for the entire surfaceome like G-protein coupled receptors as well as kinases and cell metabolism-related proteins. Each gene was targeted by a pool of four individual non-overlapping siRNAs. The Ma-Mel-86 HLA-A2+ Luc+ cells were transfected in a 384-well format and the screen including the viability (culture of cells in medium) and cytotoxicity (co-culture with FluT cells) setting was conducted in technical duplicates (Figures 19&20).

Subsequently the screen was analyzed using the programming language R for statistical computing with the package 'CellHTS2' [155]. Briefly, to be able to compare the raw luciferase unit results originating from different plates and therefore to eliminate inter-plate variability, plate normalization was applied. Also, consistency in both technical replicates was determined by calculation of the correlation coefficient for all plate pairs. All genes were afterwards scored, meaning their location among each other was estimated and their distribution was scaled (z-score). To identify each gene's immunomodulatory potential, a differential score between the cytotoxicity and viability score was calculated and corrected by applying locally estimated scatterplot smoothing (LOESS). This resulted in a final LOESS score ranking in which the genes with the highest immune resistance phenotypes receive the highest score and genes with opposite effects receive negative scores. The list of genes was filtered to eliminate genes that showed high impact on the viability of the tumor cells. As in general higher viability effects were observed for Ma-Mel-86a the range for viability z-scores was set between -3 and 1 and for Ma-Mel-86c the range between -2,5 and 1,5 was chosen.

Figure 19 shows the performance of the controls in the screens where blue dots represent the viability setting and red ones the cytotoxicity setting. For positive controls a shift in z-score can be seen confirming their immunoregulatory impact. In agreement with previous kill assays the effects were higher in Ma-Mel-86a (*SIK3* s1, *SIK3* s11, *CAMK1D* pool) than in Ma-Mel-86c (*OR10H1* s1, *OR10H1* s5, *Gal-3* pool). The Scr controls did not show immunomodulatory effects and LOESS scores were comparable to the medium, especially for Scr3 and Scr4 (Figure 19&20). As previously observed in the kill assays, Cell Death siRNA and the knockdown of *UBC* resulted in a high cell death of Ma-Mel-86a already in the viability setting while moderate effects were observed for Ma-Mel-86c.

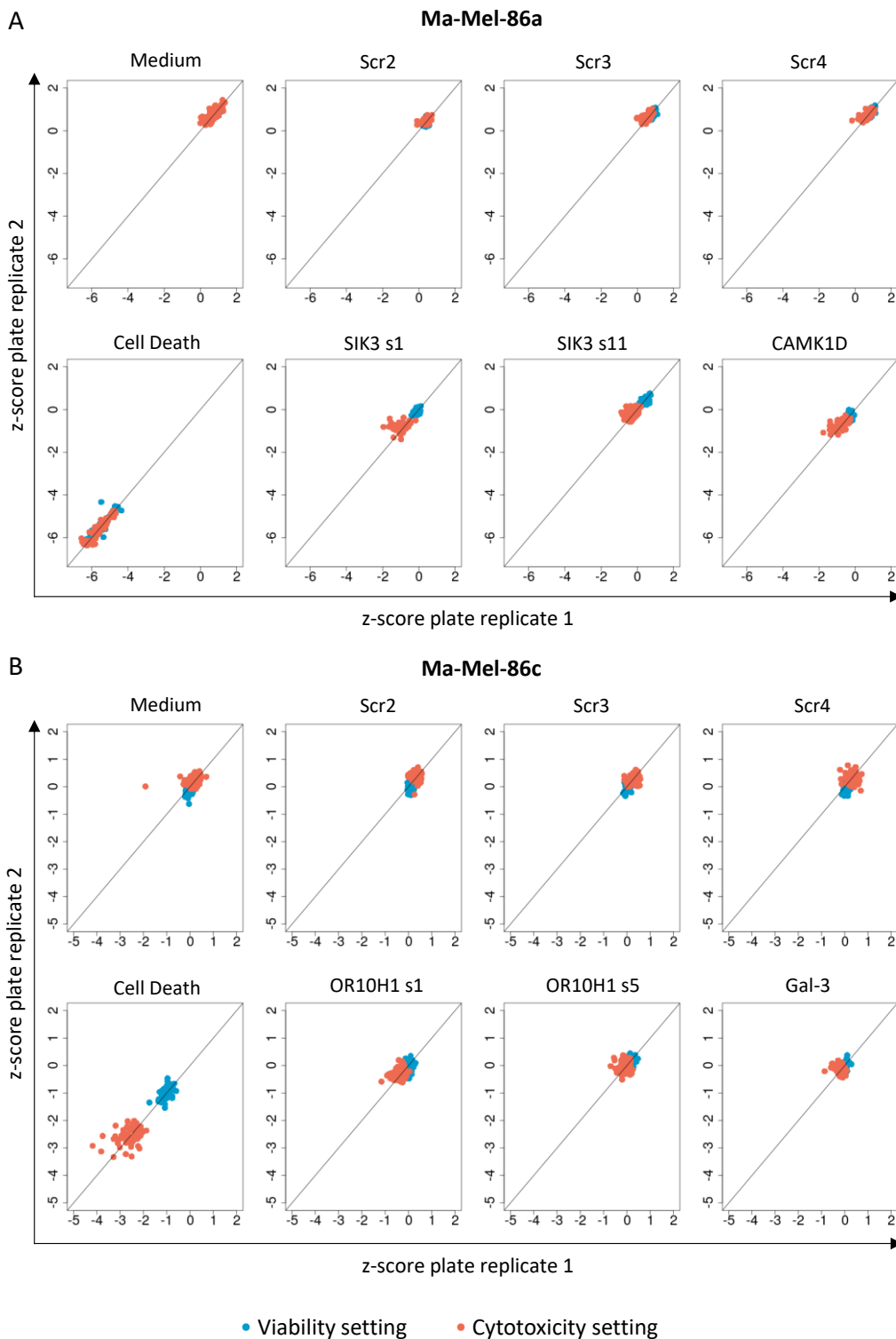


Figure 19: Performance of the controls in the primary high-throughput (HTP) RNAi screens.

A siRNA library of 5202 genes was used in the HTP screens. Additionally, non-targeting Scr controls, the transfection control ‘Cell Death’ as well as positive controls *SIK3*, *CAMK1D*, *OR10H1* and Galectin-3 were included. Viability and cytotoxicity settings were applied as described in Figure 15. HTP screens were analyzed using the programming language R for statistical computing with the package ‘CellHTS2’. Raw luciferase units (RLU) were normalized plate-wise and transformed into z-scores for each duplicate in the viability and cytotoxicity setting. Scatter plots show the z-scores of technical replicates of the controls for (A) Ma-Mel-86a and (B) Ma-Mel-86c. Blue and red dots represent the z-scores of the viability and the cytotoxicity settings, respectively.

For both cell lines a set of immunoregulatory genes showing a higher impact on tumor cell rejection by FluT cells than the positive controls could be identified. For Ma-Mel-86a the best performing positive control *SIK3* s1 occupied rank 96 of 4217 remaining genes while for Ma-Mel-86c the best performing positive control *OR10H1* s1 occupied rank 337 of 4733 (Figure 20B). Among the best performing genes (hits), genes that were previously identified in another HTP screen in our group could be found or those that are known for their immune resistance phenotype such as Janus Kinase 2 (*JAK2* - rank 12 in Ma-Mel-86a) and CASP8 And FADD Like Apoptosis Regulator (*CFLAR/FLIP* - rank 1 in Ma-Mel-86c), corroborating the validity and reliability of the outcome of the HTP screens. Taken together, the HTP screens identified novel putative immune resistance genes in melanoma that increased susceptibility to T cell-mediated tumor cell rejection stronger than previously established positive controls.

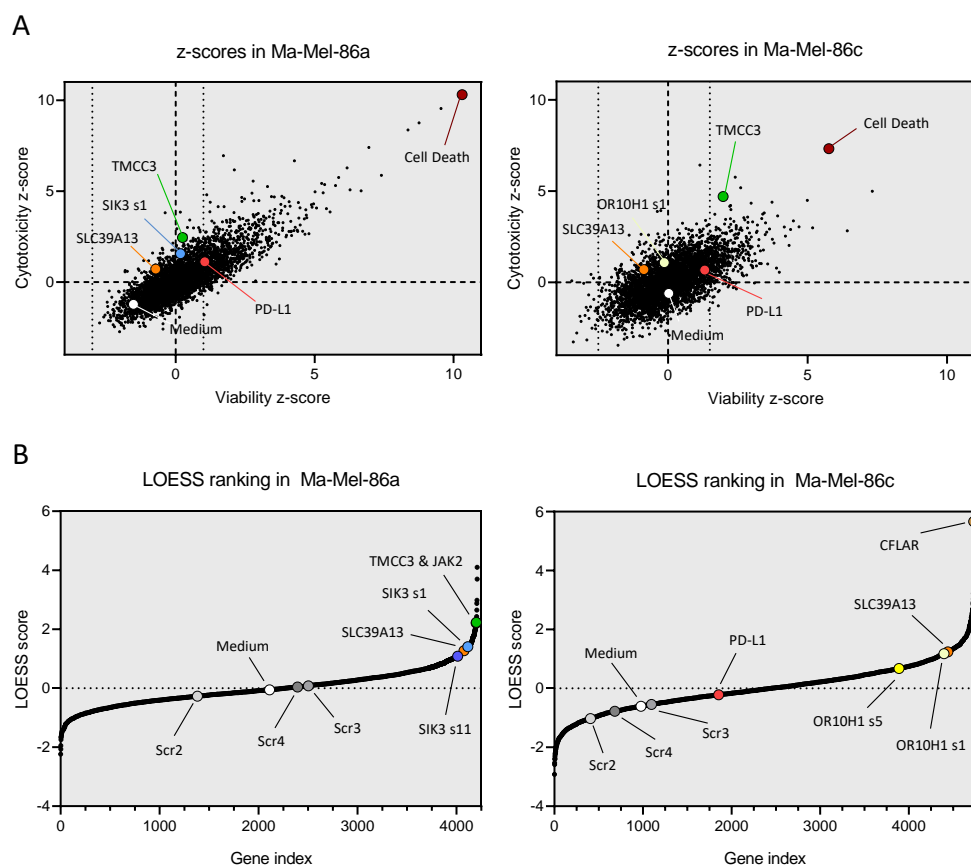


Figure 20: Outcome of the high-throughput (HTP) RNAi screens.

This figure extends Figure 19. **(A)** The mean of z-scores of both replicates of the viability setting were plotted against the cytotoxicity setting for library and control genes. Bold lines indicate a z-score of 0. Vertical faint lines indicate the threshold of the viability score for further analysis. Some control and candidate genes are highlighted. **(B)** Differential scores between viability and cytotoxicity scores were corrected by applying locally estimated scatterplot smoothing (LOESS). Library and control genes were filtered for viability thresholds in each HTP screen and ordered by their LOESS score. High values indicate cytotoxic influence on T cell-mediated rejection. Horizontal lines indicate a LOESS score of 0. Selected control and candidate genes are highlighted.

5.3.2 Design of a siRNA library for a secondary validation screen

The primary screens made use of a siRNA library comprising 5202 genes in which each gene was targeted by a pool of four individual siRNAs. In order to exclude off-target effects as well as to validate the findings from the HTP screens, a secondary screen was performed. Here, hits with strong immune resistance phenotypes were selected. In the validation screens, each gene was targeted either by one individual siRNAs or with pool of 4 siRNAs (de-convolution of the siRNA pool).

I selected hits with diverse effects to be included in the secondary screen library: genes that showed either an immune resistance phenotype in Ma-Mel-86a or in Ma-Mel-86c in the primary screens as well as common hits showing the effect in both cell lines. The z-score thresholds for viability effects for both cell lines stated in the previous chapter were applied and genes that had a LOESS score of above 1,5 in Ma-Mel-86a but below 1 in Ma-Mel-86c was considered a Ma-Mel-86a specific hit and vice versa. This selection criterion resulted in 111 and 41 of Ma-Mel-86c and Ma-Mel-86a specific hits, respectively. Accordingly, the number of Ma-Mel-86c specific hits were reduced to 41 by selecting those with the highest LOESS score and/or with the highest score difference compared to Ma-Mel-86a ($LOESS_{Ma-Mel-86c} - LOESS_{Ma-Mel-86a}$). Common hits were defined to have a LOESS score above 1 in both cell lines with a sum of both scores above 2,5. Due to their relevance for this project, I also included *MITF* and *PD-L1/CD274* in the library. Finally, a siRNA library comprising 174 genes was designed targeting hits that showed strong effects in Ma-Mel-86a and/or Ma-Mel-86c in the primary HTP screens (Figure 21, Supplementary Table 1).

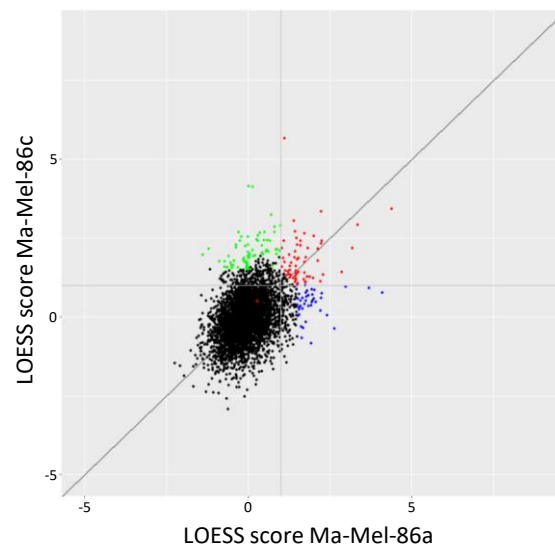


Figure 21: Selection of library genes for a secondary validation screen.

Scatter plot was created using the programming language R for statistical computing with the package “ggplot2”. LOESS scores derived from the primary high-throughput (HTP) screens in Ma-Mel-86a and Ma-Mel-86c were plotted against each other to select genes for a secondary validation screen in both cell lines. Vertical and horizontal faint lines indicate a LOESS score of 1. Viability thresholds were applied to each cell line to exclude genes that showed a high impact on tumor cell viability after knockdown. Red dots indicate common hits that displayed a strong immunomodulatory effect in both cell lines, Ma-Mel-86a and Ma-Mel-86c. Blue dots indicate

Ma-Mel-86a specific hits with a LOESS score higher than 1,5 in Ma-Mel-86a and lower than 1 in Ma-Mel-86c. Green dots indicate Ma-Mel-86c specific hits. LOESS score had to be higher than 1,5 in Ma-Mel-86c and lower than 1 in Ma-Mel-86a. Altogether, 174 genes were selected to be tested in the validation screen (Supplementary table 1).

5.3.3 Performance of the secondary validation screen

The secondary screen was performed in a similar manner as the primary HTP screens, the format was changed from 384-well to 96-well plates due to a smaller library size. Scr2-4 were included as negative controls as well as Cell Death siRNA as a transfection control. *SIK3* s1 and s11 and *CAMK1D* were used as positive controls in Ma-Mel-86a while *OR10H1* s1, *SIK3* s1 and *Gal-3* were used as positive controls in Ma-Mel-86c (Figures 22&23).

Subsequently, the analysis was performed as before with the R package 'CellHTS2'. This was valuable to get a general overview of the performance of the controls and to assess the transformation of the luciferase units to z-scores (Figure 22). Here, Cell Death control worked well in both melanoma cell lines. For Ma-Mel-86a the best positive control was again *SIK3* s1 for which a shift in the scatter plot is observed as blue dots represent the viability setting while the red ones the cytotoxicity setting. This shift is not visible for *OR10H1* s1 or another control in Ma-Mel-86c. On the other hand, medium and Scr controls show a shift in the opposite direction.

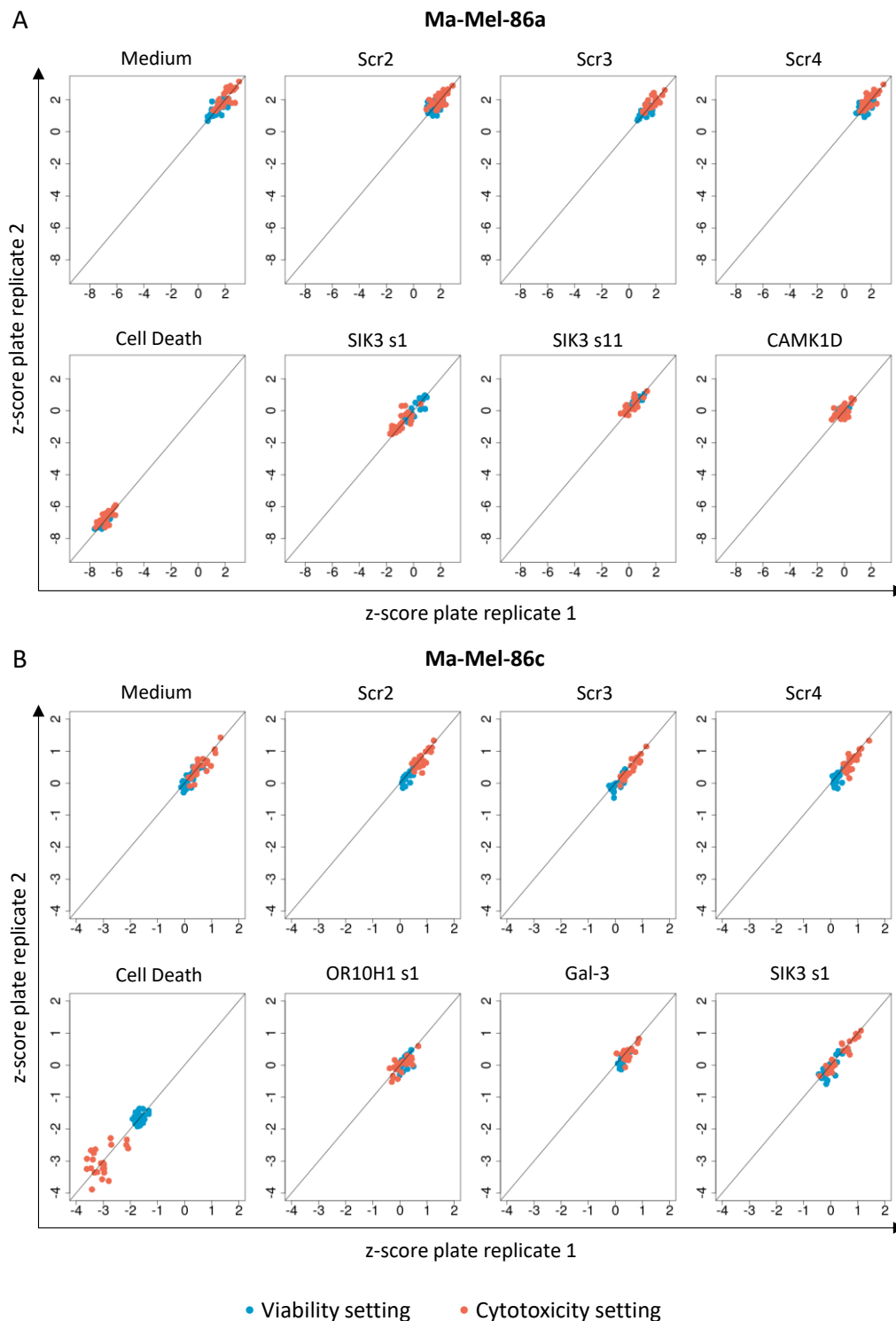


Figure 22: Performance of the controls in the secondary validation high-throughput (HTP) RNAi screens.

A siRNA library of 174 genes was used in the HTP screens. Additional indicated controls were included. As the primary HTP screens, validation screens were conducted with a viability and cytotoxicity setting as described in Figure 15. Analysis was conducted using the programming language R for statistical computing with the package 'CellHTS2'. Raw luciferase units (RLU) were normalized plate-wise and transformed into z-scores for each duplicate in the viability and cytotoxicity setting. Scatter plots show the z-scores of technical replicates of the controls for (A) Ma-Mel-86a and (B) Ma-Mel-86c. Blue dots represent z-scores of the viability setting while red dots represent z-scores of the cytotoxicity setting.

Additionally, raw luciferase units (RLU) were normalized to a Scr negative control in a plate-wise manner to directly compare the effects of the different siRNA treatments on the viability and cytotoxicity in Ma-Mel-86a and -86c for each gene. In order to select the most appropriate Scr control for each cell line, luciferase units of the medium condition were compared to the ones of the single Scr controls. Finally, in Ma-Mel-86a RLU for each gene were normalized to RLU of Scr4 while for Ma-Mel-86c values were normalized to RLU of Scr3 as those Scr controls showed highest similarity to the medium condition (Figure 23). Normalized values of Cell Death siRNA reproduced findings of the CellHTS2 analysis. Additionally, downregulation of *SIK3* by using siRNAs s1 and s11 improved T cell-mediated killing of Ma-Mel-86a while targeting *Gal-3* and *OR10H1* showed a similar phenotype in Ma-Mel-86c.

To improve comparability, I fitted the z-score viability threshold from the primary screens to the normalized values in the secondary screens. Finally, the thresholds for Scr normalization were set to 0,265 for Ma-Mel-86a and 0,772 for Ma-Mel-86c. In order to call a gene a validated hit, the following validation criteria were applied: the viability impact should be above the set thresholds and an immunomodulatory effect should be seen for the siRNA pool as well as at least two individual siRNAs of the same gene. An immunomodulatory effect was defined as a cytotoxicity/viability ratio (CV ratio) $\leq 0,85$, meaning additional 15 % more tumor cells died in the co-culture setting with FluT cells. Alternatively, if the CV ratio was above 0,85 a significant p-value between both settings was necessary, determined by an unpaired two-tailed students t-test. Finally, the phenotype should be reproduced in the same cell line as it was shown in the primary screen. For genes that showed an effect on tumor cell rejection by FluT cells in both cell lines, validation in one cell line was sufficient.

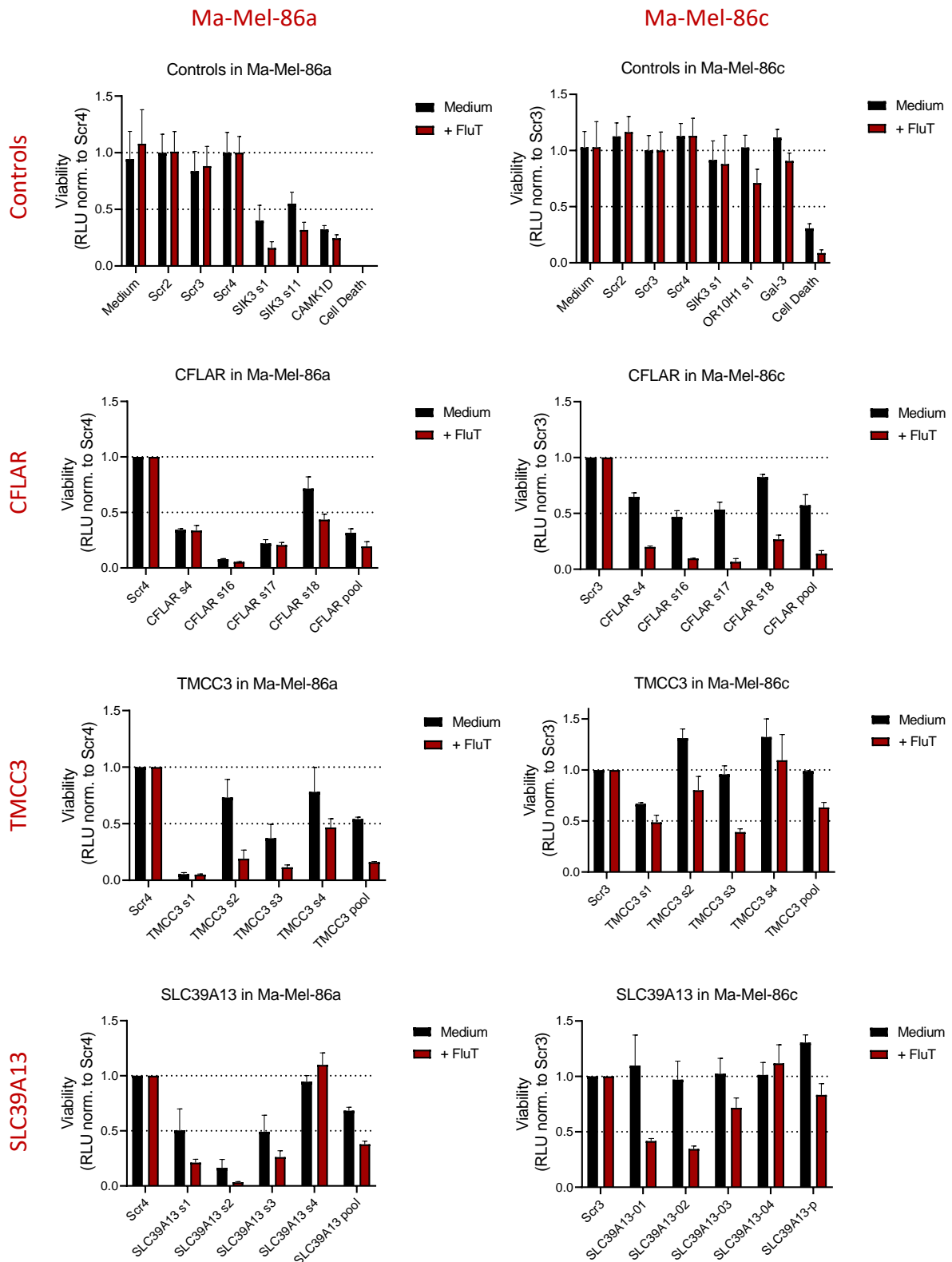


Figure 23: Performance of controls and selected genes in the secondary validation high-throughput (HTP) RNAi screens.

After implementation of the HTP screens in Ma-Mel-86, raw luciferase units (RLU) for each gene were normalized to Scr4 negative control in Ma-Mel-86a and to Scr3 negative control in Ma-Mel-86c in a plate-wise manner. Bar plots show the normalized values in the viability (culture of melanoma cells in plain medium, black bars) and cytotoxicity (co-culture with FluT cells, red bars) settings for the controls as well as the selected genes *CFLAR*, *TMCC3* and *SLC39A13*. Blots of library genes represent the different conditions using individual siRNAs or the pool of four siRNAs. Bars correspond to the mean of the duplicates + standard deviation.

From a total of 174 genes, the secondary screen validated 91 genes (53,2 %). Additionally, there were 17 genes (9,9 %) that fulfilled the basic criteria but not in the melanoma cell line from which the hit originated according to the primary HTP screen. For Ma-Mel-86c more cell line-specific genes could be validated (59,7 % compared to 24,4 % in Ma-Mel-86a). From the common hits 18,4 % were validated in both cell lines while 69,4 % were validated in at least one of the cell lines. As already observed in the primary HTP screening, genes that are known to manipulate tumor cell resistance to immune cells like TNF Receptor Superfamily Member 6b (*TNFRSF6B/DcR3*) could also be validated by this secondary screen. The phenotype of *CFLAR* which was especially strong in Ma-Mel-86c was reproduced in the secondary screen yet due to a high viability impact it was not assigned as a validated hit. Figure 23 shows the performance of *CFLAR* as well as two more selected genes in the secondary validation HTP screens as examples. In conclusion, the secondary screen validated the immune resistance phenotype of 91 genes to regulate T cell-mediated tumor cell rejection.

5.4 Bioinformatic analyses reveal clusters of co-expressed immune resistance genes with inter-individual expression patterns

Many patients do not respond to immunotherapies due to the fact that tumor cells have developed mechanisms to circumvent immune responses by using complementary proteins and pathways to those targeted by an immunotherapy [105]. This could be especially valid for resistant *MITF*^{low} melanomas. I hypothesized that immune resistance genes were co-regulated and in case one protein or pathway is affected by immunotherapy, another gene can be upregulated by the tumor cell to become resistant against apoptosis induced by immune cells.

For this reason, different bioinformatic analyses were performed using the programming language R for statistical computing. The analyses were mainly performed with expression data of genes that were validated in the secondary HTP screens. Our group had previously performed six HTP screens in tumor cell lines of different entities: breast cancer, lung adenocarcinoma, pancreatic ductal adenocarcinoma (PDAC), melanoma, multiple myeloma and glioblastoma. Each screen revealed a list of validated immunoregulatory genes that were also included in the analyses. Finally, known immune checkpoint genes that are expressed on tumor cells as well as genes that were described to be positively or negatively correlating with *MITF* were added to the list as controls. In total 265 genes were included in the bioinformatic analyses.

Publicly available RNA sequencing data sets were used as expression data input. For this thesis, the following data sets were of importance: bulk RNA-Seq data from Skin Cutaneous Melanoma (SKCM) samples of The Cancer Genome Atlas (TCGA) and healthy organ samples from the Genotype-Tissue

Expression (GTEx) project [175]. Furthermore, single cell RNA-Seq data from patient's melanoma tumors from Jerby-Arnon *et al.* [152] and bulk RNA-Seq data from patient-derived melanoma cell lines from Wouters *et al.* [83] was used. The single cell data set (Jerby-Arnon *et al.*) provided an annotation file that labeled each cell to a specific cell type like 'malignant' while the cell line data set (Wouters *et al.*) annotated each cell line by their phenotype: melanocytic ($MITF^{high}$), intermediate ($MITF^{high}$), neural crest stem cell like ($MITF^{low}$) or mesenchymal ($MITF^{low}$). Additionally, bulk RNA-Seq data was available for Ma-Mel-86 [130]. Here raw sequencing data was kindly processed by our institute's Next Generation Sequencing (NGS) core facility. Afterwards it was combined with the sequencing data of the other melanoma cell lines (Wouters *et al.*) and corrected for batch effects using ComBat-Seq to be able to analyze it as one data set (Supplementary Figure 1).

5.4.1 Melanoma and healthy tissues upregulate different sets of immune resistance genes

To get a first impression of the expression of the immune resistance genes, I was interested how they are expressed across different tissues (Figure 24). Gene expression in melanoma compared to a set of healthy organs was investigated, using TCGA data for melanoma and GTEx data for healthy samples. As the data originated from different projects and data sets, batch effects were expected. The University of California Santa Cruz (UCSC) developed the pipeline TOIL in which they processed the TCGA and GTEx data in a single analysis to remove any batch effect from the bioinformatics side [175]. Although technical batch effects were possible to remain, no further batch effect correction was performed to not overcorrect the data and lose biological information. Gene expression of the immune resistance genes from the HTP screens were tested against each other in melanoma (TCGA) and Skin, Colon, Kidney, Liver, Lung, Pancreas, Adrenal Gland, Heart and Blood (GTEx). Genes were ordered by significant overexpression in the different data sets. Analysis was performed by my colleague Leonard Bellersheim.

The heatmap is shown in Figure 24. Every column represents a single gene while rows represent single samples. The coloured bar on the left side of the heatmap indicates the different tissues. The analysis showed that melanoma as well as all healthy organs have a set of immune resistance genes that are significantly upregulated. The first block of genes on the left represents genes which are upregulated in melanoma, among them *MITF* was present. Blood has a large set of genes overexpressed compared to the other entities, but also many other genes that are low expressed indicated by the blue color. The right half of the heatmap represents genes that are not uniquely overexpressed in a single entity. Still, some genes show higher expression in melanoma. In summary, melanoma and healthy tissues showed increased expression of a specific set of immune resistance genes.

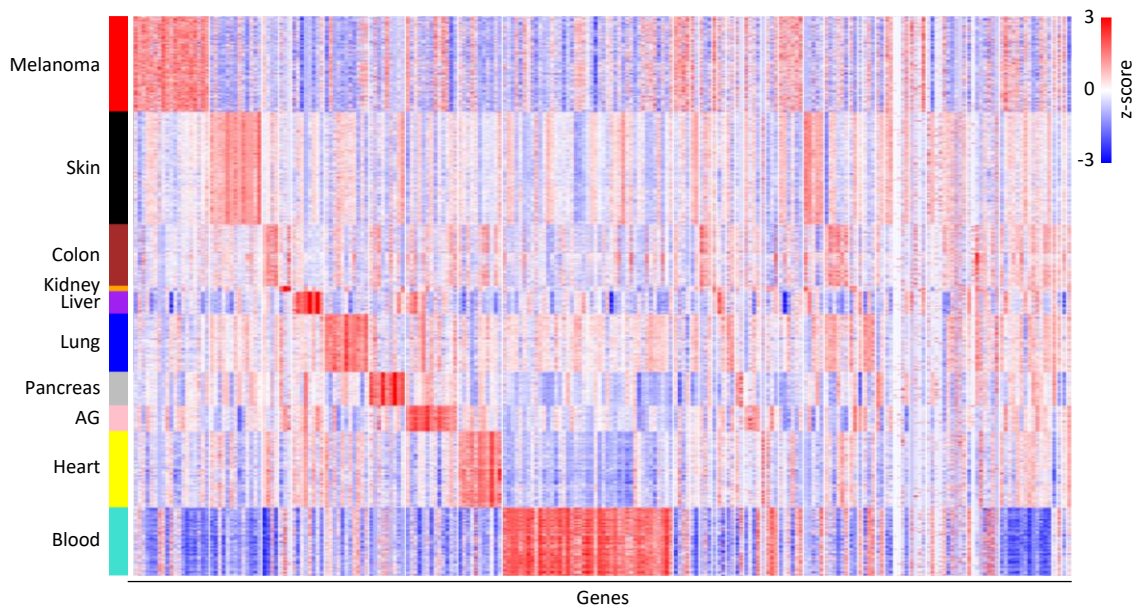


Figure 24: Expression of Immune resistance (IR) genes in melanoma and different healthy tissues.

Analysis was conducted by using the programming language R for statistical computing. Log2 transformed normalized count expression data from the pipeline TOIL from the University of California Santa Cruz (UCSC) was filtered for data of melanoma patients from TCGA and for healthy samples of skin, colon, kidney, liver, lung, pancreas, adrenal gland (AG), heart and blood from the GTEx project. Expression of each gene was tested against each other by applying a Mann-Whitney-U-Test always using two single data sets. Resulting p-values were adjusted for multiple testing and genes were ordered by their significance to be upregulated in the different data sets. Expression data was transformed into z-scores in a gene-wise manner and a heatmap was created using the R package 'pheatmap'. Analysis was performed by my colleague Leonard Bellersheim.

5.4.2 Immune resistance genes are co-expressed in clusters

In order to check for co-expression of immune resistance genes, a Weighted Gene Co-expression Network Analysis (WGCNA) was performed using the R package 'WGCNA' (Figure 25). This analysis enables the identification of clusters of correlating genes that are defined as module eigengene (ME) [162]. MEs could further be correlated to each other or to marker genes and external traits. Selected parameters were dependent on the data set *e.g.*, for TCGA data I decided to correlate the clusters to marker genes of melanoma plasticity like *MITF*, Melan-A (*MLANA/MART-1*), Tyrosinase (*TYR*) and SRY-Box Transcription Factor 10 (*SOX10*) for the melanocytic $MITF^{high}$ phenotype, *AXL* Receptor Tyrosine Kinase (*AXL*) for the mesenchymal $MITF^{low}$ phenotype or Nerve Growth Factor Receptor (*NGFR*) for the neural-crest stem cell like $MITF^{low}$ phenotype. Additionally, I correlated the expression of the clusters to the sample type, representing if the sample was obtained from a primary or a metastatic melanoma. As this is a binary category, metastatic was labeled as 1 and primary as 0. Therefore, a positive correlation means higher expression in metastasis and a negative correlation higher expression in primary melanoma. WGCNA was conducted to identify a signed correlation network meaning that genes were only associated to the same cluster when they showed a high positive correlation and negatively correlating genes were attributed to different clusters.

WGCNA was conducted for all three data sets: TCGA, Jerby-Arnon *et al.* and Wouters *et al.* together with Ma-Mel-86. In all three data sets WGCNA was able to identify clusters of co-expressed genes (Figure 25). Dendrograms of the WGCNA represent the distribution and proportion of the identified clusters depicted by the colored bars at the bottom. In all three data sets *MITF*-related clusters could be identified of which *MITF* was part of. Additionally, the correlation heatmaps demonstrated negatively correlating modules to *MITF* and *MITF* clusters.

In the TCGA data, *MITF* was attributed to the yellow module of the dendrogram (Figure 25A). The correlation heatmap confirmed the correlation of *MITF* and the yellow cluster and demonstrated that the yellow module was negatively correlating with the turquoise module (Figure 25B). Interestingly, the turquoise module contained both *MITF*^{low} markers *AXL* and *NGFR* as well as known immunoregulatory genes like *CD274/PD-L1* and *CFLAR*. Additionally, the turquoise module showed positive correlation to the sample type, thus to metastatic melanoma.

Due to low gene expression of many genes in single cell RNA-Seq data, correlations were more difficult to find in the Jerby-Arnon *et al.* data set. Here, I only focused on the 2018 annotated malignant cells and excluded other cell types of the tumor microenvironment. The dendrogram revealed that *MITF* was part of the turquoise module that showed positive correlation to all melanocytic marker genes in the correlation heatmap (Figure 25C&D). The brown module showed negative correlation to the *MITF* cluster which contained the marker gene *NGFR*. *AXL* together with *CFLAR* were not part of the turquoise but of the yellow module which didn't show negative correlation to the *MITF* cluster.

In the Wouters *et al.* data set combined with expression data of Ma-Mel-86, *MITF* was again part of the melanocytic-associated turquoise cluster in the dendrogram (Figure 25E). In the correlation heatmap the green module showed negative correlation to the *MITF* cluster and contained *AXL* which itself showed positive correlations to the pink, black and blue cluster (Figure 25F). The other *MITF*^{low}-associated gene *NGFR* was not connected to any cluster.

In conclusion, WGCNA in all data sets revealed co-expression clusters of immune resistance genes that in part, could be associated with positive or negative correlation to *MITF*^{high} or *MITF*^{low} marker genes.

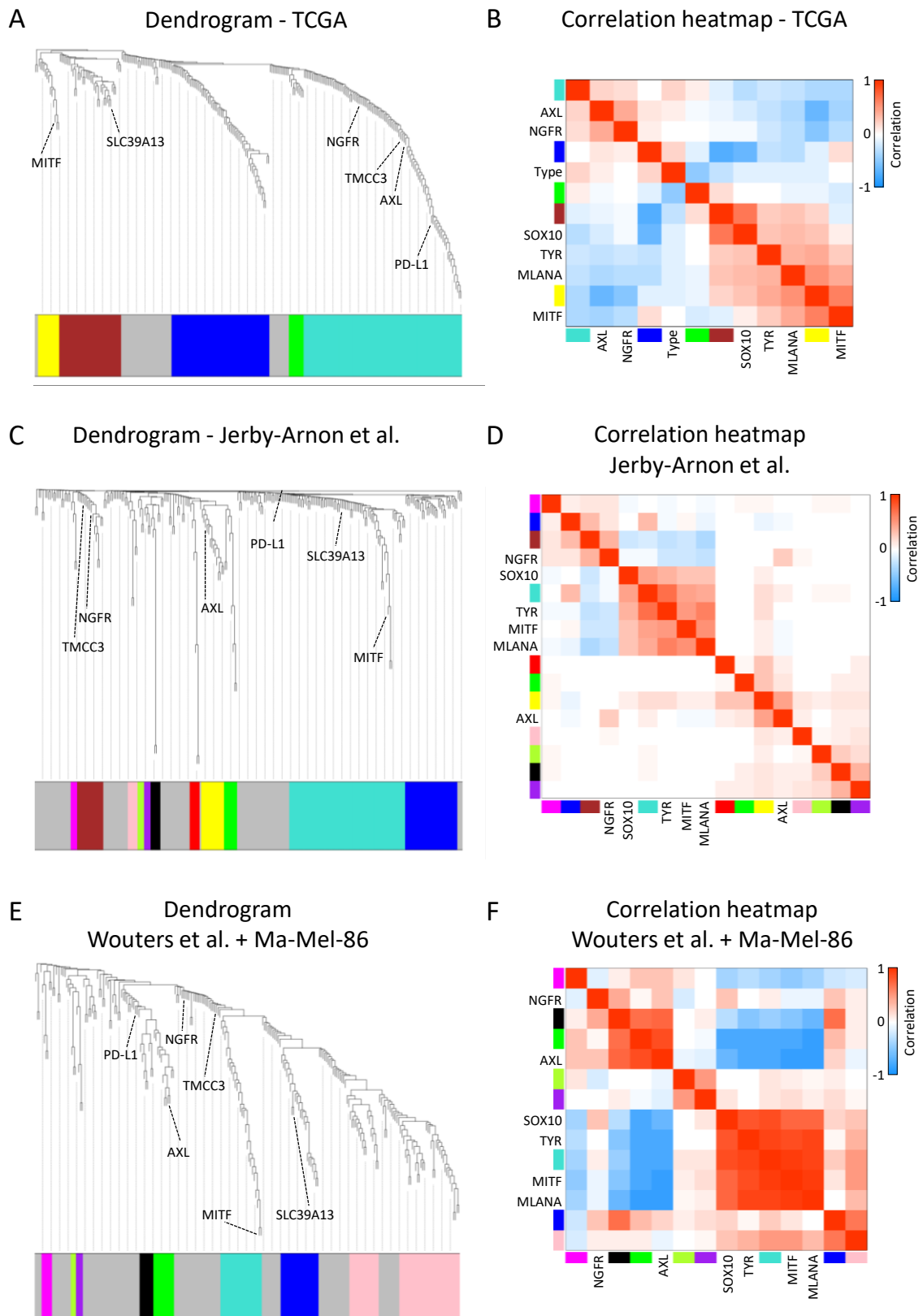


Figure 25: Weighted gene co-expression network analysis (WGCNA) in melanoma data sets.

Analysis was conducted by using the programming language R for statistical computing. Used data sets: **(A-B)** Normalized counts expression data from Skin Cutaneous Melanoma (SKCM) samples from TCGA. **(C-D)** Transcripts per million (TPM) expression data from annotated malignant cells from Jerby-Arnon *et al.* **(E-F)** Batch effect corrected normalized counts expression data from Wouters *et al.* combined with normalized counts expression data of Ma-Mel-86a and Ma-Mel-86c. **(A-F)** Expression data of all data sets were log2 transformed

and WGCNA was performed using the R package 'WGCNA'. **(A, C, E)** Dendrogram representing co-expression clusters of correlating immune resistance (IR) genes depicted by different colors. The position of melanoma marker (*MITF*, *NGFR*, *AXL*) and selected IR genes (*PD-L1*, *TMCC3*, *SLC39A13*) in the dendrogram are highlighted. **(B, D, F)** Correlation heatmap representing the correlation of the identified clusters to each other as well as to the melanoma marker genes *MITF*, *MLANA*, *TYR*, *SOX10*, *NGFR* and *AXL*. Additionally, the TCGA data (B) includes the clinical trait "Type" in which positive correlations indicate higher expression in metastatic melanoma compared to primary melanoma and vice versa.

5.4.3 Cluster expression is inter-individually heterogeneous

As it was possible to identify clusters of co-expressed genes, I was interested how these expressions were distributed within the sample populations (Figure 26). To get an impression of that, a heatmap of the expression data was generated using the R package 'pheatmap'. The genes were ordered as in the dendrogram as the columns of the heatmap depicted by the colored bar on top of the heatmap. Gene-wise standardization to z-scores was applied to see up- and downregulation of genes compared to the mean expression of each gene. Every single row was a sample, meaning a tumor sample (TCGA), a melanoma cell line (Wouters *et al.* and Ma-Mel-86) or a tumor cell (Jerby-Arnon *et al.*). Rows were either clustered by the pheatmap function or grouped by patient (single cells) or phenotype (cell lines) and ordered manually.

Upon hierarchical clustering by the pheatmap function, the TCGA data showed that the clusters are heterogeneously expressed (Figure 26A). Groups of patients share similar expression patterns and can therefore be stratified into different cohorts. Genes that were associated to one cluster show mutual down- and upregulation and for some modules their relationship to each other is clearly visible as for example a negative correlation between the brown and the blue cluster.

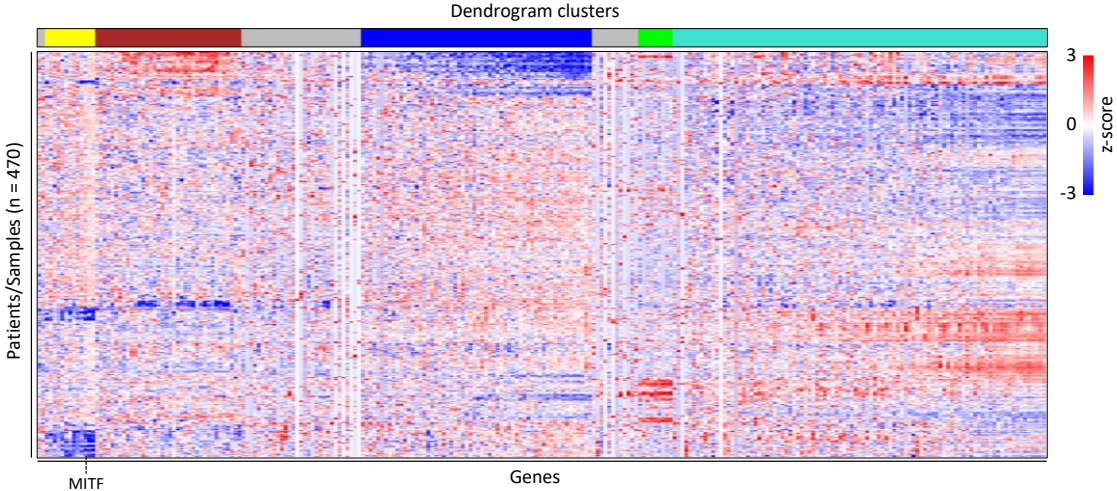
For the single cell data set of Jerby-Arnon *et al.* the tumor cells were grouped by the patients from which they originated, and patients were ordered by their mean *MITF* expression with *MITF*^{high} patients being positioned at the top of the heatmap (Figure 26B). Parts of white coloring in the heatmap indicated that the immune resistance genes and clusters are in many cases not expressed in all cells. Some clusters were exclusively expressed in one or a few patients or cells. In general, the heatmap showed that the clusters are homogeneously expressed within a patient but show heterogeneous expression patterns among the different melanoma patients. The turquoise *MITF* cluster was expressed in many cells to different degrees. In one *MITF*^{low} patient the brown cluster that contained *NGFR* was upregulated which no other patient had expressed to comparable levels.

In the Wouters *et al.* and Ma-Mel-86 data set the melanoma cell lines were grouped by their phenotype: melanocytic (*MITF*^{high}), intermediate (*MITF*^{high}), neural crest stem cell like (*MITF*^{low}) or mesenchymal (*MITF*^{low}). Similar to the melanoma cells in the Jerby-Arnon *et al.* dataset, some genes showed hardly any expression across all cell line samples (Figure 26 C). The turquoise *MITF* cluster is

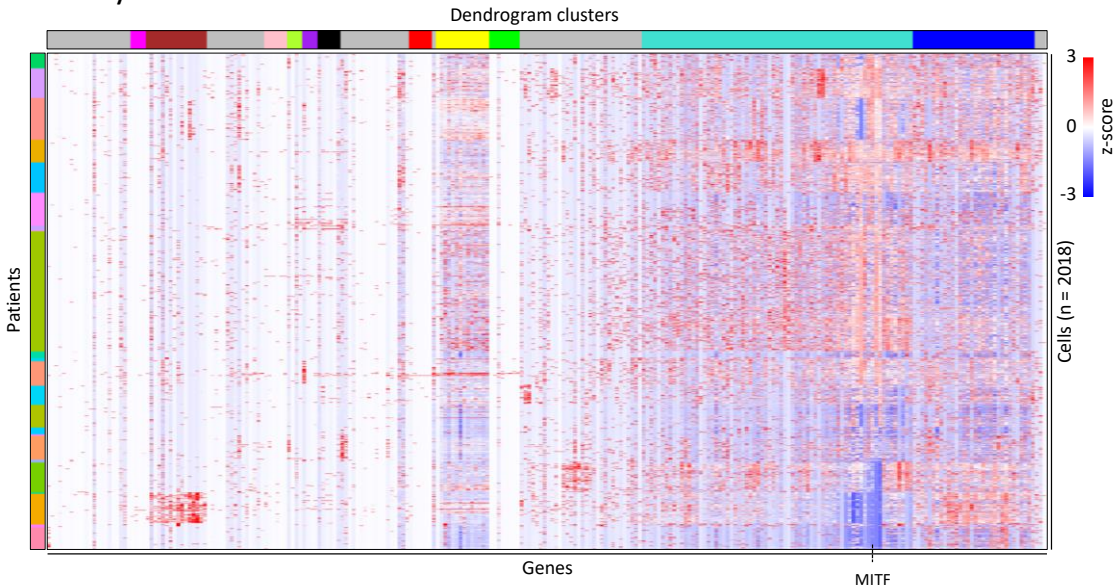
higher expressed in the MITF^{high} fraction of melanoma cell lines and the green cluster is upregulated in the MITF^{low} melanoma cell lines.

Taken together, immune resistance genes and co-expression clusters showed inter-individual expression patterns in all three data sets.

A TCGA



B Jerby-Arnon et al.



C Wouters et al. + Ma-Mel-86

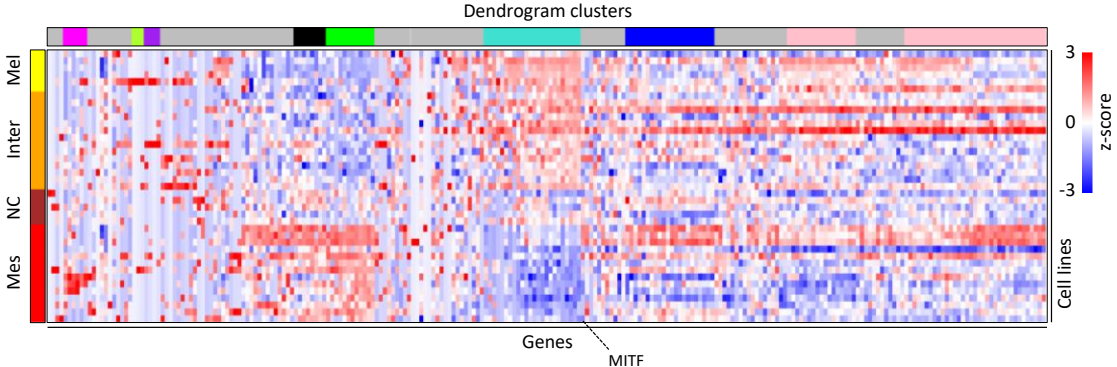


Figure 26: Differential expression patterns of immune resistance (IR) genes in melanoma data sets.

This figure extends Figure 25. Analysis was conducted by using the programming language R for statistical computing. Log₂ expression data was transformed into z-scores in a gene-wise manner and genes were ordered by their position in the dendrogram of the respective data set. On top of the heatmaps, the colored bar represents clusters of the dendrogram previously identified by WGCNA (Figure 25). Heatmaps were created using the R package 'pheatmap' and MITF is highlighted. **(A)** Heatmap of the TCGA data set. Samples were ordered by hierarchical clustering in order to group patients with similar expression patterns. **(B)** Heatmap of the Jerby-Arnon *et al.* data set. Malignant cells were grouped by annotated patient ID (colored bar on the left side of the heatmap) and patients were ordered by their mean of the MITF expression. Patients with higher MITF expression are positioned at the top of the heatmap. **(C)** Heatmap of the Wouters *et al.* dataset combined with expression data of Ma-Mel-86. Melanoma cell lines were grouped by their annotated phenotype (colored bar on the left side of the heatmap) and groups were ordered by their MITF expression. MITF^{high} cell lines are positioned at the top of the heatmap. (Phenotypes: Mel = melanocytic, Inter = intermediate, NC = neural-crest stem cell like, Mes = mesenchymal).

5.4.4 Immune resistance gene expression can be correlated to MITF expression status

As whole clusters could be attributed to low or high *MITF* expression, I investigated a general gene-wise correlation between the immune resistance genes and *MITF* (Figure 27). For this purpose, melanoma cells of Jerby-Arnon *et al.* and melanoma cell lines of Wouters *et al.* together with Ma-Me-86 were grouped into MITF^{low} and MITF^{high} and a statistical test was applied to the expression data between both groups in a gene-wise manner with subsequent correction for multiple testing. Due to low expression for some genes, I assumed that the data was not normally distributed and applied a Mann-Whitney-U-Test. Genes were ordered by their adjusted p-value of the test in columns and vertical red lines indicate the significance threshold.

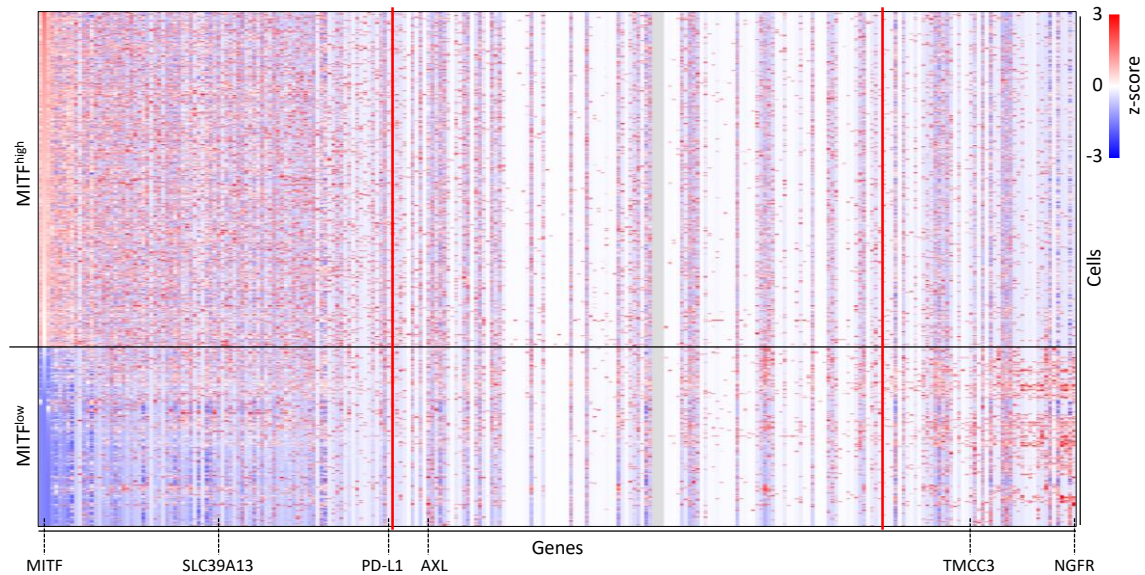
Due to a high cell number, I chose a more stringent separation factor in the single cell data set of Jerby-Arnon *et al.* (Figure 27A). The MITF^{low} group was represented by cells with a z-score below 0 for *MITF*, but also for *MLANA* and *TYR* while the MITF^{high} fraction of cells had a z-score above 0 for all three genes to retrieve a clearer melanocytic cell population. From 2018 malignant cells 430 were attributed to the MITF^{low} group while 809 were categorized as MITF^{high}. Numerous genes could be attributed to the MITF^{low} group with *NGFR* as the most significant gene ($p = 7,0 \text{ e-}41$). In the MITF^{high} group, *TYR*, *MITF* and *MLANA* were the most significant genes ($p = 2,0 \text{ e-}188 / 1,1 \text{ e-}185 / 1,7 \text{ e-}183$, respectively), underlining the reliability of the test. In total, 48 genes were significantly upregulated in MITF^{low} melanoma cells while 89 showed significant upregulation in MITF^{high} melanoma cells, interestingly among them *CD274/PD-L1* could be found ($p = 0,04$).

In the Wouters *et al.* dataset, the cells were grouped by their annotation in the publication (Figure 27B). Melanocytic and intermediate annotated cell lines together with Ma-Mel-86c represented the MITF^{high} group while mesenchymal and neural crest stem cell like annotated cell lines together with Ma-Mel-86a represented the MITF^{low} group. *MITF* was the gene with the highest significance in the MITF^{high} group ($p = 3,7 \text{ e-}9$) while *AXL* was the most significant one in the MITF^{low} group ($p = 1,1 \text{ e-}5$).

In total, 21 genes showed significant upregulation in MITF^{low} melanoma cell lines while 44 genes were significantly upregulated in MITF^{high} melanoma cell lines.

In conclusion MITF^{low} and MITF^{high} cells and cell lines showed significant upregulation of specific sets of immune resistance genes.

A Jerby-Arnon et al.



B Wouters et al. + Ma-Mel-86

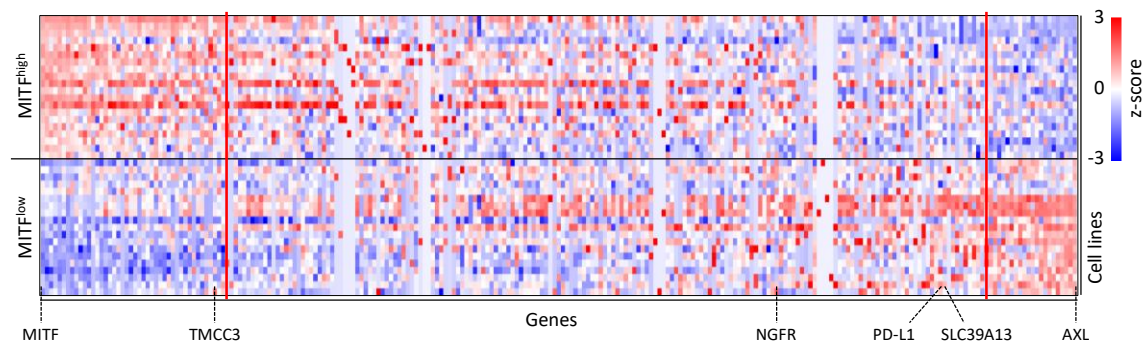


Figure 27: Significant up- and downregulation of immune resistance (IR) genes with respect to MITF expression in melanoma data sets.

This figure extends Figure 25. Analysis was conducted by using the programming language R for statistical computing. **(A)** Log₂ expression data of Jerby-Arnon *et al.* was transformed into z-scores and malignant cells were divided into a MITF^{high} group of cells with z-scores of MITF, MLANA and TYR > 0 and a MITF^{low} group of cells with z-scores of MITF, MLANA and TYR < 0. **(B)** Log₂ expression data of Wouters *et al.* combined with expression data of Ma-Mel-86 was transformed into z-scores and melanoma cell lines were divided into the MITF^{high} group of cell lines with the annotated phenotype “melanocytic” or “intermediate” or the MITF^{low} group when annotated “neural-crest stem cell like” or “mesenchymal”. **(A-B)** Gene expression in the MITF^{high} and MITF^{low} group were tested against each other by applying a Mann-Whitney-U-Test in a gene-wise manner. The resulting p-values were corrected for multiple testing and genes were ordered by their adjusted p-values. Heatmaps were created for visualization using the R package ‘pheatmap’. Vertical red lines indicate the threshold of significant upregulation in the respective group (adjusted p < 0,05). Position of selected melanoma marker genes (*MITF*, *NGFR*, *AXL*) and IR genes (*PD-L1*, *TMCC3*, *SLC39A13*) are highlighted in the heatmap.

5.4.5 Patient-derived melanoma samples reveal MITF^{low} cell subset that shows upregulation of immune resistance genes

One type of analysis that is widely used in the scientific community for single cell RNA-Seq analysis is Seurat [160]. With the help of cell marker genes, it identifies cell populations in data sets by comparing their expression profiles. The R package 'Seurat' together with 'Harmony' which eliminates patient-specific batch effects were used on raw count data of the Jerby-Arnon *et al.* data set in order to identify malignant and MITF^{low} malignant cell subsets in melanoma patient samples (Figure 28&29).

After conduction of quality control and harmony integration, 16 clusters were discovered (Figure 28A). A list of marker genes identified the malignant cell population in cluster 1, 5, 9 and 11 as well as T cells, B cells, NK cells, Macrophages, Endothelial cells, and cancer-associated fibroblasts (CAFs) (Figure 28B&C). The two smallest clusters with unclear cell assignment were eliminated from further analysis. By applying a list of marker genes to differentiate between MITF^{low} and MITF^{high} cells, one large MITF^{high} (cluster 1) and three smaller MITF^{low} (cluster 5, 9, 11) malignant cell populations were identified as melanocytic markers such as *MITF*, *TYR*, *MLANA* and Premelanosome Protein (*PMEL*) were upregulated in cluster 1 (Figure 28B&D). By applying a function to identify marker genes of each cell type and overlaying the list of marker genes with the list of immune resistance genes identified by our HTP screens I was able to identify immune resistance genes for each cell type that were upregulated (Figure 29A). Interestingly, the malignant MITF^{low} population still shared gene expression with the MITF^{high} population but at the same time, upregulated another set of genes. This was not higher expressed in the MITF^{high} population but interestingly in part in the CAF population.

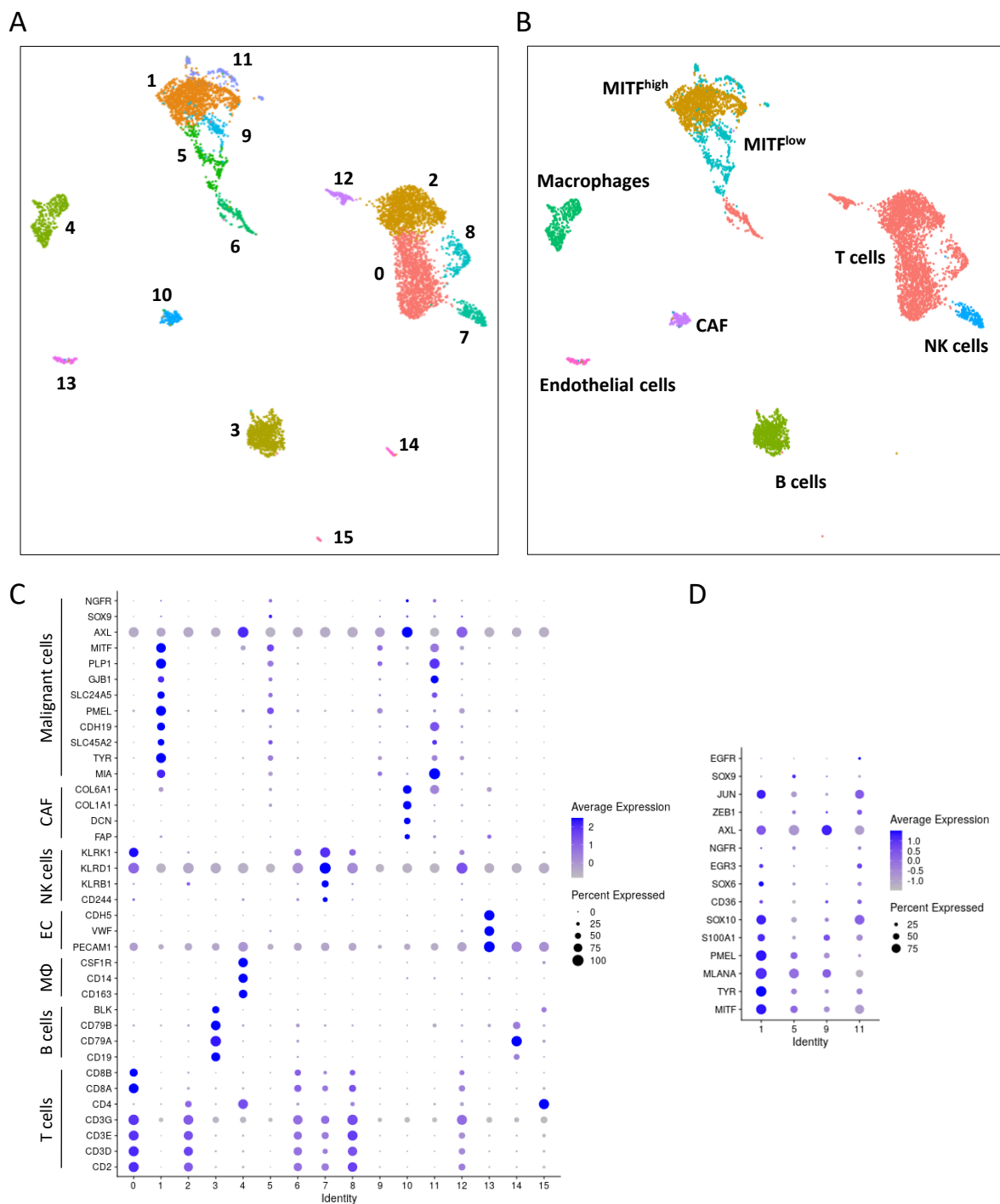


Figure 28: Malignant MITF^{high} and MITF^{low} cell subsets in patient-derived melanoma samples.

Analysis was conducted by using the programming language R for statistical computing with the packages ‘Seurat’ and ‘harmony’. Raw count data from the Jerby-Arnon *et al.* data set was subjected to quality control followed by normalization and scaling of the data. Harmony integration removed patient-specific batch effects and cells were clustered by their expression profiles. **(A)** UMAP plot of 16 identified clusters of cells. **(B)** UMAP plot with relabeled cell populations after cell type identification and exclusion of clusters 14 and 15. (CAF = cancer-associated fibroblasts, EC = endothelial cells, MΦ = macrophages). **(C-D)** Dot plots representing the expression patterns of marker genes to identify (C) melanoma cells among stromal cell populations and (D) subpopulations of MITF^{high} and MITF^{low} cells within the melanoma cell fraction of clusters 1, 5, 9 and 11.

By checking for cluster-associated marker genes within the malignant cell subpopulation and overlaying it with the list of immune resistance genes, genes that are differentially expressed between the four malignant clusters were identified (Figure 29B). *MITF*, *MLANA* and *TYR* are among those from cluster 1, the *MITF*^{high} cluster. Cluster 5 showed upregulation of several proteasomal subunit genes like Proteasome 26S Subunit, ATPase 1 (*PSMC1*), *PSMC3*, Proteasome 26S Subunit, Non-ATPase 1 (*PSMD1*), *PSMD6* and *PSMD13*. Also, Heparin Binding Growth Factor (*HDGF*) is among them, which is associated to cancer cell transformation and metastasis.

In summary, Seurat analysis revealed that immune resistance genes were differentially expressed between malignant cells and cells of the microenvironment as well as between the clusters of malignant cells.

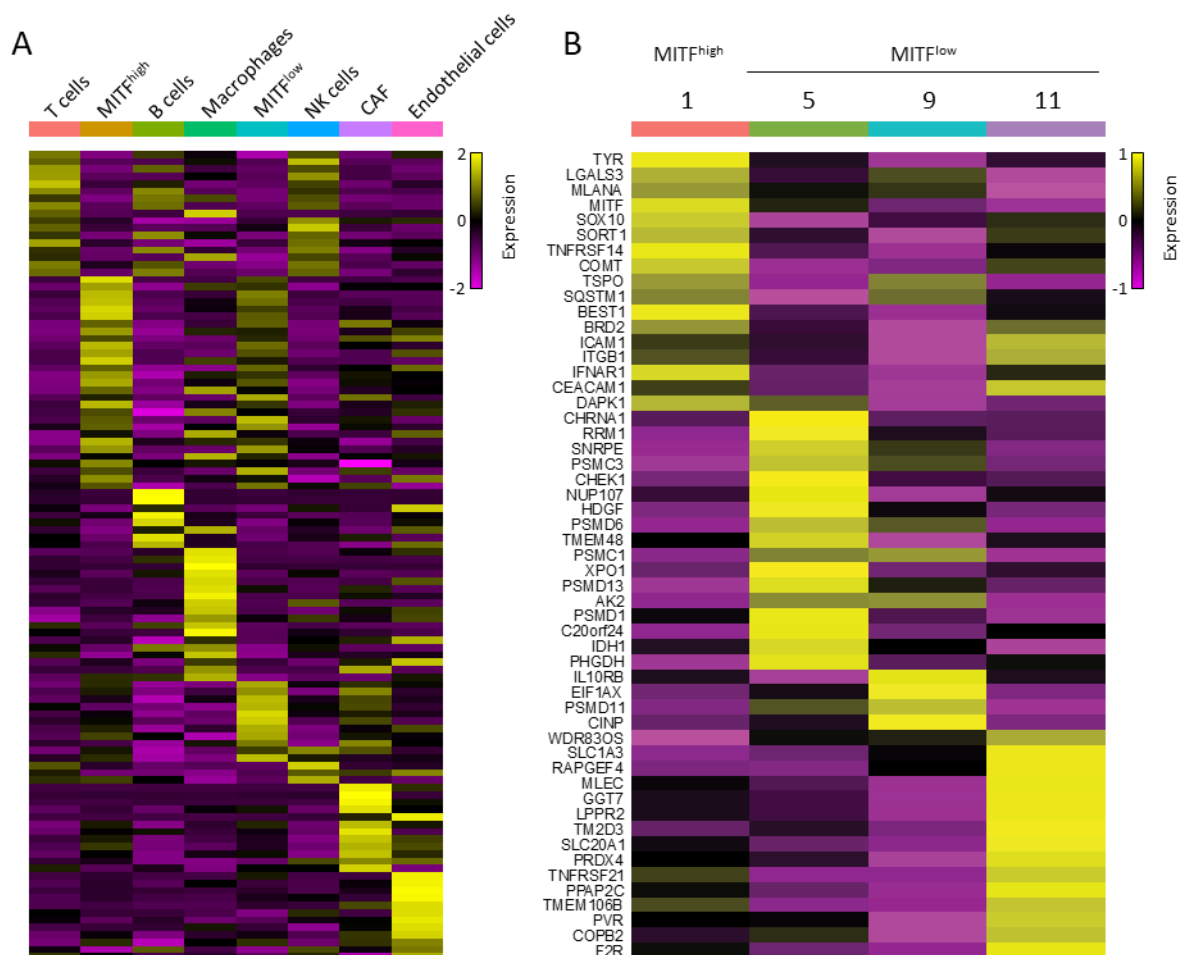


Figure 29: Overexpression of immune resistance (IR) genes in cell clusters of melanoma patients.

This figure extends Figure 28. Analysis was conducted by using the programming language R for statistical computing. **(A)** Marker genes for each cell type were identified and genes were filtered for the IR genes. Heatmap represents expression of IR marker genes in the cell subsets (CAF = cancer-associated fibroblasts). **(B)** Marker genes for each cluster of malignant cells (cluster 1, 5, 9 and 11) were filtered for immune resistance genes. Heatmap represents IR marker genes in the malignant clusters.

5.5 Functional validation of immune resistance genes

The HTP screens together with the bioinformatics aimed to identify novel immune resistance genes that showed an impact on tumor cell rejection by cytotoxic T cells, even in therapy resistant MITF^{low} melanomas. In order to finally understand the resistance mechanism, candidates for further functional validation were selected considering different parameters:

- Strong immune resistance phenotype in the HTP screens, especially in Ma-Mel-86a (MITF^{low})
- Association to a MITF^{low} co-expression cluster
- Negative correlation to MITF in gene expression data
- Low recognition in literature with regard to cancer and immunology
- Moderate to high expression levels in Ma-Mel-86, especially in Ma-Mel-86a (MITF^{low})

Validated hits from the HTP screens were filtered mainly for their recognition in literature to be included in functional analyses. Genes well known in cancer research with indications to or described resistance mechanisms were excluded. With regard to hits that were selected by their performance in the bioinformatic analyses, the genes had to be associated to MITF^{low} across multiple data sets.

5.5.1 Primary functional validation of pre-selected immune resistance genes

According to the selection parameters, a total of 17 genes were pre-selected for validation. I also included the control genes *AXL*, *NGFR*, *CFLAR* and *HDGF* which are either markers of MITF^{low} melanomas and/or genes that are known to play a role in cancer and immune resistance. Luciferase-based cytotoxicity assays for each gene were performed as in the HTP screens to check their impact on immune resistance. Additionally, gene expression levels were measured by quantitative PCR. Table 20 shows the summary of the performed experiments.

Immune resistance phenotypes of hits validated from the HTP screens were accordingly confirmed in the assays (Table 20). However, the effects in Ma-Mel-86c were not as strong as in the screen (Figure 30). Those genes that were added due to bioinformatic analyses such as Delta Like Canonical Notch Ligand 1 (*DLL1*) or Plexin A3 (*PLXNA3*) showed no or only weak immune resistance potential (Table 20). qPCR results demonstrated that many genes are expressed at low levels (Ct > 30). To narrow down the list of candidates for further functional analysis I selected hits with the strong effects and those which had a Ct value of less than 30, both conditions preferentially fulfilled in Ma-Mel-86a. Additionally, I took the gene's recognition described in literature into account. Finally, the remaining genes were MOK Protein Kinase (*MOK*), Solute Carrier Family 39 Member 13 (*SLC39A13*), Transmembrane and Coiled-Coil Domain Family 3 (*TMCC3*) and Zinc Finger Protein 443 (*ZNF443*). Of note, the protein encoded by *SLC39A13* is preferentially called ZIP13. For simplicity, I will stay with the name SLC39A13

in the upcoming sections for both, gene and protein name. Figure 30 shows the results of the kill assays for the remaining genes which show that several siRNAs of each gene affect the immunoregulatory potential of the melanoma cell. Additionally, the results for *CFLAR* and *HDGF* are displayed as control genes.

Table 20: Summary of Luciferase-based kill assays and quantitative real-time PCR

Gene	Origin	Effect in cytotoxicity assay		Ct value in qPCR	
		Ma-Mel-86a	Ma-Mel-86c	Ma-Mel-86a	Ma-Mel-86c
GJC2	Screen			29,4	29,7
MOK	Screen			23,5	22,0
ITGAX	Screen			33,4	26,9
SLC39A13	Screen			25,4	26,6
SLC13A2	Screen			31,9	33,5
TMCC3	Screen			27,5	28,0
SPNS3	Screen			30,8	32,5
ZNF443	Screen			29,1	35,2
GRM6	Screen			31,5	34,1
DLL1	Bioinformatics			30,8	30,6
CDH24	Bioinformatics			30,4	32,1
ELN	Bioinformatics			31,7	30,6
GCK	Bioinformatics			31,0	32,2
LRRN1	Bioinformatics			31,3	31,9
TMEM132E	Bioinformatics			32,8	32,2
S1PR1	Bioinformatics			27,0	31,1
PLXNA3	Bioinformatics			26,4	27,6
AXL	Bioinformatics			20,4	30,9
NGFR	Bioinformatics			30,8	27,2
HDGF	Bioinformatics			21,4	22,9
CFLAR	Screen			25,2	26,1

Column "Origin" indicates if the gene was selected primarily due to its performance in the HTP screens or because of its MITF^{low} association in the bioinformatic analyses. Blue color in the columns "Effect in cytotoxicity assay" represents immune resistance phenotype in the luciferase-based cytotoxicity assays while grey color indicates that no effect was observed. Columns "Ct value in qPCR" list the Ct values that were determined by quantitative real-time PCR with blue font highlighting a Ct value below 30. Amelie Bärnreuther contributed to the generation of the results as a student under my co-supervision.

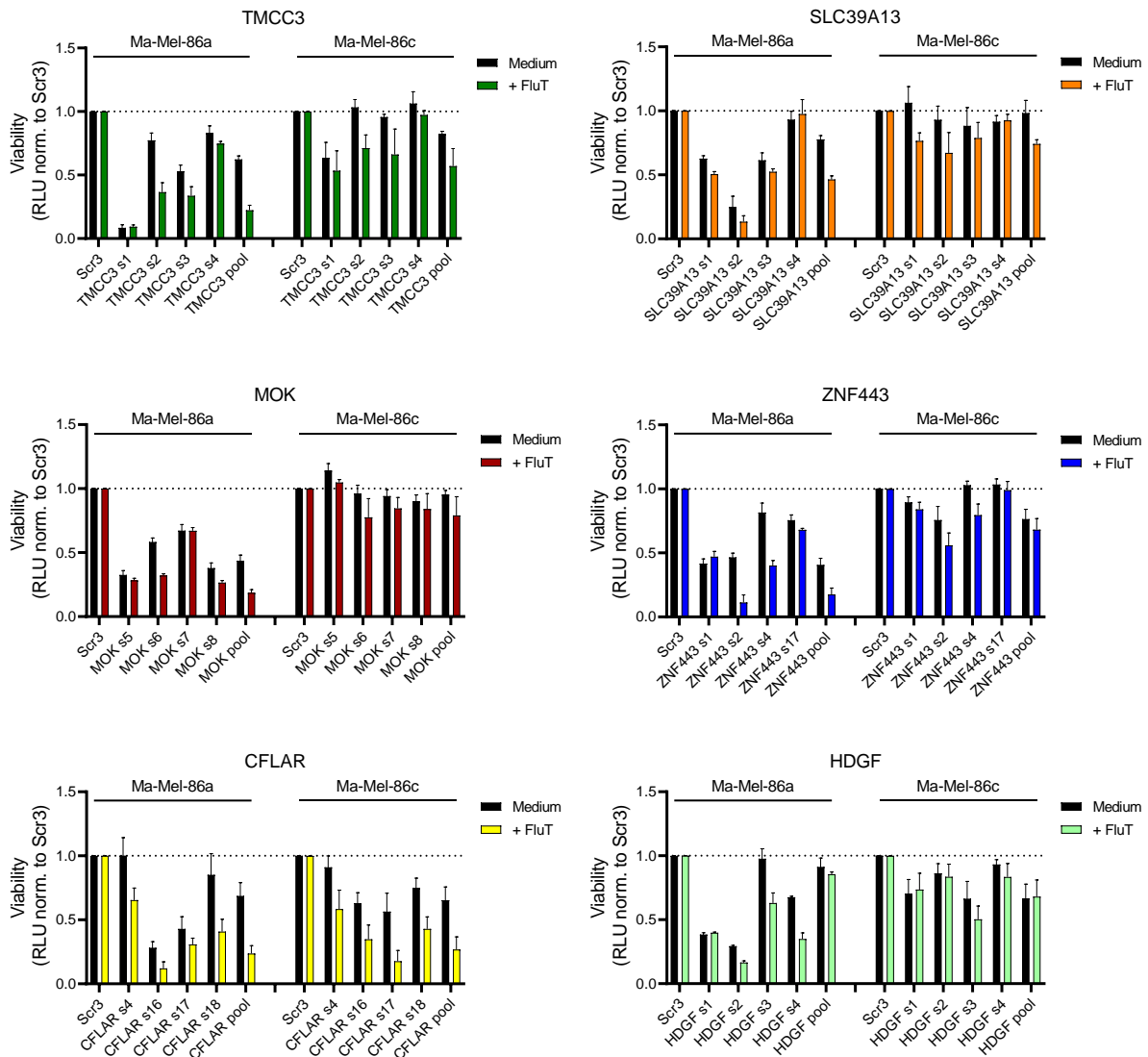


Figure 30: Performance of validated immune resistance (IR) genes in a de-convolution kill assay.

Luciferase-based cytotoxicity assay to validate the immune resistance phenotype of the candidate genes *TMCC3*, *SLC39A13*, *MOK* and *ZNF443* and re-test the effect of *CFLAR* and *HDGF*. Ma-Mel-86 HLA-A2+ Luc+ were transfected with individual or pooled siRNAs for 48 h. Melanoma cells were pulsed for 1 h and subsequently cultured in plain medium (viability setting) or co-culture with FluT cells (cytotoxicity setting) in an E:T ratio of 1:1 for Ma-Mel-86a and 0,5:1 for Ma-Mel-86c. Cells were lysed, and remaining luciferase activity was measured by luminescence. Raw luciferase units (RLU) were normalized to RLU of Scr3. Bars represent the mean of three independent experiments + standard deviation. Amelie Bärnreuther contributed to the generation of the data as a student under my co-supervision.

After confirming the immunoregulatory capacity for several siRNAs from the remaining candidate genes (Figure 30), qPCR was performed to check for the downregulation of target genes in Ma-Mel-86 cells upon transfection with siRNA (Figure 31). Just like in the previous cytotoxicity assays, individual as well as the pool of siRNAs for each gene were used (Supplementary Figure 2). Taking the cytotoxicity assays and qPCR data together, a single siRNA condition was chosen for each gene that showed a low viability impact but a strong effect on the cytotoxicity as well as strong knockdown efficiency. Further functional testing of the genes was conducted with the pool of four siRNAs for *TMCC3*, *MOK* and

SLC39A13 and with siRNA #4 for *ZNF443*. Concerning the qPCR results with these siRNAs, expression of *TMCC3*, *MOK*, *SLC39A13* and *ZNF443* was reduced in Ma-Mel-86a on average by 92 %, 86 %, 95 % and 43 % while in Ma-Mel-86c expression was reduced in average by 73 %, 39 %, 77 % and 40 %, respectively (Figure 31A). Western blot results showed downregulation of *TMCC3*, *SLC39A13* and *MOK* in Ma-Mel-86a, but hardly downregulation of *ZNF443* (Figure 31B). In Ma-Mel-86c downregulation of *MOK* was demonstrated by western blot. *TMCC3* and *SLC39A13* protein expression was difficult to detect, despite moderate mRNA expression (Table 20). Contrarily, expression of *ZNF443* was present, although mRNA expression was low (Ct = 35,2). However, protein knockdown efficiency of this gene was low both at mRNA and protein level.

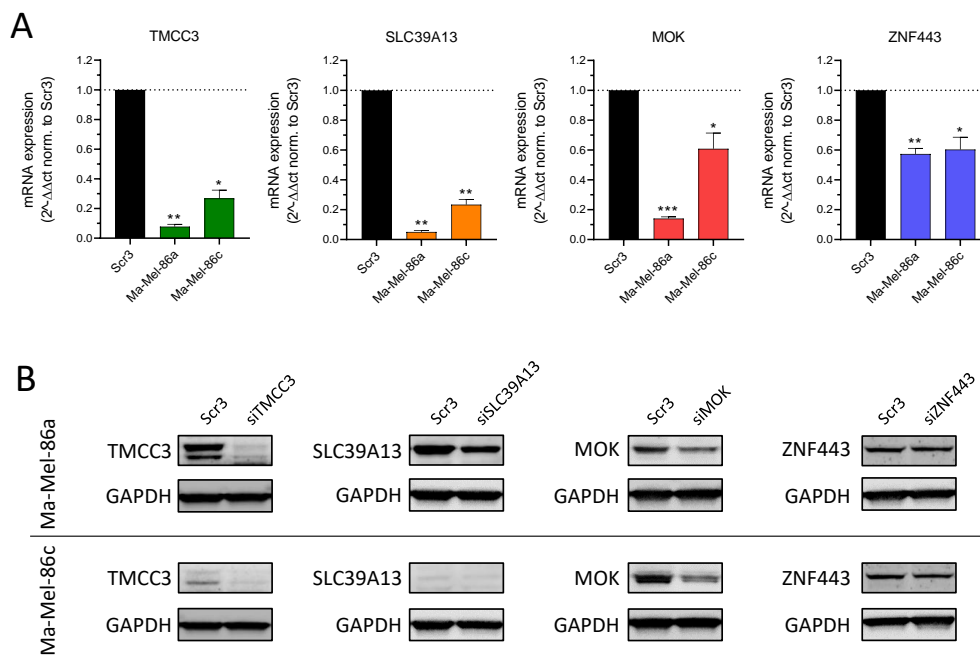


Figure 31: Knockdown efficiency of selected immune resistance (IR) genes.

Ma-Mel-86 HLA-A2+ Luc+ were transfected with Scr3, a pool of four siRNAs for *TMCC3*, *SLC39A13* and *MOK* or *ZNF443* siRNA for 48 h. **(A)** Cells were lysed for RNA isolation followed by reverse transcription to cDNA. Quantitative real-time PCR was used to measure target gene expression. Expression of Actin-beta was measured as reference gene to normalize gene expression and values were normalized to Scr3. Bars represent the mean + standard deviation of three independent experiments. Significance between siRNA and Scr3 for each cell line was calculated by applying a one-tailed ratio paired t-test (*p<0,05, **p<0,01). **(B)** Cells were lysed, and total protein was extracted. Protein expression of target genes was measured by western blot. GAPDH expression was acquired as reference gene. Verena Babl contributed to the generation of the data as a Master's student under my co-supervision.

To further validate the immunomodulatory role of the hits that was observed in the luciferase-based cytotoxicity assay with FluT cells, another assay system was chosen. Instead of measuring the remaining cell viability by luciferase activity, a real-time cytotoxicity assay was performed. Upon co-culture of Ma-Mel-86 HLA-A2+ Luc+ cells with FluT cells, the Incucyte® Cytotox Red Dye was added to measure tumor cell death. The Cytotox Dye enters cells with reduced cell membrane integrity and

binds to DNA. The GFP signal of the Luc⁺ cells was used to measure the confluency of the remaining cells to deduce the capacity of the tumor cells to continue proliferation. Every two hours green and red signal were detected in the Incucyte[®] instrument and the red signal was normalized to the green signal to measure tumor cell death in a time range up to 22-24 hours. The results of the real time cytotoxicity assay confirmed the phenotypes that were observed previously (Figure 32). siRNA transfection and knockdown of all four candidate genes caused increased tumor cell death by FluT cells in Ma-Mel-86a. While the effects were low for ZNF443 and SLC39A13, silencing of MOK and TMCC3 as well as the positive control CFLAR resulted in a stronger kill. In Ma-Mel-86c similar effects were observed (Figure 32). Downregulation of the positive control CFLAR as well as TMCC3 improved T cell-mediated tumor cell kill whereas silencing of MOK, SLC39A13 and ZNF443 showed low to no effects on the immunoregulatory capacity of the Ma-Mel-86c cells.

Taken together, the four immune resistance genes *TMCC3*, *SLC39A13*, *MOK* and *ZNF443* showed strong immune resistance phenotypes and were therefore selected for more extensive functional analyses.

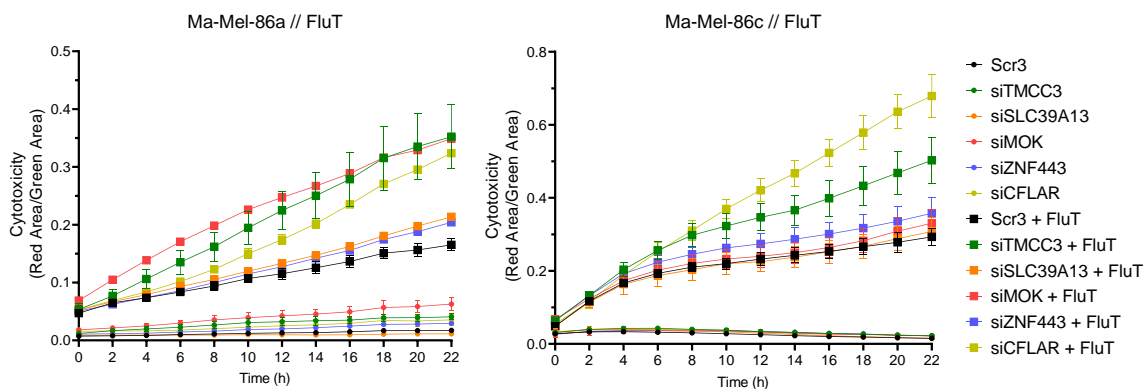


Figure 32: Impact of immune resistance genes on FluT cell-mediated tumor cell rejection.

Real time cytotoxicity assay to measure the impact of gene knockdown on the cytotoxicity of FluT cells. Ma-Mel-86 HLA-A2⁺ Luc⁺ were transfected with Scr3, a pool of four siRNAs for *TMCC3*, *SLC39A13*, *MOK* or *CFLAR* or *ZNF443* siRNA for 48 h. Melanoma cells were pulsed with flu peptide and subsequently cultured in medium or co-cultured with FluT cells at an effector to target ratio of 1:1 for Ma-Mel-86a and 0,5:1 for Ma-Mel-86c. Incucyte[®] Cytotox Red Dye was added to label dead cells and tumor cell death was measured every two hours for 22 h. The signal of the Red Area was normalized to the Green Area, representing the confluency of the tumor cells by detection of GFP. Representative data of two independent experiments.

5.5.2 Immunoregulatory potential of candidate genes is independent of T cell specificity

After performing cytotoxicity assays with FluT cells, immune resistance phenotypes of the four candidate genes were tested using melanoma specific MART-1 and TIL412 in the luciferase-based and the real-time cytotoxicity assays (Figure 33). As Figure 10 showed high resistance of Ma-Mel-86a against TIL412 and MART-1 T cells without prior pulsing with MART-1 peptide, Ma-Mel-86 HLA-A2⁺ Luc⁺ were pulsed with MART-1 peptide before co-culture with MART-1 T cells to normalize antigen

presentation between both melanoma cell lines. TIL412 were added without previous treatment to see if tumor cells can be sensitized to apoptosis in an antigen-unspecific manner.

Similar to cytotoxicity assays using FluT cells, co-culture of Ma-Mel-86a with MART-1 T cells showed increased tumor cell lysis upon knockdown of candidate genes (Figure 33A&C). Although TIL412 are not reactive to Ma-Mel-86a in principle, knockdown of all candidates and CFLAR increased tumor cell death significantly in the luciferase-based kill assay. Similarly in Ma-Mel-86c, gene knockdown increased tumor cell lysis in co-culture experiments with MART-1 and TIL412 (Figure 33B&D). Here, co-culture experiments with TIL412 showed stronger effects than in Ma-Mel-86a. In conclusion, the previously observed immune resistance phenotype of the candidate genes were confirmed in cytotoxicity assays with a different T cell co-culture system.

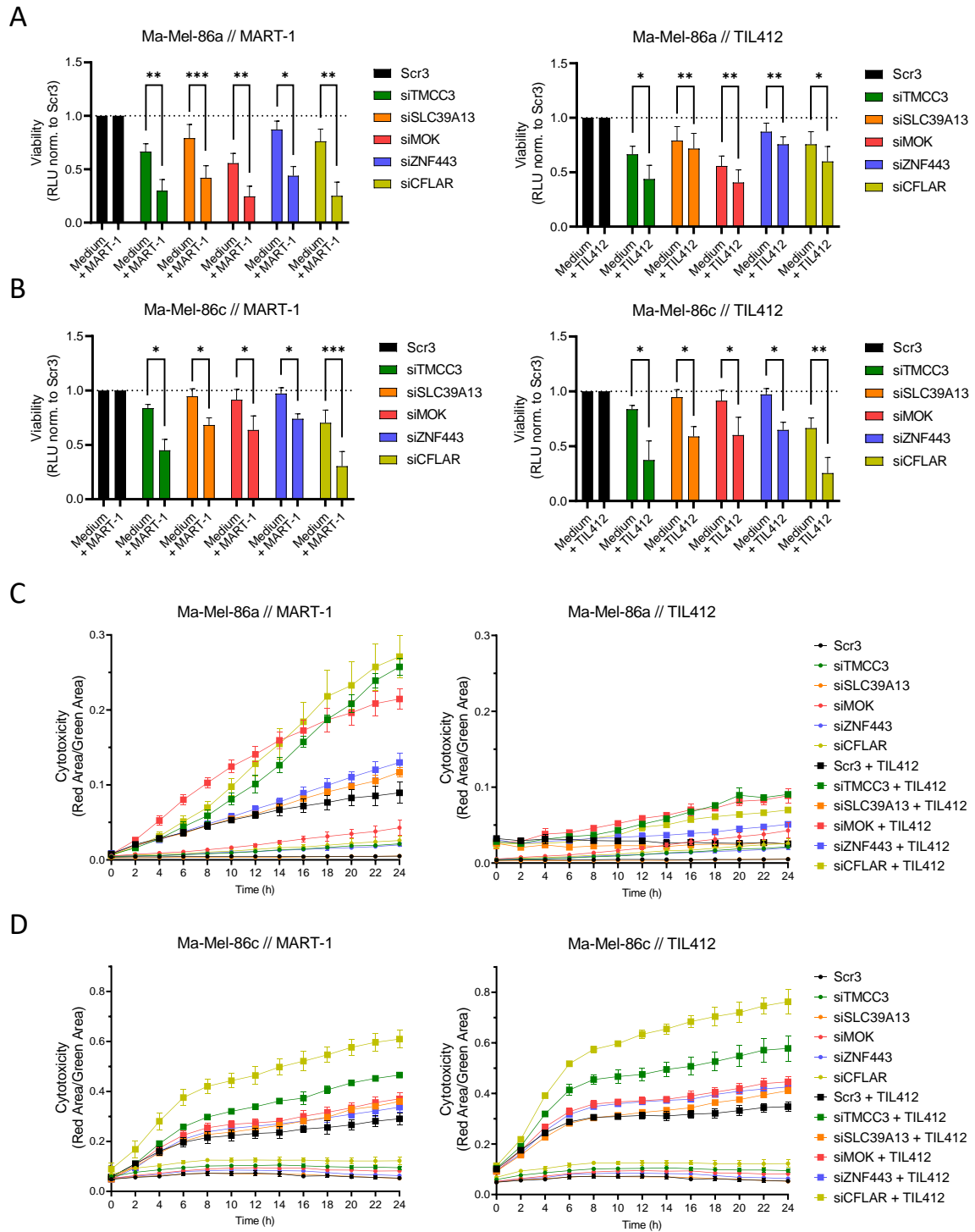


Figure 33: Impact of immune resistance genes on tumor cell rejection mediated by MART-1 T cells and TIL412. Cytotoxicity assays to measure the impact of gene knockdown on the cytotoxicity of MART-1 T cells and TIL412. Ma-Mel-86 HLA-A2+ Luc+ were transfected with Scr3, a pool of four siRNAs for *TMCC3*, *SLC39A13*, *MOK* or *CFLAR* or *ZNF443* siRNA for 48 h. In cytotoxicity assays with MART-1 T cells, the melanoma cells were pulsed with MART-1 peptide for 1 h and subsequently cultured in plain medium (viability setting) or co-cultured with MART-1 T cells (cytotoxicity setting) at an effector to target ratio of 1:1 for Ma-Mel-86a and 0,5:1 for Ma-Mel-86c. In experiments with TIL412, Ma-Mel-86 were not pulsed and cultured in plain medium (viability setting) or co-cultured with TIL412 (cytotoxicity setting) at an effector to target ratio of 5:1 for Ma-Mel-86a and 2,5:1 for Ma-Mel-86c. **(A-B)** Luciferase-based cytotoxicity assay with (A) Ma-Mel-86a and (B) Ma-Mel-86c. After co-culture of melanoma cells with T cells for 20 h, cells were lysed, and remaining luciferase activity was measured by luminescence. Raw luciferase units (RLU) were normalized to RLU of Scr3. Bars represent the mean + standard

deviation of three independent experiments. Significances between viability and cytotoxicity setting were calculated by applying a two-tailed paired t-test (* $p < 0,05$, ** $p < 0,01$, *** $p < 0,001$). **(C-D)** Real-time cytotoxicity assay with (C) Ma-Mel-86a and (D) Ma-Mel-86c. Upon co-culture of tumor cell and T cells Incucyte® Cytotox Red Dye was added to label dead cells and tumor cell death was measured every two hours for 24 h. The signal of the Red Area was normalized to the Green Area, representing the confluency of the tumor cells by detection of GFP. Representative data of two independent experiments. Verena Babl contributed to the generation of the data as a Master's student under my co-supervision.

5.5.3 Immune resistance genes show intrinsic protective effects in the tumor cells

As immune resistance of tumor cells can be caused either by inhibiting T cell function or by prevention of tumor cell apoptosis, I aimed to investigate on which side the four candidate genes act. Hence, Ma-Mel-86 HLA-A2+ Luc+ were treated with supernatant of polyclonally activated FluT cells in the cytotoxicity setting instead of co-cultured with cytotoxic T cells. The results showed that gene silencing of *TMCC3*, *MOK*, *SLC39A13* and *ZNF443* resulted in an increased cell death upon culture of tumor cells in supernatant (Figure 34). In the luciferase-based cytotoxicity assay this effect is stronger in Ma-Mal-86a than in Ma-Mel-86c. In the real-time cytotoxicity assay for both cell lines the effect is strong for *TMCC3* and the positive control *CFLAR* and weaker for the remaining three genes. Taken together, all genes showed intrinsic protective effects in Ma-Mel-86 against the treatment with T cell supernatant.

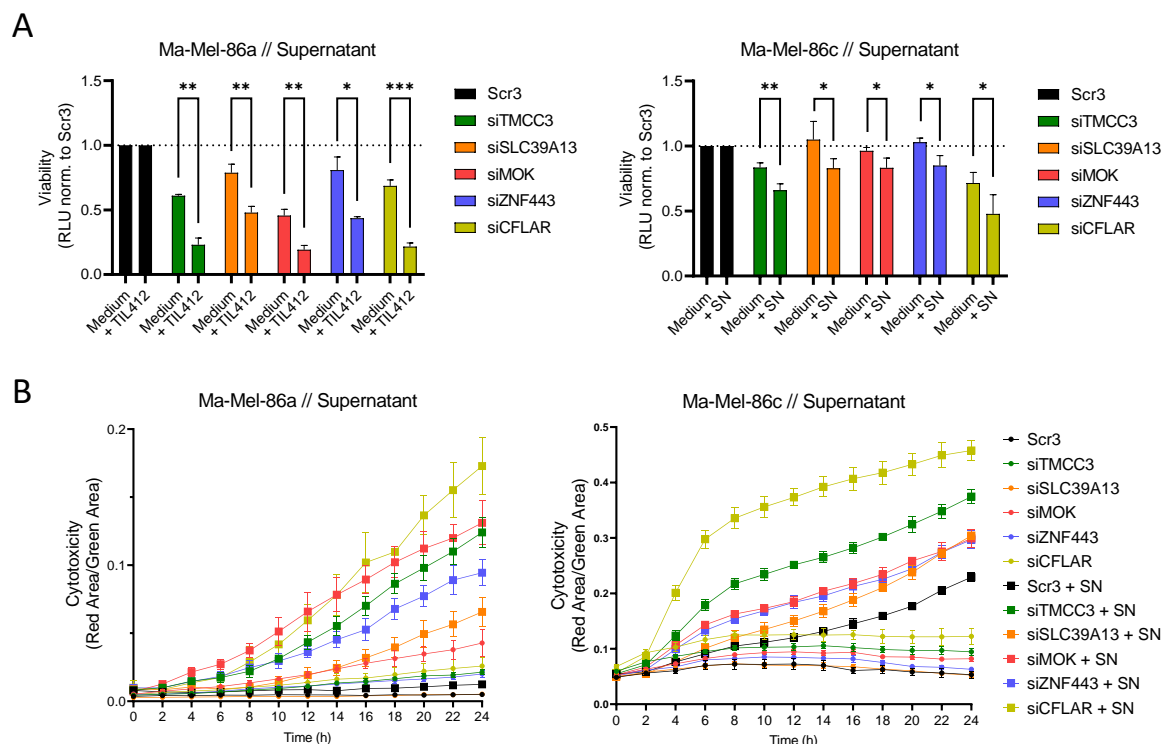


Figure 34: Impact of immune resistance genes on supernatant-mediated tumor cell rejection.

Cytotoxicity assays to measure the impact of gene knockdown on the cytotoxicity of supernatant of polyclonally activated FluT cells. Ma-Mel-86 HLA-A2+ Luc+ were transfected with Scr3, a pool of four siRNAs for *TMCC3*, *SLC39A13*, *MOK* or *CFLAR* or *ZNF443* siRNA for 48 h. Subsequently, cells were cultured in plain medium (viability setting) or in supernatant of FluT cells that were polyclonally activated for 24 h (cytotoxicity setting).

(A) Luciferase-based cytotoxicity assay with Ma-Mel-86a and Ma-Mel-86c. After treatment of melanoma cells

with supernatant for 20 h, cells were lysed, and remaining luciferase activity was measured by luminescence. Raw luciferase units (RLU) were normalized to RLU of Scr3. Bars represent the mean + standard deviation of three independent experiments. Significances between viability and cytotoxicity setting were calculated by applying a two-tailed paired t-test (* $p < 0,05$, ** $p < 0,01$, *** $p < 0,001$). **(B)** Real-time cytotoxicity assay with Ma-Mel-86a and Ma-Mel-86c. Upon treatment of tumor cells with supernatant Incucyte® Cytotox Red Dye was added to label dead cells and tumor cell death was measured every two hours for 24 h. The signal of the Red Area was normalized to the Green Area, representing the confluency of the tumor cells by detection of GFP. Representative data of two independent experiments. Verena Babl contributed to the generation of the data as a Master's student under my co-supervision.

5.5.4 Silencing of immune resistance genes sensitizes tumor cells to death receptor ligands

Figure 14 shows primary resistance of Ma-Mel-86 to treatments with the death receptor ligands TRAIL, TNF α , FasL, LT α and LIGHT. In order to investigate if silencing of candidate genes sensitizes tumor cells to apoptosis induced by death receptor ligands, cytotoxicity assays were performed by treating Ma-Mel-86 HLA-A2+ Luc+ with TRAIL, TNF α , FasL, LT α , LIGHT as well as IFN γ after gene knockdown. Figure 35A shows exemplary results of the luciferase-based cytotoxicity assay in Ma-Mel-86a for TRAIL and IFN γ treatment. Knockdown of the genes sensitized tumor cells to TRAIL induced tumor cell death, with the weakest effect with *SLC39A13* siRNA. On the other hand, *SLC39A13* silencing increased apoptosis upon IFN γ treatment more than other genes such as *TMCC3* and *CFLAR*. This was also observed in the real-time cytotoxicity assay measuring tumor cell death over a time of 48 h (Figure 35 B). The whole set of results can be found in Supplementary Figures 3 and 4.

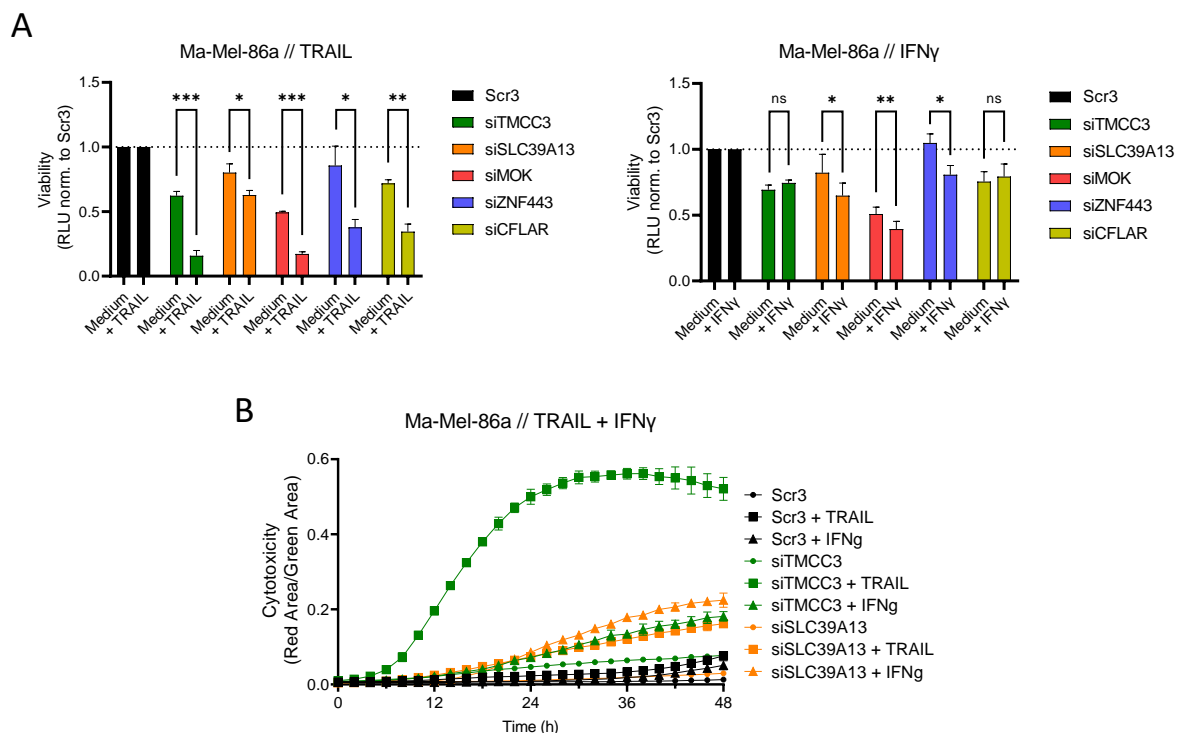


Figure 35: Impact of immune resistance genes on tumor cell rejection mediated by TRAIL or IFN γ .

Cytotoxicity assays to measure the impact of gene knockdown on the cytotoxicity of TRAIL or IFN γ treatment. Ma-Mel-86 HLA-A2+ Luc+ were transfected with Scr3, a pool of four siRNAs for *TMCC3*, *SLC39A13*, *MOK* or *CFLAR*

or *ZNF443* s4 siRNA for 48 h. Subsequently, cells were cultured in plain medium (viability setting) or treated with 100 ng/ml recombinant TRAIL or IFN γ (cytotoxicity setting). **(A)** Luciferase-based cytotoxicity assay with Ma-Mel-86a and Ma-Mel-86c. After treatment of melanoma cells with TRAIL or IFN γ for 20 h, cells were lysed, and remaining luciferase activity was measured by luminescence. Raw luciferase units (RLU) were normalized to RLU of Scr3. Bars represent the mean + standard deviation of three independent experiments. Significances between viability and cytotoxicity setting were calculated by applying a two-tailed paired t-test (* $p < 0,05$, ** $p < 0,01$, *** $p < 0,001$, ns=not significant). **(B)** Real-time cytotoxicity assay with Ma-Mel-86a and Ma-Mel-86c. Upon treatment of tumor cells with TRAIL or IFN γ Incucyte[®] Cytotox Red Dye was added to label dead cells and tumor cell death was measured every two hours for 48 h. The signal of the Red Area was normalized to the Green Area, representing the confluency of the tumor cells by detection of GFP. Representative data of two independent experiments. Verena Babl contributed to the generation of the data as a Master's student under my co-supervision.

In order to increase the comparability of the impact of gene knockdown on the different treatments, the ratio of cytotoxicity and viability setting (CV ratio) for each condition was determined. Thereby it was investigated to which treatments and putative pathways a gene can contribute to resistance. Generally, these resistance profiles were similar between Ma-Mel-86a and Ma-Mal-86c but as observed before, effects in Ma-Mel-86a were stronger than in Ma-Mel-86c, except for co-culture experiments with TIL412 (Figure 36). In general, gene silencing in the MITF^{high} cell line Ma-Mel-86c did not sensitize the cells to treatment with FasL and LT α . TMCC3 knockdown increased susceptibility of tumor cell death to the death receptor ligands TNF α , TRAIL, FasL and LT α . Compared to the co-culture with FluT and MART-1 or treatment with supernatant of polyclonally activated FluT cells, tumor cell death was even increased when treated with TRAIL in Ma-Mal-86a (75 % vs. 60 %). There was no enhanced apoptosis of the cells after treatment with LIGHT or IFN γ . Similar results could be observed for MOK and ZNF443, however effects were generally weaker while IFN γ treatment showed an increase of tumor cell death of about 20 %. On the other hand, downregulation of SLC39A13 sensitized Ma-Mel-86a against IFN γ stronger compared to its impact on TNF α or TRAIL treatment. However, no single treatment was able to induce tumor cell death to a similar level as co-culture with T cells or treatment with supernatant (Figure 36).

In summary, knockdown of immune resistance genes resulted in increased sensitivity of Ma-Mel-86 towards cytotoxic ligands with differential protective effects of the genes towards single treatments.

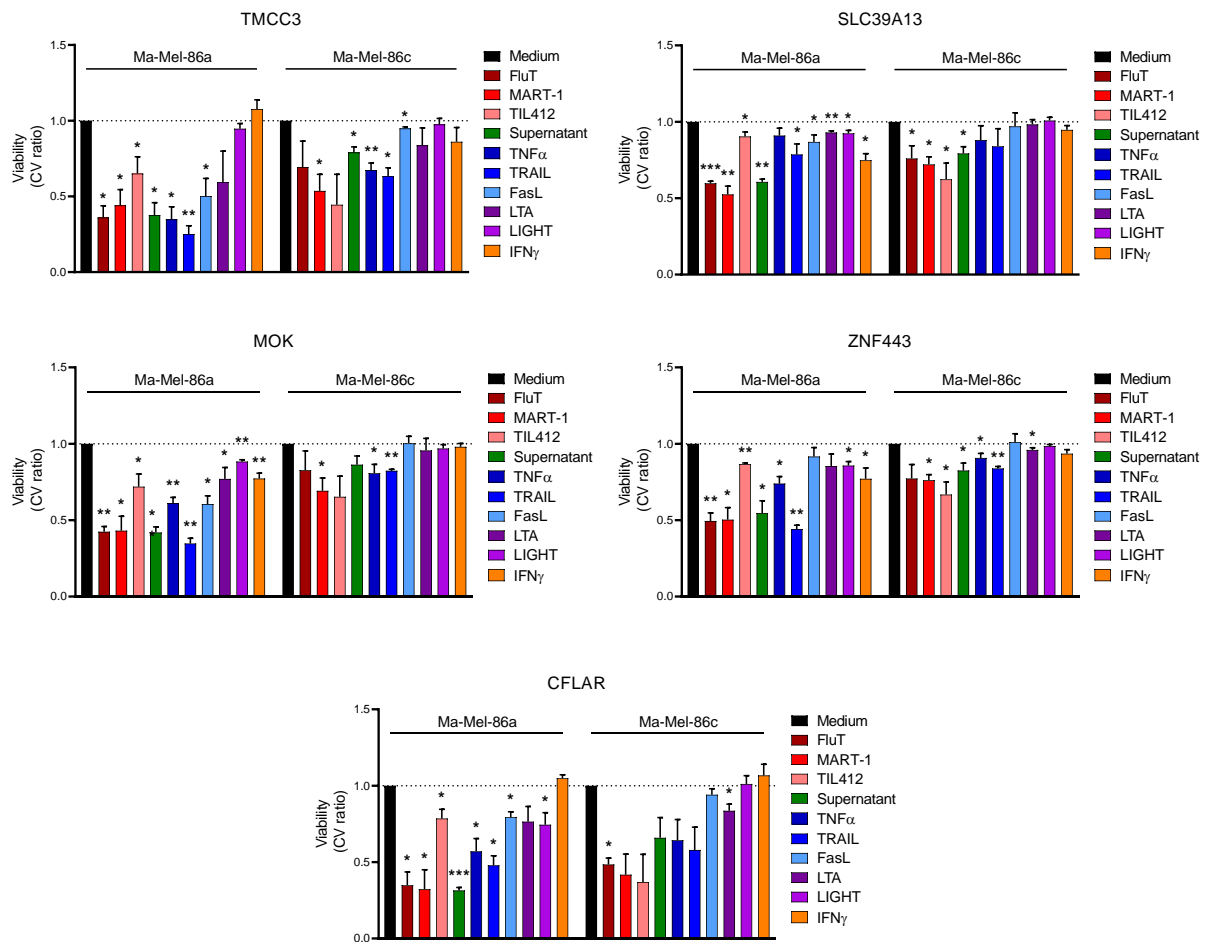


Figure 36: Cytotoxicity profiles of the immune resistance (IR) genes.

Summary of luciferase-based cytotoxicity assays. Ma-Mel-86 HLA-A2+ Luc+ were transfected with Scr3, a pool of four siRNAs for *TMCC3*, *SLC39A13*, *MOK* or *CFLAR* or *ZNF443* s4 siRNA for 48 h. Melanoma cells were cultured in plain medium (viability setting) or co-cultured with different T cell sources, treated with 100 ng/ml of single cytotoxic ligands or the supernatant of polyclonally activated FluT cells (cytotoxicity setting) for 20 h as described in Figures 30, 33-35 and Supplementary Figure 3. Normalized values of the cytotoxicity setting were divided by values of the viability setting, resulting in the CV ratio. Bars represent the mean of the CV ratios + standard deviation of three independent experiments for all different treatments. Significances between viability and each cytotoxicity setting were calculated by applying a two-tailed ratio paired t-test (* $p < 0,05$, ** $p < 0,01$, *** $p < 0,001$, no asterisk means not significant).

5.6 *TMCC3* and *SLC39A13* use different mechanisms to prevent tumor cell apoptosis

TMCC3 and *SLC39A13* were selected for further mode of action analysis in order to investigate how exactly they impact immune resistance in the MITF^{low} cell line Ma-Mel-86a. While *TMCC3* downregulation showed increased cell death upon TRAIL treatment, *SLC39A13* knockdown increased the susceptibility to IFN γ the most. Therefore, I picked two genes that could impact different pathways in the tumor cells. Additionally, knockdown efficiency was strong on both, the mRNA and protein level in Ma-Mel-86a. Both genes could also be associated with MITF^{low} in bioinformatic analysis: *TMCC3* was associated to the turquoise MITF^{low} gene cluster in the TCGA data as well as was part of the brown single cell cluster in the Jerby-Arnon *et al.* data set that was upregulated in a MITF^{low} patient (Figures

25&26). Additionally, *TMCC3* and *SLC39A13* were each higher expressed in one of the three *MITF*^{low} cell clusters in the Seurat analysis compared to the *MITF*^{high} cell cluster (Supplementary Figure 5). Also, *SLC39A13* was higher expressed in *MITF*^{low} cell lines compared to *MITF*^{high} cell lines, although not significantly (Figure 27).

5.6.1 The relationship between the expression of *MITF* and that of *TMCC3* or *SLC39A13*

In order to better understand if the expression of *MITF* and the two selected immune resistance genes influence each other in the *MITF*^{low} melanoma cell line Ma-Mel-86a I checked for the expression of *TMCC3* and *SLC39A13* after transfection of tumor cells with Scr3 or *MITF* siRNA (Figure 37A). The results showed that neither *TMCC3* nor *SLC39A13* expression was significantly affected by the downregulation of *MITF*.

Furthermore, *TMCC3* and *SLC39A13* were silenced and alterations of the expression of *MITF* were investigated (Figure 37B). Here, results demonstrated that upon knockdown of *TMCC3*, *MITF* was induced significantly. In contrast, *MITF* did not show changes in expression upon *SLC39A13* downregulation.

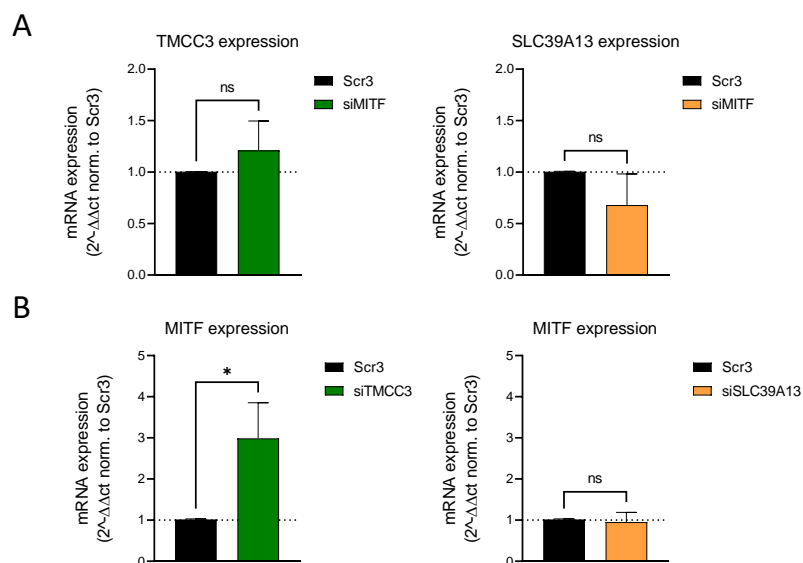


Figure 37: Relationship of gene expression between *MITF* and *TMCC3* or *SLC39A13*.

Quantitative real-time PCR to measure the gene expression of *MITF*, *TMCC3* and *SLC39A13*. Ma-Mel-86a HLA-A2+ Luc+ were transfected with Scr3 or a pool of four siRNAs for *TMCC3*, *SLC39A13* or *MITF* for 48 h. Subsequently, cells were lysed for RNA isolation followed by reverse transcription to cDNA. Quantitative real-time PCR was used to measure target gene expression. Expression of Actin-beta was measured to normalize gene expression and values were normalized to Scr3. Bars represent the mean + standard deviation of three independent experiments. Significance between siRNA and Scr3 was calculated by applying a two-tailed ratio paired t-test (*p<0,05, ns=not significant). **(A)** Expression of *TMCC3* and *SLC39A13* upon *MITF* knockdown. **(B)** Expression of *MITF* upon knockdown of *TMCC3* and *SLC39A13*, respectively.

5.6.2 Supernatant of activated FluT cells induces TMCC3 expression

I also investigated whether *TMCC3* and *SLC39A13* are upregulated as a resistance mechanism in response to cytotoxic ligands expressed by T cells to induce tumor cell apoptosis. For that reason, expression of the two genes was measured after treatment of Ma-Mel-86 with supernatant of polyclonally activated FluT cells, TNF α or IFN γ . Expression changes of *MITF* in response to these treatments was also investigated (Figure 38).

The results demonstrated that *TMCC3* expression was significantly increased by 2,5-fold in Ma-Mel-86a upon treatment with the supernatant of polyclonally activated FluT cells while *SLC39A13* induction was not significant (Figure 38A). TNF α treatment did not alter the expression of both genes while IFN γ treatment had no impact on the expression of *TMCC3* and decreased *SLC39A13* levels significantly by around 50 % (Figure 38B&C). *MITF* was downregulated significantly by 40 % in response to treatment with supernatant (Figure 38A). IFN γ treatment led to an insignificant decrease of *MITF* expression, while TNF α treatment didn't change *MITF* expression (Figure 38B&C).

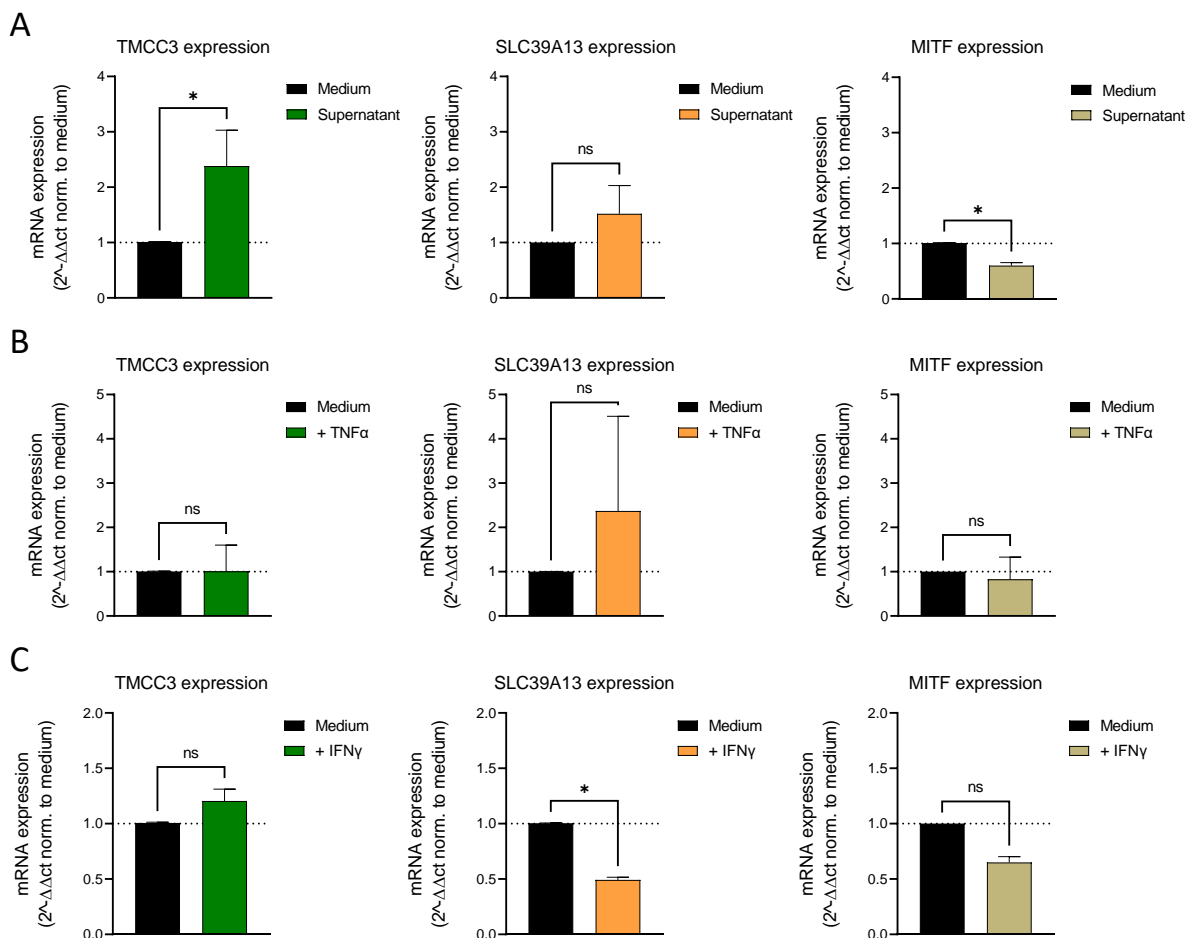


Figure 38: Expression of TMCC3, SLC39A13 and MITF after various treatments of Ma-Mel-86a.

Quantitative real-time PCR to measure the gene expression of *MITF*, *TMCC3* and *SLC39A13* in Ma-Mel-86a HLA-A2+ Luc after 20 h of culture in plain medium or treatment with 100 ng/ml TNF α or IFN γ or supernatant of FluT cells that were polyclonally activated for 24 h. Subsequently, cells were lysed for RNA isolation followed by reverse transcription to cDNA. Quantitative real-time PCR was used to measure target gene expression.

Expression of Actin-beta was measured to normalize gene expression and values were normalized to those of cells that were cultured in plain medium. Bars represent the mean + standard deviation of (A) three or (B-C) two independent experiments. Significance between untreated and treated cells was calculated by applying a two-tailed ratio paired t-test (* $p < 0,05$, ns=not significant). **(A)** Expression of *TMCC3*, *SLC39A13* and *MITF* upon treatment with supernatant. **(B)** Expression of *TMCC3*, *SLC39A13* and *MITF* upon treatment with TNF α . **(C)** Expression of *TMCC3*, *SLC39A13* and *MITF* upon treatment with IFN γ .

5.6.3 Simultaneous knockdown of *TMCC3* and *SLC39A13* does not increase tumor cell rejection by FluT cells

As a proportion of tumor cells survive after co-culture with T cells or treatment with cytotoxic ligands, I investigated whether combined knockdown of the genes could increase tumor cell lysis especially as the hypothesis indicated that *TMCC3* and *SLC39A13* could impact different signaling pathways (Figure 39). Both genes were silenced simultaneously, and luciferase-based and real-time cytotoxicity assays were performed. The results showed that tumor cell death was not increased by combining *TMCC3* and *SLC39A13* siRNAs, observed in both assay systems (Figure 39A&B).

In order to exclude the possibility that only cells survived that were not affected by gene silencing of the genes, gene expression was measured by qPCR in cells cultured in plain medium and in remaining cells after the co-culture with FluT cells. The results demonstrated that gene knockdown of *TMCC3* and *SLC39A13* was present before and after co-culture (Figure 39C).

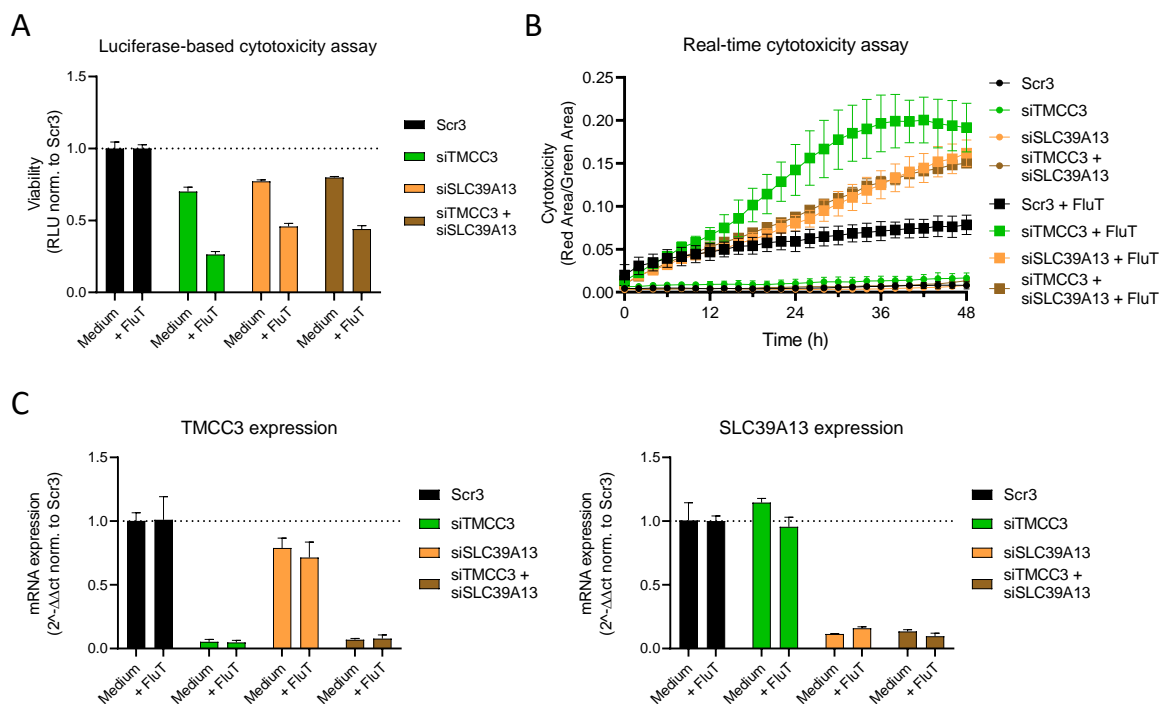


Figure 39: Co-knockdown of *TMCC3* and *SLC39A13* in Ma-Mel-86a.

Ma-Mel-86a HLA-A2⁺ Luc⁺ were transfected with Scr3 or a pool of four siRNAs for *TMCC3* or *SLC39A13* or *TMCC3+SLC39A13* for 48 h. Melanoma cells were pulsed with flu peptide for 1 h and subsequently cultured in plain medium (viability setting) or co-cultured with FluT cells (cytotoxicity setting) at an effector to target ratio

of 1:1. **(A)** Luciferase-based cytotoxicity assay. After co-culture of melanoma cells with FluT cells for 20 h, cells were lysed, and remaining luciferase activity was measured by luminescence. Raw luciferase units (RLU) were normalized to RLU of Scr3. Bars represent the mean of technical replicates + standard deviation. **(B)** Real-time cytotoxicity assay. Upon co-culture of tumor cell and FluT cells Incucyte® Cytotox Red Dye was added to label dead cells and tumor cell death was measured every two hours for 48 h. The signal of the Red Area was normalized to the Green Area, representing the confluency of the tumor cells by detection of GFP. **(C)** Quantitative real-time PCR to measure the expression of *TMCC3* and *SLC39A13*. After culture in plain medium or co-culture of melanoma cells with FluT cells for 20 h, cells were lysed for RNA isolation followed by reverse transcription to cDNA. Quantitative real-time PCR was used to measure target gene expression. Expression of Actin-beta was measured as reference gene to quantify gene expression and values were normalized to Scr3 in both, the viability and cytotoxicity setting. Bars represent the mean of technical replicates + standard deviation. Representative data of two independent experiments.

5.6.4 Co-culture with FluT cells downregulate expression of receptors that are important for antigen expression as well as induction of apoptosis

As simultaneous knockdown of *TMCC3* and *SLC39A13* did not increase tumor cell death compared to a single knockdown, it was further investigated whether surface expression of receptors that are involved in tumor cell death was reduced in Scr3 and *TMCC3* and/or *SLC39A13* silenced Ma-Mel-86a cells. After co-culture with FluT cells expression of DR5/TRAILR2, TNFR1, FAS, and IFN γ R1 as well as the expression of HLA-A2 being responsible for flu peptide antigen presentation was analyzed by flow cytometry (Figure 40). To characterize receptor expression on live or apoptotic cells a live/dead marker was used. Zombie NIR dye enters dying cells and therefore separates the population of dying and living cells. Zombie NIR staining interestingly showed that among the fraction of living cells two subpopulations after FluT co-culture were present, mainly in *TMCC3* silenced cells (Figure 40A). Receptor expression was differentially investigated in the Zombie NIR^{low} population (most viable cells) and the Zombie NIR^{medium} population. Figure 40B shows exemplary histograms of the flow cytometry analysis in which expression of DR5 and HLA-A2 is lower in the NIR^{low} fraction, especially in the *TMCC3* silenced cells.

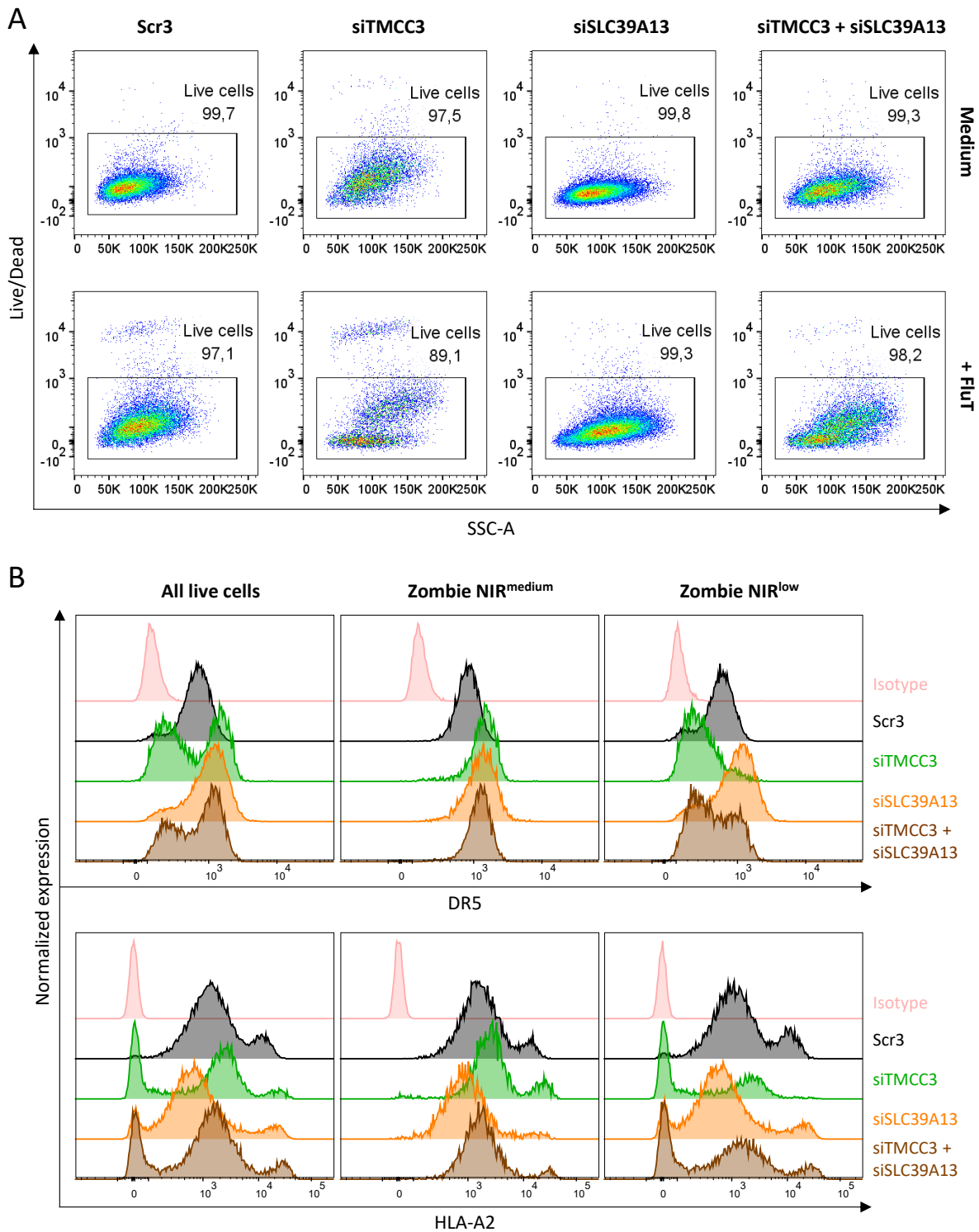


Figure 40: Flow cytometry analysis after co-culture of Ma-Mel-86a with FluT cells.

Ma-Mel-86a HLA-A2⁺ were transfected with Scr3 or a pool of four siRNAs for *TMCC3* or *SLC39A13* or *TMCC3+SLC39A13* for 48 h. Melanoma cells were pulsed with flu peptide for 1 h and subsequently cultured in plain medium (viability setting) or co-cultured with FluT cells (cytotoxicity setting) at an effector to target ratio of 1:1 for 20 h. Subsequently, cells were stained with Zombie NIR as well as isotype or antigen-specific antibodies for DR5/TRAILR2, TNFR1, FAS, IFN γ R1 and HLA-A2. Representative data of three independent experiments. **(A)** Dot plots representing the positivity of Zombie NIR in Ma-Mel-86a in order to identify the fraction of living cells. The upper lane shows plots for cells in the viability setting while the lower lane shows plots for cells in the cytotoxicity setting after co-culture with FluT cells. **(B)** Histogram plots of DR5 (upper lane) and HLA-A2 (lower lane) expression in all living cells (left), in cells with medium Zombie NIR positivity (center) and in cells with low

Zombie NIR positivity (right). One plot represents the histograms for the isotype of Scr3 treated cells (pink curve) as well as the staining with receptor-specific antibodies in all different siRNA conditions after co-culture of Ma-Mel-86a with FluT cells.

Flow cytometry analysis demonstrated that upon co-culture tumor cells downregulated the majority of the acquired receptors (Figure 41). Death receptors DR5/TRAILR2 and TNFR1 as well as IFN γ R1 and HLA-A2 were lower expressed while expression of FAS was increased. Receptor downregulation was even more prominent in the Zombie NIR^{low} cell subpopulation, for example up to 80 % for IFN γ R1 after co-culture. Here, TMCC3 silenced cells also lost their phenotype of FAS upregulation. Regarding the co-knockdown, the expression levels of the receptors were between those of the single knockdowns in Ma-Mel-86a.

Taken together, upon co-culture with FluT cells, Ma-Mel-86 decreased susceptibility to T cell-mediated rejection by downregulation of several receptors that are important for apoptosis induction and antigen presentation.

All live cells

Zombie NIR^{low}

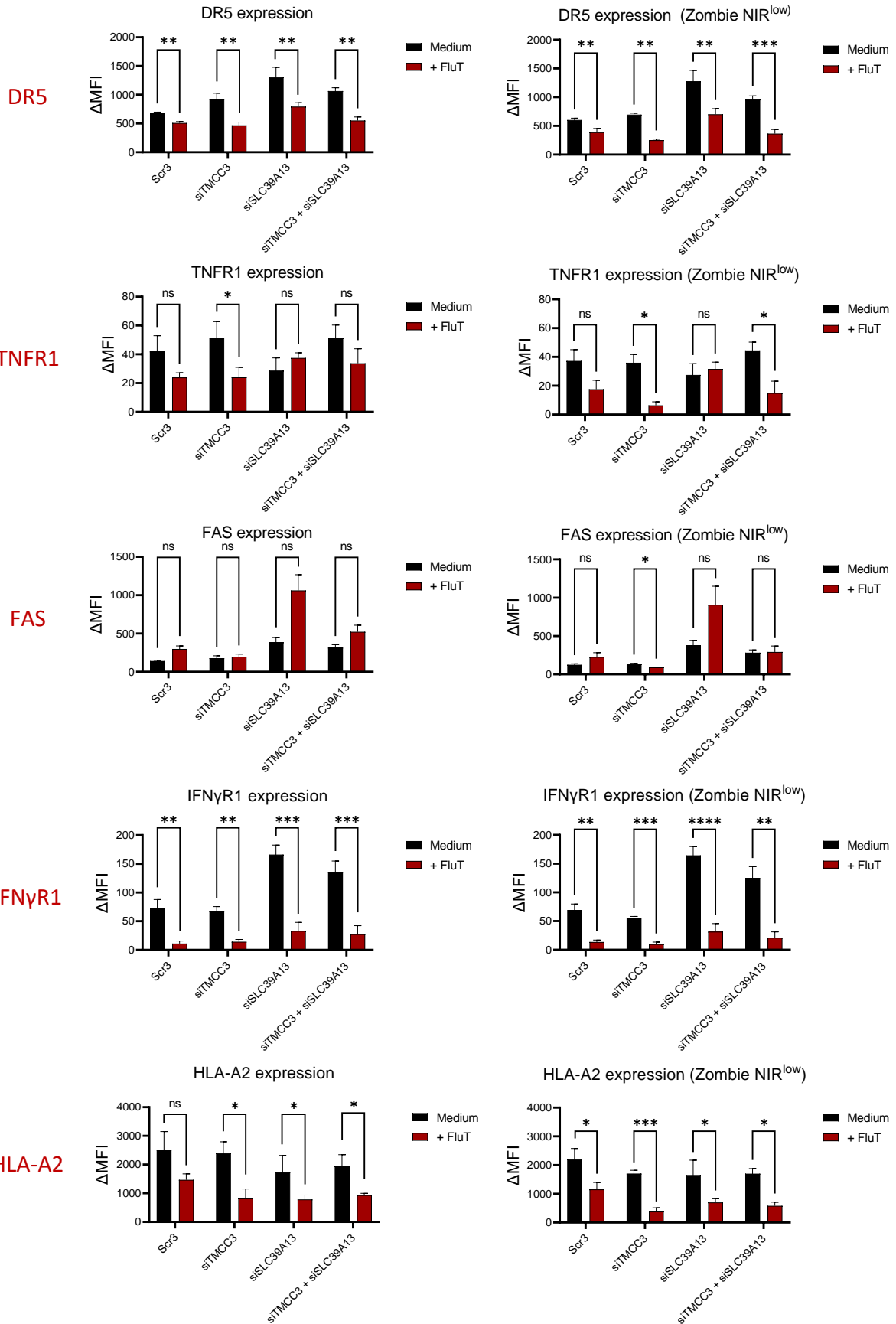


Figure 41: Regulation of surface receptors after co-culture of Ma-Mel-86a with FluT cells.

This figure extends Figure 40. Flow cytometry analysis was used to calculate the Δ MFI (MFI: mean fluorescence intensity using the geometric mean), representing the difference between the MFI of receptor-stained cells and the MFI of the respective isotype. Δ MFI was calculated for all acquired receptors DR5/TRAILR2, TNFR1, FAS, IFN γ R1 and HLA-A2 in the viability and cytotoxicity setting for all living cells (left panel) and the cells with low Zombie NIR positivity (right panel). Bars represent the mean of Δ MFI + standard deviation of three independent experiments. Significances between viability and cytotoxicity setting were calculated by applying a one-tailed paired t-test (* $p < 0,05$, ** $p < 0,01$, *** $p < 0,001$, **** $p < 0,0001$, ns = not significant).

5.6.5 Downregulation of TMCC3 and SLC39A13 alter receptor expression *per se*

In order to understand increased T cell-mediated tumor cell death after silencing of TMCC3 and SLC39A13, it was investigated if the downregulation of the two proteins alter the expression of surface receptors that are important for apoptosis of Ma-Mel-86a. In the context of the previous experiment, I also checked by flow cytometry analysis if the knockdown of TMCC3 and SLC39A13 altered the expression of DR5/TRAILR2, TNFR1, FAS, IFN γ R1 and HLA-A2 *per se* (Figure 42).

The results indicated that TMCC3 silencing did not change the expression of HLA-A2, IFN γ R1, TNFR1 and FAS (Figure 42A). Surface expression of DR5/TRAILR2 was increased, although not significantly. SLC39A13 knockdown on the other hand increased expression of DR5/TRAILR2, FAS and IFN γ R1 significantly. Expression of HLA-A2 was decreased with significance upon SLC39A13 silencing while TNFR1 expression was reduced insignificantly. Figure 43B shows exemplary histograms for the expression of DR5, IFN γ R1 and HLA-A2 after knockdown of TMCC3 and SLC39A13. In conclusion, downregulation of TMCC3 or SLC39A13 altered the expression of receptors that are important for apoptosis induction and antigen presentation, *per se*.

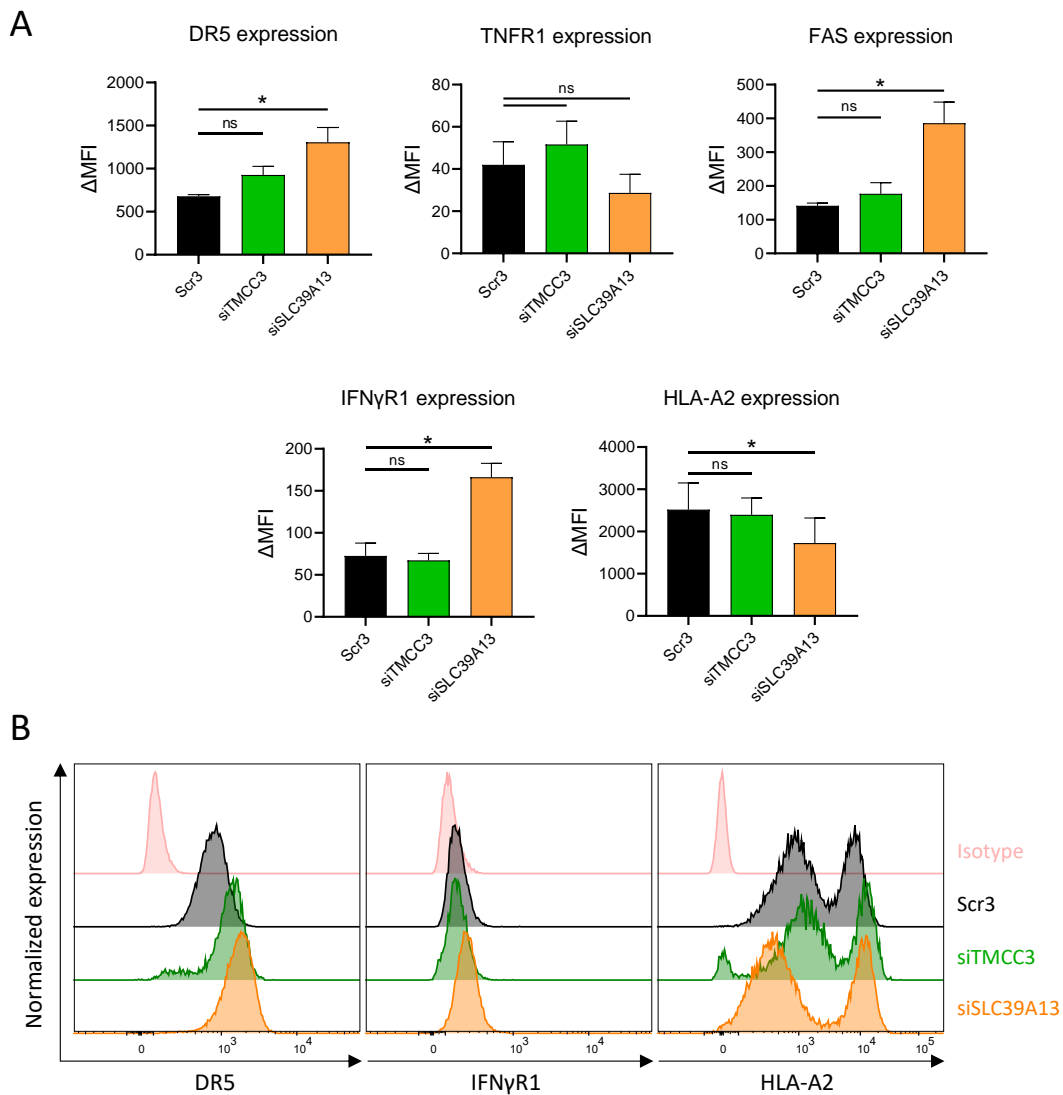


Figure 42: Regulation of surface receptors upon knockdown of TMCC3 and SLC39A13.

This figure extends Figure 40. Flow cytometry analysis was used to calculate the Δ MFI (MFI: mean fluorescence intensity using the geometric mean), representing the difference between the MFI of receptor-stained cells and the MFI of the respective isotype. Δ MFI was calculated for all acquired receptors DR5/TRAILR2, TNFR1, FAS, IFN γ R1 and HLA-A2 in the viability setting for all living cells in Scr3 and single knockdowns of TMCC3 and SLC39A13. **(A)** Bars represent the mean of Δ MFI + standard deviation of three independent experiments. Significances between Scr3 and TMCC3 or SLC39A13 knockdown were calculated by applying a two-tailed paired t-test (* $p < 0,05$, ns = not significant). **(B)** Histogram plots of DR5 (left panel), IFN γ R1 (center panel) and HLA-A2 (right panel) expression. One plot represents the histograms for the isotype of Scr3 treated cells (pink curve) as well as the staining with receptor-specific antibodies in all different siRNA conditions. Representative data of three independent experiments.

5.6.6 Downregulation of TMCC3 and SLC39A13 sensitize Ma-Mel-86a to apoptosis by regulating the expression of caspases and BCL-2

After demonstration of increased tumor cell lysis by various treatments upon knockdown of TMCC3 and SLC39A13 and alteration of expression of receptors playing a role in antigen presentation and apoptosis induction, tumor cell intrinsic pathways were further investigated. Initially, the protein

expression of apoptotic proteins such as cleaved Caspase-3, Caspase-8 and Caspase-9 as well anti-apoptotic protein B-cell lymphoma 2 (BCL-2) was measured by western blot (Figure 43).

The results showed that downregulation of TMCC3 and SLC39A13 impacted the expression of caspases and BCL-2. TMCC3 knockdown didn't affect expression of Caspase-9 but enhanced Caspase-3 and Caspase-8 expression and downregulated BCL-2. Cleavage of caspases, especially of caspase-8 could be detected upon TMCC3 silencing. SLC39A13 knockdown did not alter the expression of Caspase-3, but increased expression of Caspase-8 and Caspase-9. Furthermore, BCL-2 expression was downregulated. In contrast to TMCC3 silencing, cleavage of caspases is hardly present in the SLC39A13 knockdown cells. In summary, downregulation of both immune resistance gene increased susceptibility towards tumor cell death by upregulation of caspases as well as downregulation of BCL-2.

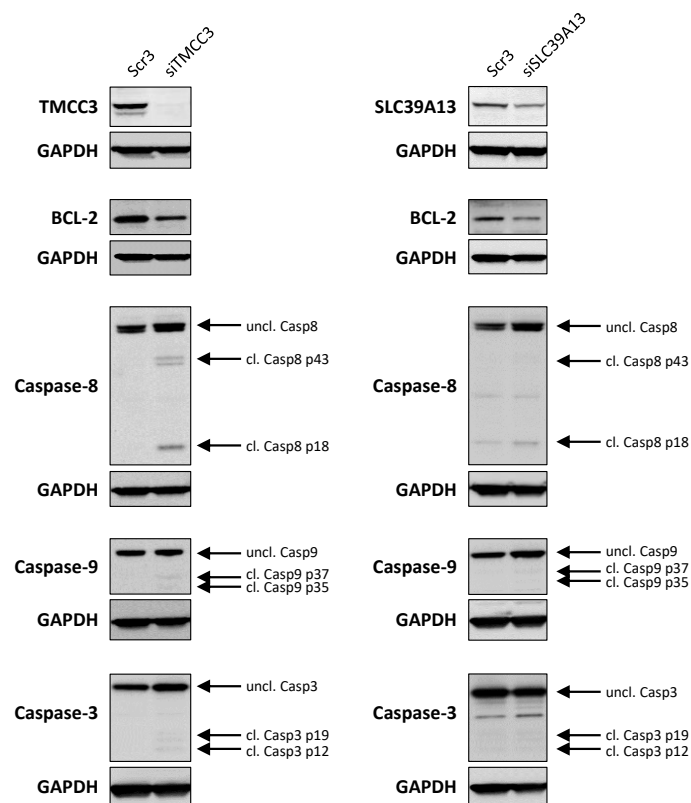


Figure 43: Expression of apoptotic genes in TMCC3 or SLC39A13 proficient/deficient Ma-Mel-86a.

Ma-Mel-86a HLA-A2+ Luc+ were transfected with Scr3 or a pool of four siRNAs for *TMCC3* or *SLC39A13* for 48 h. Cells were lysed, and total protein was extracted. Expression of TMCC3, SLC39A13, BCL-2 and activity of Caspase-3/-8/-9 was detected by western blot. GAPDH expression was acquired as reference gene. Representative data of two independent experiments. Verena Babl contributed to the generation of the data as a Master's student under my co-supervision.

5.6.7 TRAIL treatment increases caspase activity in TMCC3 silenced Ma-Mel-86a

As TRAIL showed strong capacity in inducing tumor cell death after TMCC3 knockdown, the induction of the caspase activity and the expression of BCL-2 was monitored upon TRAIL treatment for 30 min, 2 h and 4 h by western blot (Figure 44). The results demonstrated that caspases were cleaved upon TRAIL treatment preferentially in the TMCC3 silenced tumor cells. In Scr3 transfected cells Caspase-8 as well as Caspase-3 cleavage was present in later time points of TRAIL treatment, but in the TMCC3 knockdown cells this was highly increased. BCL-2 expression is not altered upon TRAIL treatment, and it remained to be lower expressed in the TMCC3 silenced cells. In summary, TRAIL treatment induced apoptosis preferentially in TMCC3 deficient Ma-Mel-86a.

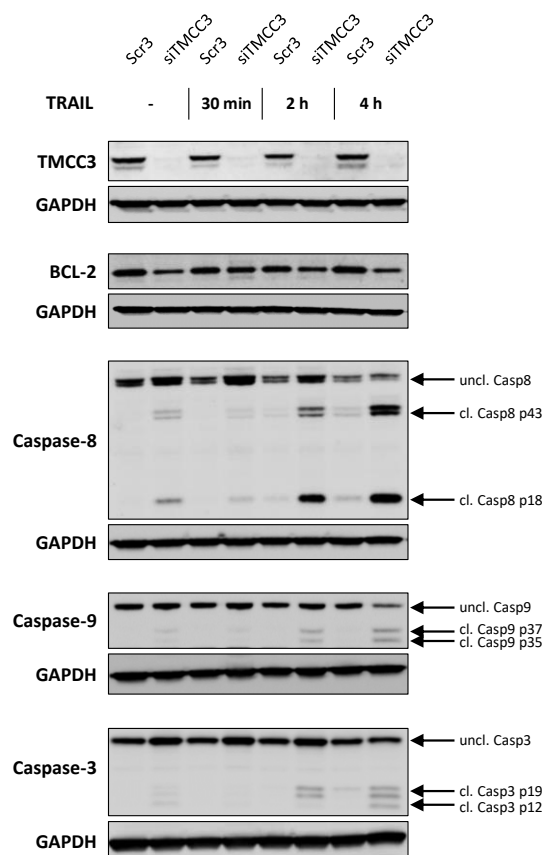


Figure 44: Expression of apoptotic genes in TMCC3 proficient/deficient Ma-Mel-86a upon TRAIL treatment.

This figure extends Figure 43. Ma-Mel-86a HLA-A2+ Luc+ were transfected with Scr3 or a pool of four siRNAs for *TMCC3* for 48 h. Subsequently, cells were treated with 100 ng/ml of recombinant TRAIL for 30 min, 2 h or 4 h or cultured in plain medium for 4 h. Cells were lysed, and total protein was extracted. Expression of *TMCC3* (same as in Figure 43), *BCL-2* and activity of Caspase-3/-8/-9 were detected by western blot. GAPDH expression was acquired as reference gene. Representative data of two independent experiments. Verena Babl contributed to the generation of the data as a Master's student under my co-supervision.

5.6.8 TMCC3 silencing activates Akt survival pathway

TMCC3 was described to be able to regulate the activation of Protein kinase B (PKB/Akt). In breast cancer stem cells, it was shown that a downregulation of *TMCC3* is concomitant with a lower

phosphorylation of AKT, therefore decreasing its activity [182]. Hence, the impact of TMCC3 knockdown on survival and apoptosis-related downstream proteins of AKT was investigated upon TRAIL treatment (Figure 45). Related to the experiment mentioned in 5.6.7, I checked for the expression of AKT, phosphorylated AKT (pAKT) and the phosphorylation of target genes BCL2 Associated Agonist Of Cell Death (pBAD), RELA Proto-Oncogene, NF-KB Subunit p65 (pRELA) as well as Tumor Protein P53 (p53) and X-Linked Inhibitor Of Apoptosis (XIAP).

While expression of total AKT was not impacted by the knockdown of TMCC3 in Ma-Mel-86a, TRAIL treatment slightly decreased its expression after 4 h. In contrast to its reported impact on breast cancer cells, TMCC3 downregulation did not decrease the phosphorylation of AKT but instead increased it in Ma-Mel-86a. Like total AKT, pAKT expression was lower after 4 h of TRAIL treatment. Furthermore, a higher phosphorylation of RELA and BAD and an increased expression of p53 and XIAP can be observed in the TMCC3 silenced cells which is more prominent upon TRAIL treatment (Figure 45). Taken together, TMCC3 deficient Ma-Mel-86a increased pro-survival AKT signaling as well as expression of p53.

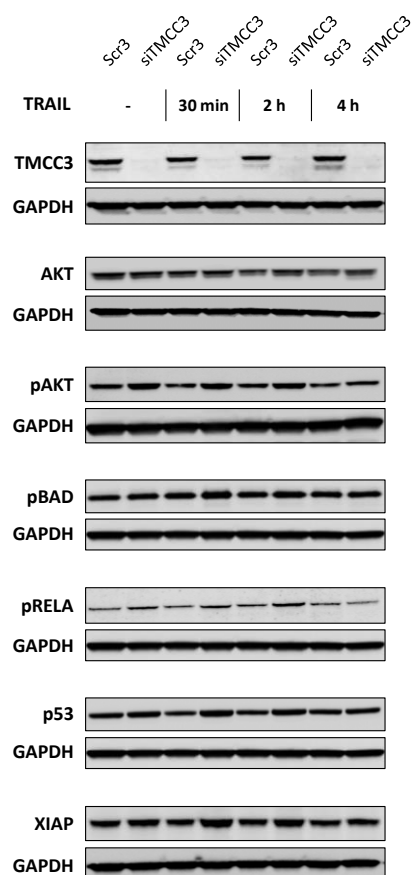


Figure 45: Expression of AKT pathway-related genes in TMCC3 proficient/deficient Ma-Mel-86a without and with TRAIL treatment.

Ma-Mel-86a HLA-A2+ Luc+ were transfected with Scr3 or a pool of four siRNAs for *TMCC3* for 48 h. Subsequently, cells were treated with 100 ng/ml of recombinant TRAIL for 30 min, 2 h or 4 h or cultured in plain medium for 4 h. Cells were lysed, and total protein was extracted. Expression of TMCC3 (same as in Figure 43/44), AKT, pAKT,

pBAD, pRELA, p53 and XIAP was detected by western blot. GAPDH expression was acquired as reference gene. The same GAPDH blots can be displayed more than one time due to detection of several proteins on the same membrane. Representative data of two independent experiments. Verena Babl contributed to the generation of the data as a Master's student under my co-supervision.

5.6.9 TMCC3 silencing results in perturbation of ER homeostasis

As I observed contrary results to previously published data with regard to AKT phosphorylation and as survival signaling by AKT was increased in TMCC3 silenced Ma-Mel-86a, another mechanism had to be responsible for the increased tumor cell death. TMCC3 is an important protein for the tubular network of the endoplasmic reticulum (ER) by working together with atlastins to build three-way junctions [183]. Therefore, the expression of proteins regulated during ER stress was investigated, namely Binding-Immunoglobulin Protein (BiP), C/EBP homologous protein (CHOP), total and phosphorylated Inositol-Requiring Protein 1 (IRE1 α), phosphorylated JUN N-Terminal Kinase (JNK) as well as the large fragment of CFLAR as downstream target of pJNK. As in the experiment in 5.6.7 and 5.6.8 protein expression was measured by western blot after knockdown of TMCC3 and upon treatment with TRAIL in Ma-Mel-86a (Figure 46).

Results showed that the expression of BiP was neither affected by knockdown of TMCC3 nor by treatment with TRAIL. TMCC3 downregulation resulted in decreased CHOP expression compared to Scr3 but upon treatment with TRAIL expression levels became similar. TMCC3 knockdown did not alter expression of total IRE1 α but induced phosphorylation of IRE1 α as well as of JNK. TRAIL treatment enhanced levels of pIRE1 α and stronger of pJNK, especially in the TMCC3 silenced cells. After 4 h of TRAIL treatment, phosphorylation of JNK was decreased. TMCC3 knockdown led to undetectable levels of the large fragment of CFLAR independent of TRAIL treatment. In the Scr3 treated cells, TRAIL treatment reduced CFLAR_L expression, but protein expression was still detectable (Figure 46). In conclusion, TMCC3 deficient Ma-Mel-86a induced ER stress which is enhanced upon treatment with TRAIL.

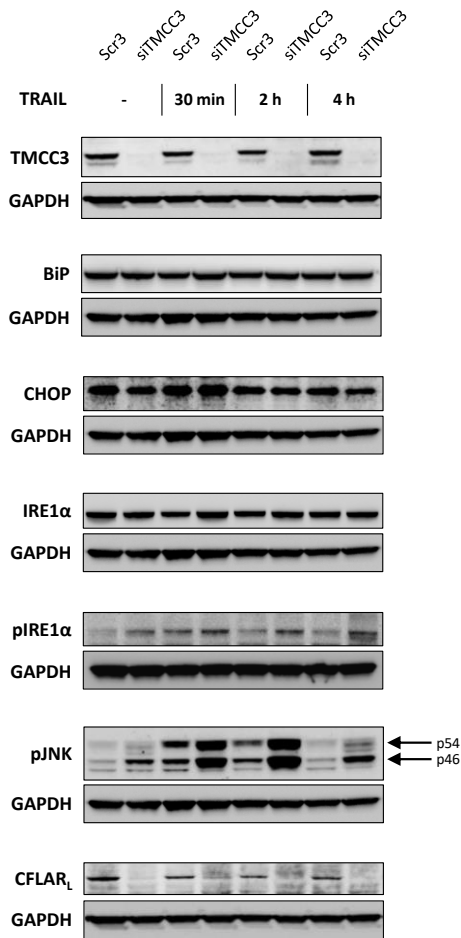


Figure 46: Expression of ER stress-related genes in TMCC3 proficient/deficient Ma-Mel-86a without and with TRAIL treatment.

Ma-Mel-86a HLA-A2+ Luc+ were transfected with Scr3 or a pool of four siRNAs for *TMCC3* for 48 h. Subsequently, cells were treated with 100 ng/ml of recombinant TRAIL for 30 min, 2 h or 4 h or cultured in plain medium for 4 h. Cells were lysed, and total protein was extracted. Expression of *TMCC3* (same as in Figure 44/45/46), BiP, CHOP, IRE1 α , pIRE1 α , pJNK and CFLAR_L was detected by western blot. GAPDH expression was acquired as reference gene. The same GAPDH blots can be displayed more than one time due to detection of several proteins on the same membrane. Representative data of two independent experiments.

5.6.10 IFN γ treatment increases caspase activity in SLC39A13 silenced Ma-Mel-86a

Upon SLC39A13 silencing, IFN γ was the cytotoxic ligand with the strongest phenotype in terms of cell death of Ma-Mel-86a. In order to investigate expression of apoptosis-related markers, cells were treated with IFN γ for 30 min, 4 h and 20 h. Expression and cleavage of Caspases-3/-8/-9 and BCL-2 were subsequently measured by western blot (Figure 47). In SLC39A13 proficient Ma-Mel-86a no activation of Caspase-3/-8/-9 could be observed. Caspase cleavage of all three measured caspases occurred only in the SLC39A13 knockdown cells after 20 h of IFN γ treatment. BCL-2 expression remained to be downregulated in SLC39A13 silenced cells, only after 4 h of IFN γ treatment expression is slightly increased but downregulated again after 20 h. In Scr3 treated cells BCL-2 expression

remained unchanged in all conditions. In summary, only SLC39A13 deficient Ma-Mel-86a induced apoptosis after 20 h of treatment with IFN γ .

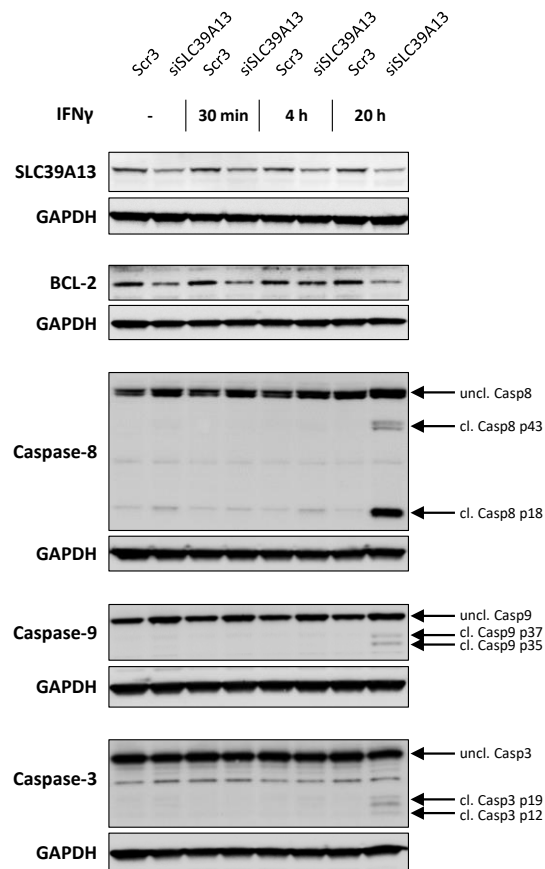


Figure 47: Expression of apoptotic genes in SLC39A13 proficient/deficient Ma-Mel-86a upon IFN γ treatment. This figure extends Figure 43. Ma-Mel-86a HLA-A2+ Luc+ were transfected with Scr3 or a pool of four siRNAs for *SLC39A13* for 48 h. Subsequently, cells were treated with 100 ng/ml of recombinant IFN γ for 30 min, 4 h or 20 h or cultured in plain medium for 20 h. Cells were lysed, and total protein was extracted. Expression of SLC39A13 (same as in Figure 43), BCL-2 and Caspase-3/-8/-9 was detected by western blot. GAPDH expression was acquired as reference gene. Representative data of two independent experiments.

5.6.11 SLC39A13 silencing shifts STAT1/STAT3 ratio to induce apoptosis

SLC39A13 was described to be involved in activation of Src/FAK pathway which is associated with cell survival by activating among others the PI3K/AKT pathway or STAT3 signaling [184]. Therefore, expression and phosphorylation of AKT, STAT3 as well as STAT1 being downstream of IFN γ signaling was measured by western blot in Ma-Mel-86a equally treated as in 5.6.10 (Figure 48).

The results demonstrated that expression of AKT was neither affected by knock-down of SLC39A13 nor IFN γ treatment of Ma-Mel-86. Phosphorylation of AKT was slightly increased in the SLC39A13 silenced cells, but IFN γ induced phosphorylation also in the Scr3 treated cells. After 20 h pAKT expression went down in both conditions. SLC39A13 knockdown cells increased total STAT1 protein expression. IFN γ treatment increased STAT1 and STAT3 expression in general with higher expression in the knockdown

cells. Baseline phosphorylation of STAT3 was higher in the SLC39A13 silenced cells but IFN γ treatment increased pSTAT3 in the Scr3 treated cells. However, after 20 h of treatment pSTAT3 levels were still increased in the knockdown cells. pSTAT1 was not present in both conditions without IFN γ treatment. IFN γ induced phosphorylation of STAT1 in Ma-Mel-86a but the level of pSTAT1 was higher in the SLC39A13 silenced cells after 20 h of treatment. Taken together, SLC39A13 deficient Ma-Mel-86a showed increased STAT1 signaling upon treatment with IFN γ .

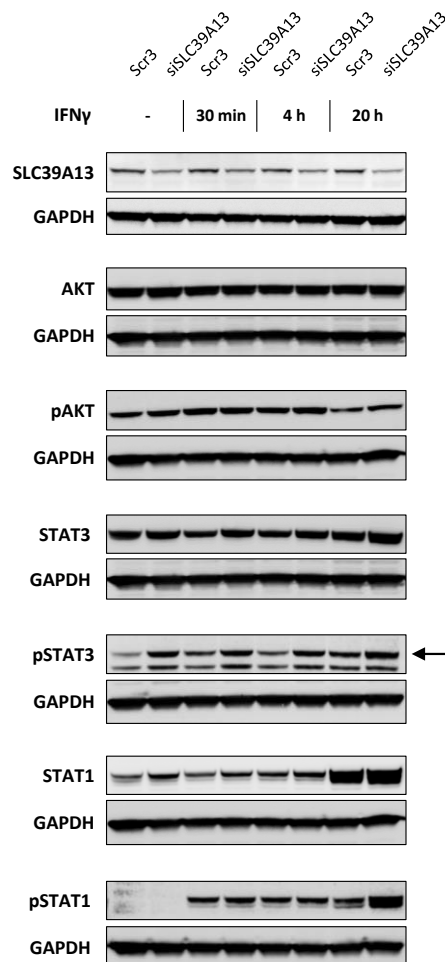


Figure 48: Expression of FAK/Src and IFN γ R pathway-related genes in SLC39A13 proficient/deficient Ma-Mel-86a without and with IFN γ treatment.

Ma-Mel-86a HLA-A2+ Luc+ were transfected with Scr3 or a pool of four siRNAs for *SLC39A13* for 48 h. Subsequently, cells were treated with 100 ng/ml of recombinant IFN γ for 30 min, 4 h or 20 h or cultured in plain medium for 20 h. Cells were lysed, and total protein was extracted. Expression of SLC39A13 (same as in Figure 43/47), AKT, pAKT, STAT3, pSTAT3, STAT1 and pSTAT1 was detected by western blot. GAPDH expression was acquired as reference gene. The same GAPDH blots can be displayed more than one time due to detection of several proteins on the same membrane. Representative data of two independent experiments.

5.6.12 Overexpression of TMCC3 decreases FluT cell-mediated tumor cell death

As downregulation of TMCC3 and SLC39A13 resulted in an increased tumor cell death upon co-culture with FluT cells and other death-inducing treatments, I investigated if overexpression of these genes

leads to a protective effect (Figure 49). Stable transfection with an overexpression plasmid increased *TMCC3* and *SLC39A13* expression in Ma-Mel-86 HLA-A2+ Luc+ more than 200-fold on the mRNA level compared to an empty vector control (Figure 49A). Normalized to the empty vector control, the results of the luciferase-based cytotoxicity assay showed overexpression of *TMCC3* and *SLC39A13* resulted in increased raw luciferase values without treatment (Figure 49B). Upon co-culture with FluT cells this is enhanced for *TMCC3* but not for *SLC39A13*. However, overexpression of *TMCC3* decreased tumor cell death to 18 % compared to 35 % in the empty vector control when normalized to the untreated condition (Figure 49C). Here, *SLC39A13* overexpression showed similar levels of tumor cell lysis as the empty vector control. In conclusion, overexpression of *TMCC3* showed protective effects towards FluT cell-mediated lysis of Ma-Mel-86a.

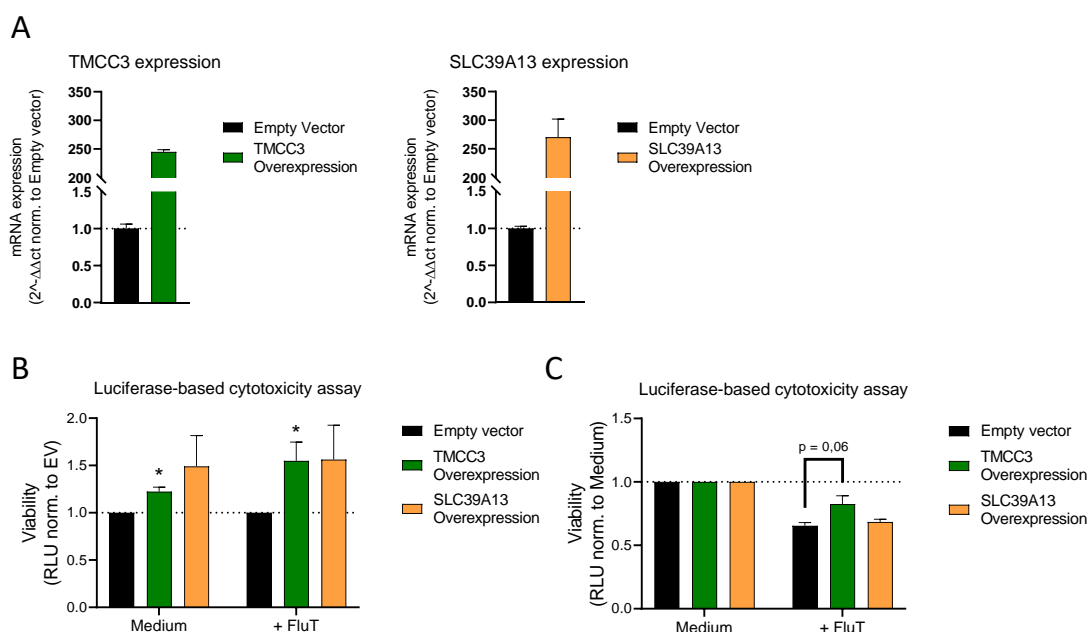


Figure 49: Overexpression of *TMCC3* and *SLC39A13* and their impact on T cell-mediated rejection.

Ma-Mel-86a HLA-A2+ Luc+ were stably transfected with an empty vector or overexpression vector for *TMCC3* and *SLC39A13*. **(A)** Cells were lysed for RNA isolation which was reversely transcribed into cDNA. Gene expression of *TMCC3* and *SLC39A13* was measured by quantitative real-time PCR (qPCR). Expression of Actin-beta was measured as reference gene and used for normalization of *TMCC3* and *SLC39A13* in the qPCR, respectively. Gene expression was normalized to expression levels of cells transfected with an empty vector. Bars represent the mean of technical replicates + standard deviation. **(B-C)** Luciferase-based cytotoxicity assay to investigate the immunoregulatory effect of overexpression of *TMCC3* and *SLC39A13*. Cells were cultured for 48 h in complete medium. Subsequently, cells were cultured in plain medium (viability setting) or co-cultured with FluT cells (cytotoxicity setting) in an E:T ratio of 1:1 for 20 h. Cells were lysed, and remaining luciferase activity was measured by luminescence. Raw luciferase units (RLU) were normalized to RLU of the empty vector cells (B) or to the viability setting (C). Bars represent the mean of three independent experiments + standard deviation.

6 Discussion

6.1 MITF downregulation increases resistance of melanoma cells

MITF is the key transcriptional factor of melanocytes and a marker of melanoma plasticity [71, 88]. A dedifferentiation of melanoma cells is concomitant with a more invasive and resistant phenotype. The cell line pair Ma-Mel-86 is derived from different lesions of the same melanoma patient and were reported to differ in their MITF expression [130]. In a first experiment I confirmed the phenotype of Ma-Mel-86a as MITF^{low} and Ma-Mel-86c as MITF^{high} cell line. Co-culture experiments with melanoma specific tumor infiltrating lymphocytes (TILs) showed that only Ma-Mel-86c were efficiently killed by these T cells. Ma-Mel-86a were not targeted by TIL412 or MART-1 specific T cells, even in higher E:T ratios. These results confirmed the expression of typical melanoma differentiation antigens (MDA) such as MART-1 and gp100 in Ma-Mel-86c making them susceptible to TIL412 and MART-1 specific T cells [130]. Dedifferentiated MITF^{low} cells like Ma-Mel-86a lose MDAs and become resistant which often occurs during immunotherapy [185]. The authors of the original study of Ma-Mel-86 showed that both tumor cell lines induced the expansion of T cell clones with hardly any cross-reactivity [130]. For further experiments, it was therefore necessary to either increase the expression of antigens which TIL412 and MART-1 T cells can recognize or choose a melanoma-unspecific T cell system. Addition of MART-1 peptide resulted in lysis of Ma-Mel-86a upon co-culture with MART-1 TILs. However, the degree of tumor cell death was higher in the MITF^{high} cell line Ma-Mel-86c. Co-culture of the cell lines with FluT cells after pulsing with flu peptide confirmed the increased resistance of the MITF^{low} cell line. After stable transfection, both cell lines highly expressed HLA-A2 which presented the A2-matched flu peptide to FluT cells generated from HLA-A2+ donors. However, HLA-A2 independent treatment of Ma-Mel-86 with supernatant of polyclonally activated FluT cells demonstrated a higher tumor cell lysis of Ma-Mel-86c. ELISA of the supernatant showed that the supernatant contained cytotoxic molecules like TNF α and IFN γ . Death receptor ligands such as TRAIL, FasL, LT α and LIGHT are expressed on the T cell surface and were detected by flow cytometry. Initially surface-expressed ligands are proteolytically cleaved from activated T cells [186]. Receptors of the ligands such as TNFR1, DR5 and FAS showed generally a higher expression in Ma-Mel-86a. Therefore, the T cell co-culture experiments and treatment with FluT supernatant underlines stronger cell intrinsic resistance mechanisms in the MITF low cell line. Despite receptor expression, treatment of Ma-Mel-86 with individual ligands showed a primary resistance to TRAIL, TNF α , FasL, LT α and LIGHT. Resistance of melanoma cells against death receptor ligands have been previously reported [187]. As described in 1.1.4 different mechanisms contribute to resistance like elevated pro-survival and anti-apoptotic signaling [28, 54]. Also, the soluble form of ligands like TRAIL and FasL show decreased cytotoxic potential [28, 186]. However,

synergistic activity of several death receptor ligands can improve apoptosis induction in target cells [188]. Furthermore, binding of several ligands to their cognate receptors on the tumor cells in close proximity could enhance receptor oligomerization for successful signal transduction [189]. Therefore, despite resistance to death receptor ligands in individual treatments, they might still be able to contribute to tumor cell lysis in treatment experiments with supernatant. Individual treatment of IFN γ induced tumor cell death in both melanoma cell lines which was more pronounced in Ma-Mel-86c. A similar degree of tumor cell lysis was achieved as treatment with supernatant. Reducing the cytotoxic effect of the supernatant to the properties of IFN γ would be short-sighted as I observed cell apoptosis mediated by IFN γ at concentrations above 1 ng/ml (data not shown) which was higher than in the supernatant. Besides IFN γ and death receptor ligands, the supernatant contains other cytotoxic molecules such as perforin and granzyme B whose expression have not been investigated.

PD-L1 is upregulated on cancer cells in order to escape immune responses [190]. It is the ligand for PD-1 which is expressed on T cells and ligand-receptor interaction results in inhibition of T cell activation and survival. The PD-1/PD-L1 axis has been the target of many antibody therapies inhibiting PD-1 (Nivolumab/Pembrolizumab) or PD-L1 (Atezolizumab). In melanoma plasticity, higher expression of PD-L1 is more associated with low MITF expression and it has been described that MITF contributes to lysosomal degradation of PD-L1 [88, 191, 192]. This supports increased resistance of dedifferentiated melanoma cells against T cell-based therapies. The patient Ma-Mel-86 received different immunotherapies although no PD-1/PD-L1 treatment [130]. Both Ma-Mel-86 cell lines expressed high levels of PD-L1. The expression was higher in the MITF^{low} cell line Ma-Mel-86a which can explain why T cell-mediated killing was decreased in co-culture experiments with this cell line. Therefore, I investigated whether downregulation of PD-L1 would increase susceptibility to FluT cell-mediated tumor cell lysis. MITF^{low} cell line Ma-Mel-86a showed reduction of viability upon siRNA transfection but PD-L1 silencing did not further improve T cell cytotoxicity. To a certain degree, this was the case for the MITF^{high} cell line Ma-Mel-86c. The increased resistance of Ma-Mel-86a could be due to additional proteins that inhibit T cell function. Tumor cells are able to express various molecules targeting different immune checkpoints to prevent antitumor immunity [193]. Alternatively, as expression of PD-L1 was initially higher in Ma-Mel-86a, downregulation to a degree that is achieved by siRNA treatment might not be sufficient to overcome PD-L1-mediated resistance.

6.2 A high-throughput RNAi screen in melanoma

Despite improved median overall survival in malignant melanoma patients since the advent of immunotherapy, especially by immune checkpoint inhibitors, patients still die from this disease due to primary or acquired therapy resistance [105]. Melanoma is highly plastic and phenotype switching of

differentiated melanoma cells with increased expression of antigens to a dedifferentiated and invasive state is common and associated with increased resistance to immunotherapy [88]. Within one tumor, different phenotypes coexist, and resistant clones are able to outgrow during immunotherapy [70]. Therefore, finding alternative targets for immunotherapy that increase activity of effector immune cells even against dedifferentiated, resistant tumor cells, are of great importance to further improve patient survival rates.

6.2.1 Rationale and design

In order to identify novel immune resistance genes in melanoma, a high-throughput (HTP) RNAi screen was performed. The original method of the RNAi screen was developed in our group by Dr. Nisit Khandelwal and resulted in the identification of several genes that tumor cells of different entities use to circumvent immune cell responses [143-145]. Interestingly, the lists of identified genes from the different screens showed small overlap, indicating tumor entity specificity of immune resistance mechanisms. The cell lines used in this project were derived from lesions of the same melanoma patient Ma-Mel-86 at different phases of the disease [130]. Among others, the cell lines showed mutations in *BRAF*, *PTEN* and *TP53*. The patient received several immunotherapies such as tumor lysate-loaded DC vaccine and IFN α but finally deceased after relapse. While Ma-Mel-86c showed a differentiated melanoma phenotype with high MITF expression, Ma-Mel-86a expressed low levels of MITF while the receptor tyrosine kinase AXL was upregulated. In first experiments, I demonstrated that the MITF^{low} cell line Ma-Mel-86a showed features of increased resistance, confirming the phenotype of dedifferentiated melanoma cells [88].

The HTP screens were performed in both cell lines to identify immune resistance genes that can mediate resistance in melanoma in general but also to investigate whether there are selective mechanisms in the different phenotypes. Due to the association to increased resistance, immune resistance genes showing an effect in the MITF^{low} cell line Ma-Mel-86a were of particular interest and importance. As the patient was HLA-A2 negative, the cell lines were stably transfected with HLA-A2 and transduced with luciferase for eligibility of the screening approach. Afterwards, both cell lines expressed high levels of HLA-A2 and luciferase. Flu peptide specific cytotoxic T (FluT) cells were chosen as effector T cells in the screen. The protocol for the generation of FluT cells from PBMCs of HLA-A2+ donors was previously established in our group by Dr. Ayşe Menevşe. Pulsing of tumor cell lines with HLA-A2 matched flu peptide resulted in recognition of the target cells by the FluT cells and approved to be an effective assay system [144, 194]. Apart from adjustment of the effector to target ratio, the degree of tumor cell death could also be regulated by defining an optimal peptide concentration. For this project, the assay system was especially reasonable as typical melanoma differentiation antigens

such as MART-1 and gp100 targeted by tumor infiltrating lymphocytes (TILs) like TIL412 are downregulated upon dedifferentiation of melanoma hence making the MITF^{low} melanoma cell line Ma-Mel-86a resistant to co-culture with such T cells.

Since the first screen in our group more than a decade ago the used siRNA libraries were enlarged from 520 to 5202 genes. The library used in this project comprised genes encoding for the whole surfaceome as well as kinases and genes involved in cell metabolism. Surface genes are of particular interest as they are more likely to directly interact with the T cells potentially modifying T cell function. Additionally, surface molecules are easier to target in a therapeutic approach as seen for the immune checkpoint molecule PD-L1 targeted by monoclonal antibodies. Kinases are important regulators of intrinsic cell signaling and in melanoma, frequent mutations result in increased MAPK signaling. Kinase inhibitors against BRAF or MEK are in use and show improved survival of melanoma patients. In our group both, surface molecules as well as kinases have been identified to mediate resistance to T cell-mediated killing [143-145]. By enlarging the siRNA library to more than 5200 genes with additional functions it was possible to identify yet unknown resistance mechanisms, even in therapy resistant MITF^{low} melanoma cells.

Since the advent of CRISPR in genetic manipulation, CRISPR screens are nowadays widely used as alternative to RNAi. However, there are several advantages to use RNAi over CRISPR. Complete loss of a target gene is not always favorable as knockout of genes with essential functions can be lethal for the cells [137]. Furthermore, CRISPR can introduce random mutations that don't disrupt the open reading frame (ORF) and makes it difficult to interpret the resulting phenotype. Here, transient downregulation of transcriptional products is more straightforward. Finally, siRNA-based RNAi is faster as well as better represents the application of drugs which usually downregulate protein function instead of preventing transcription [137].

6.2.2 Optimization of the screening protocol

In advance to the primary HTP screens, the setup of the cytotoxicity assay was optimized in terms of appropriate transfection and co-culture conditions as well as inclusion of positive and negative controls. In a transfection experiment with siRNAs targeting *SIK3* and *PD-L1*, I showed that a transfection of 48 h resulted in a more reduced gene expression compared to 72 h. In co-culture experiments, FluT cells killed tumor cells only when cells were previously pulsed with flu peptide, validating the efficiency and reliability of the assay system. Increased concentration of flu peptide accordingly resulted in increased tumor cell lysis. Higher effector to target (E:T) ratios enhanced tumor cell death more in Ma-Mel-86c compared to Ma-Mel-86a. Overall, I chose a peptide concentration of 0,01 µg/ml for both melanoma cell lines with an E:T ratio of 1:1 for Ma-Mel-86a and 0,5:1 for Ma-Mel-

86c. This resulted on average in 40-50 % tumor cell lysis of Ma-Mel-86a and 60-80 % lysis of Ma-Mel-86c, respectively. Degree of tumor cell death was also dependent on the expansion experiment in which FluT cells were generated.

The selection of appropriate negative and positive controls was important to confirm the validity of the approach and to interpret the outcome of the screen [142]. Negative controls were siRNA sequences that do not target any gene. Additionally, effects of positive controls were normalized to sequence-independent siRNAs due to higher similarity between targeting and non-targeting siRNA settings than to a setting without any siRNA treatment (mock). For my cytotoxicity assay and screening approach I used positive control genes that are well established in the literature to have an impact on resistance as well as genes that have been identified in our group to show the same phenotype. Comparison of candidate genes to positive controls enabled me to assess the impact of novel immune resistance genes. Interestingly, differences between Ma-Mel-86a and Ma-Mel-86c were observed. While in Ma-Mel-86a, the kinase *SIK3* showed a strong impact on T cell-mediated rejection of tumor cells, in Ma-Mel-86c this was the case for *OR10H1*. The kinase *SIK3* was previously identified in a pancreatic cancer screen in our group having an impact on TNF α -mediated apoptosis [145]. Olfactory receptor *OR10H1* playing a superior role in *MITF*^{high} cell line Ma-Mel-86c was particularly interesting as *OR10H1* was identified in a melanoma screen in our group in which the melanoma cell line M579 was used that showed expression of melanocytic markers similarly to Ma-Mel-86c [181]. The performance of positive controls therefore already indicated that different genes could mediate resistance in melanoma cells with different phenotypes. Finally, transfection controls that compromised cell viability were included such as siRNA targeting *UBC* or the 'Cell Death' siRNA cocktail. Transfection of Ma-Mel-86a resulted in complete loss of tumor cells while for Ma-Mel-86c, only 30-50 % of tumor cells died. Only upon co-culture with FluT cells the proportion of dead melanoma cells increased.

Overall, Ma-Mel-86a showed higher response to transfection controls than Ma-Mel-86c. This was accompanied by general stronger viability effects upon transfection as well as increased effect sizes of immune resistance genes in cytotoxicity assays. Finally, as seen in later experiments, the knockdown efficiency of most target genes was higher in Ma-Mel-86a. Therefore, it is plausible that transfection efficiency was enhanced in the *MITF*^{low} cell line resulting in the observed phenotypes. *MITF* or the differentiation status of melanoma cells could impact the transfection efficiency. *MITF* is able to regulate the transcription of *DICER1* encoding Dicer, an important nuclease that processes dsRNAs to siRNAs before RISC assembly [195, 196]. Although commercially available siRNA duplexes don't require processing, increased Dicer expression could impact the amount of siRNA available for targeted gene knockdown. *MITF*-induced Dicer expression could also be concomitant with counterregulatory mechanisms to limit production of siRNAs. Furthermore, experiments investigating intracellular duplex

siRNA trafficking showed that siRNA-lipid complexes are not simply incorporated into the cell to be processed and integrated into the RISC. siRNA complexes can lose integrity by remaining in endosomal structures or accumulate in perinuclear structures or the nucleus [197]. MITF as key regulator in melanocytes can regulate hundreds of other genes *e.g.*, genes involved in lysosome and endosome function [71]. Hence, differentiation status and differential gene expression might impact the distribution and availability of siRNAs for gene knockdown. Of note, the melanoma cell line M579 as well as another tested cell line with high MITF expression similarly showed decreased cell death upon transfection with UBC siRNA or the 'Cell Death' (data not shown) [181].

6.2.3 Performance of primary and validation screens

HTP screens in Ma-Mel-86a and Ma-Mel-86c were performed in the viability setting in which siRNA transfected tumor cells were cultured in plain medium and in the cytotoxicity setting in which cells were co-cultured with FluT cells. Genes with an immune resistance phenotype ideally would not show an impact on the viability of the cells but would enhance T cell-mediated lysis compared to a non-targeting siRNA control. As recommended, screens were conducted in technical duplicates to increase the reliability of observed effects [142].

In the primary screens, each gene was targeted by a pool of four non-overlapping siRNAs. In the subsequent analysis, the performance of control and library genes were scored, and the regressed differential score termed LOESS score was used to rank all genes. I was able to reproduce the phenotypes of the controls in previous cytotoxicity assays including the pattern of increased viability impacts as well as cytotoxicity effects in Ma-Mel-86a. Using the 'Cell Death' siRNA cocktail resulted in strong tumor cell death and *SIK3* was the best performing positive control in Ma-Mel-86a. In the LOESS score ranking, it occupied rank 96 among the library genes while in Ma-Mel-86c, the best performing positive control *OR10H1* ranked at position 337. Corroborating the reliability of the approach and outcome of the screens, genes that were previously identified in our group and those with known resistance phenotypes were among the best performing candidates. *JAK2* occupied rank 12 in Ma-Mel-86a and was also a hit in the M579 screen [181]. *JAK2* is involved in pro-survival JAK2-STAT3 signaling that promotes expression of anti-apoptotic proteins like BCL-2 or immunosuppressive checkpoint molecules like PD-L1 [198]. *CFLAR* was the strongest hit in the Ma-Mel-86c screen. *CFLAR* is an anti-apoptotic protein that shows structural similarities to caspase-8 [199]. In death receptor signaling, it binds to FADD in the DISC in order to prevent caspase-8 induction and activity.

Despite various advantages of the use of siRNAs in RNAi screens, one concern of their use are off-target effects and concomitantly the production of false positive results. Off-target effects are sequence dependent or independent and can be assigned to three categories [137, 200, 201]. Due to partial

sequence complementarity, siRNAs bind to the 3'UTR of other mRNAs leading to their unintended degradation. Furthermore, siRNAs compete with endogenous miRNAs resulting in RISC saturation. Therefore, miRNAs are not able anymore to execute their function properly. Finally, both siRNAs as well as the delivery vehicles can activate Toll-like receptors of the target cells which induce inflammatory responses. It could be the combination of sequence dependence and independence together with the differential gene and miRNA expression profiles in MITF^{low} and MITF^{high} melanoma cells that result in general stronger viability impacts in Ma-Mel-86a upon siRNA transfection. In order to validate the findings of the primary screens and to identify false positives, secondary screens were performed in which the siRNA pool was deconvoluted [142, 202]. This means, apart from using the pool of four siRNAs, each individual siRNA was used separately. I selected 174 genes to be tested in the validation screens that showed either strong effects in both cell lines or differential effects in Ma-Mel-86a and Ma-Mel-86c. In order to define a gene as validated immune resistance gene, the pool and at least two single siRNAs had to increase tumor cell lysis by at least 15 % compared to a Scr control as described in 5.3.3. Another validation criterion comprised a viability threshold in Ma-Mel-86a of 0,265 and in Ma-Mel-86c of 0,772. The threshold of 0,265 in Ma-Mel-86a was very low, meaning that more than 70 % of viability loss was in range. However, viability thresholds were adapted to LOESS score thresholds in the primary screens to increase comparability.

Normalization of the controls reproduced their phenotype in previous cytotoxicity assays confirming that the implementation of the screen was generally successful. In contrast, Figure 22 shows the z-score analysis of the controls which indicates that negative controls increase the viability upon co-culture with FluT cells while positive controls don't show an impact. The z-score of a gene represents its localization within a distribution. As I aimed to validate strong phenotypes from the primary screens that distribution is shifted. In the cytotoxicity setting, many genes decrease tumor cell viability, therefore increasing the z-scores of the negative controls. Overall, 91 of 174 library genes (53,2 %) were validated in the secondary screens. Furthermore, 17 genes (9,9 %) fulfilled the general criteria but in the other cell line as in the primary screen. Similar to the primary screen, genes that are known to mediate immune resistance like *TNFRSF6B* were validated, corroborating the reliability of the approach. *TNFRSF6B/DcR3* is a decoy receptor that binds to death receptor ligands such as FasL and LIGHT to neutralize their function therefore preventing apoptosis of tumor cells [56]. Despite the validation of the majority of genes, the secondary screens at the same time identified false positive phenotypes in the primary screens, underlining this important step in advance of functional analysis of hits.

6.3 Selection of novel immune resistance genes for functional analyses

6.3.1 Performance of bioinformatic analyses

Transcriptome analysis by RNA-Seq has become a popular tool to study the biology of cancer [148]. Especially the advent of single cell RNA-Seq made it possible to define cancer heterogeneity and cell subsets with distinct transcriptional profiles. Using bulk and scRNA-Seq of patient-derived melanomas and melanoma cell lines lead to the discovery of marker genes and gene regulatory networks of specific phenotypes of melanoma plasticity as well as signatures associated with immune resistance and therapy response [83, 86, 123, 152].

Generally, differential gene expression (DGE) analysis of two or more conditions is applied to define sets of genes or functions that can be attributed to one condition [203]. Furthermore, Seurat analysis on scRNA-Seq data is used to define cell populations by measuring the differential expression of marker genes in identified cell clusters [160]. In DGE analysis, usually the expression of the whole genome is investigated. In contrast, our group has validated more than 200 genes that are able to regulate T cell-mediated rejection of tumor cells in a tumor entity-specific context. This is an enormous advantage as we can selectively investigate DGE of immune resistance (IR) genes in various data sets. For the analyses in this project, I focused on bulk and scRNA-Seq data from human melanomas and patient-derived melanoma cell lines to investigate individual co-expression patterns and associations of gene expression with the *MITF* status. As a decrease of *MITF* is associated with invasion and immunotherapy resistance [88], it was particularly interesting to identify IR genes that are upregulated in *MITF*^{low}, potentially contributing to this melanoma phenotype. The screens in Ma-Mel-86 identified 91 genes that regulated T cell-mediated rejection of tumor cells. For the bioinformatic analyses I also included the 17 genes that showed an impact in the other melanoma cell line as in the primary screens. The library of the validation screen was designed by applying thresholds of the LOESS scores and therefore categorizing the genes into common and cell line-specific hits. Cell line specificity did not exclude the possibility that a gene showed an impact on cytotoxicity in the other cell line but rather that the gene could not reach the LOESS score threshold. Hence, effects of some genes in the secondary screen were expected and therefore, including them in the bioinformatic analyses was appropriate. Furthermore, I included validated genes that were previously identified by other HTP screens in our group. Thereby, I was able to investigate their correlation patterns to melanoma-specific hits and *MITF*. Additionally, genes with a strong *MITF*^{low} association were eligible for re-evaluation in functional assays as they potentially failed to be included in the secondary library due to LOESS score thresholds or off-target effects in the primary screen.

By using WGCNA I was able to identify co-expression clusters of IR genes. Analyses of bulk RNA-Seq data revealed larger clusters with stronger correlation patterns. This is expectable due to generally

higher coverage of genes as many cell types contribute to the averaged gene expression data in one sample while in scRNA-Seq data cell subsets are defined by differential gene expression with occurrence of a higher number of zero read counts [204]. In all data sets I was able to identify a *MITF*-related cluster. Part of the same cluster were also genes that are known to be upregulated by *MITF* such as *MLANA*, *TYR* and *CEACAM1* which were added to the analyses as controls. Being able to reconstruct their co-expression in dendrograms and correlation heatmaps confirmed WGCNA to be an appropriate method of choice and increased on the other hand the reliability of negatively correlating clusters and genes to *MITF*. In every data set used for WGCNA clusters were identified that showed negative correlation to the *MITF* cluster and *MITF* itself. This was more prominent in the bulk RNA-Seq data due to the previously mentioned zero counts in scRNA-Seq data which impedes high correlations. In the bulk TCGA and melanoma cell line data the clusters that clearly anticorrelated with *MITF* contained the gene *AXL*. *AXL* is a receptor tyrosine kinase that is a marker for mesenchymal *MITF*^{low} melanomas [88]. Additionally, it was previously described that on the bulk level melanomas can be categorized into *MITF*^{high} and *AXL*^{high} while this is not the case for the single cell level [70]. Hence, my analyses were able to reconstruct these phenotypes. The only cluster that was negatively correlating with *MITF* in the scRNA-Seq data set of Jerby-Arnon *et al.* did not contain *AXL* but instead *NGFR* which is a marker gene of neural crest stem cell (NCSC)-like *MITF*^{low} melanomas [88]. According to single expression data from the Human Protein Atlas, *NGFR* as well as other genes from the same cluster such as *TMCC3*, *CDH24* and *LRRN1* are more associated to neuronal and glial cells [205, 206]. Interestingly, the publication of the TCGA network described as well that the identified *MITF*-low cluster was enriched with genes associated to the nervous system and neuronal development [149]. By separation of the single cells in *MITF*^{low} and *MITF*^{high} cells and performing statistical tests between both groups, *NGFR* was identified as the most significant gene upregulated in the *MITF*^{low} population. In total, 48 genes showed significance in this population while *MITF* and *MITF*-regulated genes were significantly upregulated in the *MITF*^{high} population, underlining the rationale of the analyses. Similar results were observed in the RNA-Seq data of the patient-derived melanoma cell lines in which 21 genes showed significant upregulation in *MITF*^{low} cell lines with *AXL* showing the highest significance. Heatmaps displayed in Figure 26 show expression patterns between melanoma patients and melanoma cells. Hierarchical clustering of TCGA samples indicated that the gene and also the cluster expression is heterogeneous between patients and would allow to stratify the patients into cohorts (Figure 26A). Correlations between the clusters are visually apparent as for example the heatmap shows a clear negative correlation between the brown and the blue cluster. The heatmap of the scRNA-Seq data confirms heterogeneous expression of IR gene clusters between patients after grouping of cells from the same patient (Figure 26B). On the other hand, the expression of a cluster within a patient is rather homogeneous. As previously mentioned, scRNA-Seq data features higher number of zero read

counts [204] which is also represented in the heatmap by white coloring. Clusters like the brown one show mainly expression in one patient and in general some clusters show expression only in a few patients or even cells while other clusters like the yellow, turquoise and blue ones are expressed in more patients but with varying degree. The inter-individual differences of IR gene expression can underline the meaningfulness of personalized or precision medicine in which therapies are tailor-made for each patient depending on the profile of each tumor [207].

The Seurat analysis of the scRNA-Seq data set was performed to identify cell populations of patient-derived melanoma samples with a focus on subsets of malignant cells and their expression of IR genes, independent of individual expression patterns. Patient-specific batch effects were therefore removed by using harmony integration. By applying a list of cell type signature genes, I was able to assign cell types to the identified clusters. In a next step, I differentiated between $MITF^{high}$ and $MITF^{low}$ populations within the four malignant cell clusters. Cluster 1 was identified as one large $MITF^{high}$ cluster as *MITF* and melanocytic genes were identified as marker genes. Hence, clusters 5, 9 and 11 were identified as $MITF^{low}$ cell populations. Seurat analysis enabled the determination of marker genes of each cell type. The resulting list was filtered for IR genes and displayed two interesting features. First, malignant cells as well as cells of the microenvironment upregulated a specific set of IR genes. Second, the $MITF^{low}$ cells showed higher expression of two sets of IR genes. On the one hand they still expressed genes of the $MITF^{high}$ cluster although to a lower extent. Considering that $MITF^{low}$ cells still originate from melanocytes, expression of $MITF^{high}$ marker genes compared to stromal cells was plausible. On the other hand, $MITF^{low}$ cells upregulated a set of IR genes that were not expressed in the $MITF^{high}$ population. In contrast, it was rather expressed by cancer-associated fibroblasts (CAFs). In a tumor, CAFs contribute to an immunosuppressive environment by the secretion of IL-6 and TGF β and are associated with remodeling of the extracellular matrix, invasion and modulation of therapy response [208]. These features overlap with those of $MITF^{low}$ melanoma cells [87, 88]. Phenotype switching of melanoma cells have also been described in the context of transdifferentiation in which cells can convert into a CAF-like or endothelial-like phenotype [87, 209]. Also, neural differentiation has long been observed in melanoma [210]. These events are associated with melanoma progression and might be induced during therapy to establish resistance. The expression of IR genes in the cell subsets underline the trajectories from differentiation via dedifferentiation to transdifferentiation. Identification of marker genes between the malignant clusters similarly showed cluster-specific IR gene features. While in the $MITF^{high}$ cluster *MITF* and melanocytic genes are upregulated, others take over in the $MITF^{low}$ population. Cluster 5 for example shows increased expression of *HDGF*, a growth factor which was shown to play a role in cell transformation and metastasis [211]. HDGF stimulated pro-survival pathways such as MAPK or PI3K and the production of HDGF itself as well as factors like VEGF by binding to genomic DNA [212]. Cluster 11 showed upregulation of *PRDX4* which is often

overexpressed in cancer and is described to promote therapy resistance and protection of cell homeostasis by regulating ROS metabolism [213].

By investigating the differential expression of IR genes between malignant melanoma and a set of healthy tissues I similarly could identify sets of genes that were significantly upregulated in single entities. Interestingly, some genes that showed higher expression in melanoma overlapped with marker genes of MITF^{high} and MITF^{low} melanoma cells from the Seurat analysis including *MITF* and *MOK*. On the one hand, melanoma selective genes appear to be more biased towards general melanoma-associated genes like MITF making it difficult to differentiate between MITF^{high} and MITF^{low}. On the other hand, scRNA-Seq data is successfully able to reproduce observations of bulk RNA-Seq data despite the presence of other cell types in bulk samples. A large set of IR genes was upregulated in blood samples. Blood samples are comprised of hematopoietic stem/progenitor cells and differentiated lymphocytes, myeloid cells and erythrocytes [214]. Various blood cell types express a low number of different genes. In relative terms this results in a higher number of very high and very low expressed genes which is represented by the intense coloring of the genes in the blood samples in the heatmap.

Despite increased understanding of melanoma biology due to bulk and single cell transcriptomics, many mechanisms of melanoma resistance to targeted and immunotherapy remain unclear or at least incomplete. New technologies and more studies on therapy-matched patient samples are necessary to increase the resolution of the complexity of melanoma and therapy resistance. Investigating the expression of validated immune resistance genes improves the interpretation but a drawback is the limited sequencing depth that is currently possible in single cells. Comprehension of IR gene expression by epigenetic mechanisms as well as posttranslational activity of IR proteins will be complemented by broad multiomics studies.

6.3.2 Hit selection and refinement

The HTP screens identified a set of strong immune resistance genes eligible for functional analysis. Bioinformatic analyses were performed to further select validated IR genes that showed strong association to a low expression of *MITF*, therefore putatively contributing to melanoma dedifferentiation and therapy resistance. These features together with a low profile in literature resulted in a pre-selection of 17 genes to re-evaluate their impact on T cell-mediated rejection in Ma-Mel-86 in cytotoxicity assays.

As expected, luciferase-based cytotoxicity assays confirmed the immune resistance phenotype of those genes that were identified in the Ma-Mel-86 screen. However, those genes that were primarily

selected due to an association to a low *MITF* expression in the bioinformatic analyses, did not or hardly increased T cell-mediated rejection upon knockdown. High impacts of these genes were less probable as otherwise these genes would have performed well in the primary screens. On the other side, off-target effects of the individual siRNAs could have prevented immune resistance phenotypes of the pool in the primary screens. Therefore, re-evaluation of genes identified by bioinformatic analyses was reasonable. Low effects of these genes could also be due to dependence on the cell line or tumor entity. Bioinformatic analyses showed inter-individual differences in the gene expression of IR genes pointing to selective effects in cell lines. qPCR analyses of the genes mostly confirmed higher expression in the *MITF*^{low} cell line Ma-Mel-86a, but gene expression was in general low for various genes (Ct value above 30). Low expression of target genes could therefore result in low impacts on T cell-mediated rejection. At the same time, complementary immune resistance mechanisms could easily fill in upon downregulation. Alternatively, the identification of these IR genes proposes novel biomarkers of resistant *MITF*^{low} melanomas that facilitate the interpretation of the disease but failed to show biological impact, at least in Ma-Mel-86a. In general, omics studies discover many potential biomarkers with only a few that survive pre-clinical and clinical validation [215].

Finally, I selected *TMCC3*, *MOK*, *SLC39A13* and *ZNF443* for further functional analyses due to their higher mRNA expression levels and their performance in the cytotoxicity assays as well as their low recognition in the literature. Additionally, some genes showed upregulation in *MITF*^{low} (*TMCC3*, *SLC39A13*, *ZNF443*) or were selectively upregulated in melanoma compared to healthy tissues (*MOK* – not indicated in heatmap). For each gene, I selected a single siRNA condition (pooled or individual siRNAs) that showed low to moderate viability effects but enhanced cytotoxic potential of T cells as well as reasonable knockdown efficiencies. Detection of knockdown on the protein level was difficult due to the availability of antibodies as the genes were not yet much of interest in research. While knockdown of *TMCC3*, *SLC39A13* and *MOK* was observed in Ma-Mel-86a, this was only the case for *MOK* in Ma-Mel-86c. Protein expression of *TMCC3* and *SLC39A13* was very low in the *MITF*^{high} cell line Ma-Mel-86c. This was especially surprising for *SLC39A13* as mRNA expression was reasonably high. The Human Protein Atlas describes several splice variants of *SLC39A13* that could result in proteins with different molecular size than the one predicted to be detected by the antibody [206]. Different isoforms could be apparent in *MITF*^{high} and *MITF*^{low} cell lines. Furthermore, it is possible that mRNA and protein expression show only limited correlation [216]. This is due to the regulation of transcription, RNA degradation, translation and protein degradation [217]. This would also contribute to the contrary expression on mRNA and protein level of *ZNF443* in both cell lines. Despite higher mRNA expression in Ma-Mel-86a, the protein expression in both cell lines is comparable. Upon siRNA transfection, mRNA levels drop by 40 % with hardly any changes on the protein level.

The effects observed in the luciferase-based cytotoxicity assays were further confirmed in real-time cytotoxicity assays which measured the degree of dying cells upon co-culture with cytotoxic T cells. TMCC3 showed the strongest effects of the four candidates in both cell lines while MOK was especially strong in Ma-Mel-86a. To that point, experiments were performed with the FluT cell system. To validate the findings, the effect of the genes was investigated in co-culture experiments with MART-1 T cells in the presence of MART-1 peptide and with TIL412. Both systems confirmed the results of the cytotoxicity assays with FluT cells. Although Ma-Mel-86a were initially not targeted by TIL412 due to the lack of melanoma differentiation antigens gene knockdown resulted in a sensitization toward TIL412-mediated tumor cell killing. This was surprising as non-activated TIL412 did not show expression or secretion of cytotoxic molecules. However, how IR gene knockdown remodeled the phenotype of Ma-Mel-86a making them susceptible to TIL412-mediated lysis by for example induction of the expression of melanoma differentiation antigens or release of mediators that lead to activation of TIL412 was not further investigated.

In order to investigate whether IR genes modulate T cell function or increase the resistance of the tumor cells intrinsically, tumor cells were treated with supernatant of polyclonally activated T cells. Knockdown of all genes increased tumor cell lysis upon supernatant treatment. As T cells were absent in the experiment, I concluded that the genes convey resistance mechanisms within the melanoma cells. Subsequently, I was able to show that knockdown of IR genes sensitized tumor cells to treatment with cytotoxic ligands like TRAIL, TNF α , FasL and IFN γ . This was particularly interesting as both cell lines showed primary resistance against death receptor ligands. In order to investigate how the proteins contribute to resistance, I selected TMCC3 and SLC39A13 for deeper mode of action analyses. TMCC3 showed generally very strong phenotypes in the experiments. Treatment with TRAIL resulted even in a stronger tumor cell death compared to co-culture assays upon gene knockdown. In general susceptibility to several death receptor ligands was affected in Ma-Mel-86a. This was strongly in contrast to SLC39A13 which is the reason this protein was additionally selected for mode of action analyses. Of the single treatments, SLC39A13 silencing resulted in the sensitization mostly to IFN γ treatment and not to death receptor ligands. Therefore, two opposing and complementary signaling pathways could be affected and could contribute to the resistance. As low MITF expression is associated with increased resistance, functional analyses of TMCC3 and SLC39A13 were performed in the MITF^{low} cell line Ma-Mel-86a. Here, protein expression was detectable, and knockdown of these genes resulted in decreased expression on the mRNA and protein level. Although both genes were primarily selected due to their performance in the HTP screens, both genes were associated with increased expression in MITF^{low} melanoma cells in the Seurat analysis. Additionally, TMCC3 was associated with clusters identified by WGCNA that negatively correlated to the MITF clusters in the

TCGA and the single cell RNA-Seq data, further supporting the rationale for mode of action analyses of these genes.

6.4 TMCC3 and SLC39A13 as immune resistance genes in melanoma

TMCC3 and SLC39A13 were selected for further mode of action analyses and were associated with MITF^{low} and an increased resistance. Therefore, I investigated whether the expression of the two genes were affected by MITF or by various treatments of Ma-Mel-86a. Downregulation of MITF did not change the expression of *TMCC3* or *SLC39A13*, but TMCC3 knockdown increased *MITF* expression. MITF is a key transcription factor in melanocytes and its expression can be regulated by various activating and repressing mechanisms [71]. As TMCC3 silencing increased T cell-mediated rejection of Ma-Mel-86a, multiple pathways could be affected by the knockdown that induce MITF expression. Treatment of Ma-Mel-86a with supernatant of activated FluT cells induced *TMCC3*. Taken into account that TMCC3 was identified as an immune resistance gene, it could well be upregulated as a resistance mechanism of the tumor cells. While no significant difference of *SLC39A13* expression was detected, *MITF* expression was downregulated upon treatment with supernatant. Inflammation and cytokines such as TNF α and IL-6 can induce phenotype switching and downregulate MITF in melanoma cells [71, 88, 124]. However, treatment of cells with TNF α alone did not alter *MITF* or *TMCC3* mRNA expression. The expression of *SLC39A13* was only affected by IFN γ treatment. This was interesting as a knockdown of this gene resulted in higher susceptibility of Ma-Mel-86a to IFN γ -mediated apoptosis.

As downregulation of TMCC3 and SLC39A13 resulted in an increased susceptibility towards T cell-mediated tumor cell lysis, I investigated whether overexpression of the genes would increase the protection against T cell attack. Ma-Mel-86a were stably transfected with overexpression plasmids for TMCC3 and SLC39A13 or with an empty vector control. The luciferase-based cytotoxicity assay showed increased luciferase values when both genes were overexpressed, assuming that proliferation was enhanced. Upon FluT cell co-culture, SLC39A13 overexpressing cells showed similar proportion of dying cells as the empty vector control. In contrast, TMCC3 overexpression resulted in a decreased degree of tumor cell death indicating that this gene increases resistance towards T cell-mediated lysis. SLC39A13 overexpression did not demonstrate the desired effect. As protein levels were already high in wildtype cells, increased expression potentially didn't improve immune resistance. This would also be supported by the fact that by treatment of Ma-Mel-86a with T cell supernatant SLC39A13 is not further increased while this is the case for TMCC3.

6.4.1 TMCC3 and SLC39A13 knockdown changes the expression of receptors important for antigen presentation and apoptosis induction

As downregulation of either TMCC3 or SLC39A13 increased T cell-mediated rejection of melanoma cells, both genes were silenced simultaneously. The genes were associated to different clusters in the bioinformatic analyses while in functional analyses TMCC3 showed protective effects against death receptor ligands and SLC39A13 to IFN γ . Therefore, I investigated whether co-knockdown resulted in an additive effect towards T cell cytotoxicity. Tumor cell death was not increased upon simultaneous gene silencing, so I assessed whether the surviving cells after co-culture with T cells were still TMCC3 and SLC39A13 proficient to protect the tumor cells. Knockdown was still present, so tumor cells were apparently using a complementary resistance mechanism.

Flow cytometry analyses revealed that after co-culture, expression of DR5, TNFR1, IFN γ R1 and HLA-A2 was decreased, receptors that are important for apoptosis induction or antigen presentation [218, 219]. Downregulated receptor expression was especially present in cells with the strongest viability phenotype. The identified subset of cell death resistant cells that emerge during the experiment can originate by two different hypotheses that represent the categories described in 1.3.2: Either resistant clones with low receptor expression existed prior to co-culture with FluT cells and outgrew during the experiment or the receptors were downregulated in the course of the experiment. As untreated wild-type cells did not show receptor negative populations the knockdown would need to be the reason for its generation. Generally, the second hypothesis is more probable. In the homeostatic resistance model, clones emerge under immune pressure during treatment [122]. HLA and death receptor expression can be downregulated by epigenetic, transcriptional and posttranslational silencing [220-223]. The expression of HLA on the surface is further dependent on the stability of the HLA-peptide complex [224]. If the peptide is removed from the complex, the β_2M subunit gets lost and HLA will be internalized, ubiquitinated and proteolytically degraded. Moreover, it was shown in PDAC that NBR1 mediates HLA internalization and localization to lysosomes for autophagy-mediated degradation [225]. Similar to HLA-A2, DR5 and IFN γ R1 expression can be downregulated by autophagy [222, 226]. Autophagy is induced by stress and is associated to tumor progression and drug resistance [227]. It was shown to induce STAT3 signaling in cancer cells to prevent sensitivity to T cell cytotoxicity. Therefore, autophagic processes in Ma-Mel-86a could be induced by the FluT cells to enhance stress tolerance and downregulate expression of HLA-A2, DR5 and IFN γ R1 as a resistance mechanism. Additionally, expression of IL-3 by T cells can induce downregulation of TNFR1 [228, 229]. In contrast, co-culture of Ma-Mel-86a with FluT cells resulted in stronger FAS expression which could be induced by IFN γ release of the T cells [230]. However, sensitivity to FAS-induced apoptosis is not necessarily increased by higher FAS expression [231]. In cell lines that are initially resistant to FAS-mediated apoptosis (like Ma-Mel-86), stimulation of FAS is more tumorigenic as it stimulates pathways involved

in invasiveness and growth [232]. At the same time, resistant cells often increase the expression of FasL to induce apoptosis in T cells.

The analysis revealed that co-culture of Ma-Mel-86a with FluT cells generates an immune resistant cell population by downregulation of receptors important for antigen recognition and induction of apoptosis, potentially due to degradation initiated by autophagy. Additionally, I observed that the knockdown of TMCC3 and SLC39A13 changed the receptor expression *per se*. Although TMCC3 knockdown did not alter expression significantly, there was an increase of DR5 expression. This could be one aspect explaining the increased susceptibility to TRAIL of TMCC3 deficient cells. SLC39A13 silencing increased the expression of DR5, FAS, IFN γ R1 and decreased the one of HLA-A2 significantly. As SLC39A13 knockdown increased the susceptibility of Ma-Mel-86a slightly to TRAIL and stronger to IFN γ , the increased receptor expression could be a reason. On the other hand, downregulation of HLA-A2 in SLC39A13 deficient cells can contribute to explain why TMCC3 showed a stronger IR phenotype in co-culture experiments with T cells. The expression levels of the receptors in simultaneous knockdown of TMCC3 and SLC39A13 were constantly between those of the single knockdowns. As there were no opposite effects in receptor alterations between TMCC3 and SLC39A13, flow cytometry analysis could not clarify why there is no additive effect upon simultaneous knockdown. Overall, altered receptor expression was no sufficient characterization of how TMCC3 and SLC39A13 protect Ma-Mel-86a. This was further investigated by western blot analysis.

6.4.2 Structure and function of TMCC3

Transmembrane and coiled-coil domain family 3 (TMCC3) belongs along with TMCC1, TMCC2 and TEX28 to the testis-expressed 28 (TEX28) family that typically contain two transmembrane domains and cytoplasmic coiled-coil domains [183, 233]. TMCC3 is highly expressed in the nervous system and the testis, and it is located in the endoplasmic reticulum membrane (ER). Here, it works in tandem with atlastins and lunapark in order to build three-way junctions of the tubular network of the ER [183, 234]. The ER plays a major role in cell homeostasis being important for protein synthesis as well as calcium and lipid metabolism [235]. The network of the tubular ER is highly dynamic and characterized by a rather peripheral cell localization and by three-way junctions that connect tubules with each other. The smooth tubular network is not defined by high density of ribosomes and is therefore more important for lipid synthesis, calcium signaling and contact sites for other organelles [235]. Indeed, TMCC1-3 have also been associated to the regulation of endosome trafficking from the ER [236]. Downregulation of TMCC3 resulted in the decrease of three-way junctions and changes of the ER morphology [183]. TMCC3 has been shown to bind to the 14-3-3 protein family [233, 234]. The 14-3-3 protein family are phosphoserine/phosphothreonine-binding proteins that interact with various

proteins to regulate for example their localization or activity [237]. Overexpression of 14-3-3 γ reduced the localization of TMCC3 to three-way junctions of the ER and the number of three-way-junctions [234]. TMCC3 possesses a long cytoplasmic domain that can be phosphorylated which facilitates the binding of 14-3-3 γ [183, 234]. The kinase that is responsible for the phosphorylation is yet unknown [234].

In cancer research, TMCC3 has not drawn much attention so far. TMCC3 protein expression was reported to be upregulated in Chronic lymphocytic leukemia (CLL) vs. healthy B-cells [238]. In pancreatic cancer, expression of *TMCC3* and neighboring genes was induced by increased expression of miR-492 [239]. miR-492 expression was associated to cell proliferation and EMT by TGF β /Smad3 signaling. Enhanced characterization of TMCC3 was performed in a study in breast cancer stem cells (BCSCs) [182]. TMCC3 expression was increased in BCSCs and knockdown of TMCC3 resulted in decreased cell migration and metastasis *in vitro* and *in vivo*, respectively. The authors described that TMCC3 can interact with AKT with its cytoplasmic coiled-coil domain in order to activate AKT [182].

6.4.3 TMCC3 sensitizes melanoma cells to TRAIL-mediated apoptosis

As TMCC3 was described to interact with AKT and promote its activation in BCSCs [182], I wanted to investigate how this impacts the sensitivity to apoptosis in Ma-Mel-86a. AKT was characterized to promote pro-survival signaling for example by inhibition of anti-apoptotic BAD [240]. I showed in my experiments that TMCC3 downregulation increased susceptibility of Ma-Mel-86a towards TRAIL treatment. Therefore, I investigated expression and activation of AKT signaling and apoptosis-related proteins upon TMCC3 knockdown and TRAIL treatment. In contrast to the published data, silencing of TMCC3 did not reduce phosphorylation and thereby activation of AKT but promoted it in Ma-Mel-86a. Consequently, pAKT target genes BAD and NF-kB/RELA were likewise phosphorylated and the expression of anti-apoptotic XIAP was upregulated, especially during TRAIL treatment [240, 241]. pAKT activates MDM2, an E3 ubiquitin ligase leading to the degradation of p53 that induces apoptosis [240]. In TMCC3 silenced cells, p53 expression was enhanced which is on the one hand contrary to increased phosphorylation of AKT, but on the other hand it can contribute to increased tumor cell death upon treatment. p53 is able to induce pro-apoptotic proteins and the expression of death receptors [242].

Apart from AKT pathway-related genes, the expression of caspases and anti-apoptotic BCL-2 indicated anti-survival features. BCL-2 was downregulated and caspase-3 and -8 were upregulated which favored pro-apoptotic signaling. This supported increased tumor cell lysis upon co-culture with FluT cells or treatment with death receptor ligands like TRAIL. Accordingly, treatment with TRAIL induced caspase cleavage much stronger in TMCC3 deficient cells. Caspase activity was also apparent in the absence of TRAIL which explains the viability impact in *TMCC3* siRNA-treated cells. Expression of Caspase-9 was

not increased potentially due to counter regulatory mechanisms by increased AKT activation [243]. In conclusion, TMCC3 downregulation sensitized Ma-Mel-86a towards apoptosis by death receptor signaling which was counter regulated by increased AKT activity.

6.4.4 Downregulation of TMCC3 induces perturbation of ER homeostasis

In contrast to published data, my results showed that TMCC3 knockdown resulted in increased activity of AKT and consequently of proteins downstream of AKT. I therefore had to investigate other mechanisms how TMCC3 could protect Ma-Mel-86a from T cell or TRAIL-mediated lysis. As described previously, TMCC3 is important for the generation of three-way junctions of the tubular ER [183]. In the respective publication they investigated if downregulation of TMCC3 results in ER stress in U2OS cells by measurement of the expression of BiP and CHOP, two important markers of ER stress. This was not the case [183]. If ER homeostasis is disturbed by protein misfolding or disturbance of lipid and calcium metabolism, ER stress occurs resulting in the unfolded protein response (UPR) [244, 245]. In the homeostatic condition, BiP binds to the three important proteins Inositol Requiring 1 (IRE1), PKR-like ER kinase (PERK), and Activating Transcription Factor 6 (ATF6) [244]. If ER stress occurs, BiP dissociates and IRE1, PERK and ATF6 are activated and induce the UPR in which different pathways try to either resolve the stress situation or induce apoptosis. Phosphorylation of IRE1 α and PERK results in signaling cascades that stimulate apoptosis by phosphorylation of JNK and expression of CHOP, respectively [244]. The results of my experiments showed that TMCC3 increased susceptibility to death receptor ligand-mediated apoptosis. Phosphorylated JNK is able to promote death receptor-mediated apoptosis via downregulation of CFLAR_L and in tandem with CHOP also of BCL-2 while upregulating DR5 [245-247]. Additionally, TMCC3 silencing promoted AKT activity. Increased activity of AKT and expression of XIAP was shown to be induced to by ER stress [248]. The published data and previous results therefore supported the hypothesis that TMCC3 knockdown induces ER stress in Ma-Mel-86a. Although TMCC3 downregulation did not induce ER stress in U2OS cells, I did not exclude this possibility in Ma-Mel-86a. In melanoma plasticity, MITF^{low}/AXL^{high} cells like Ma-Mel-86a can be induced by nutrient starvation or inflammation via eIF2 α and ATF4 [88, 249]. ATF4 is also induced during the UPR and regulates CHOP expression potentially linking melanoma plasticity to susceptibility of ER stress [244].

I therefore investigated if the knockdown of TMCC3 induces ER stress in Ma-Mel-86a in order to sensitize the cells to apoptosis which is counter regulated by increased AKT signaling. I measured the expression and/or phosphorylation of BiP, CHOP, IRE1 α , JNK and CFLAR_L. As hypothesized, TMCC3 silencing resulted in phosphorylation of JNK and degradation of CFLAR_L which explains enhanced susceptibility of tumor cell lysis upon TRAIL treatment and together with increased p53, could be

associated to increased DR5 expression. Upstream of JNK is IRE1 α which also shows phosphorylation upon TMCC3 downregulation and indicates ER stress. The expression of other two proteins BiP and CHOP was not induced by TMCC3 knockdown. CHOP expression under homeostatic conditions is in general very low and increases strongly upon ER stress [250]. The high expression that was observed in Scr3 cells could be due to expression of ATF4 that is associated with low MITF expression. However, ATF4 expression was not measured in the experiment. A reason why there is no induction of CHOP upon knockdown and potentially also of BiP could be due to general high protein expression that is not further enhanced. However, phosphorylation of IRE1 α demonstrate the presence of ER stress. Furthermore, increased expression of p53 can also be attributed to ER stress [242, 251]. Treatment of TRAIL enhanced pIRE1 α and stronger pJNK, especially in TMCC3 deficient cells, but expression and phosphorylation levels of the BiP, CHOP, CFLAR_L as well as total IRE1 α did not show alterations during treatment. The degree and the precise source of the ER stress upon downregulation could further be investigated by measurement of more ER stress-related proteins as well as the involvement of calcium due to the calcium storage function of the tubular ER network. However, these measurements were not part of this thesis.

Taken together, knockdown of TMCC3 induces ER stress in Ma-Mel-86a that on the one hand induces pro-survival signaling via AKT but also brings the cells into an apoptosis sensitive state. Downregulation of anti-apoptotic proteins BCL-2 and CFLAR_L in combination with upregulation of DR5 make TMCC3 deficient Ma-Mel-86a cells highly susceptible to TRAIL-mediated cell death.

6.4.5 Structure and function of SLC39A13/ZIP13

Solute Carrier Family 39 Member 13 (SLC39A13) whose gene product is preferentially called ZIP13 protein belongs to the LIV-1 subfamily of ZIP zinc transporters [252]. ZIP family members possess eight transmembrane (TM) domains and enable zinc influx into the cytoplasm [253]. Zinc is an important regulator of the function of enzymes such as histone acetyltransferases (HATs) and histone deacetylases (HDACs) as well as DNA methyltransferases (DNMTs), therefore regulating gene expression by epigenetic mechanisms. Apart from bones, also skin is abundant of zinc, especially in the epidermis [254]. Here, ZIP13 is mainly expressed by fibroblasts for the development of connective tissue [255]. It was shown to be important for bone morphogenetic protein (BMP) and TGF β signaling by regulating the nuclear localization of Smad proteins. In contrast to other family members, ZIP13 is not located in the cytoplasmic membrane but located in the Golgi apparatus transporting zinc out of the Golgi compartment. Both the N and the C terminus of the eight TM domain protein face the luminal side on the Golgi [252]. Between TM3 and TM4 resides a hydrophilic loop located in the cytoplasm that is unique from the other ZIP family members.

A loss of SLC39A13 has been linked to the spondylocheiro dysplastic form of Ehlers-Danlos syndrome which is characterized by alterations of the extracellular matrix (ECM) and skin fragility [256, 257]. In terms of cancer biology, the gene has not been extensively studied. SLC39A13/ZIP13 was reported to be higher expressed in pancreatic and breast cancers compared to respective healthy tissues [258, 259]. One study reported that SLC39A13/ZIP13 activated the Focal adhesion kinase (FAK)/Src signaling pathway in ovarian cancer [184]. Establishment of ZIP13 knockout cell lines showed reduced growth potential and decreased generation of tumors *in vivo*. Differential gene expression analyses between wildtype and knockout cell lines revealed that ZIP13 is important for various pathways such as ECM-receptor interaction, cytokine signaling and focal adhesion. Proteins like STAT3 and ERK that are involved in FAK/Src signaling were downregulated upon ZIP13 knockdown [184]. FAK/Src pathway activity promoting tumorigenesis and metastasis is well established in cancers like lung and pancreatic cancer [260]. As this pathway is required for mesenchymal invasion and related to inflammatory signaling, it might well play a role in MITF^{low} cells such as Ma-Mel-86a. The study on ZIP13 in ovarian cancer proposed its role in the Zinc distribution in the cell in order enable FAK/Src pathways signaling and expression of proinflammatory and invasion-related genes [184].

6.4.6 SLC39A13/ZIP13 sensitizes melanoma cells to IFN γ -mediated apoptosis by increasing STAT1/STAT3 ratio

MITF^{low} cell line Ma-Mel-86a was previously shown to have increased phosphorylation of STAT3 compared to the MITF^{high} cell line Ma-Mel-86c [130]. This could indicate an increased activation of the FAK/Src pathway upon dedifferentiation in melanoma. Knockdown of SLC39A13 increased the susceptibility of Ma-Mel-86a towards T cells as well as IFN γ . IFN γ binding to IFN γ R results in canonical JAK-STAT1 signaling that can induce apoptosis in the target cancer cell [21, 261]. If STAT1 is absent, STAT3 can be stimulated for pro-survival signaling [261]. I therefore decided to investigate the expression and phosphorylation of STAT1, STAT3 as well as of AKT as another pro-survival pathway that can be activated by FAK/Src. I determined protein expression upon SLC39A13 knockdown and during IFN γ treatment. I was not able to reproduce the phenotype described in the publication, in which it was shown that SLC39A13 deficiency decreased STAT3 expression and phosphorylation [184]. Knockdown of SLC39A13 did not change the expression of total STAT3 and even increased its phosphorylation in Ma-Mel-86a. On the other side, total STAT1 was upregulated making the cells more prone to IFN γ -mediated apoptosis. Upon IFN γ treatment total and phosphorylated STAT1 levels increased, especially in the SLC39A13 silenced cells while phosphorylation of STAT3 showed small changes. STAT1 activation in SLC39A13 proficient cells can explain cell death of Ma-Mel-86a upon IFN γ treatment. Knockdown of SLC39A13 however increases STAT1 expression prior to treatment and enhances the phosphorylation to induce apoptosis. I therefore concluded, by increasing the ratio of

STAT1/STAT3, Ma-Mel-86a became more prone to apoptosis induction in ZIP13 deficient cells. In a mathematical model this balance was similarly described [262]. It determined if cancer cells are promoting apoptosis (high STAT1) or repress it (high STAT3).

Apoptosis in ZIP13 deficient Ma-Mel-86a is also enhanced by the increased expression of caspases and decreased expression of BCL-2 upon gene knockdown. The previously described mathematical model of STAT1/STAT3 balance further proposed that the higher STAT1 results in BCL-2 downregulation as well as upregulation of pro-apoptotic BAX [262]. Reduced BCL-2 expression was achieved by SLC39A13 downregulation without IFN γ treatment. STAT1 is generally activated through phosphorylation [263]. However, experiments showed that transfection of U3A cells with STAT1 reduced BCL-2 promoter activity without IFN γ treatment [264]. Similarly, in U3A unphosphorylated STAT1 was able to induce expression of caspases 1, 2 and 3 [265]. It is therefore possible that STAT1 is responsible for the upregulation of other caspases upon SLC39A13 knockdown. STAT1 has additionally been described to upregulate death receptors like FAS or DR5 [265]. Here, upregulation was dependent on IFN γ -induced STAT1 activity. However, due to regulation of expression of BCL-2 and caspases, it should not be ruled out that also unphosphorylated STAT1 can induce death receptor expression. This could also explain why downregulation of SLC39A13 resulted in altered expression of death receptor expression in Ma-Mel-86a. Another possibility was the previously mentioned autophagic processes. In fibrosarcoma, it was shown that ZIP13 can inhibit autophagy [266]. As autophagy could be a reason for reduced receptor expression of DR5 and IFN γ R1, SLC39A13/ZIP13 knockdown could reduce this process, therefore increasing the surface expression of the receptors.

Taken together, SLC39A13/ZIP13 increased the STAT1/STAT3 ratio which brings Ma-Mel-86a into an apoptosis sensitive state by downregulation of BCL-2 and which works in tandem with increased IFN γ R1 expression to increase IFN γ -STAT1 dependent apoptosis.

6.5 Translational implications of SLC39A13 and TMCC3 in malignant melanoma

As many melanoma patients still do not respond to immunotherapies and melanoma cells dedifferentiate into MITF^{low} cells and acquire resistance mechanisms, alternative targets are in need to overcome tumor immunity. This project aimed to identify complementary resistance mechanisms and identified with TMCC3 and SLC39A13/ZIP13 two proteins that protected melanoma cells with low MITF expression.

In immunotherapeutic approaches, antibody therapies and small molecules are used to improve benefits for cancer patients [267]. Small molecules have the advantage of modulating intracellular targets and pathways. As neither TMCC3 nor ZIP13 are expressed on the cell surface, they are not

eligible for antibody therapies and would rather be targeted by small molecules. TMCC3 has been subject of a patent for an antibody therapy for breast cancer [268]. However, the patent was issued before it was published that the protein is not expressed on the surface but the endoplasmic reticulum. Downregulation of TMCC3 activated an ER stress response in Ma-Mel-86a bringing the cell into an apoptosis sensitive state that can be killed through death receptor signaling. Targeting TMCC3 intracellularly would be difficult as the protein is not an enzyme or a channel. Increased research on the different domains of the protein is highly necessary for development of an appropriate therapy. 14-3-3 γ was shown to bind to phosphorylated TMCC3 which regulated the location of TMCC3 and reduced the number of three-way junctions [234]. However, the kinase that phosphorylates TMCC3 remains unknown so far and inducing a kinase or 14-3-3 γ activity would probably have very broad effects in the target cells.

SLC39A13 downregulation sensitized Ma-Mel-86a to IFN γ -mediated apoptosis by upregulation of IFN γ R1 and STAT1 paralleled by downregulation of BCL-2. Inhibitors of Zinc transporters are under development [269]. Although ZIP13 has not directly been targeted by an inhibitor, the ZIP7 inhibitor NVS-ZP7-4 has been shown to target ZIP7 in the ER to regulate intracellular zinc levels. Therefore, ZIP13 could be similarly inhibited by a compound to reproduce the reported sensitivity to tumor cell apoptosis.

Also, TMCC3 expression is elevated in the nervous system and the testis while SLC39A13 is highly expressed in the bone and in hard and connective tissue [233, 269]. Targeting these proteins systemically could therefore be accompanied with severe adverse events and damage of healthy tissues. Application of a drug at a specific location like the tumor microenvironment could be achieved for example by 4th generation CAR T cells. As previously described, CAR T cells are not restricted to antigen recognition on HLA and express synthetic receptors for improved T cell activity [99, 270]. 4th generation CAR T cells are designed to produce and release proteins such as cytokines or antibodies upon activation [270]. Hence, activation of CAR T cells in the tumor microenvironment could induce the expression and secretion of small inhibitory proteins or mediators targeting TMCC3 and SLC39A13 locally. However, applying CAR T cell therapy to MITF^{low} melanoma would be concomitant with two major difficulties. Despite successful application against hematological cancers, solid tumors like melanoma didn't show promising results yet [271]. Also, the selection of an appropriate melanoma specific surface antigen for CAR T cell receptor activation is compromised. Melanoma differentiation antigens (MDAs) are often targets for T cell therapy, but MITF^{low} melanoma cells don't express MDAs. Alternative but more unspecific targets could be cancer germline antigens (CGA) like NY-ESO-1 or even better, neoantigens. Neoantigen therapy would be a highly personalized, but also expensive approach [271].

References

Journal Articles

1. Hanahan, D. and R.A. Weinberg, *The hallmarks of cancer*. Cell, 2000. **100**(1): p. 57-70.
2. Hanahan, D. and R.A. Weinberg, *Hallmarks of cancer: the next generation*. Cell, 2011. **144**(5): p. 646-74.
3. Hanahan, D., *Hallmarks of Cancer: New Dimensions*. Cancer Discov, 2022. **12**(1): p. 31-46.
4. Dunn, G.P., L.J. Old, and R.D. Schreiber, *The three Es of cancer immunoediting*. Annu Rev Immunol, 2004. **22**: p. 329-60.
5. Ehrlich, P., *Ueber den jetzigen Stand der Karzinomforschung*. Ned Tijdschr Geneesk, 1909(5): p. 273-90.
6. Burnet, M., *Cancer: a biological approach. III. Viruses associated with neoplastic conditions. IV. Practical applications*. Br Med J, 1957. **1**(5023): p. 841-7.
7. Waldman, A.D., J.M. Fritz, and M.J. Lenardo, *A guide to cancer immunotherapy: from T cell basic science to clinical practice*. Nat Rev Immunol, 2020. **20**(11): p. 651-668.
8. Chen, D.S. and I. Mellman, *Oncology meets immunology: the cancer-immunity cycle*. Immunity, 2013. **39**(1): p. 1-10.
9. Mittal, D., et al., *New insights into cancer immunoediting and its three component phases-- elimination, equilibrium and escape*. Curr Opin Immunol, 2014. **27**: p. 16-25.
10. Munhoz, R.R. and M.A. Postow, *Recent advances in understanding antitumor immunity*. F1000Res, 2016. **5**: p. 2545.
11. Demaria, O., et al., *Harnessing innate immunity in cancer therapy*. Nature, 2019. **574**(7776): p. 45-56.
12. Paul, S. and G. Lal, *The Molecular Mechanism of Natural Killer Cells Function and Its Importance in Cancer Immunotherapy*. Front Immunol, 2017. **8**: p. 1124.
13. Weigelin, B. and P. Friedl, *T cell-mediated additive cytotoxicity - death by multiple bullets*. Trends Cancer, 2022. **8**(12): p. 980-987.
14. Raskov, H., et al., *Cytotoxic CD8(+) T cells in cancer and cancer immunotherapy*. Br J Cancer, 2021. **124**(2): p. 359-367.
15. Chowdhury, D. and J. Lieberman, *Death by a thousand cuts: granzyme pathways of programmed cell death*. Annu Rev Immunol, 2008. **26**: p. 389-420.
16. Keefe, D., et al., *Perforin triggers a plasma membrane-repair response that facilitates CTL induction of apoptosis*. Immunity, 2005. **23**(3): p. 249-62.
17. Pipkin, M.E. and J. Lieberman, *Delivering the kiss of death: progress on understanding how perforin works*. Curr Opin Immunol, 2007. **19**(3): p. 301-8.
18. Adrain, C., B.M. Murphy, and S.J. Martin, *Molecular ordering of the caspase activation cascade initiated by the cytotoxic T lymphocyte/natural killer (CTL/NK) protease granzyme B*. J Biol Chem, 2005. **280**(6): p. 4663-73.
19. Buzza, M.S., et al., *Extracellular matrix remodeling by human granzyme B via cleavage of vitronectin, fibronectin, and laminin*. J Biol Chem, 2005. **280**(25): p. 23549-58.
20. de Araújo-Souza, P.S., S.C. Hanschke, and J.P. Viola, *Epigenetic control of interferon-gamma expression in CD8 T cells*. J Immunol Res, 2015. **2015**: p. 849573.
21. Jorgovanovic, D., et al., *Roles of IFN- γ in tumor progression and regression: a review*. Biomark Res, 2020. **8**: p. 49.

22. Negishi, H., T. Taniguchi, and H. Yanai, *The Interferon (IFN) Class of Cytokines and the IFN Regulatory Factor (IRF) Transcription Factor Family*. Cold Spring Harb Perspect Biol, 2018. **10**(11).
23. Yang, M.Q., et al., *Interferon regulatory factor 1 priming of tumour-derived exosomes enhances the antitumour immune response*. Br J Cancer, 2018. **118**(1): p. 62-71.
24. Dostert, C., et al., *The TNF Family of Ligands and Receptors: Communication Modules in the Immune System and Beyond*. Physiol Rev, 2019. **99**(1): p. 115-160.
25. Suo, F., et al., *Receptor Specificity Engineering of TNF Superfamily Ligands*. Pharmaceutics, 2022. **14**(1).
26. Diaz Arguello, O.A. and H.J. Haisma, *Apoptosis-Inducing TNF Superfamily Ligands for Cancer Therapy*. Cancers (Basel), 2021. **13**(7).
27. Kucka, K., et al., *Membrane lymphotoxin- α (2) β is a novel tumor necrosis factor (TNF) receptor 2 (TNFR2) agonist*. Cell Death Dis, 2021. **12**(4): p. 360.
28. E, O.R., et al., *The Janus Face of Death Receptor Signaling during Tumor Immunoediting*. Front Immunol, 2016. **7**: p. 446.
29. Micheau, O. and J. Tschopp, *Induction of TNF receptor I-mediated apoptosis via two sequential signaling complexes*. Cell, 2003. **114**(2): p. 181-90.
30. Hu, X., et al., *Lymphotoxin β receptor mediates caspase-dependent tumor cell apoptosis in vitro and tumor suppression in vivo despite induction of NF- κ B activation*. Carcinogenesis, 2013. **34**(5): p. 1105-14.
31. Chen, M.C., et al., *The role of apoptosis signal-regulating kinase 1 in lymphotoxin-beta receptor-mediated cell death*. J Biol Chem, 2003. **278**(18): p. 16073-81.
33. Kim, S.K. and S.W. Cho, *The Evasion Mechanisms of Cancer Immunity and Drug Intervention in the Tumor Microenvironment*. Front Pharmacol, 2022. **13**: p. 868695.
34. Chen, Q., T. Sun, and C. Jiang, *Recent Advancements in Nanomedicine for 'Cold' Tumor Immunotherapy*. Nanomicro Lett, 2021. **13**(1): p. 92.
35. Bourhis, M., et al., *Direct and Indirect Modulation of T Cells by VEGF-A Counteracted by Anti-Angiogenic Treatment*. Front Immunol, 2021. **12**: p. 616837.
36. Turley, S.J., V. Cremasco, and J.L. Astarita, *Immunological hallmarks of stromal cells in the tumour microenvironment*. Nat Rev Immunol, 2015. **15**(11): p. 669-82.
37. Zong, J., et al., *Tumor-derived factors modulating dendritic cell function*. Cancer Immunol Immunother, 2016. **65**(7): p. 821-33.
38. Chen, L. and D.B. Flies, *Molecular mechanisms of T cell co-stimulation and co-inhibition*. Nat Rev Immunol, 2013. **13**(4): p. 227-42.
39. Taylor, B.C. and J.M. Balko, *Mechanisms of MHC-I Downregulation and Role in Immunotherapy Response*. Front Immunol, 2022. **13**: p. 844866.
40. Pan, Y., et al., *Tumor-Associated Macrophages in Tumor Immunity*. Front Immunol, 2020. **11**: p. 583084.
41. Veglia, F., E. Sanseviero, and D.I. Gabrilovich, *Myeloid-derived suppressor cells in the era of increasing myeloid cell diversity*. Nat Rev Immunol, 2021. **21**(8): p. 485-498.
42. Batlle, E. and J. Massagué, *Transforming Growth Factor- β Signaling in Immunity and Cancer*. Immunity, 2019. **50**(4): p. 924-940.
43. Chen, B.J., et al., *Immunotherapy of Cancer by Targeting Regulatory T cells*. Int Immunopharmacol, 2022. **104**: p. 108469.

44. Peng, S. and Y. Bao, *A narrative review of immune checkpoint mechanisms and current immune checkpoint therapy*. *Annals of Blood*, 2021. **7**.
45. Lo, W.L., et al., *Lck promotes Zap70-dependent LAT phosphorylation by bridging Zap70 to LAT*. *Nat Immunol*, 2018. **19**(7): p. 733-741.
46. Zhu, Y., S. Yao, and L. Chen, *Cell surface signaling molecules in the control of immune responses: a tide model*. *Immunity*, 2011. **34**(4): p. 466-78.
47. Walunas, T.L., et al., *CTLA-4 can function as a negative regulator of T cell activation*. *Immunity*, 1994. **1**(5): p. 405-13.
48. Parry, R.V., et al., *CTLA-4 and PD-1 receptors inhibit T-cell activation by distinct mechanisms*. *Mol Cell Biol*, 2005. **25**(21): p. 9543-53.
49. He, X. and C. Xu, *Immune checkpoint signaling and cancer immunotherapy*. *Cell Res*, 2020. **30**(8): p. 660-669.
50. Köhler, N., et al., *The Role of Immune Checkpoint Molecules for Relapse After Allogeneic Hematopoietic Cell Transplantation*. *Front Immunol*, 2021. **12**: p. 634435.
51. Lao, Y., et al., *Immune Checkpoint Inhibitors in Cancer Therapy-How to Overcome Drug Resistance?* *Cancers (Basel)*, 2022. **14**(15).
52. Beatty, G.L. and W.L. Gladney, *Immune escape mechanisms as a guide for cancer immunotherapy*. *Clin Cancer Res*, 2015. **21**(4): p. 687-92.
53. Mohammad, R.M., et al., *Broad targeting of resistance to apoptosis in cancer*. *Semin Cancer Biol*, 2015. **35** Suppl(0): p. S78-s103.
54. Zhang, L. and B. Fang, *Mechanisms of resistance to TRAIL-induced apoptosis in cancer*. *Cancer Gene Ther*, 2005. **12**(3): p. 228-37.
55. Jong, K.X.J., E.H.M. Mohamed, and Z.A. Ibrahim, *Escaping cell death via TRAIL decoy receptors: a systematic review of their roles and expressions in colorectal cancer*. *Apoptosis*, 2022. **27**(11-12): p. 787-799.
56. Hsieh, S.L. and W.W. Lin, *Decoy receptor 3: an endogenous immunomodulator in cancer growth and inflammatory reactions*. *J Biomed Sci*, 2017. **24**(1): p. 39.
57. McIlwain, D.R., T. Berger, and T.W. Mak, *Caspase functions in cell death and disease*. *Cold Spring Harb Perspect Biol*, 2013. **5**(4): p. a008656.
58. Jan, R. and G.E. Chaudhry, *Understanding Apoptosis and Apoptotic Pathways Targeted Cancer Therapeutics*. *Adv Pharm Bull*, 2019. **9**(2): p. 205-218.
59. Li, H., et al., *Cleavage of BID by caspase 8 mediates the mitochondrial damage in the Fas pathway of apoptosis*. *Cell*, 1998. **94**(4): p. 491-501.
60. Roberts, J.Z., N. Crawford, and D.B. Longley, *The role of Ubiquitination in Apoptosis and Necroptosis*. *Cell Death Differ*, 2022. **29**(2): p. 272-284.
61. Silke, J. and P. Meier, *Inhibitor of apoptosis (IAP) proteins-modulators of cell death and inflammation*. *Cold Spring Harb Perspect Biol*, 2013. **5**(2).
62. Lomonosova, E. and G. Chinnadurai, *BH3-only proteins in apoptosis and beyond: an overview*. *Oncogene*, 2008. **27** Suppl 1(Suppl 1): p. S2-19.
63. Banjara, S., et al., *The Bcl-2 Family: Ancient Origins, Conserved Structures, and Divergent Mechanisms*. *Biomolecules*, 2020. **10**(1).
64. Qian, S., et al., *The role of BCL-2 family proteins in regulating apoptosis and cancer therapy*. *Front Oncol*, 2022. **12**: p. 985363.
65. Khan, N.H., et al., *Skin cancer biology and barriers to treatment: Recent applications of polymeric micro/nanostructures*. *J Adv Res*, 2022. **36**: p. 223-247.

67. Davey, M.G., N. Miller, and N.M. McInerney, *A Review of Epidemiology and Cancer Biology of Malignant Melanoma*. *Cureus*, 2021. **13**(5): p. e15087.
68. Wagstaff, W., et al., *Melanoma: Molecular genetics, metastasis, targeted therapies, immunotherapies, and therapeutic resistance*. *Genes Dis*, 2022. **9**(6): p. 1608-1623.
69. Liu, J., et al., *Developmental pathways activated in melanocytes and melanoma*. *Arch Biochem Biophys*, 2014. **563**: p. 13-21.
70. Massi, D., et al., *Dedifferentiated melanomas: Morpho-phenotypic profile, genetic reprogramming and clinical implications*. *Cancer Treat Rev*, 2020. **88**: p. 102060.
71. Goding, C.R. and H. Arnheiter, *MITF-the first 25 years*. *Genes Dev*, 2019. **33**(15-16): p. 983-1007.
72. Huber, W.E., et al., *A tissue-restricted cAMP transcriptional response: SOX10 modulates alpha-melanocyte-stimulating hormone-triggered expression of microphthalmia-associated transcription factor in melanocytes*. *J Biol Chem*, 2003. **278**(46): p. 45224-30.
73. Ferguson, J., et al., *Glucose availability controls ATF4-mediated MITF suppression to drive melanoma cell growth*. *Oncotarget*, 2017. **8**(20): p. 32946-32959.
74. Strub, T., et al., *Essential role of microphthalmia transcription factor for DNA replication, mitosis and genomic stability in melanoma*. *Oncogene*, 2011. **30**(20): p. 2319-32.
75. Cheli, Y., et al., *Fifteen-year quest for microphthalmia-associated transcription factor target genes*. *Pigment Cell Melanoma Res*, 2010. **23**(1): p. 27-40.
76. Malcov-Brog, H., et al., *UV-Protection Timer Controls Linkage between Stress and Pigmentation Skin Protection Systems*. *Mol Cell*, 2018. **72**(3): p. 444-456.e7.
77. Sholl, L.M., *A narrative review of BRAF alterations in human tumors: diagnostic and predictive implications*. *Precision Cancer Medicine*, 2020. **3**.
78. Dankner, M., et al., *Classifying BRAF alterations in cancer: new rational therapeutic strategies for actionable mutations*. *Oncogene*, 2018. **37**(24): p. 3183-3199.
79. Guarneri, C., et al., *NF- κ B inhibition is associated with OPN/MMP-9 downregulation in cutaneous melanoma*. *Oncol Rep*, 2017. **37**(2): p. 737-746.
80. Yin, M., et al., *Osteopontin promotes the invasive growth of melanoma cells by activating integrin α v β 3 and down-regulating tetraspanin CD9*. *Am J Pathol*, 2014. **184**(3): p. 842-58.
81. Deng, W., et al., *WNT1-inducible signaling pathway protein 1 (WISP1/CCN4) stimulates melanoma invasion and metastasis by promoting the epithelial-mesenchymal transition*. *J Biol Chem*, 2019. **294**(14): p. 5261-5280.
82. Agaimy, A., et al., *Metastatic Malignant Melanoma With Complete Loss of Differentiation Markers (Undifferentiated/Dedifferentiated Melanoma): Analysis of 14 Patients Emphasizing Phenotypic Plasticity and the Value of Molecular Testing as Surrogate Diagnostic Marker*. *Am J Surg Pathol*, 2016. **40**(2): p. 181-91.
83. Wouters, J., et al., *Robust gene expression programs underlie recurrent cell states and phenotype switching in melanoma*. *Nat Cell Biol*, 2020. **22**(8): p. 986-998.
84. Rambow, F., et al., *Toward Minimal Residual Disease-Directed Therapy in Melanoma*. *Cell*, 2018. **174**(4): p. 843-855.e19.
85. Tsoi, J., et al., *Multi-stage Differentiation Defines Melanoma Subtypes with Differential Vulnerability to Drug-Induced Iron-Dependent Oxidative Stress*. *Cancer Cell*, 2018. **33**(5): p. 890-904.e5.
86. Tirosh, I., et al., *Dissecting the multicellular ecosystem of metastatic melanoma by single-cell RNA-seq*. *Science*, 2016. **352**(6282): p. 189-96.

87. Rambow, F., J.C. Marine, and C.R. Goding, *Melanoma plasticity and phenotypic diversity: therapeutic barriers and opportunities*. *Genes Dev*, 2019. **33**(19-20): p. 1295-1318.
88. Huang, F., et al., *Melanoma Plasticity: Promoter of Metastasis and Resistance to Therapy*. *Front Oncol*, 2021. **11**: p. 756001.
89. Nieto, M.A., et al., *EMT: 2016*. *Cell*, 2016. **166**(1): p. 21-45.
90. Goodall, J., et al., *Brn-2 represses microphthalmia-associated transcription factor expression and marks a distinct subpopulation of microphthalmia-associated transcription factor-negative melanoma cells*. *Cancer Res*, 2008. **68**(19): p. 7788-94.
91. O'Connell, M.P., et al., *Hypoxia induces phenotypic plasticity and therapy resistance in melanoma via the tyrosine kinase receptors ROR1 and ROR2*. *Cancer Discov*, 2013. **3**(12): p. 1378-93.
92. Smith, M.P. and C. Wellbrock, *Molecular Pathways: Maintaining MAPK Inhibitor Sensitivity by Targeting Nonmutational Tolerance*. *Clin Cancer Res*, 2016. **22**(24): p. 5966-5970.
93. Haq, R., et al., *Oncogenic BRAF regulates oxidative metabolism via PGC1 α and MITF*. *Cancer Cell*, 2013. **23**(3): p. 302-15.
94. Nayak, A.P., et al., *Oxidative Phosphorylation: A Target for Novel Therapeutic Strategies Against Ovarian Cancer*. *Cancers (Basel)*, 2018. **10**(9).
95. Ashton, T.M., et al., *Oxidative Phosphorylation as an Emerging Target in Cancer Therapy*. *Clin Cancer Res*, 2018. **24**(11): p. 2482-2490.
96. Stanley, J.O. and S.A. Mohamed, *Cancer immunotherapy: a brief review of the history, possibilities, and challenges ahead*. *J Cancer Metastasis Treat*, 2017. **3**: p. 250-261.
97. Hoteit, M., et al., *Cancer immunotherapy: A comprehensive appraisal of its modes of application*. *Oncol Lett*, 2021. **22**(3): p. 655.
98. Fukuhara, H., Y. Ino, and T. Todo, *Oncolytic virus therapy: A new era of cancer treatment at dawn*. *Cancer Sci*, 2016. **107**(10): p. 1373-1379.
99. Sterner, R.C. and R.M. Sterner, *CAR-T cell therapy: current limitations and potential strategies*. *Blood Cancer J*, 2021. **11**(4): p. 69.
100. Thomas, S. and H. Abken, *CAR T cell therapy becomes CHIC: "cytokine help intensified CAR" T cells*. *Front Immunol*, 2022. **13**: p. 1090959.
101. He, M., et al., *Immune Checkpoint Inhibitor-Based Strategies for Synergistic Cancer Therapy*. *Adv Healthc Mater*, 2021. **10**(9): p. e2002104.
102. Herzberg, B., M.J. Campo, and J.F. Gainor, *Immune Checkpoint Inhibitors in Non-Small Cell Lung Cancer*. *Oncologist*, 2017. **22**(1): p. 81-88.
103. Hodi, F.S., et al., *Improved survival with ipilimumab in patients with metastatic melanoma*. *N Engl J Med*, 2010. **363**(8): p. 711-23.
104. Guruprasad, P., et al., *The current landscape of single-cell transcriptomics for cancer immunotherapy*. *J Exp Med*, 2021. **218**(1).
105. Knight, A., L. Karapetyan, and J.M. Kirkwood, *Immunotherapy in Melanoma: Recent Advances and Future Directions*. *Cancers (Basel)*, 2023. **15**(4).
106. Wolchok, J.D., et al., *Long-Term Outcomes With Nivolumab Plus Ipilimumab or Nivolumab Alone Versus Ipilimumab in Patients With Advanced Melanoma*. *J Clin Oncol*, 2022. **40**(2): p. 127-137.
107. Robert, C., et al., *Ipilimumab plus dacarbazine for previously untreated metastatic melanoma*. *N Engl J Med*, 2011. **364**(26): p. 2517-26.

108. Ribas, A., et al., *Association of Pembrolizumab With Tumor Response and Survival Among Patients With Advanced Melanoma*. *Jama*, 2016. **315**(15): p. 1600-9.
109. Robert, C., et al., *Pembrolizumab versus ipilimumab in advanced melanoma (KEYNOTE-006): post-hoc 5-year results from an open-label, multicentre, randomised, controlled, phase 3 study*. *Lancet Oncol*, 2019. **20**(9): p. 1239-1251.
110. Weber, J.S., et al., *Nivolumab versus chemotherapy in patients with advanced melanoma who progressed after anti-CTLA-4 treatment (CheckMate 037): a randomised, controlled, open-label, phase 3 trial*. *Lancet Oncol*, 2015. **16**(4): p. 375-84.
111. Robert, C., et al., *Five-Year Outcomes With Nivolumab in Patients With Wild-Type BRAF Advanced Melanoma*. *J Clin Oncol*, 2020. **38**(33): p. 3937-3946.
112. Weber, J., et al., *Adjuvant Nivolumab versus Ipilimumab in Resected Stage III or IV Melanoma*. *N Engl J Med*, 2017. **377**(19): p. 1824-1835.
113. Postow, M.A., et al., *Nivolumab and ipilimumab versus ipilimumab in untreated melanoma*. *N Engl J Med*, 2015. **372**(21): p. 2006-17.
114. Workman, C.J., et al., *Lymphocyte activation gene-3 (CD223) regulates the size of the expanding T cell population following antigen activation in vivo*. *J Immunol*, 2004. **172**(9): p. 5450-5.
115. Hemon, P., et al., *MHC class II engagement by its ligand LAG-3 (CD223) contributes to melanoma resistance to apoptosis*. *J Immunol*, 2011. **186**(9): p. 5173-83.
116. Milhem, M.M., et al., *Phase 1b/2, open label, multicenter, study of the combination of SD-101 and pembrolizumab in patients with advanced melanoma who are naïve to anti-PD-1 therapy*. *Journal of Clinical Oncology*, 2019. **37**(15_suppl): p. 9534-9534.
117. Milhem, M., et al., *304 Intratumoral injection of CMP-001, a toll-like receptor 9 (TLR9) agonist, in combination with pembrolizumab reversed programmed death receptor 1 (PD-1) blockade resistance in advanced melanoma*. *Journal for ImmunoTherapy of Cancer*, 2020. **8**(Suppl 3): p. A186-A187.
118. Sun, L., et al., *Talimogene Laherparepvec combined with anti-PD-1 based immunotherapy for unresectable stage III-IV melanoma: a case series*. *J Immunother Cancer*, 2018. **6**(1): p. 36.
119. Mullinax, J.E., et al., *Combination of Ipilimumab and Adoptive Cell Therapy with Tumor-Infiltrating Lymphocytes for Patients with Metastatic Melanoma*. *Front Oncol*, 2018. **8**: p. 44.
120. Davar, D., et al., *Fecal microbiota transplant overcomes resistance to anti-PD-1 therapy in melanoma patients*. *Science*, 2021. **371**(6529): p. 595-602.
121. Tawbi, H.A., et al., *Relatlimab and Nivolumab versus Nivolumab in Untreated Advanced Melanoma*. *N Engl J Med*, 2022. **386**(1): p. 24-34.
122. Zhou, B., et al., *Acquired Resistance to Immune Checkpoint Blockades: The Underlying Mechanisms and Potential Strategies*. *Front Immunol*, 2021. **12**: p. 693609.
123. Hugo, W., et al., *Genomic and Transcriptomic Features of Response to Anti-PD-1 Therapy in Metastatic Melanoma*. *Cell*, 2016. **165**(1): p. 35-44.
124. Landsberg, J., et al., *Melanomas resist T-cell therapy through inflammation-induced reversible dedifferentiation*. *Nature*, 2012. **490**(7420): p. 412-6.
125. Douglass, S.M., et al., *Myeloid-Derived Suppressor Cells Are a Major Source of Wnt5A in the Melanoma Microenvironment and Depend on Wnt5A for Full Suppressive Activity*. *Cancer Res*, 2021. **81**(3): p. 658-670.
126. Reinhardt, J., et al., *MAPK Signaling and Inflammation Link Melanoma Phenotype Switching to Induction of CD73 during Immunotherapy*. *Cancer Res*, 2017. **77**(17): p. 4697-4709.

127. Furuta, J., et al., *CD271 on melanoma cell is an IFN- γ -inducible immunosuppressive factor that mediates downregulation of melanoma antigens*. *J Invest Dermatol*, 2014. **134**(5): p. 1369-1377.
128. Sucker, A., et al., *Acquired IFN γ resistance impairs anti-tumor immunity and gives rise to T-cell-resistant melanoma lesions*. *Nat Commun*, 2017. **8**: p. 15440.
129. Zaretsky, J.M., et al., *Mutations Associated with Acquired Resistance to PD-1 Blockade in Melanoma*. *N Engl J Med*, 2016. **375**(9): p. 819-29.
130. Zhao, F., et al., *Melanoma Lesions Independently Acquire T-cell Resistance during Metastatic Latency*. *Cancer Res*, 2016. **76**(15): p. 4347-58.
131. Sucker, A., et al., *Genetic evolution of T-cell resistance in the course of melanoma progression*. *Clin Cancer Res*, 2014. **20**(24): p. 6593-604.
132. Maleno, I., et al., *Frequent loss of heterozygosity in the $\beta 2$ -microglobulin region of chromosome 15 in primary human tumors*. *Immunogenetics*, 2011. **63**(2): p. 65-71.
133. Restifo, N.P., et al., *Loss of functional beta 2-microglobulin in metastatic melanomas from five patients receiving immunotherapy*. *J Natl Cancer Inst*, 1996. **88**(2): p. 100-8.
134. Koyama, S., et al., *Adaptive resistance to therapeutic PD-1 blockade is associated with upregulation of alternative immune checkpoints*. *Nat Commun*, 2016. **7**: p. 10501.
135. Riaz, N., et al., *Tumor and Microenvironment Evolution during Immunotherapy with Nivolumab*. *Cell*, 2017. **171**(4): p. 934-949.e16.
136. Kakavand, H., et al., *Negative immune checkpoint regulation by VISTA: a mechanism of acquired resistance to anti-PD-1 therapy in metastatic melanoma patients*. *Mod Pathol*, 2017. **30**(12): p. 1666-1676.
137. Boettcher, M. and M.T. McManus, *Choosing the Right Tool for the Job: RNAi, TALEN, or CRISPR*. *Mol Cell*, 2015. **58**(4): p. 575-85.
138. Bock, C., et al., *High-content CRISPR screening*. *Nature Reviews Methods Primers*, 2022. **2**(1): p. 8.
139. Fire, A., et al., *Potent and specific genetic interference by double-stranded RNA in *Caenorhabditis elegans**. *Nature*, 1998. **391**(6669): p. 806-11.
140. Elbashir, S.M., et al., *Duplexes of 21-nucleotide RNAs mediate RNA interference in cultured mammalian cells*. *Nature*, 2001. **411**(6836): p. 494-8.
141. Doudna, J.A. and E. Charpentier, *Genome editing. The new frontier of genome engineering with CRISPR-Cas9*. *Science*, 2014. **346**(6213): p. 1258096.
142. Boutros, M. and J. Ahringer, *The art and design of genetic screens: RNA interference*. *Nat Rev Genet*, 2008. **9**(7): p. 554-66.
143. Khandelwal, N., et al., *A high-throughput RNAi screen for detection of immune-checkpoint molecules that mediate tumor resistance to cytotoxic T lymphocytes*. *EMBO Mol Med*, 2015. **7**(4): p. 450-63.
144. Volpin, V., et al., *CAMK1D Triggers Immune Resistance of Human Tumor Cells Refractory to Anti-PD-L1 Treatment*. *Cancer Immunol Res*, 2020. **8**(9): p. 1163-1179.
145. Sorrentino, A., et al., *Salt-inducible kinase 3 protects tumor cells from cytotoxic T-cell attack by promoting TNF-induced NF- κ B activation*. *J Immunother Cancer*, 2022. **10**(5).
146. Sontheimer, E.J., *Assembly and function of RNA silencing complexes*. *Nat Rev Mol Cell Biol*, 2005. **6**(2): p. 127-38.
147. Li, Y., et al., *Advances in bulk and single-cell multi-omics approaches for systems biology and precision medicine*. *Brief Bioinform*, 2021. **22**(5).

148. Hong, M., et al., *RNA sequencing: new technologies and applications in cancer research*. J Hematol Oncol, 2020. **13**(1): p. 166.
149. Network, C.G.A., *Genomic Classification of Cutaneous Melanoma*. Cell, 2015. **161**(7): p. 1681-96.
150. Gide, T.N., et al., *Distinct Immune Cell Populations Define Response to Anti-PD-1 Monotherapy and Anti-PD-1/Anti-CTLA-4 Combined Therapy*. Cancer Cell, 2019. **35**(2): p. 238-255.e6.
151. Liu, D., et al., *Integrative molecular and clinical modeling of clinical outcomes to PD1 blockade in patients with metastatic melanoma*. Nat Med, 2019. **25**(12): p. 1916-1927.
152. Jerby-Arnon, L., et al., *A Cancer Cell Program Promotes T Cell Exclusion and Resistance to Checkpoint Blockade*. Cell, 2018. **175**(4): p. 984-997.e24.
153. Sade-Feldman, M., et al., *Defining T Cell States Associated with Response to Checkpoint Immunotherapy in Melanoma*. Cell, 2018. **175**(4): p. 998-1013.e20.
154. Gentleman, R.C., et al., *Bioconductor: open software development for computational biology and bioinformatics*. Genome Biol, 2004. **5**(10): p. R80.
155. Boutros, M., L.P. Brás, and W. Huber, *Analysis of cell-based RNAi screens*. Genome Biol, 2006. **7**(7): p. R66.
156. Zhang, Y., G. Parmigiani, and W.E. Johnson, *ComBat-seq: batch effect adjustment for RNA-seq count data*. NAR Genom Bioinform, 2020. **2**(3): p. lqaa078.
157. Tang, Y., M. Horikoshi, and W. Li, *ggfortify: Unified Interface to Visualize Statistical Results of Popular R Packages*. The R Journal, 2016. **8**(2): p. 474-485.
158. Korsunsky, I., et al., *Fast, sensitive and accurate integration of single-cell data with Harmony*. Nat Methods, 2019. **16**(12): p. 1289-1296.
159. Butts, C.T., *network: A Package for Managing Relational Data in R*. Journal of Statistical Software, 2008. **24**(2): p. 1 - 36.
160. Stuart, T., et al., *Comprehensive Integration of Single-Cell Data*. Cell, 2019. **177**(7): p. 1888-1902.e21.
161. Wickham, H., et al., *Welcome to the Tidyverse*. Journal of open source software, 2019. **4**(43): p. 1686.
162. Langfelder, P. and S. Horvath, *WGCNA: an R package for weighted correlation network analysis*. BMC Bioinformatics, 2008. **9**: p. 559.
175. Vivian, J., et al., *Toil enables reproducible, open source, big biomedical data analyses*. Nat Biotechnol, 2017. **35**(4): p. 314-316.
179. Jin, J., et al., *Simplified method of the growth of human tumor infiltrating lymphocytes in gas-permeable flasks to numbers needed for patient treatment*. J Immunother, 2012. **35**(3): p. 283-92.
180. Livak, K.J. and T.D. Schmittgen, *Analysis of relative gene expression data using real-time quantitative PCR and the 2(-Delta Delta C(T)) Method*. Methods, 2001. **25**(4): p. 402-8.
182. Wang, Y.H., et al., *Transmembrane and coiled-coil domain family 3 (TMCC3) regulates breast cancer stem cell and AKT activation*. Oncogene, 2021. **40**(16): p. 2858-2871.
183. Wisesa, S., Y. Yamamoto, and T. Sakisaka, *TMCC3 localizes at the three-way junctions for the proper tubular network of the endoplasmic reticulum*. Biochem J, 2019. **476**(21): p. 3241-3260.

184. Cheng, X., et al., *Zinc transporter SLC39A13/ZIP13 facilitates the metastasis of human ovarian cancer cells via activating Src/FAK signaling pathway*. J Exp Clin Cancer Res, 2021. **40**(1): p. 199.
185. Mehta, A., et al., *Immunotherapy Resistance by Inflammation-Induced Dedifferentiation*. Cancer Discov, 2018. **8**(8): p. 935-943.
186. Kucka, K. and H. Wajant, *Receptor Oligomerization and Its Relevance for Signaling by Receptors of the Tumor Necrosis Factor Receptor Superfamily*. Front Cell Dev Biol, 2020. **8**: p. 615141.
187. Thomas, W.D. and P. Hersey, *TNF-related apoptosis-inducing ligand (TRAIL) induces apoptosis in Fas ligand-resistant melanoma cells and mediates CD4 T cell killing of target cells*. J Immunol, 1998. **161**(5): p. 2195-200.
188. Corazza, N., et al., *TRAIL receptor-mediated JNK activation and Bim phosphorylation critically regulate Fas-mediated liver damage and lethality*. J Clin Invest, 2006. **116**(9): p. 2493-9.
189. Naval, J., et al., *Importance of TRAIL Molecular Anatomy in Receptor Oligomerization and Signaling. Implications for Cancer Therapy*. Cancers (Basel), 2019. **11**(4).
190. Han, Y., D. Liu, and L. Li, *PD-1/PD-L1 pathway: current researches in cancer*. Am J Cancer Res, 2020. **10**(3): p. 727-742.
191. Ahn, A., et al., *Transcriptional Reprogramming and Constitutive PD-L1 Expression in Melanoma Are Associated with Dedifferentiation and Activation of Interferon and Tumour Necrosis Factor Signalling Pathways*. Cancers (Basel), 2021. **13**(17).
192. Zhang, N., et al., *SA-49, a novel aloperine derivative, induces MITF-dependent lysosomal degradation of PD-L1*. EBioMedicine, 2019. **40**: p. 151-162.
193. Pant, A., R. Medikonda, and M. Lim, *Alternative Checkpoints as Targets for Immunotherapy*. Curr Oncol Rep, 2020. **22**(12): p. 126.
194. Menevse, A.N., et al., *TSP0 acts as an immune resistance gene involved in the T-cell mediated immune control of glioblastoma (accepted)*. Acta Neuropathol., 2023.
195. Levy, C., et al., *Lineage-specific transcriptional regulation of DICER by MITF in melanocytes*. Cell, 2010. **141**(6): p. 994-1005.
196. Agrawal, N., et al., *RNA interference: biology, mechanism, and applications*. Microbiol Mol Biol Rev, 2003. **67**(4): p. 657-85.
197. Hirsch, M. and M. Helm, *Live cell imaging of duplex siRNA intracellular trafficking*. Nucleic Acids Res, 2015. **43**(9): p. 4650-60.
198. Huang, B., X. Lang, and X. Li, *The role of IL-6/JAK2/STAT3 signaling pathway in cancers*. Front Oncol, 2022. **12**: p. 1023177.
199. Fulda, S., *Targeting c-FLICE-like inhibitory protein (CFLAR) in cancer*. Expert Opin Ther Targets, 2013. **17**(2): p. 195-201.
200. Jackson, A.L. and P.S. Linsley, *Recognizing and avoiding siRNA off-target effects for target identification and therapeutic application*. Nat Rev Drug Discov, 2010. **9**(1): p. 57-67.
201. Khan, A.A., et al., *Transfection of small RNAs globally perturbs gene regulation by endogenous microRNAs*. Nat Biotechnol, 2009. **27**(6): p. 549-55.
202. Echeverri, C.J., et al., *Minimizing the risk of reporting false positives in large-scale RNAi screens*. Nat Methods, 2006. **3**(10): p. 777-9.
203. McDermaid, A., et al., *Interpretation of differential gene expression results of RNA-seq data: review and integration*. Brief Bioinform, 2019. **20**(6): p. 2044-2054.

204. Hegenbarth, J., et al., *Perspectives on Bulk-Tissue RNA Sequencing and Single-Cell RNA Sequencing for Cardiac Transcriptomics*. *Frontiers in Molecular Medicine*, 2022. **2**.
205. Karlsson, M., et al., *A single-cell type transcriptomics map of human tissues*. *Sci Adv*, 2021. **7**(31).
207. Tsimberidou, A.M., et al., *Review of precision cancer medicine: Evolution of the treatment paradigm*. *Cancer Treat Rev*, 2020. **86**: p. 102019.
208. Sahai, E., et al., *A framework for advancing our understanding of cancer-associated fibroblasts*. *Nat Rev Cancer*, 2020. **20**(3): p. 174-186.
209. Li, X., et al., *Disseminated Melanoma Cells Transdifferentiate into Endothelial Cells in Intravascular Niches at Metastatic Sites*. *Cell Rep*, 2020. **31**(11): p. 107765.
210. Maddodi, N. and V. Setaluri, *Prognostic significance of melanoma differentiation and trans-differentiation*. *Cancers (Basel)*, 2010. **2**(2): p. 989-99.
211. Bao, C., et al., *HDGF: a novel jack-of-all-trades in cancer*. *Future Oncol*, 2014. **10**(16): p. 2675-85.
212. Enomoto, H., et al., *Hepatoma-Derived Growth Factor: An Overview and Its Role as a Potential Therapeutic Target Molecule for Digestive Malignancies*. *Int J Mol Sci*, 2020. **21**(12).
213. Jia, W., P. Chen, and Y. Cheng, *PRDX4 and Its Roles in Various Cancers*. *Technol Cancer Res Treat*, 2019. **18**: p. 1533033819864313.
214. Xie, X., et al., *Single-cell transcriptomic landscape of human blood cells*. *Natl Sci Rev*, 2021. **8**(3): p. nwa180.
215. Frangogiannis, N.G., *Biomarkers: hopes and challenges in the path from discovery to clinical practice*. *Transl Res*, 2012. **159**(4): p. 197-204.
216. Fu, N., et al., *Comparison of protein and mRNA expression evolution in humans and chimpanzees*. *PLoS One*, 2007. **2**(2): p. e216.
217. Cheng, Z., et al., *Differential dynamics of the mammalian mRNA and protein expression response to misfolding stress*. *Mol Syst Biol*, 2016. **12**(1): p. 855.
218. Kumar, R., P.E. Herbert, and A.N. Warrens, *An introduction to death receptors in apoptosis*. *Int J Surg*, 2005. **3**(4): p. 268-77.
219. Krensky, A.M., *The HLA system, antigen processing and presentation*. *Kidney Int Suppl*, 1997. **58**: p. S2-7.
220. Hazini, A., K. Fisher, and L. Seymour, *Deregulation of HLA-I in cancer and its central importance for immunotherapy*. *J Immunother Cancer*, 2021. **9**(8).
221. Dhatchinamoorthy, K., J.D. Colbert, and K.L. Rock, *Cancer Immune Evasion Through Loss of MHC Class I Antigen Presentation*. *Front Immunol*, 2021. **12**: p. 636568.
222. Min, K.J., et al., *Elucidation for modulation of death receptor (DR) 5 to strengthen apoptotic signals in cancer cells*. *Arch Pharm Res*, 2019. **42**(1): p. 88-100.
223. Puimège, L., C. Libert, and F. Van Hauwermeiren, *Regulation and dysregulation of tumor necrosis factor receptor-1*. *Cytokine Growth Factor Rev*, 2014. **25**(3): p. 285-300.
224. Pishesha, N., T.J. Harmand, and H.L. Ploegh, *A guide to antigen processing and presentation*. *Nat Rev Immunol*, 2022. **22**(12): p. 751-764.
225. Yamamoto, K., et al., *Autophagy promotes immune evasion of pancreatic cancer by degrading MHC-I*. *Nature*, 2020. **581**(7806): p. 100-105.
226. Du, W., et al., *Loss of Optineurin Drives Cancer Immune Evasion via Palmitoylation-Dependent IFNGR1 Lysosomal Sorting and Degradation*. *Cancer Discov*, 2021. **11**(7): p. 1826-1843.
227. Yun, C.W. and S.H. Lee, *The Roles of Autophagy in Cancer*. *Int J Mol Sci*, 2018. **19**(11).

228. Yogesha, S.D., S.M. Khapli, and M.R. Wani, *Interleukin-3 and granulocyte-macrophage colony-stimulating factor inhibits tumor necrosis factor (TNF)-alpha-induced osteoclast differentiation by down-regulation of expression of TNF receptors 1 and 2*. J Biol Chem, 2005. **280**(12): p. 11759-69.
229. Dilloo, D., et al., *Differential production of interleukin-3 in human T lymphocytes following either CD3 or CD2 receptor activation*. Exp Hematol, 1996. **24**(4): p. 537-43.
230. Dörrie, J., et al., *Regulation of CD95 expression and CD95-mediated cell death by interferon-gamma in acute lymphoblastic leukemia with chromosomal translocation t(4;11)*. Leukemia, 1999. **13**(10): p. 1539-47.
231. Ramaswamy, M., et al., *Many checkpoints on the road to cell death: regulation of Fas-FasL interactions and Fas signaling in peripheral immune responses*. Results Probl Cell Differ, 2009. **49**: p. 17-47.
232. Peter, M.E., et al., *The role of CD95 and CD95 ligand in cancer*. Cell Death Differ, 2015. **22**(4): p. 549-59.
233. Sohn, W.J., et al., *Expression and characterization of transmembrane and coiled-coil domain family 3*. BMB Rep, 2016. **49**(11): p. 629-634.
234. Suhda, S., et al., *The 14-3-3 γ isoform binds to and regulates the localization of endoplasmic reticulum (ER) membrane protein TMCC3 for the reticular network of the ER*. J Biol Chem, 2023. **299**(2): p. 102813.
235. Schwarz, D.S. and M.D. Blower, *The endoplasmic reticulum: structure, function and response to cellular signaling*. Cell Mol Life Sci, 2016. **73**(1): p. 79-94.
236. Hoyer, M.J., et al., *A Novel Class of ER Membrane Proteins Regulates ER-Associated Endosome Fission*. Cell, 2018. **175**(1): p. 254-265.e14.
237. Freeman, A.K. and D.K. Morrison, *14-3-3 Proteins: diverse functions in cell proliferation and cancer progression*. Semin Cell Dev Biol, 2011. **22**(7): p. 681-7.
238. Johnston, H.E., et al., *Proteomics Profiling of CLL Versus Healthy B-cells Identifies Putative Therapeutic Targets and a Subtype-independent Signature of Spliceosome Dysregulation*. Mol Cell Proteomics, 2018. **17**(4): p. 776-791.
239. Liu, S., et al., *NamiRNA-enhancer network of miR-492 activates the NR2C1-TGF- β /Smad3 pathway to promote epithelial-mesenchymal transition of pancreatic cancer*. Carcinogenesis, 2023.
240. Song, G., G. Ouyang, and S. Bao, *The activation of Akt/PKB signaling pathway and cell survival*. J Cell Mol Med, 2005. **9**(1): p. 59-71.
241. Liu, R., et al., *PI3K/AKT pathway as a key link modulates the multidrug resistance of cancers*. Cell Death Dis, 2020. **11**(9): p. 797.
242. Aubrey, B.J., et al., *How does p53 induce apoptosis and how does this relate to p53-mediated tumour suppression?* Cell Death Differ, 2018. **25**(1): p. 104-113.
243. Li, P., et al., *Caspase-9: structure, mechanisms and clinical application*. Oncotarget, 2017. **8**(14): p. 23996-24008.
244. Osowski, C.M. and F. Urano, *Measuring ER stress and the unfolded protein response using mammalian tissue culture system*. Methods Enzymol, 2011. **490**: p. 71-92.
245. Bahar, E., H. Kim, and H. Yoon, *ER Stress-Mediated Signaling: Action Potential and Ca(2+) as Key Players*. Int J Mol Sci, 2016. **17**(9).
246. Chang, L., et al., *The E3 ubiquitin ligase itch couples JNK activation to TNF α -induced cell death by inducing c-FLIP(L) turnover*. Cell, 2006. **124**(3): p. 601-13.

247. Tiwary, R., et al., *Role of endoplasmic reticulum stress in alpha-TEA mediated TRAIL/DR5 death receptor dependent apoptosis*. PLoS One, 2010. **5**(7): p. e11865.
248. Hu, P., et al., *Critical role of endogenous Akt/IAPs and MEK1/ERK pathways in counteracting endoplasmic reticulum stress-induced cell death*. J Biol Chem, 2004. **279**(47): p. 49420-9.
249. Falletta, P., et al., *Translation reprogramming is an evolutionarily conserved driver of phenotypic plasticity and therapeutic resistance in melanoma*. Genes Dev, 2017. **31**(1): p. 18-33.
250. Hu, H., et al., *The C/EBP Homologous Protein (CHOP) Transcription Factor Functions in Endoplasmic Reticulum Stress-Induced Apoptosis and Microbial Infection*. Front Immunol, 2018. **9**: p. 3083.
251. Lin, W.C., et al., *Endoplasmic reticulum stress stimulates p53 expression through NF- κ B activation*. PLoS One, 2012. **7**(7): p. e39120.
252. Bin, B.H., et al., *Biochemical characterization of human ZIP13 protein: a homo-dimerized zinc transporter involved in the spondylocheiro dysplastic Ehlers-Danlos syndrome*. J Biol Chem, 2011. **286**(46): p. 40255-65.
253. Brito, S., et al., *Zinc and Its Transporters in Epigenetics*. Mol Cells, 2020. **43**(4): p. 323-330.
254. Ogawa, Y., et al., *Zinc and Skin Disorders*. Nutrients, 2018. **10**(2).
255. Fukada, T., et al., *The zinc transporter SLC39A13/ZIP13 is required for connective tissue development; its involvement in BMP/TGF-beta signaling pathways*. PLoS One, 2008. **3**(11): p. e3642.
256. Yamauchi, T., et al., *Changes in skin structure of the Zip13-KO mouse by Makomo (Zizania latifolia) feeding*. J Vet Med Sci, 2017. **79**(9): p. 1563-1568.
257. Hirose, T., et al., *Comparative study of dermal components and plasma TGF- β 1 levels in Slc39a13/Zip13-KO mice*. J Vet Med Sci, 2015. **77**(11): p. 1385-9.
258. Zhu, B., et al., *Increased expression of zinc transporter ZIP4, ZIP11, ZnT1, and ZnT6 predicts poor prognosis in pancreatic cancer*. J Trace Elem Med Biol, 2021. **65**: p. 126734.
259. Liu, L., J. Yang, and C. Wang, *Analysis of the prognostic significance of solute carrier (SLC) family 39 genes in breast cancer*. Biosci Rep, 2020. **40**(8).
260. Parkin, A., et al., *Targeting the complexity of Src signalling in the tumour microenvironment of pancreatic cancer: from mechanism to therapy*. Febs j, 2019. **286**(18): p. 3510-3539.
261. Green, D.S., H.A. Young, and J.C. Valencia, *Current prospects of type II interferon γ signaling and autoimmunity*. J Biol Chem, 2017. **292**(34): p. 13925-13933.
262. Lee, J., D. Lee, and Y. Kim, *Mathematical model of STAT signalling pathways in cancer development and optimal control approaches*. R Soc Open Sci, 2021. **8**(9): p. 210594.
263. Barnholt, K.E., et al., *Adenosine blocks IFN-gamma-induced phosphorylation of STAT1 on serine 727 to reduce macrophage activation*. J Immunol, 2009. **183**(10): p. 6767-77.
264. Stephanou, A., et al., *Opposing actions of STAT-1 and STAT-3 on the Bcl-2 and Bcl-x promoters*. Cell Death Differ, 2000. **7**(3): p. 329-30.
265. Kim, H.S. and M.S. Lee, *STAT1 as a key modulator of cell death*. Cell Signal, 2007. **19**(3): p. 454-65.
266. Lee, M.G., et al., *Loss of the dermis zinc transporter ZIP13 promotes the mildness of fibrosarcoma by inhibiting autophagy*. Sci Rep, 2019. **9**(1): p. 15042.
267. Chen, S., Z. Song, and A. Zhang, *Small-Molecule Immuno-Oncology Therapy: Advances, Challenges and New Directions*. Curr Top Med Chem, 2019. **19**(3): p. 180-185.

269. Hara, T., et al., *Zinc transporters as potential therapeutic targets: An updated review*. J Pharmacol Sci, 2022. **148**(2): p. 221-228.
270. Hawkins, E.R., R.R. D'Souza, and A. Klampatsa, *Armored CAR T-Cells: The Next Chapter in T-Cell Cancer Immunotherapy*. Biologics, 2021. **15**: p. 95-105.
271. Winge-Main, A.K., S. Wälchli, and E.M. Inderberg, *T cell receptor therapy against melanoma-Immunotherapy for the future?* Scand J Immunol, 2020. **92**(4): p. e12927.

Webpages

32. BioRender. *BioRender*. Available from: <https://www.biorender.com/>.
66. Maßberg, D. and S. von dem Hagen. *Hautkrebs*. 2021; Available from: <https://www.krebshilfe.de/informieren/ueber-krebs/krebsarten/hautkrebs/>.
163. Bengtsson, H. *aroma.light: Light-Weight Methods for Normalization and Visualization of Microarray Data using Only Basic R Data Types*. Available from: <https://bioconductor.org/packages/aroma.light>.
164. Dowle, M. and A. Srinivasan. *data.table: Extension of 'data.frame'*. Available from: <https://CRAN.R-project.org/package=data.table>.
165. Langfelder, P., B. Zhang, and S. Horvath. *dynamicTreeCut: Methods for Detection of Clusters in Hierarchical Clustering Dendrograms*. Available from: <https://cran.r-project.org/web/packages/dynamicTreeCut/index.html>.
166. Wickham, H., et al. *dplyr: A Grammar of Data Manipulation*. Available from: <https://CRAN.R-project.org/package=dplyr>.
167. Wickham, H., et al. *ggplot2: Create Elegant Data Visualisations Using the Grammar of Graphics*. Available from: <https://CRAN.R-project.org/package=ggplot2>.
168. Warnes, G.R., et al. *gplots: Various R Programming Tools for Plotting Data*. Available from: <https://CRAN.R-project.org/package=gplots>.
169. Kolberg, L. *gprofiler2: Interface to the 'g:Profiler' Toolset*. Available from: <https://CRAN.R-project.org/package=gprofiler2>.
170. Pau, G. *hwriter: HTML Writer - Outputs R Objects in HTML Format*. Available from: <https://CRAN.R-project.org/package=hwriter>.
171. Kolde, R. *pheatmap: Pretty Heatmaps*. Available from: <https://CRAN.R-project.org/package=pheatmap>.
172. Huber, W. and O. Sklyar. *splots: Visualization of high-throughput assays in microtitre plate or slide format*. 2022; Available from: <https://bioconductor.org/packages/splots>.
173. Leek, J.T., et al. *sva: Surrogate Variable Analysis*. 2022; Available from: <https://bioconductor.org/packages/sva>.
174. Dragulescu, A. and C. Arendt. *xlsx: Read, Write, Format Excel 2007 and Excel 97/2000/XP/2003 Files*. Available from: <https://CRAN.R-project.org/package=xlsx>.
176. Center for Cancer Genomics, N. *The Cancer Genome Atlas Program (TCGA)*. Available from: <https://www.cancer.gov/tcga>.
177. Harvard, B.I.o.M.a. *The Genotype-Tissue Expression (GTEx) project*. Available from: <https://gtexportal.org/home/>.
206. HPA. *The Human Protein Atlas*. Available from: <https://www.proteinatlas.org/>.

Theses

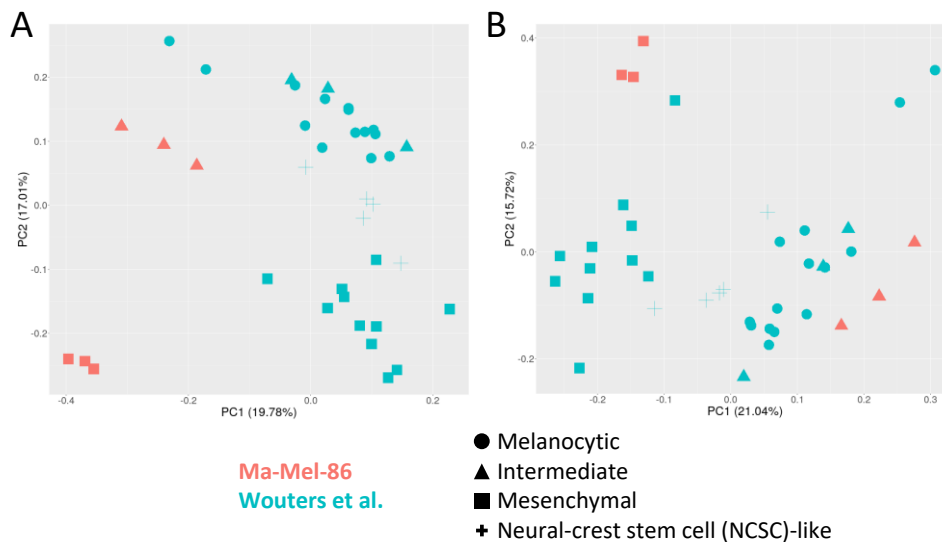
178. Menevse, A.N., *Identification of EFNB1 as a key immune modulator in brain with a dual role in T cell co-stimulation and glial cell immune resistance*. 2020, Regensburg.
181. Michels, T., *A high-throughput RNAi screening identifies olfactory receptor signaling as a novel immune checkpoint in solid tumors*. 2017, Heidelberg.

Patents

268. Yu, A.L., et al., *Methods for suppressing cancer by inhibition of TMCC3* 2016: United States.

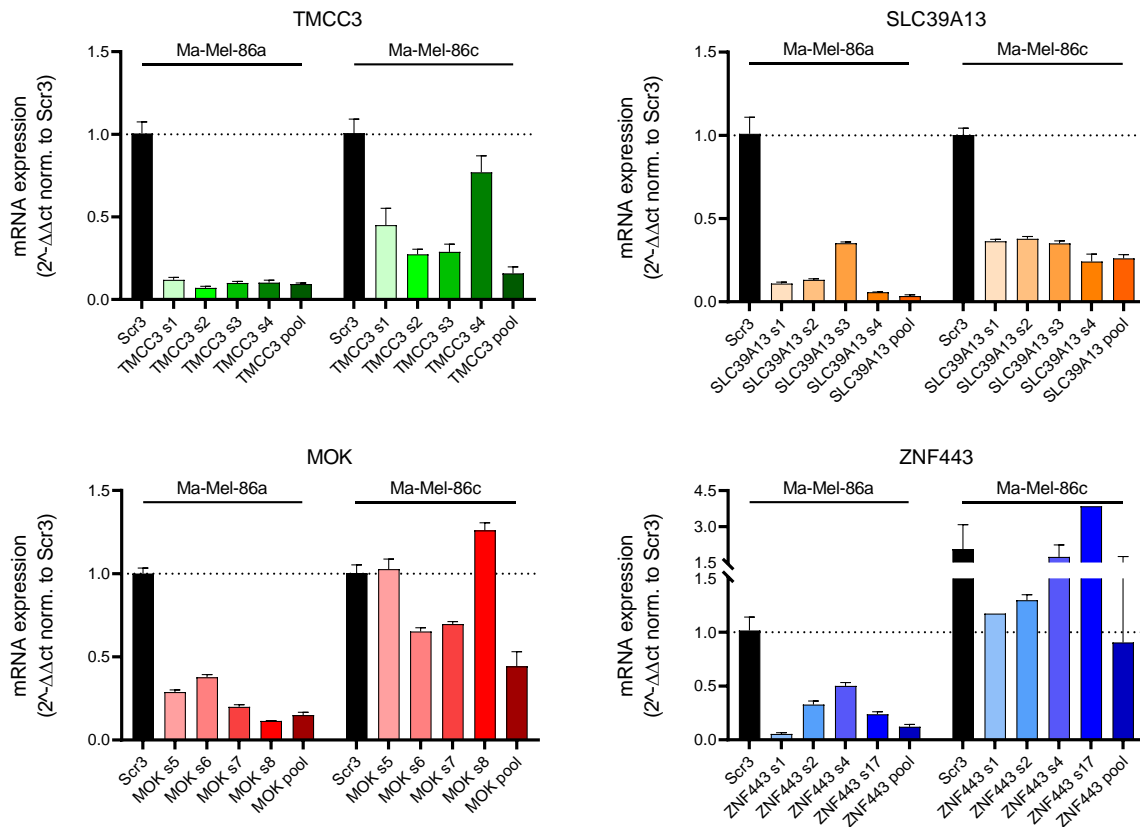
Appendix

I. Supplementary Figures



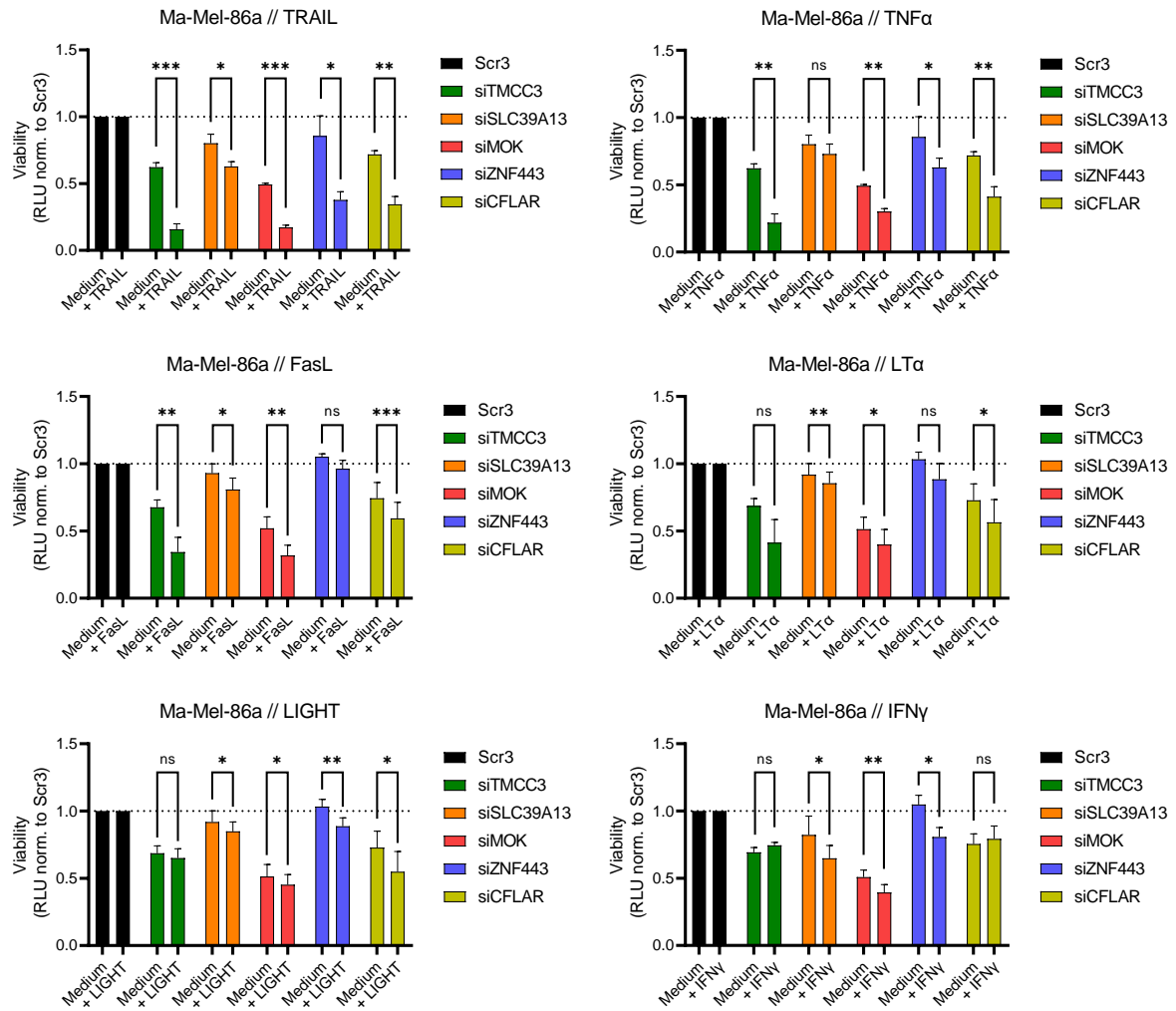
Supplementary Figure 1: ComBat-seq to remove dataset specific batch effects.

Raw count RNA-Seq data from Wouters *et al.* and Ma-Mel-86 in triplicates was combined and subjected to ComBat-seq in order to remove batch effects that were introduced due to the different origin of the two data sets. Principle component analysis (PCA) was conducted to represent the similarity of the samples **(A)** before and **(B)** after ComBat-seq. Red colored samples represent RNA-Seq data of Ma-Mel-86 while blue colored samples represent cell lines from Wouters *et al.* The different symbols represent the melanoma cell line subtypes melanocytic (MITF^{high}), intermediate (MITF^{high}), mesenchymal (MITF^{low}) and neural-crest stem cell (NCSC)-like (MITF^{low}).



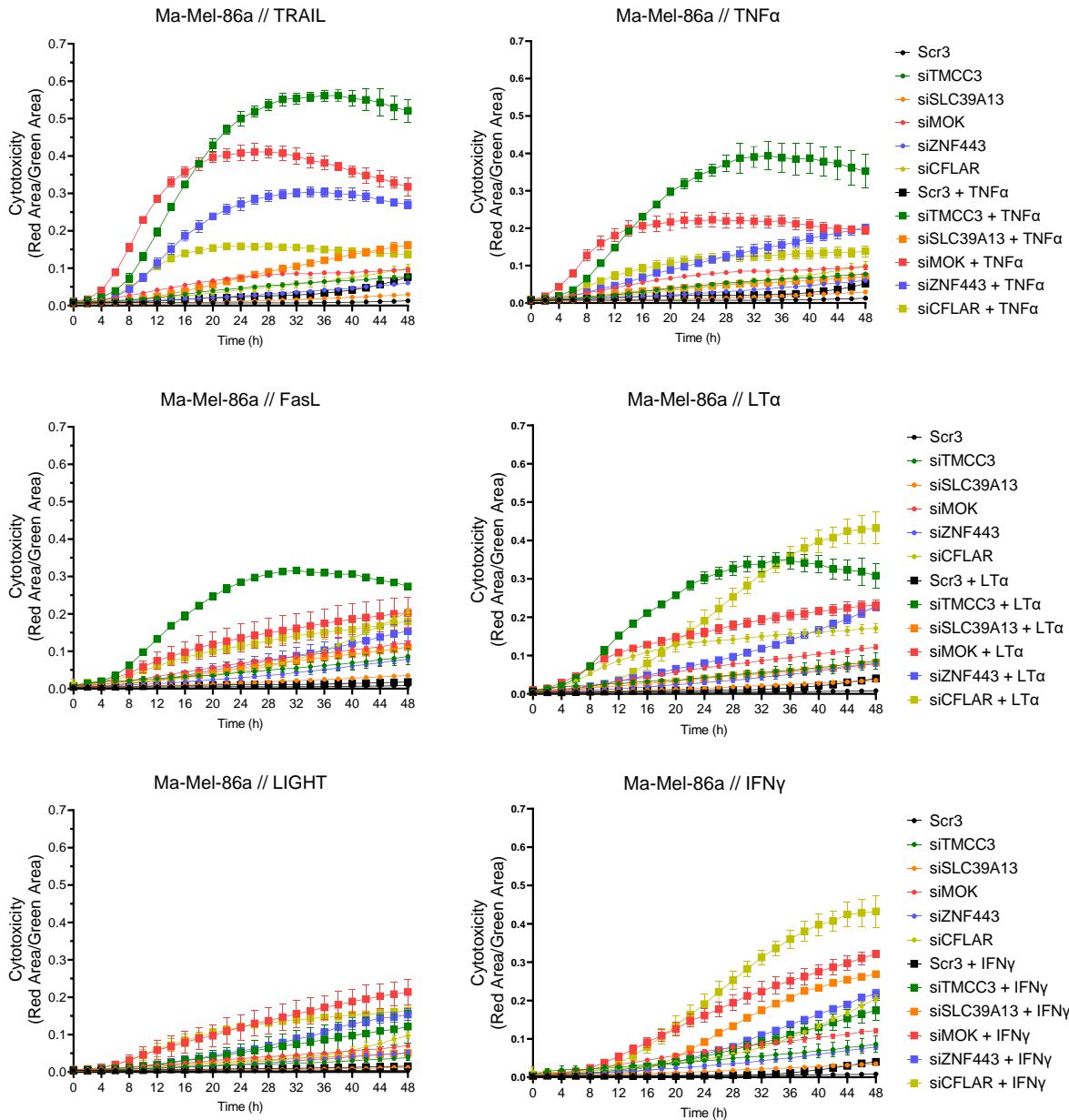
Supplementary Figure 2: Knockdown efficiency of selected immune resistance (IR) genes.

Ma-Mel-86 HLA-A2+ Luc+ were transfected with Scr3 and individual or pooled siRNAs for *TMCC3*, *SLC39A13*, *MOK* or *ZNF443* for 48 h. Cells were lysed for RNA isolation followed by reverse transcription to cDNA. Quantitative real-time PCR was used to measure target gene expression. Expression of Actin-beta was measured as reference gene to normalize gene expression and values were normalized to Scr3. Bars represent the mean of technical replicates + standard deviation.



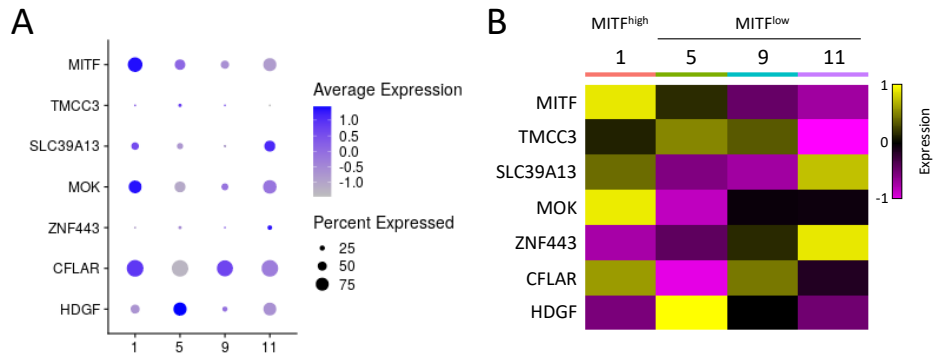
Supplementary Figure 3: Impact of immune resistance genes on tumor cell rejection mediated by cytotoxic ligands I.

Luciferase-based cytotoxicity assays to measure the impact of gene knockdown on the cytotoxicity of TRAIL, TNF α , FasL, LT α , LIGHT or IFN γ . Ma-Mel-86 HLA-A2+ Luc⁺ were transfected with Scr3, a pool of four siRNAs for *TMCC3*, *SLC39A13*, *MOK* or *CFLAR* or *ZNF443* siRNA for 48 h. Subsequently, cells were cultured in plain medium (viability setting) or treated with 100 ng/ml recombinant TRAIL, TNF α , FasL, LT α , LIGHT or IFN γ (cytotoxicity setting). After 20 h of treatment, cells were lysed, and remaining luciferase activity was measured by luminescence. Raw luciferase units (RLU) were normalized to RLU of Scr3. Bars represent the mean + standard deviation of three independent experiments. Significances between viability and cytotoxicity setting were calculated by applying a two-tailed paired t-test (* $p < 0,05$, ** $p < 0,01$, *** $p < 0,001$, ns=not significant).



Supplementary Figure 4: Impact of immune resistance genes on tumor cell rejection mediated by cytotoxic ligands II.

Real-time cytotoxicity assays to measure the impact of gene knockdown on the cytotoxicity of TRAIL, TNF α , FasL, LT α , LIGHT or IFN γ . Ma-Mel-86 HLA-A2+ Luc+ were transfected with Scr3, a pool of four siRNAs for *TMCC3*, *SLC39A13*, *MOK* or *CFLAR* or *ZNF443* siRNA for 48 h. Subsequently, cells were cultured in plain medium (viability setting) or treated with 100 ng/ml recombinant TRAIL, TNF α , FasL, LT α , LIGHT or IFN γ (cytotoxicity setting). Upon treatment Incucyte[®] Cytotox Red Dye was added to label dead cells and tumor cell death was measured every two hours for 48 h. The signal of the Red Area was normalized to the Green Area, representing the confluency of the tumor cells by detection of GFP. Representative data of two independent experiments.



Supplementary Figure 5: Expression of control and immune resistance genes in different melanoma cell subsets.

This figure extends Figures 28 and 29. Seurat analysis was conducted by using the programming language R for statistical computing. Expression of control and immune resistance genes was investigated in the four melanoma cell clusters 1, 5, 9 and 11 and represented as **(A)** dotplot or **(B)** heatmap.

II. Supplementary Tables

Supplementary Table 21: siRNA library of the secondary validation screen.

AATK	CCDC51	FAT4	KCNK5	NINJ2	PLA2G1B	RIPK1	TGFA
ABCA13	CCL4	FES	KCNS2	NLK	PLD2	RNF19A	TMCC3
ABCA5	CD274	FGFR2	KLRC3	NROB2	PLPP2	RPS6KA2	TMEM106B
ABHD13	CDH24	FLVCR2	LETM1	OR11G2	PLPP4	SCARA3	TMEM132E
ADIPOR2	CFLAR	GABRA4	LNPB	OR1E2	PLPP6	SERTM1	TMEM165
AK2	CHEK1	GABRB1	LRFN3	OR1S1	POLR2G	SIGLEC6	TMEM248
AKAP1	CHRNA7	GCK	LRFN4	OR2H1	PRDX4	SLC12A1	TMEM42
ALDH2	CHRNA7	GJB1	LTB4R	OR2K2	PRKD2	SLC13A2	TMEM63C
ANO8	CLEC12B	GJC2	MAK	OR4A47	PRKD3	SLC13A5	TNFRSF13B
APOA2	CNOT3	GPAT4	MALT1	OR51G2	PRRT1	SLC20A1	TNFRSF1A
ASTL	CNTNAP1	GPR142	MAP3K14	OR5AN1	PSMC1	SLC26A11	TNFRSF6B
ATP13A5	COASY	GPR87	MAP3K9	OR7A5	PSMC3	SLC34A2	TNIK
ATP1A4	DCK	GRK1	MAP4K1	OR8U8	PSMD13	SLC39A13	TP53AIP1
ATP2B4	DDIT3	GRM6	MARK3	PCDHAC2	PSMD3	SLC7A10	TPD52L3
ATP8A1	DENND6B	HAS1	MARK4	PHGDH	PSMD6	SLC9A5	TRPC7
ATP8B2	DGKQ	HTR1A	MAT2A	PI4KA	PTCHD3	SNRPE	WDR83OS
BCAP29	DUOX2	HYAL1	MITF	PIEZO1	RAPGEF4	SPNS3	XPO1
BCL10	DYRK2	ITGAX	MOK	PIGP	RBBP4	SSPN	ZNF443
BCL2L10	DYRK3	JAK2	MURF1	PIK3C2G	RELT	STAB1	ZNF705A
BRD2	EDNRA	JAKMIP3	MURF2	PIK3CG	RETREG1	STX17	
BTN2A2	ELFN2	KCNJ9	NCCRP1	PKD2	RETREG2	TAAR8	
C1orf162	ELN	KCNK13	NDC1	PKLR	RHBDD3	TAS2R43	